Evaluation of M102 as a novel therapeutic in Amyotrophic Lateral Sclerosis (ALS)

By

Amy Francesca Amanda Keerie

Submitted for the degree of Doctor of Philosophy (PhD)

February 2022

Supervisors:
Dr Richard Mead, Dr Guillaume Hautbergue, Prof Dame Pamela Shaw

Department of Neuroscience
Sheffield Institute for Translational Neuroscience
University of Sheffield

This thesis is dedicated to my aunt Amanda and my nan Brenda.

Thank you for your continued support and encouragement throughout my life and my studies, the inspiration to pursue my interest in science and obviously the chocolate packages to keep me going.

Acknowledgements

Firstly, a huge thanks to my supervisors, Dr Richard Mead, Dr Guillaume Hautbergue and Professor Dame Pamela Shaw for their support throughout my PhD. I am incredibly grateful to Richard, who has been extremely helpful and encouraging during my time at SITraN and has allowed me to develop as a researcher. Thanks for believing in me even when I didn't believe in myself. I couldn't have wished for a better supervisor. A huge thanks to Dr Ning Shan, Raymond Houck and Dr Joseph Reiser from Aclipse Therapeutics for funding my PhD and giving guidance and support throughout the project, helping to make it a success.

Thank you to everyone who has taught me techniques: Lydia Castelli and Mirinda Tattan for their advice on RT-qPCR, Ryan West for Drosophila techniques and motivational speeches, James Alix for his expert knowledge in electrophysiology and Ian Coldicott for tolerating spending time with me. Thank you to Dan Fillingham and Lynne Baxter for their support with histology and to Khoa Pharm for his mass spec analysis. A huge thanks to the team at the BSU for helping with animal care, especially Carol Pentland, who is an absolute angel, is calm in a crisis and keeps the place running. Thanks to Alex Daniel, Shivani Suresh and Isaac Kirkland who aided with the project and helped conduct some studies for my thesis.

To all the members of the Mead team and SITraN past and present, thank you for your support, advice, and friendship, you have made working at SITraN much more enjoyable. I am extremely grateful for Scott McKinnon's help, especially during the pandemic when he was one of the only humans I would see and for our weekly gaming session with Paddy. A huge shout out to Charlotte Mason, who has helped me to keep as sane as possible during these difficult years and for being by my side as we strive to be the best humans we can be.

A special thanks to my parents, nan and Amanda for their love and support throughout my whole education. Being far away is difficult but FaceTime has made it more bearable. A huge thanks to my sister for coming to visit so we can pet animals, but not for giving me COVID. I couldn't not mention my cat Phoebe, who has sat beside me throughout my entire write up. Finally, a huge thank you to Sam for his continued support in everything I do.

Doing a PhD during a pandemic has not been ideal, I am extremely grateful to everyone for their support and friendship during this time. I am so lucky to have such a supportive network.

Table of Contents

List of Figures

List of Tables

Abstract

ALS is a devastating neurodegenerative disease affecting both motor and cognitive function for which new therapies are urgently needed. M102 and M102R are electrophilic enantiomers previously shown to activate the NFE2-related factor 2 (NRF2) pathway. Electrophilic molecules often activate other pathways such as heat shock factor 1 (HSF1), which activates heat shock proteins (HSPs) and chaperones that aid with correct folding of proteins and removal of misfolded proteins. Since protein aggregates are a hallmark of ALS, activation of HSF1 has the potential to be neuroprotective.

The objectives of the PhD were to further investigate the pharmacodynamic response to M102 *in vivo* by measuring gene induction for NRF2 and HSF1 pathways in dose response experiments. This enabled identification of the optimal dose for further testing in a TDP-43^{Q331K} transgenic mouse model of ALS to increase confidence in clinical translation. In addition, oral dosing of M102 was explored in the $SOD1^{G93A}$ model to support the clinical development of this route of administration.

After identifying for the first time that M102 can activate downstream targets of NRF2 and HSF1 pathways in WT mice, it was shown that this activity was dampened in a $SOD1^{G93A}$ mouse model at both early and intermediate stages of disease, particularly for NRF2 targets. M102 was also shown to increase levels of reduced glutathione (GSH), showing activation of downstream pathways of NRF2.

Results from both $SOD1^{G93A}$ and TDP-43^{Q331K} mouse models showed improvement in weight and electrophysiological parameters. In the TDP-43^{Q331K} model, there was also an improvement in gait parameters and an increase in HSF1 and NRF2 gene targets in cortex tissue. This suggests neuroprotective effects of M102 and because both models showed responses in the same parameters, it gives confidence that the same pathways are driving the effects seen. This data has contributed to the advancement of M102 towards clinical testing.

Abbreviations

AD	Alzheimer's disease
ALS	Amyotrophic Lateral Sclerosis
ALSFRS	Amyotrophic Lateral Sclerosis Functional Rating Scale
ARE	Antioxidant Response Element
AUC	Area under the curve
B-TrCP	Beta-transducin repeat containing protein
BAC	Bacterial artificial chromosome
BBB	Blood brain barrier
BOS	Base of support
BTB	broad complex/ tramtrack/ bric a brac
bZIP	basic leucine zipper
C9orf72	Chromosome 9 open reading frame 72
CBP	CREB-binding protein
CDDO-me	2-cyano-3,12-dioxoolean-1,9-dien-28-oic acid, Bardoxolone methyl
CHO	Chinese hamster ovary
CMAP	Compound muscle action potential
CNC	Cap 'N' Collar
CNS	Central nervous system
cT	Cycle threshold
CUL3	Cullin3
DEPC	Diethyl pyrocarbonate
DGR	Double glycine repeat
DMEM	Dulbecco's Modification of Eagle's Medium
DMF	Dimethyl fumarate
dNTP	Deoxynucleotide triphosphate
DPR	Dipeptide repeat proteins
EAAT2	Excitatory amino acid transporter
EC50	Half maximal effective concentrations
ER	Endoplasmic reticulum
ESG	N-ethylsuccinimido-S-glutathione
FALS	Familial ALS
FDA	U.S. Food and Drug Administration

FTD	Frontal temporal dementia
FUS	Fused in Sarcoma
GA	Glycine- alanine
GP	Glycine- proline
GR	Glycine - arginine
GSH	Reduced glutathione
GSK-3β	Glycogen synthase kinase 3β
GSSG	Oxidised glutathione
HP- β -CD	(2-hydroxypropyl)-beta-cyclodextrin
HPLC	High-Performance Liquid Chromatography
HSE	Heat shock element
HSF1	Heat shock factor 1
hSOD1	human SOD1
HSP	Heat shock protein
HSR	Heat shock response
huRNP	Heterogeneous ribonucleoprotein
ITC	Isothermal calorimetry
IVR	Intervening region
KEAP1	Kelch-like ECH-associated protein 1
MAREs	MAF recognition elements
MC	Methyl cellulose
MMF	Monomethyl fumarate
MS	Multiple sclerosis
Neh	NRF2-ECH homology
NF-kB	Nuclear factor kB
NLS	Nuclear localisation signal
NMJ	Neuromuscular junction
NMR	Nuclear magnetic resonance
NRF2	Nuclear factor erythroid 1-like 2
NT	Non transgenic
NTC	Non template control
PD	Parkinson’s disease
PPARγ	Peroxisome proliferator-activator receptor γ

PPI	Protein protein interaction
PG	Proline- glycine
PR	Proline- arginine
Prx	Peroxiredoxins
RAN	Repeat association non-ATG
RNS	Repetitive nerve stimulation
ROS	Reactive oxygen species
RT	Reverse transcriptase
RXRα	Retinoid X receptor alpha
SALS	sporadic ALS
sMAF	Small muscle aponeurosis fibromatosis
SOD1	Super oxide dismutase
SRM	Selected reaction monitoring
T	transgenic
TDP-43	Transactive response DNA binding protein 43kDa
TK	Thymidine kinase
WT	Wild type

1. Introduction

1.1. ALS background

Amyotrophic lateral sclerosis (ALS) is a progressive neurodegenerative disease caused by the loss of upper and lower motor neurons that leads to weakness and degeneration of muscles. Patients experience progressive paralysis, with death occurring in an average of 3-5 years post disease onset.

ALS affects 2 to 5 individuals per 100,000, although this is predicted to rise in the future due to an aging population (Arthur *et al.*, 2016). There are currently only two U.S. Food and Drug Administration (FDA) approved drugs for the treatment of ALS: riluzole and edaravone. Riluzole extends lifespan by an average of approximately 3 months (Miller *et al.*, 2003), without improving quality of life. Edavarone originally did not show any benefit to patients in phase 3 trials (Abe *et al.*, 2014). However, after further analysis it was found that a small subset of patients responded better than others. Using this information a further phase 3 trial began recruiting using stringent inclusion criteria and found a 2.5 point reduction in ALS functional rating scale (ALSFRS) decline over 6 months when compared to placebo (Abe *et al.*, 2017). Edaravone was approved by the FDA for use in ALS Patients in 2017. Although the exact mechanism of action is not known, it is thought to predominantly scavenge free radicals, reducing oxidative stress (Shou *et al.*, 2019). There is a desperate need for the development of new therapeutics that will improve and lengthen life for patients suffering with ALS.

Treatment of ALS is multi-disciplinary and is designed to minimise pain and control symptoms of ALS to maximise quality of life. Medication to help with muscle cramps and spasticity, pain, sleep and depression can be prescribed depending on each patient's experience and stage of disease. Most patients also benefit from a wide range of adaptive equipment in order to help them carry out day to day tasks (Paganoni *et al.*, 2015). The treatment and care of patients with ALS can require many specialists and cost of treatment increases over time with every milestone (Meng *et al.*, 2018). Analysis in Germany showed the average cost per patient was €78,256 per year (Schönfelder *et al.*, 2020).

Some patients diagnosed with ALS also show clinical frontotemporal dementia (FTD) (Burrell *et al.*, 2016). In a study by Ringholz and colleagues, it was found that 50% of ALS patients had

some cognitive impairment with 15% of ALS patients meeting criteria for FTD (Ringholz *et al.*, 2005). It was also discovered that 30% of patients initially diagnosed with FTD develop features of ALS (Burrell *et al.*, 2011). FTD and ALS share a number of genetic mutations leading to the idea of a disease continuum between the two diseases previously considered to be separate entities (Murphy *et al.*, 2007).

1.2. Genetics

Approximately 10% of ALS cases are familial (FALS) and the remaining 90% of cases are sporadic (SALS). There have been more than 30 genes associated with ALS (Chia *et al.*, 2018), the four most common being: S*OD1*, *C9orf72*, *TARDBP* and *FUS*.

Table 1.1: Major genes associated with ALS. The major genes associated with ALS showing the pathogenic mechanisms, year of discovery and discovery method.

Gene	Gene name	Locus	Pathogenic mechanism	Year discovered	Discovery method	References
SOD1	Superoxide dismutase 1	ALS1	Oxidative stress, Glutamate excitotoxicity, axonal transport defect, calcium imbalance, ER stress	1993	Linkage analysis	(Rosen *et al.*, 1993)
ALSIN	Alsin	ALS2	Endosomal trafficking, glutamate excitotoxicity, extracellular vesicles	2001	Linkage analysis	(Yang *et al.*, 2001)
SETX	Senataxin	ALS4	RNA processing, DNA damage	1998	Linkage analysis	(Chance *et al.*, 1998)
SPG11	spatacsin	ALS5	DNA damage repair	2010	Linkage analysis	(Orlacchio *et al.*, 2010)
FUS	Fused in Sarcoma	ALS6	RNA processing, mitochondiral functioning, protein aggregation	2009	Linkage analysis	(Kwiatkowski *et al.*, 2009; Vance *et al.*, 2009)
VAPB	vesicle-associated membrane protein B	ALS8	Endosomal trafficking, calcium signalling, mitochondiral signalling	2004	Linkage analysis	(Nishimura *et al.*, 2004)
ANG	Angiogenin	ALS9	RNA processing	2006	Candidate gene	(Greenway *et al.*, 2006)
TARDBP	TAR DNA-binding protein 43	ALS10	RNA processing, mitochondiral functioning, protein aggregation	2008	Linkage analysis	(Sreedharan *et al.*, 2008)
FIG4	Phosphoinositide 5-phosphatase	ALS11	Endosomal trafficking	2009	Candidate gene	(Chow *et al.*, 2009)
OPTN	Optineurin	ALS12	Endosomal trafficking, Autophagy, ER stress, protein aggregation, Mitophagy, immune response	2010	Homozygosity mapping	(Maruyama *et al.*, 2010)
ATXN2	Ataxin-2	ALS13	Protein aggregation, RNA processing	2010	Candidate gene	(Elden *et al.*, 2010)
VCP	Valosin-containing protein	ALS14	Protein aggregation, Endosomal trafficking, extracellular vesicles	2010	Candidate gene	(Johnson *et al.*, 2010)
UBQLN2	Ubiquilin-2	ALS15	Autophagy	2011	Linkage analysis	(Deng *et al.*, 2011)
SIGMAR1	Sigma non-opioid intracellular receptor 1	ALS16	Endosomal trafficking, Calcium signalling	2011	Candidate gene	(Al-Saif *et al.*, 2011)
CHMP2B	Charged multivesicular protein 2B	ALS17	Endosomal trafficking	2006	Candidate gene	(Parkinson *et al.*, 2006)

PFN1	Profilin	ALS18	Axonal transport defect	2012	Exome sequencing	(Wu *et al.*, 2012)
ERBB4	erb-b2 receptor tyrosine kinase 4	ALS19	Axonal development, apoptosis	2013	Linkage analysis	(Takahashi *et al.*, 2013)
HNRNPA1	Heterogeneous nuclear ribonucleoprotein A1	ALS20	RNA processing	2013	Linkage analysis	(Kim *et al.*, 2013)
MATR3	Matrin 3	ALS21	Protein aggregation, RNA processing	2014	Linkage analysis	(Johnson *et al.*, 2014)
TUBA4A	Tubulin alpha 4a	ALS22	Cytoskeleton	2014	Exome sequencing	(Smith *et al.*, 2014)
ANXA11	Annexin A11	ALS23	Vesicle trafficking, apoptosis	2017	Whole exome sequencing	(Smith *et al.*, 2017)
NEK1	(NIMA)-related kinase 1	ALS24	DNA damage	2016	Exome sequencing	(Brenner *et al.*, 2016)
KIF5A	Kinesin heavy-chain isoform 5A	ALS25	Axonal transport defect, mitochondrial damage	2018	Genome wide-association study	(Brenner *et al.*, 2018; Nicolas *et al.*, 2018; Simone *et al.*, 2018)
TIA1	TIA1 cytotoxic granule-associated RNA-binding protein	ALS26	RNA processing	2017	Genetic association study	(Mackenzie *et al.*, 2017)
GLT8D1	Glycosyltransferase 8 domain containing 1		Processing of glycoproteins and glycolipids	2019	Linkage analysis	(Cooper-Knock *et al.*, 2019)
DNAJC7	DnaJ heat shock protein family (Hsp40) member C7		Loss of heat shock response	2019	Whole exome sequencing	(Farhan *et al.*, 2019)
C9ORF72	Chromosome 9 open reading frame 72	ALS-FTD1	Glutamate excitotoxicity, ER stress, Endosomal trafficking, autophagy	2011	Linkage analysis	(DeJesus-Hernandez *et al.*, 2011; Renton *et al.*, 2011)
CHCHD10	coiled-coil helix coiled-coil helix domain-containing 10	ALS-FTD2	Mitochondrial function, mitophagy	2014	Linkage analysis	(Bannwarth *et al.*, 2014)
SQSTM1	Sequestosome 1	ALS-FTD3	Protein aggregation	2011	Candidate gene	(Fecto *et al.*, 2011)
TBK1	TANK-binding kinase 1	ALS-FTD4	Mitophagy, immune response, Autophagy	2016	Whole exome sequencing	(Freischmidt *et al.*, 2015; Le Ber *et al.*, 2015)

1.2.1. SOD1

In 1993 mutations in the Cu/Zn-binding superoxide dismutase (*SOD1*) gene were the first to be linked with familial ALS (Rosen *et al.*, 1993). There are currently over 200 mutations identified in SOD1 (www.alsod.iop.kcl.ac.uk) that account for 15-30% of FALS and only around 2% of sporadic cases (Zou *et al.*, 2017). There is no localisation of mutations to a particular region of the protein and most mutations lead to single amino acid substitutions.

Under physiological conditions, SOD1 forms a stable homodimer that binds copper and zinc and protects against reactive oxygen species (ROS) by catalysing the reactions of superoxide anions into molecular oxygen and hydrogen peroxide. Hydrogen peroxide can then be converted to water by either catalase enzymes or glutathione (Barber *et al.*, 2006). Reduced glutathione (GSH) acts as a cofactor in the reaction in which GSH peroxidase converts hydrogen peroxide to water, creating oxidised glutathione (GSSG) in the process (Fernadez-checa *et al.*, 1997). GSSG is quickly reduced to GSH by glutathione reductase using NADPH, therefore levels of GSSG are kept low in basal conditions. Under oxidative stress levels of GSSG are increased. As well as its role in countering ROS, it has been found that SOD1 has other roles in gene transcription in response to oxidative stress and RNA metabolism (Eleutherio *et al.*, 2021).

Mutations in SOD1 can affect the enzymatic activity, although the change in enzymatic activity varies based on the mutation (Salehi *et al.*, 2015). However, loss or reduction of enzymatic activity of SOD1 does not correlate with disease severity (Al-Chalabi *et al.*, 2012), suggesting a toxic gain of function for mutant SOD1.

In *SOD1* FALS there are often aggregates of SOD1 and more recently they have also been seen in SALS cases (Paré *et al.*, 2018). SOD1 is a disordered protein, meaning that the conformation of SOD1 is fairly flexible (Santamaria *et al.*, 2017). This disorder allows SOD1 to have a degree of flexibility in its structure, which may allow it to carry out different roles and bind to different targets. However, this flexibility, combined with mutations that interfere with metal ion binding, or formation of homodimers can cause SOD1 to misfold and aggregate. Oxidation of SOD1 can also lead to aggregation of SOD1 (Kabashi *et al.*, 2007). There is evidence that misfolded SOD1 can propagate misfolding of WT SOD1 and that these can spread in a prion-like fashion (Münch *et al.*, 2011). More recently it has been suggested that SOD1 trimers are

the cause of toxicity in ALS and that large aggregates of SOD1 are neuroprotective (Proctor *et al.*, 2016; Zhu *et al.*, 2018).

SOD1 aggregates can interact with membranes through the exposed hydrophobic surfaces of misfolded proteins. There has been evidence that SOD1 aggregates are localised to mitochondrial membranes in mouse models (Vande Velde *et al.*, 2008). Aggregates, especially oligomeric intermediates, are able to cause disruption to the mitochondrial membrane and release of mitochondrial enzymes, implementing SOD1 mutations to mitochondrial dysfunction in ALS (Salehi *et al.*, 2015).

1.2.2. TDP-43

The transactive response DNA binding protein 43kDa (TDP-43) protein, encoded by the *TARDBP* gene, was found to be a major component of motor neuronal cytoplasmic inclusions in ALS patients in 2006 (Arai *et al.*, 2006). Mutations in the *TARDBP* gene have also been identified and linked with familial and sporadic ALS. *TARDBP* mutations account for 4-5% of FALS and 1% of SALS (Millecamps *et al.*, 2010), although mutation of TDP-43 is not required for aggregation.

TDP-43 has a variety of roles within the cell mostly binding to RNA and DNA including involvement in transcription, RNA splicing and mRNA stability (Ederle and Dormann, 2017). TDP-43 depletion has been shown to change the transcription level of 601 mRNAs and alter the splicing of 965 mRNAs, showing the extent of the function of TDP-43 in the cell (Polymenidou *et al.*, 2011).

Aggregation of proteins leads to both loss of protein function and potential toxic-gain-of function. Aggregation of TDP-43 in the cytoplasm also recruits miRNAs due to the RNA binding nature of TDP-43, therefore reducing the activity of miRNAs as well as TDP-43 function, which leads to altered regulation of a large number of proteins (Zuo *et al.*, 2021).

Although the aggregation of TDP-43 in the cytoplasm of motor neurons and nuclear depletion of this protein are hallmarks of ALS, it may reflect the end stage of disease. This is shown in TDP-43 mouse models of ALS, where mice develop motor phenotypes with the lack of TDP-43

aggregation in neurons (Arnold *et al.*, 2013). The mechanism by which TDP-43 aggregation or TDP-43 mutation causes toxicity in ALS is still currently unknown.

1.2.3. FUS

Fused in Sarcoma (FUS) was found to be associated with ALS in 2009 when it was discovered as a component of protein inclusions in patients (Kwiatkowski *et al.*, 2009; Vance *et al.*, 2009). FUS mutations are found in approximately 3% of FALS and 0.4% of SALS patients (Zou *et al.*, 2017) as well as very occasionally in FTD patients. Mutations in FUS are clustered around the nuclear localisation signal (NLS), leading to mislocalisation of FUS in the cytoplasm (Kwiatkowski *et al.*, 2009; Vance *et al.*, 2009). There are currently over 50 FUS mutations associated with ALS (Deng *et al.*, 2014). The mutations in FUS tend to be associated with earlier onset ALS, with over 60% of FUS ALS patients displaying symptoms before 40 years of age (Shang and Huang, 2016).

FUS is a heterogeneous ribonucleoprotein (huRNP) and in normal physiological conditions FUS has many roles including mRNA translation, involvement in alternative splicing, mRNA transport, stress-granule formation and DNA repair (Ratti and Buratti, 2016). Some of these functions are similar to and overlap with the functions of TDP-43, however they bind to different RNA and protein targets. In ALS, mutations in FUS lead to mislocalisation of FUS to the cytoplasm and aggregation in a prion-like fashion (Deng *et al.*, 2014). This aggregation may be caused by the disruption of nuclear shuttling of the protein and due to the aggregation-prone nature of FUS. There is a discussion of whether ALS symptoms in FUS mutant patients are created through a toxic gain-of-function of the FUS aggregates or through loss-of-function of RNA regulation in the nucleus. Due to the large number of RNA targets and proteins that FUS is hypothesised to bind to and the large number of RNA processing steps that FUS is involved in (Ederle and Dormann, 2017), disruption of FUS function could lead to a change in a lot of different mRNAs, which can have a massive effect on neuronal activity.

1.2.4. C9ORF72

A hexanucleotide repeat (GGGGCC) expansion within the first intron of the chromosome 9 open reading frame 72 (*C9ORF72*) gene was found as a genetic cause of ALS and FTD in 2011 (Renton *et al.*, 2011). Previously, expansions or mutations in introns or regulatory regions of genes were commonly overlooked, however the expansion in *C9ORF72* is the most common

mutation found in ALS and FTD so far, accounting for 30-40% of familial cases and ~6% of sporadic cases, as well as accounting for 25% of FTD cases (Majounie *et al.*, 2012).

Healthy individuals usually have below 30 repeats, whereas patients with ALS or FTD can have upwards of 1000 hexanucleotide repeats (DeJesus-Hernandez *et al.*, 2011; Renton *et al.*, 2011), however there is not a precise cut-off that is widely accepted to determine if an individual will develop ALS or FTD. Determining the length of the C9ORF72 expansion in patients is difficult due to somatic instability meaning repeat sizes vary between tissues. For example, it has been found that DNA from blood can have fewer repeats than DNA isolated from the CNS, and repeat length can vary with brain region (Nordin *et al.*, 2015; van Blitterswijk *et al.*, 2013). Another issue with determining precise values for the number of repeats is the difficulty sequencing an intronic region that is so GC rich. It is not feasible to use PCR as some expansions may be too large to accurately measure the repeat size, so southern blotting is usually used. Using newer long-read sequencing technology, such as the nanopore developed by Oxford Nanopore Technologies, is making it easier and more accurate to detect these repeats (van der Ende *et al.*, 2021).

There are three current theories of how *C9ORF72* mutations may cause motor neuron injury: haploinsufficiency, RNA toxicity and toxic dipeptide repeats. There is evidence supporting all three of these mechanism as disease causing and it is possible that all of these mechanisms contribute to disease pathophysiology and the mechanisms may not being exclusive (Balendra and Isaacs, 2018). The evidence for haploinsufficiency includes defects in cellular mechanisms, where C9orf72 function has been associated with autophagy and has recently been shown to interact with RABA1 in the initial stages of autophagy (Webster *et al.*, 2016).

Toxic dipeptide repeats are formed from the repeat expansion as it can be transcribed in both the sense and antisense direction to form repeat RNA that can then be translated in all three reading frames into repeat dipeptide proteins through a process called repeat association non-ATG (RAN) translation (Zu *et al.*, 2013) leading to the formation of dipeptide repeat proteins (DPR). These DPRs consist of glycine-alanine (GA), glycine-arginine (GR), glycine-proline (GP), proline-arginine (PR) and proline-glycine (PG) species (Haeusler *et al.*, 2016). DPRs have been shown to be aggregation prone leading to varying levels of toxicity in drosophila models (West *et al.*, 2020), and longer repeat lengths giving more severe disease

phenotypes (Bennion Callister *et al.*, 2016). As well as forming toxic dipeptide repeats, the RNA from the RAN translation itself is also toxic and can form RNA foci that are neurotoxic and can bind to and sequester RNA binding proteins (Lee *et al.*, 2013). These RNA foci have been detected in the CNS of ALS patients (Cooper-Knock *et al.*, 2014).

1.2.5. Other genes associated with ALS

These genes discussed so far cover the genes that have the most common mutations linked to ALS patients. However, there are a large number of other genes that have been implicated in ALS or FTD that are mutated in a smaller percentage of patients (Table 1.1).

1.3. Mechanisms of ALS

ALS is a complicated disease with many mechanisms associated with motor neuronal death (Hardiman *et al.*, 2017). Many of the mechanisms are interlinked, and different mechanisms may be more prevalent in patients with different genetic mutations, further complicating the disease process.

1.3.1. Oxidative stress

ROS are highly reactive oxygen molecules that at low levels are important for activating various signalling pathways. However, ROS can cause damage to proteins, RNA and DNA and oxidative stress is described as the imbalance between production and removal of ROS, leading to increased levels of ROS and ROS damage in the cell. The oxygen requirements in the brain are higher than other organs, meaning the central nervous system (CNS) is at higher risk of oxidative damage.

There is evidence that oxidative stress biomarkers are increased in the blood and urine of SALS patients (Mitsumoto *et al.*, 2008), as well as evidence of oxidative damage to proteins in the spinal cords of post mortem ALS patients (Shaw *et al.*, 1995), suggesting oxidative stress is linked to ALS pathology.

ROS can come from within the cell or from external sources. The main source of internal ROS is the mitochondria as ROS are produced as electrons leak from the process of aerobic metabolism in the electron transport chain (Guo *et al.*, 2013). As well as being the major source of ROS, mitochondria are also more susceptible to damage by ROS, due to their

proximity to the source of ROS and the fact that mitochondrial DNA does not contain protective histones.

There are different mechanisms in place that have evolved to remove ROS from the cell to reduce the toxic effects. One of the mechanisms is SOD1, which converts superoxide radicals into molecular oxygen and hydrogen peroxide (Barber *et al.*, 2006). Another mechanism of protection is the activation of the NRF2 transcription factor, which activates a large number of proteins to help alleviate oxidative stress (Petri *et al.*, 2012).

Oxidative stress overlaps with many other mechanisms of neuron death, such as excitotoxicity, protein aggregation, ER stress and mitochondrial dysfunction (Ferraiuolo *et al.*, 2011). It has been shown that patients and $SOD1^{G93A}$ mice have increased mRNA oxidation, which is seen primarily in motor neurons and oligodendrocytes (Chang *et al.*, 2008). The oxidation of mRNAs was specific to mRNAs that encode proteins involved in known ALS mechanisms, such as mitochondrial electron transport, protein folding, neurofilament subunits and proteins that have previously been linked to FALS such as SOD1. Oxidative stress has also been linked to an early step in the aggregation of TDP-43 (Cohen *et al.*, 2015). Therefore, targeting oxidative stress could also alleviate other pathways that cause motor neuron death, therefore making it a good target for therapeutic intervention.

1.3.2. Mitochondrial dysfunction

Mitochondria play a major role in energy production within a cell, especially in neurons, which require large amounts of energy to function correctly. As well as their role in energy production, mitochondria have roles in calcium homeostasis, regulation of apoptosis and regulation of the cell cycle (McBride *et al.*, 2006). Therefore, dysregulation of mitochondria can have a large impact on many pathways within neurons which may lead to motor neuron death. Correct size, structure, distribution, and maintenance of mitochondria is required for motor neurons to function correctly and efficiently. Mitochondrial dysfunction is seen in many neurodegenerative diseases such as Alzheimer's disease (AD), Parkinson's disease (PD), Huntington's disease and ALS (Hroudová *et al.*, 2014).

Mitochondria are the main source of ROS inside cells, as they are produced as a by-product of energy production via the electron transport chain (Guo *et al.*, 2013). Mitochondria are also

particularly susceptible to ROS damage, probably due to their proximity to the production of ROS, and the resulting mitochondrial damage can lead to mitochondrial dysfunction, which can lead to overproduction of ROS in a feedback loop. Therefore, oxidative stress and mitochondrial dysfunction are highly linked mechanisms in ALS.

Calcium levels are tightly maintained in cells, as calcium is used for a range of signalling pathways, including apoptosis. Links between mitochondria defects and calcium homeostasis were seen in muscle fibres of $SOD1^{G93A}$ mice at the neuromuscular junction (NMJ) before symptom onset, suggesting a link between mitochondria dysfunction and excitotoxicity (Zhou *et al.*, 2010).

Disruption of the transport and distribution of mitochondria has also been implicated in ALS (De Vos *et al.*, 2007), with SOD1 and TDP-43 mouse models showing disruption of mitochondrial transport (Magrané *et al.*, 2014). Motor neurons may be particularly susceptible to this due to the large size and the length of the axons, as well as the requirement to move proteins, membrane bound vesicles and mitochondria along axons to axon terminals. Transport of mitochondria is carried out by the molecular motors kinesin, which moves towards the axon terminals (anterograde transport), and dynein, which moves towards the nucleus (retrograde transport). These molecular motors move mitochondria, and other cargoes, along microtubules. Dysregulation of this transport mechanism can cause mislocalisation of mitochondria throughout motor neurons and abnormal clusters of mitochondria have been shown in a $SOD1^{G93A}$ rat model (Sotelo-Silveira *et al.*, 2009).

1.3.3. Excitotoxicity

Glutamate signalling plays a major role in brain function, and glutamate is the main excitatory neurotransmitter in the CNS. However, overstimulation of glutamate receptors leads to excitotoxicity that can lead to cell death (Wang and Qin, 2010). Any disruption in the peak concentration of glutamate in the extrasynaptic space or an increase in the length of time that glutamate accumulates for can cause excitotoxicity as the signalling is dysfunctional and glutamate receptors can become over stimulated. Increased glutamate leads to abnormal activation of NMDA and AMPA receptors on neurons leading to calcium and sodium influxes and excitotoxicity in neurons. Excitotoxicity has been linked to a number of different neurological disorders, such as PD, AD, autism, epilepsy and ALS (Pajarillo *et al.*, 2019).

The cause of increased glutamate can be due to increased release of glutamate from the pre-synaptic neuron, reduced clearance of glutamate from the synaptic cleft or altered regulation of interneurons (Armada-Moreira *et al.*, 2020). AMPA receptors on motor neurons of ALS patients have a lower level of the subunit, GluA2, leading to selective vulnerability of motor neurons due to increased calcium permeability (Van Damme *et al.*, 2005).

Excess glutamate is cleared from the synapse by glial cells through the excitatory amino acid transporter (EAAT2) found mostly on astrocytes (Le Gall *et al.*, 2020). Alterations in EAAT2 activity through post-translational modifications have been implicated in ALS, as although there are no differences in *EAAT2* mRNA levels between ALS patients and controls, ALS patients showed a 95% decreased in EAAT2 protein levels (Bristol and Rothstein, 1996). In a mouse model of ALS, activating the translation of EAAT2 with a small molecule provided neuroprotection (Kong *et al.*, 2014).

Excitotoxicity is closely linked to other mechanisms of ALS pathology. The calcium ion influx caused by excitotoxicity can lead to mitochondrial dysfunction and increased ROS production leading to oxidative stress (Armada-Moreira *et al.*, 2020). It has also been shown that glutamate can activate JNK which phosphorylates kinesin motors and disrupts their binding to microtubules, therefore linking excitotoxicity with impaired axonal transport (Ackerley *et al.*, 2000).

1.3.4. Neuroinflammation

Activated astrocytes and microglia are hallmarks of ALS (Hall *et al.*, 1998). The combination of activated glial cells and infiltrating lymphocytes is termed neuroinflammation and causes complications in the CNS that can lead to motor neuron death. Neuroinflammation was initially seen as a product of motor neuron death but now is acknowledged as a mechanism that can contribute to motor neuron injury (Komine and Yamanaka, 2015).

Astrocytes and microglia have many important roles in the CNS as microglia monitor the environment and act as the innate immune system for the CNS and astrocytes have important functions in maintaining correct motor neuron function including clearance of glutamate from the synaptic cleft (Komine and Yamanaka, 2015). It has been shown that astrocytes from ALS

patients are toxic to neurons, suggesting that astrocyte dysfunction plays an important role in the death of motor neurons (Haidet-Phillips *et al.*, 2011). The level of microglial activity correlates with disease progression, suggesting that microgliosis is an important step in the death of motor neurons (Brettschneider *et al.*, 2012). Neuroinflammation is closely linked with oxidative stress as glial cells produce large amounts of ROS (Obrador *et al.*, 2020).

1.3.5. Protein and RNA aggregation

Nuclear inclusions of aggregated proteins are present in a range of different neurodegenerative diseases such as AD, PD and ALS (Eisele *et al.*, 2015). Protein aggregates in motor neurons are a hallmark of ALS. The major component of these inclusions is TDP-43, which is found in aggregates in the cytoplasm of around 97% of ALS patients (Prasad *et al.*, 2019). There are several mutations found in the *TARDBP* gene that are associated with ALS, however these mutations are not required in order for the protein to aggregate. The only cases of ALS without aggregation of TDP-43 are patients with *SOD1* or *FUS* mutations, however mutated SOD1 and FUS can also form aggregates with a different protein composition.

The process of protein aggregation comes from the misfolding of proteins that can bind together on the hydrophobic surfaces that become exposed. Some proteins are more prone to aggregation than others and TDP-43 is an aggregation prone protein due to its C terminal domain. Mechanisms that cause aggregation include mutations in proteins and dysregulation of molecular chaperone pathways (Malik and Wiedau, 2020).

Transcription of the C9orf72 repeat expansion can lead to aggregation of RNA binding proteins to the RNA foci (Lee *et al.*, 2013). TDP-43 in aggregates also causes accumulations of miRNAs as TDP-43 is an RNA binding protein. The lack of function of the RNA binding proteins and miRNAs due to their accumulation in aggregates leads to increased levels of certain proteins and decreased levels of others due to lack of appropriate regulation of mRNAs (Zuo *et al.*, 2021).

TDP-43 aggregation has been shown to alter a number of mitochondrial function genes through the sequestering and therefore reduced ability of miRNAs, leading to mitochondrial dysfunction and potential ROS induction (Zuo *et al.*, 2021). This links protein aggregation with oxidative stress and mitochondrial dysfunction.

1.3.6. ER stress

The endoplasmic reticulum (ER) plays major roles in the correct folding, post-translational modification and targeted transport of new proteins, as well as having roles in calcium homeostasis. Loss of correct functioning of the ER can lead to ER stress. ER stress, caused by altered calcium signalling or accumulation of misfolded proteins, leads to upregulation of the unfolded protein response pathways including an increase in ER chaperones, but can eventually lead to autophagy if the stress is not dealt with sufficiently (Rao *et al.*, 2004).

A number of other ALS mechanisms are linked to ER stress such as protein aggregation, dysfunctional axonal transport, ER degradation and changes in autophagy (Matus *et al.*, 2013). The ER functions in close proximity with mitochondria and correct signalling between them is vital for correct function and morphology of both organelles (Dafinca *et al.*, 2021), suggesting a connection between mitochondrial dysfunction and ER stress.

1.3.7. Dysregulation of axonal transport

Neurons are large cells, where axons can be up to 1m in length, and transport of different cargoes is vital for correct functioning. There is a link between mutations in genes associated with axonal transport and ALS, such as *TUBA4A* and *PFN1* (Smith *et al.*, 2014; Wu *et al.*, 2012), suggesting that impaired axonal transport is a mechanism involved in the process of ALS. Mutations that can cause dysregulation of axonal transport include disruption to microtubules, changes to microtubule architecture or disruption of motor proteins (De Vos and Hafezparast, 2017).

As mentioned previously, axonal defects can affect the distribution and transport of mitochondria, leading to defects in energy production and calcium buffering (section 1.3.2). However, transport and localisation of many other cargoes is also vital to the correct functioning of neurons. These cargoes include membrane bound vesicles, organelles, DNA and protein. Due to the transport of so many cargoes, a defect in axonal transport can also affect protein degradation pathways and RNA distribution (Le Gall *et al.*, 2020).

1.3.8. Dysregulated RNA processing

TDP-43 and FUS are RNA binding proteins that have many different targets and perform roles in RNA processing and transport (Sephton *et al.*, 2011; Tollervey *et al.*, 2011). Mutations within genes of RNA binding proteins in ALS patients showed that dysregulation of RNA metabolism is involved in ALS. Loss of function of these proteins due to their involvement in protein aggregates has the potential to alter the expression of a large number of genes and proteins.

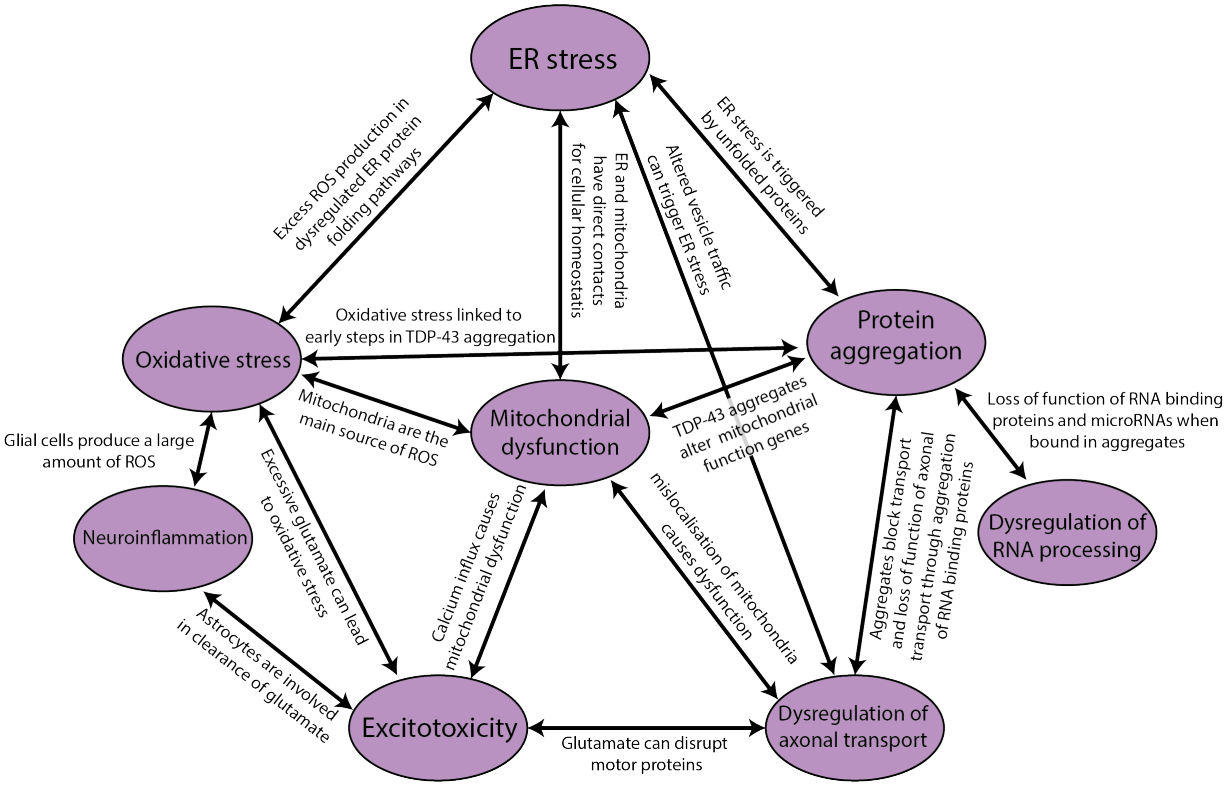

Figure 1.1: The interconnected mechanisms of ALS showing examples of how the mechanisms can impact each other.

The mechanisms involved in ALS are formed of a complex network of pathways that interact and influence each other (Figure 1.1). It can be difficult to determine which of the mechanisms cause disease, and which of the mechanisms are a result of dysfunctions in the cell.

1.4. Mouse models of ALS

Mouse models of ALS have been created based on different mutations found in genes linked to ALS. Mouse models offer the benefit of looking at tissue from the central nervous system at differing time points throughout the disease, therefore allowing a more in depth understanding of disease pathophysiology and discovery of new mechanisms. This is a limitation of humans, as differences in tissue can only be investigated at the end point of disease and therefore the mechanisms that lead to the loss of motor neurons can be hard to determine. Animal models also allow for the testing of potential therapeutics to see if they can impact on the progression of the disease.

1.4.1. SOD1

The first mouse model was created in 1994 following the finding that mutations in the *SOD1* gene were linked to FALS. In this model, human *SOD1* (hSOD1) with a clinically relevant substitution of a glycine residue for an alanine residue at position 93 (G93A), was overexpressed in transgenic mice (Gurney *et al.*, 1994). Mice with this transgene develop MND-like symptoms beginning with signs of hind limb weakness at 3-4 months of age, then paralysis as a result of loss of motor neurons in the spinal cord (Gurney *et al.*, 1994). Severity and age of onset were found to be correlated with the level of transgene expression, with mice expressing higher amounts of hSOD1 protein showing a more rapid progression of disease (Chiu *et al.*, 1995).

The $SOD1^{G93A}$ model relies heavily on an overexpression of a mutant form of *SOD1* where the expression level is 17 times the endogenous levels of mouse *Sod1* (Jonsson *et al.*, 2006). However, overexpression of wild type human *SOD1* also causes disease (Jaarsma *et al.*, 2000). Knock-in models of disease may more closely mimic human disease as they are driven by endogenous promoters to give physiological expression of the gene of interest. A knock-in model has been created by inducing a point mutation in the endogenous mouse *Sod1* gene ($SOD1^{D83G}$), a mutation found in a small number of MND patients (Joyce *et al.*, 2014). Mice homozygous for this mutation display loss of upper and lower motor neurons as well as a progressive motor phenotype similar to the $SOD1^{G93A}$ model (Joyce *et al.*, 2014). As these mice develop a motor phenotype at endogenous expression levels, this suggests that mutations in *SOD1* contribute to disease and not just overexpression of the protein. Heterozygous

$SOD1^{D83G}$ mice don't show motor neuron loss or a neurodegenerative phenotype, which could be due to a protective effect of WT SOD1 (Joyce *et al.*, 2014).

So far there has been a huge reliance on this original $SOD1^{G93A}$ model of ALS, and this model is the most extensively used for preclinical testing as it is the most commonly used mouse model for ALS (Ittner *et al.*, 2015).

The $SOD1^{G93A}$ mouse model that I used in this project is from the original Gurney model that has been back crossed onto a C57BL/6J OlaHsd background and has been extensively characterised and shown to produce robust and minimally variable results (Mead *et al.*, 2011). These mice develop progressive motor symptoms that can be tracked throughout the disease through a variety of behavioural tests that have been proven to show differences between wild-type and transgenic mice. The progression leads to progressive paralysis and an end-stage at around 140 days of age, however studies can be carried out to 90 days of age to reduce the suffering for the animals and still collect robust data on disease progression (Mead *et al.*, 2011) (Figure 1.2).

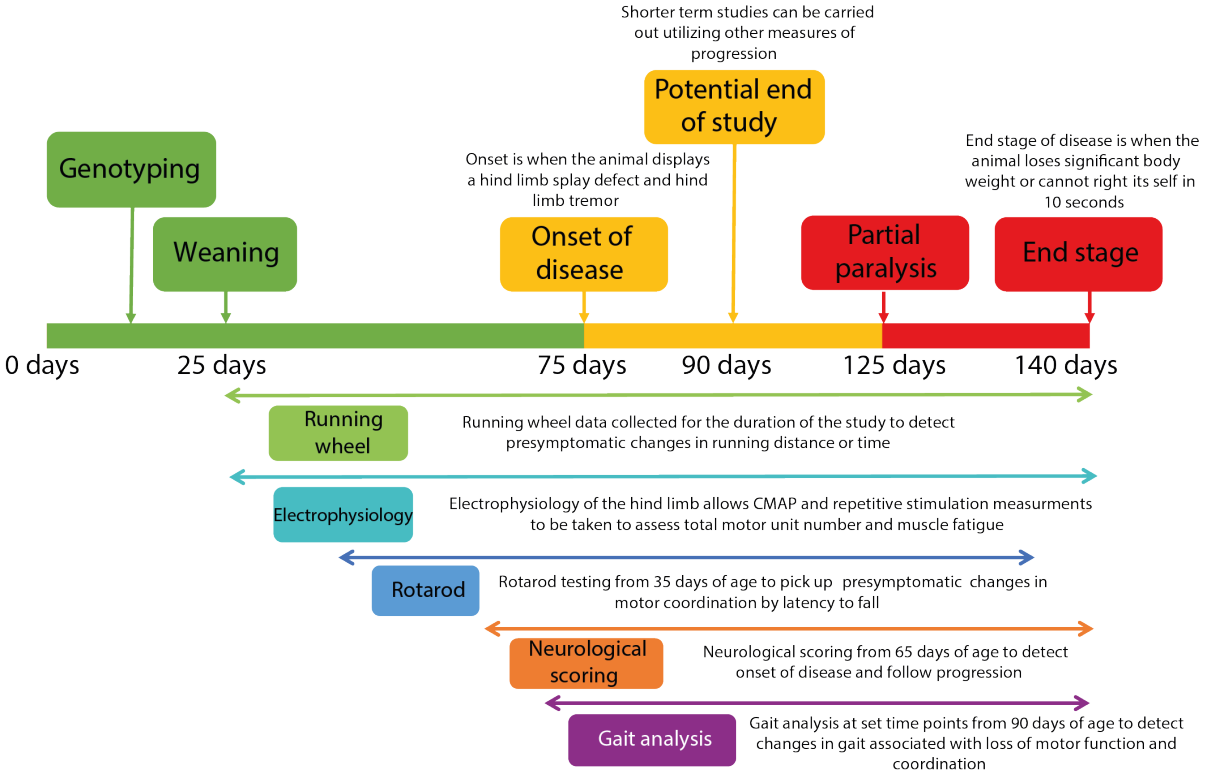

Figure 1.2: Disease course of SOD1^{G93A} C57BL/6 mice used in this thesis with major timepoints and timings of behavioural analysis. Animals are genotyped from 2 weeks of age. They are then weaned and recruited onto studies at 25 days of age. For dosing studies, dosing starts at 25 days of age and dosing regimens may differ. Onset of visible signs of disease is around 75 days of age and is determined through neuroscoring, which is carried out three times a week from 60 days of age. At 125 days of age the mice enter the substantial stage of the disease where the paralysis becomes progressively worse and end stage is around 140 days of age, which is determined by significant weight loss or a righting reflex of greater than 10 seconds. At 90 days of age there are significant changes in tissue samples and behavioural parameters between wild type and transgenic mice, meaning that there is potential for shorter studies that limit the substantial distress to the animals while still gaining robust data. Behavioural tests such as running wheel analysis, neurological scoring, gait analysis and electrophysiological analysis are carried out at multiple time points throughout the disease course that have previously shown to have significant differences between transgenic and wild type animals.

Although the mouse models of ALS have been extremely useful for understanding of the disease and for testing compounds, there is some controversy surrounding them due to the lack of translation between mouse models and patients in clinical trials. There have been over 50 publications since 1994 showing beneficial effects of compounds in the mouse model,

despite only one new treatment being approved for use by the FDA (Scott *et al.*, 2008). The positive effects described in the mouse model can lead to clinical trials being conducted, and it has been shown that 78% of negative clinical trials carried out between 2004 and 2014 were said to have been pursued following positive data in a mouse model of ALS (Mitsumoto *et al.*, 2014).

There are many factors that have led to this lack of translation between mice and humans, such as poor pre-clinical design using the mouse model (Scott *et al.*, 2008), mutations on differing background strains of mice (Heiman-Patterson *et al.*, 2011), publication bias (Benatar, 2007) or dose selection within clinical trials. Many of these have been addressed through regulations to improve pre-clinical mouse designs (Ludolph *et al.*, 2010), better characterisation of mouse models on more robust backgrounds (Mead *et al.*, 2011), increasing the number of mouse models and better design of clinical trials.

1.4.2. TDP-43

Since the discovery of TDP-43 mutations in ALS and the large proportion of patients with TDP-43 aggregates, there have been several transgenic and knock-in mouse models created based on *TARDBP* mutations. These models each lead to differing lengths of disease course and phenotypes (Joyce *et al.*, 2014; Stephenson and Amor, 2017).

Overexpression of wild type or mutant TDP-43 in mouse models causes a disease phenotype (Xu *et al.*, 2011, 2010). This could be due to overexpression of TDP-43 causing altered expression of many genes involved in mitochondrial function and axonal transport function.

A mouse model of human TDP-43^{A315T} under a mouse prion promoter has been created and characterized. However, alongside slight motor phenotypes, mice died prematurely due to severe gastrointestinal pathology (Esmaeili *et al.*, 2013; Hatzipetros *et al.*, 2014). Although these gastrointestinal effects can be reduced through feeding the mice a liquified diet (Herdewyn *et al.*, 2014), this side effect reduces the usefulness of this particular mouse model.

In a mouse model containing a knock-in of a mutated human TDP-43^{Q331K}, cognitive impairments were detected in animals similar to a FTD phenotype (White *et al.*, 2019). This is interesting as half of all FTD patients as well as 97% of ALS patients have TDP-43 inclusions

and there is significant disease overlap between the two. Therefore, having an animal model that can show signs of motor loss as well as cognitive impairment will be extremely useful when exploring different mechanisms of disease and in the development of new therapies. It may also be more representative of ALS patients than the SOD1 model, which may only represent a small subset (approximately 2%) of patients.

The mouse model used in this thesis is the transgenic TDP-43^{Q331K} mouse model that was originally created by Arnold *et al*. on a C57BL/6Ncrl background (Arnold *et al.*, 2013). This model was chosen due to the minimal overexpression of TDP-43. The mice showed progressive ALS phenotypes and significant loss of motor neuron at 10 months of age (Arnold *et al.*, 2013). These mice were then backcrossed onto a C57BL/6NJ model and have been extensively characterised in house (Watkins *et al.*, 2021). These animals show a less severe disease phenotype than the SOD1^{G93A} model described previously and have no end point based on ALS disease symptoms such as paralysis. Instead they show a progressive development of ALS phenotypes such as muscle mass loss, reduced performance on rotarod, unstable gait, tremor and also significant weight gain, which could be a symptom of an FTD-like phenotype (Watkins *et al.*, 2021). Statistical analysis on previous data showed that there is a significant difference between wild type and transgenic mice in a variety of behavioural parameters and tissue pathology at 6 months of age (Figure 1.3).

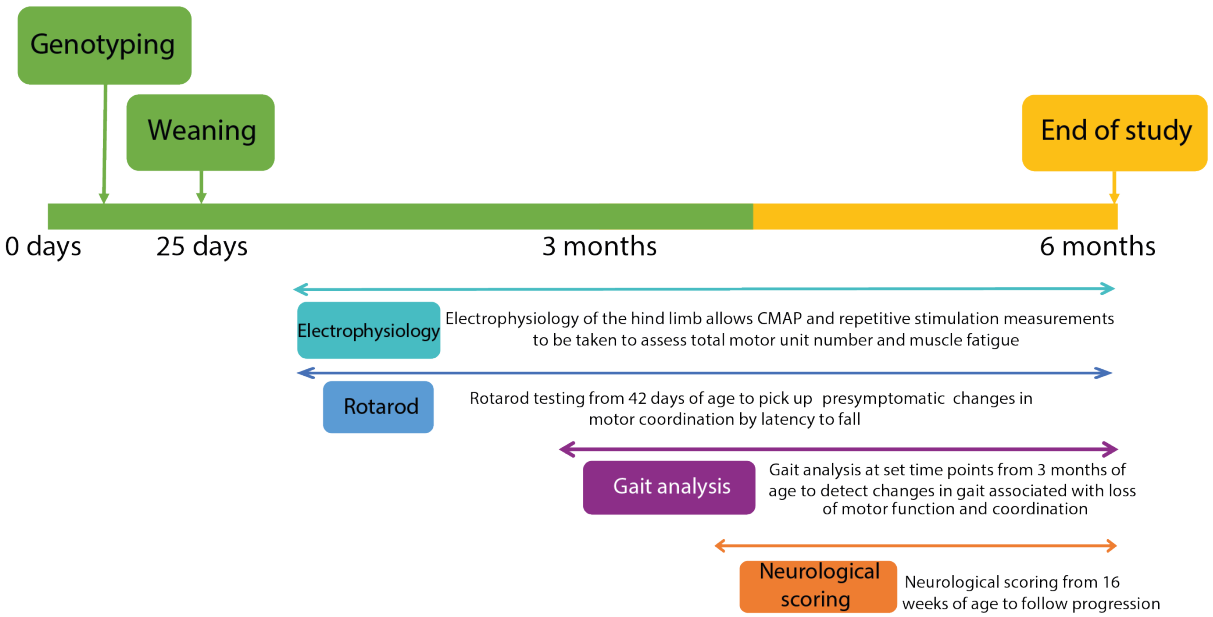

Figure 1.3: Disease course of TDP-43^{Q331K} C57BL/6NJ mouse model showing major timepoints and windows for behavioural analysis. Mice are genotyped from 2 weeks of age then weaned and recruited onto studies at 25 days of age. Behavioural tests are carried out at various timepoints throughout the progression of disease, based on timepoints where differences have been observed previously between wild type and transgenic mice. The end of the study is set at 6 months of age as these animals do not reach an end stage.

1.4.3. C9ORF72

Until recently, none of the *C9ORF72* knockout mouse models showed any ALS phenotype and no models have shown loss of motor neurons, suggesting that the loss of function of C9ORF72 has very little impact on disease progression (Balendra and Isaacs, 2018). Part of the difficulty of creating a C9ORF72 mouse model is the large expansion within the gene, making it difficult to insert into the mouse genome and difficult to genotype to ensure the gene expansion remains over generations.

In 2016 a C9ORF72 bacterial artificial chromosome (BAC) transgenic mouse model was created that contains the full-length human *C9ORF72* gene and large amounts of flanking sequence in an attempt to incorporate all endogenous aspects of gene regulation (Liu *et al.*, 2016). These mice show decreased survival, gait abnormalities, paralysis and pathology linked to both ALS and FTD. They also found significant denervation of neuromuscular junctions in the symptomatic mice (Liu *et al.*, 2016). An interesting finding from this mouse model was the variability in disease progression of mice, with some mice developing severe disease and

death within one year, while other mice developed mild symptoms, despite all carrying the mutated *C9ORF72* gene. Although this would be difficult to address if carrying out studies for potential therapeutics, the variability resembles some of the variability seen within patients and therefore could be a better model for ALS.

Once the Liu *et al.* C9ORF72 model had been shared with the wider research community, other researchers were unable to replicate the phenotypes previously reported. Mordes et al. investigated two cohorts of the C9ORF72 BAC mice at two separate institutes and although they were able to confirm that the mice expressed the correct number of hexanucleotide repeats, they were unable to detect any phenotype that distinguished the transgenic mice from NT litter mates and found no evidence of neurodegeneration or neuroinflammation (Mordes *et al.*, 2020).

Mordes *et al.* suggest several reasons for the disparity in the phenotype seen by the different groups. These reasons include the FVB/N background strain originally used, as FVB/N mice have been shown to be susceptible to seizure behaviour (Goelz *et al.*, 1998), which is potentially similar to the phenotype described for the transgenic mice. This could be possible as there is a percentage of WT mice in the original study that showed a phenotype or died before 1 year of age (Liu *et al.*, 2016). Another potential reason for the difference is that the original analysis split the mice into symptomatic vs asymptomatic groups, whereas the analysis of the Mordes et al. was carried out on all transgenic mice vs wild type. Differences in micro-organisms in different laboratories may also play a role in the phenotype differences seen, and this has been previously seen in another C9ORF72 model (Burberry *et al.*, 2020).

At the same time as the Mordes *et al.* study was published, the original team also published an article highlighting differences between analysis methods and included more data showing that their model showed a phenotype in the original laboratory and another location (Nguyen *et al.*, 2020). The debate is currently ongoing, but highlights the points made earlier about good design of *in vivo* studies and the need for careful characterisation of models.

No animal model will ever be the perfect representation of human ALS, especially in a disease which is so diverse with many mechanisms contributing to the progression of the disease.

However, using multiple relevant animal models can be useful in providing insight into the progression of the disease or the impact of potential therapeutics.

1.5. NRF2-ARE pathway

1.5.1. NRF2

Nuclear factor erythroid 1-like 2 (NRF2) is a transcription factor that belongs to the Cap N' Collar (CNC) subfamily of basic leucine zipper (bZIP) proteins (Suzuki and Yamamoto, 2015). NRF2 is a master regulator of antioxidant response within the cell and activates the expression of over 1000 genes with cytoprotective properties (Kopacz *et al.*, 2020). In the nucleus, NRF2 forms heterodimers with small muscle aponeurosis fibromatosis (sMAF) proteins and recruits binding cofactor CREB-binding protein (CBP), allowing it to bind to antioxidant response elements (AREs) in the enhancer regions of a wide range of genes with anti-inflammatory, anti-oxidant and detoxification properties, increasing their transcription (Itoh *et al.*, 1997; Katoh *et al.*, 2001).

The NRF2 protein is 605 amino acids long in humans and contain seven NRF2-ECH homology (Neh) domains (Canning *et al.*, 2015), which are highly conserved across vertebrates (Fuse and Kobayashi, 2017) (Figure 1.4). At the N terminus, the Neh2 domain contains DLG and ETGE motifs that bind to the C terminal kelch domain of KEAP1 (Tong *et al.*, 2006).

The Neh4 and Neh5 domains located after the Neh2 domain at the N terminal are transactivating domains that recruit CBP (Katoh *et al.*, 2001). Neh3 at the C terminus is also a transactivating domain that recruits machinery for transcription. The Neh7 and Neh6 domains are involved in other methods of KEAP1-independent negative regulation of NRF2 (discussed later) (Cuadrado, 2015; H. Wang *et al.*, 2013). The Neh1 domain contains the CNC bZip and is responsible for the binding of NRF2 to sMAFs and DNA, it also contains the nuclear import and nuclear export signals (Figure 1.4).

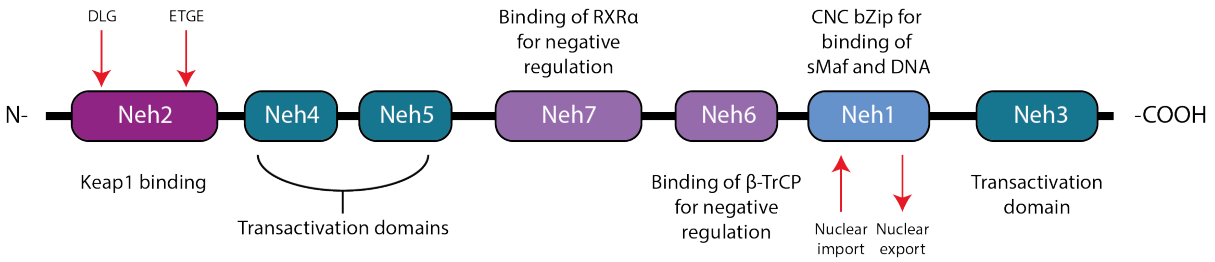

Figure 1.4: Domain structure of NRF2. NRF2 is 605 amino acids long in humans and comprises of 7 NRF2-ECH homology (Neh) domains. The Neh2 domain at the N terminal is responsible for the binding of KEAP1 through two distinct motifs. The Neh4, Neh5 and Neh3 domains are transactivation domains. Neh7 is responsible for the binding of RXRα and therefore negative regulation of NRF2. Neh6 domain is also used for negative regulation due to ß-TrCP binding. The Neh1 domain contains the nuclear export and import signals and also binds to DNA and sMaf proteins.

The activity of NRF2 is tightly controlled as disrupted NRF2 activity is found in multiple diseases, such as cancer and neurodegenerative diseases (Bono *et al.*, 2021; Jung *et al.*, 2018). Constitutive activation of NRF2 has been shown to lead to overexpression of cytoprotective enzymes and death postnatally (Wakabayashi *et al.*, 2003) and conversely, *NRF2* null mice are more susceptible to stressors due to the lack of antioxidant response (Suzuki and Yamamoto, 2015). This shows that over or under expression of NRF2 levels can be detrimental to cells and that tight regulation of NRF2 activity is required for correct functioning. Many mechanisms are involved in the regulation of NRF2, and these mechanisms work together to fine tune the levels of NRF2 to meet the requirements of the cell. NRF2 as a protein has a short half-life of around 20 minutes (Kobayashi *et al.*, 2004) and the majority of regulation occurs at the protein level, so that the response to cellular stress can be quickly activated.

1.5.2. NRF2 regulation by KEAP1

The main regulator of NRF2 activity is the adaptor protein Kelch-like ECH-associated protein 1 (KEAP1) and associated ubiquitin E3 ligase, Cullin 3 (CUL3). KEAP1 is part of the BTB-Kelch family of proteins and is made of three functional domains (Figure 1.5). At the N terminal is a broad complex/ tramtrack/ bric a brac (BTB) domain that is responsible for the dimerization and formation of the homodimer of KEAP1 as well as having a role in binding CUL3 (Cullinan *et al.*, 2004). At the C terminal is a Kelch/double glycine repeat (DGR) domain that contains the binding sites for NRF2. The Kelch domain consists of 6 Kelch repeats that form a β-

propeller (Li *et al.*, 2004) and, surprisingly, this structure can bind both of the motifs on NRF2 despite their very different structures (Tong *et al.*, 2006). The domain connecting the BTB and Kelch domain is the intervening region (IVR), which is responsible for the interaction with CUL3 and is cysteine rich (Kobayashi *et al.*, 2004).

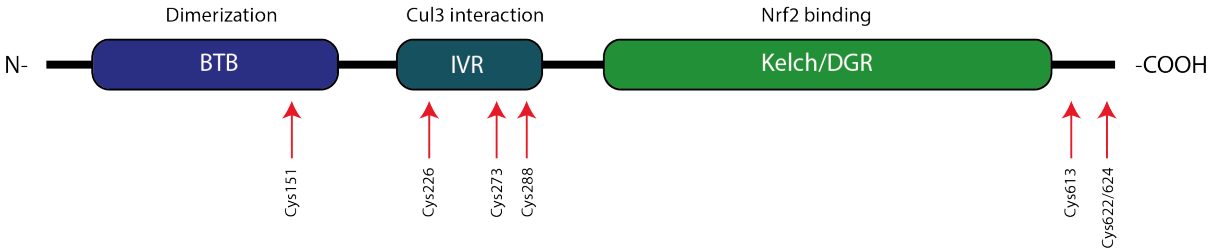

Figure 1.5: Structure of KEAP1 showing the main domains and the locations of the cysteine residues that are altered to regulate NRF2 activity.

Under basal conditions, homodimers of KEAP1 bind NRF2 in the cytoplasm allowing CUL3 to target NRF2 for proteasomal degradation through ubiquitination leading to low levels of NRF2 within the cell. Under oxidative stress, or in response to electrophiles, KEAP1 activity is reduced, leading to reduced degradation of NRF2 and therefore an increase in NRF2 concentration in the cell (Keum and Choi, 2014).

NRF2 binds to KEAP1 through two distinct motifs: DLG and ETGE. Using these motifs, one molecule of NRF2 binds to two Kelch domains on a homodimer of KEAP1 (Tong *et al.*, 2006). The ETGE motif binds to KEAP1 with higher affinity than the DLG motif, which was found using nuclear magnetic resonance (NMR) and isothermal calorimetry (ITC) methods (Tong *et al.*, 2006). This has led to the hinge and latch theory of NRF2/KEAP1 binding, in which KEAP1 recognises and binds to the higher affinity ETGE motif first, followed by the lower affinity DLG motif. The DLG motif is important in correctly orientating NRF2 to be ubiquitinated, as shown by various mutations within this motif which lower the rate of ubiquitination of NRF2 (Tong *et al.*, 2007). Under oxidative conditions or in the presence of electrophiles, a conformational change within the KEAP1 homodimers releases the DLG motif, whilst the ETGE motif remains bound to KEAP1, therefore NRF2 cannot be ubiquitinated as it is not in the correct orientation. This leads to an increase in newly synthesised NRF2 as it is not degraded and cannot bind to KEAP1.

KEAP1 has the ability to sense oxidative stress through a number of conserved cysteine residues found throughout the protein. Human KEAP1 contains 27 cysteine residues and mouse KEAP1 contains 25 (Dinkova-Kostova *et al.*, 2017). Modification of one of the most reactive cysteine molecules (Cys151) has been shown to cause a conformational change within KEAP1 that leads to the dislocation of CUL3 from the complex, meaning that NRF2 cannot be ubiquitinated (Rachakonda *et al.*, 2008). This may not be how all of the cysteine molecules carry out their function, but any conformation of KEAP1 that moves the orientation of NRF2, such as causing dissociation of the DLG motif, has the potential to block the ubiquitination of the protein.

Many studies have been carried out using various techniques such as site-directed mutagenesis to determine which of the cysteine residues are the most important altering the function of KEAP1 (Sekhar *et al.*, 2009). The cysteine residues that are best characterised and shown to be involved in regulation of NRF2 activity are Cys151, Cys273 and Cys288 (Saito *et al.*, 2015). Electrophiles are molecules that can alter the cysteine residues on KEAP1 (and various other proteins with similar reactive cysteines) and therefore increase NRF2 expression in a similar way to how oxidative stress activates NRF2. However, it has been shown that different electrophiles can react with different cysteines on KEAP1 (Holland *et al.*, 2008; Kobayashi *et al.*, 2009), meaning that there is not one cysteine that regulates the function of KEAP1, but rather a cysteine-code that is created with different molecules having different cysteine signatures on KEAP1. NRF2 activators can be divided into classes based on the cysteine residues that they interact with (Baird and Yamamoto, 2020).

1.5.3. Other mechanisms of NRF2 regulation

Although the KEAP1 mechanism of NRF2 regulation is arguably the most understood regulation mechanism, there are other mechanisms that regulate NRF2 levels and the transcription of downstream targets (Figure 1.6). Some KEAP1-independent methods of regulation involve direct regulation of NRF2. One of these methods is via the beta-transducin repeat containing protein (β-TrCP), an E3 ubiquitin ligase adaptor which binds to the Neh6 domain of NRF2 leading to ubiquitination and degradation of NRF2 (Cuadrado, 2015). This was originally found using mutant NRF2 proteins that lacked the Neh2 domain, which showed lack of binding with KEAP1 but were still degraded in a ubiquitin based manner, although with a longer half-life than NRF2 proteins containing the Neh2 domain (McMahon *et al.*, 2004). This

interaction is regulated by glycogen synthase kinase 3β (GSK-3β), which phosphorylates serine residues within the Neh6 domain therefore allowing β-TrCP to bind and target NRF2 for degradation (Rada *et al.*, 2011). The interaction of GSK-3β and NRF2 has been shown in neuronal cell models, where GSK-3β inhibitors have shown to increase levels of NRF2 and downstream targets of the NRF2 pathway following oxygen and glucose deprivation to cells (Chen *et al.*, 2016). It has been proposed that the KEAP1 and β-TrCP NRF2 degradation mechanisms work together to fine tune the NRF2 levels (Rada *et al.*, 2011).

Another KEAP1-independent method of regulation of NRF2 has been found by Wang *et al.*. Retinoid X receptor alpha (RXRα) overexpression in cells shows suppression of ARE related genes in a KEAP1-independent manner (H. Wang *et al.*, 2013). RXRα has since been shown to bind to the Neh7 domain of NRF2 through a series of binding experiments with truncated NRF2 proteins. Interestingly, the binding of RXRα and NRF2 still leads to binding of AREs, however transcription of genes is repressed (H. Wang *et al.*, 2013). This is hypothesized to be due to RXRα blocking the cofactor CBP binding to NRF2 (Namani *et al.*, 2014).

As well as the direct methods of NRF2 regulation, there are a few indirect methods. One indirect method of regulation of ARE gene expression is through the competition of NRF2 with another CNC family protein, BACH1. BACH1 forms heterodimers with sMAFs and binds to MAF recognition elements (MAREs) in the promoter region of NRF2 target genes (Oyake *et al.*, 1996), however BACH1 represses the transcription of a typical ARE regulated gene, heme oxygenase-1 (Dhakshinamoorthy *et al.*, 2005).

P62 is a key component of autophagy and regulates the formation of protein aggregates (Komatsu *et al.*, 2010). P62 can bind to KEAP1 in a similar way to the ETGE and DLG binding of NRF2 to KEAP1 in the kelch domain. P62 therefore competes for binding with NRF2 to KEAP1, and an increase in P62 can cause an increase in NRF2 activity (Komatsu *et al.*, 2010). P62 has also been shown to sequester KEAP1 into protein aggregates in the cytoplasm, again stabilizing NRF2 and increasing NRF2 activity (Lau *et al.*, 2010).

Because of these various mechanisms that have evolved to regulate NRF2 levels, correct regulation of NRF2 is important within cells. Dysregulation of NRF2 is associated with various diseases including cancer, cardiovascular disease and a number of neurodegenerative

diseases, including ALS. These differing mechanisms of NRF2 regulation have possibly evolved to accurately adjust or fine tune NRF2 activity within cells depending on many different environments and conditions.

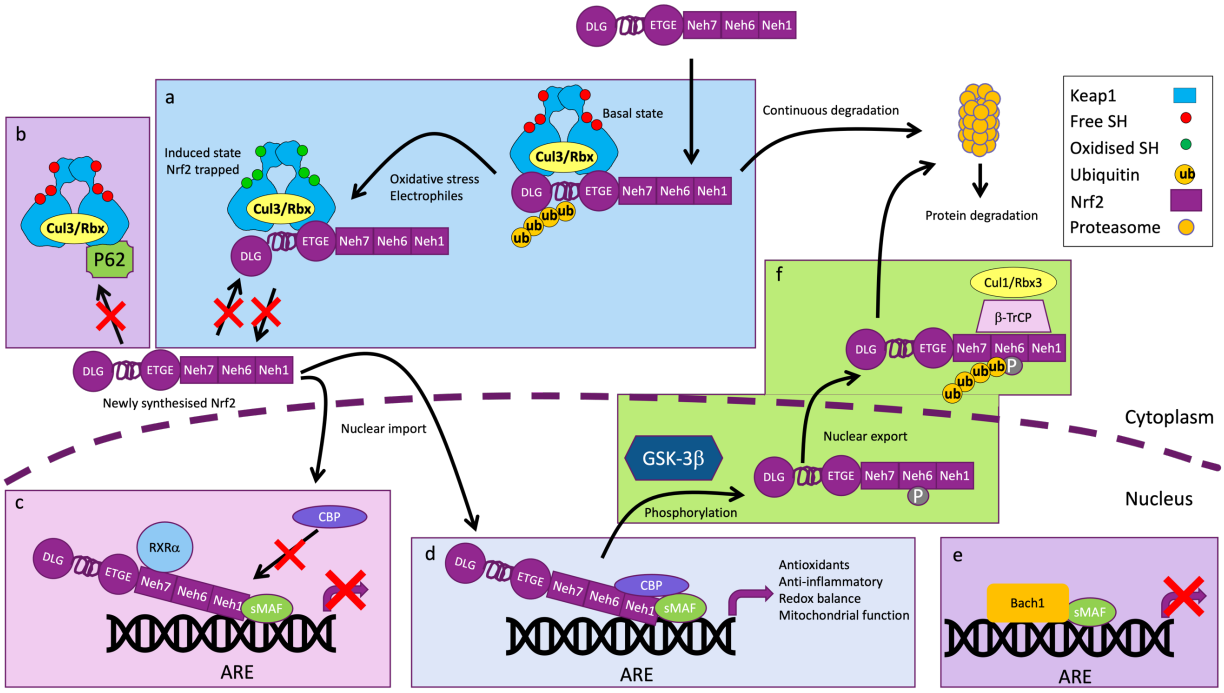

Figure 1.6: Regulation mechanisms for NRF2. NRF2 has various methods of regulation A) KEAP1 homodimers binds to two motifs within the Neh2 domain of NRF2. In basal conditions KEAP1 binds to NRF2 and leads to its ubiquitination and continuous degradation via the proteasome. Under oxidative stress or in response to electrophiles, cysteine residues are modified on KEAP1, inactivating the E3 ubiquitin ligase activity and trapping NRF2 on KEAP1. This leads to the increase in newly synthesised NRF2. B) P62 is a competitive inhibitor and binds to the kelch domain of KEAP1 stopping NRF2 from binding and being degraded, therefore increasing NRF2 levels. D) Once inside the nucleus NRF2 forms heterodimers with sMAFs and binds to ARE in the enhancer regions of target genes. Cofactors such as CBP are also recruited to allow transcription of genes. C) RXRα can bind to the Neh7 domain of Nrf2 and stop transcription of ARE regulated genes by blocking the recruitment of CBP. E) BACH1 is from the same CNC family as NRF2 and forms heterodimers with sMAFs, binding to ARE and stopping transcription of ARE regulated genes. This method of regulation relies on the competition between BACH1 and NRF2 for binding to sMAF and ARE binding sites. F) GSK-3β phosphorylates the Neh6 domain of NRF2, allowing the binding of E3 ubiquitin ligase adaptor β-TrCP, ubiquitination of NRF2 and protein degradation.

1.5.4. NRF2 in ALS

The NRF2 pathway has been shown to be dysregulated in patients as well as cellular and animal models of ALS. Kirby *et al.* showed that NRF2 and its downstream targets were decreased in a NSC32 cellular model of ALS (Kirby *et al.*, 2005). A similar trend was seen in ALS patient post mortem samples, with NRF2 mRNA and protein levels being lower in patients compared to control and *KEAP1* mRNA levels increased in the motor cortex (Sarlette *et al.*, 2008). Whereas animal models, although showing changes in NRF2 levels, have an increase of NRF2 protein in the nucleus and cytoplasm of MNs and glial cells of $SOD1^{G93A}$ mice from 10 weeks of age (Mimoto *et al.*, 2012). The transgenic mice also show increased levels of stress response proteins such as HMOX1 and glutathione in glial cells when compared to wild type controls. In this study there were differences seen in protein levels between MNs and glial cells, suggesting that different populations of cells may respond in distinctive ways in response to stress stimulus.

More recently, RNA binding proteins have been implemented in the regulation of the NRF2 pathway. RBM45 is an RNA binding protein that is shown to have increased expression in ALS patients and stabilizes KEAP1, therefore decreasing the levels of NRF2 (Bakkar *et al.*, 2015). Another RNA binding protein, hnRNP K, aids with translation of NRF2 transcripts, however TDP-43 mutants affect the localisation of hnRNP K therefore leading to a reduction in translation of NRF2 transcripts (Moujalled *et al.*, 2017).

1.5.5. Activators of Nrf2

Oxidative stress has been shown as a major component of ALS pathology (Barber *et al.*, 2006). Whether oxidative stress is a cause or consequence of ALS pathology is currently unknown, however it is shown that decreasing oxidative stress in ALS models is effective at reducing ALS effects. The interlocking network of the different mechanisms of ALS shows that the interaction between pathways is complex. The NRF2 pathway can activate pathways that are able to affect many of these mechanisms. This together with the NRF2 dysregulation seen in ALS, suggests that elevating levels of NRF2 in cells could be beneficial to alleviate oxidative stress, through the activation of antioxidant pathways downstream of NRF2 signalling and therefore decreasing ALS symptoms. $SOD1^{G93A}$ mice were crossed with mice overexpressing NRF2 in astrocytes and mice with both mutations showed an improvement of disease (Vargas

et al., 2008). This suggested that increasing expression of NRF2 could relieve effects of neurodegeneration and potentially benefit patients with ALS.

As well as increasing the transcription of antioxidant genes, NRF2 also increases the transcription of genes involved in anti-inflammatory pathways, mitochondrial function, and autophagy, which have all shown to be involved in ALS pathology (Ferraiuolo *et al.*, 2011). So far targeting just one pathway or mechanism of ALS has been mostly unsuccessful, with many drugs that go into clinical trial having limited effects in patients, despite positive effects in cellular and animal models. Therefore, by activating NRF2 and therefore targeting multiple mechanisms of ALS at once, there may be a potential to slow progression of disease in ALS.

Many NRF2 activators have been explored for the treatment of neurodegenerative diseases, such as ALS, as well as other diseases that are centred around oxidative stress. The most explored NRF2 activators are electrophiles, that exert their function by reducing the activity of KEAP1 by modifying cysteine residues used for detecting oxidative stress, leading to upregulation of NRF2 target genes (He and Ma, 2009).

Dimethyl fumarate (DMF), derived from fumaric acid, is rapidly converted into monomethyl fumarate (MMF) in the gastrointestinal tract (Werdenberg *et al.*, 2003). Both DMF and MMF have been shown to activate NRF2 through electrophilic interaction with cysteine residues on KEAP1, however, DMF and MMF have been shown to bind to different cysteines on KEAP1, therefore providing differing levels of NRF2 Activity (Brennan *et al.*, 2015). DMF and MMF can also modify glutathione levels and were shown to reduce levels of GSH (Lehmann *et al.*, 2007). DMF has previously been used to treat psoriasis, an inflammatory skin condition, and since 2013 has been used to treat relapsing multiple sclerosis (MS) under the brand name Tecfidera (Satoh and Lipton, 2017).

Because of the anti-inflammatory effects and activation of NRF2, DMF has been tested in animal models of PD, in which it showed some neuroprotective properties (Lastres-Becker *et al.*, 2016) indicating a potential for DMF treatment in ALS patients. However, a phase 2 trial of DMF in ALS patients failed to show efficacy (Vucic *et al.*, 2021).

Bardoxolone methyl is the methyl ester of 2-cyano-3,12-dioxoolean-1,9-dien-28-oic acid (CDDO-me) and a derivative of the naturally occurring triterpenoid oleanolic acid. It has been shown to activate NRF2 (Liby *et al.*, 2005) and inhibit NF-kB (Ahmad *et al.*, 2006), displaying anti-inflammatory and neuroprotective effects, therefore making it a potential therapeutic in a wide range of disease areas, including cancer, diabetes, kidney disease and neurodegenerative diseases.

A phase 3 trial investigating bardoxolone as a therapy in patients with stage 4 chronic kidney disease and type 2 diabetes had to be terminated in 2012 as the rate of cardiovascular disease was increased in patients given bardoxolone compared with patients given placebo (de Zeeuw *et al.*, 2013). A related molecule omaveloxolone (RTA408), is in clinical trials for Fredreich's ataxia (NCT02255435), a disease where NRF2 activity is low.

These electrophilic molecules are the most researched so far. Other electrophiles that are currently in preclinical or clinical testing for a range of different diseases are: CXA10 (NCT04125745), TFM735 (Higashi *et al.*, 2017) and sulforaphane (NCT05084365).

One of the potential disadvantages of electrophiles is their ability to react with a wide range of molecules via modification of cysteine residues, not just the intended target of KEAP1. In a study by Yore and colleagues it was shown that Bardoxolone methyl bound to 577 different proteins, indicating that electrophiles have the potential to interact with and alter a large number of pathways (Yore *et al.*, 2011).

Generating small molecules to physically block the interaction between NRF2 and KEAP1, or CUL3 and KEAP1, by directly binding to KEAP1 is an attractive strategy as they have the potential to have fewer off target effects potentially leading to compounds that have a higher potency or that are better tolerated. These are known as KEAP1 protein-protein interaction (PPI) inhibitors. An example of a molecule that has been developed to block this interaction between NRF2 and KEAP1 is KI-969 (Davies *et al.*, 2016). This molecule was developed using fragment-based drug discovery using X-ray crystal structures to optimise binding of a molecule to the Kelch1 domain of KEAP1. This molecule shows high potency and selectivity *in vitro* as well as activation of NRF2 in animal models and may be beneficial in treating other diseases associated with disfunction of NRF2 signalling. However, due to lack of brain penetrance it

would not be beneficial to patients with neurodegenerative diseases. PPI inhibitors tend to be large molecules which are difficult to transport through the blood brain barrier (BBB), although these may be useful for other diseases that are driven by oxidative stress, the lack of CNS penetrance reduces the potential for these drugs to be therapeutic agents for neurodegenerative diseases (Bono *et al.*, 2021).

Other methods of NRF2 activation are more indirect and work through KEAP1-independent mechanisms. One mechanism is through inhibiting BACH1. BACH1 competes with NRF2 to form heterodimers with sMAF proteins and bind to MAREs in the promoter region of NRF2 target genes sites downregulating gene expression of NRF2 targets (Dhakshinamoorthy *et al.*, 2005; Tian *et al.*, 2019). BACH1 deficient mice were shown to be protected against MPTP neurotoxicity by upregulation of NRF2 regulated genes and also some non NRF2 regulated genes (Ahuja *et al.*, 2021). Downregulation of BACH1 showed protection from oxidative stress in osteoblasts, a protection that was reversed with NRF2 knockdown (Tian *et al.*, 2019), suggesting that BACH1 inhibitors could have protective effects through the activation of NRF2.

GSK-3β is involved in the negative regulation of NRF2 by phosphorylating the Neh6 domain allowing β-TrCP to bind and target NRF2 for degradation (Rada *et al.*, 2011). Therefore, inhibiting GSK-3β should lead to upregulation of NRF2 as it is no longer degraded, making GSK-3β a potential therapeutic target (Cuadrado, 2015). In a mouse model of traumatic brain injury, lithium, an inhibitor of GSK-3β, was given post trauma and it lessened neuronal degradation and neuroinflammation (Yu *et al.*, 2012). Lithium is currently used as a treatment of bipolar disorder and has shown neuroprotective properties that may be due to its effect on GSK-3β and regulation of NRF2 (Cuadrado, 2015).

P62 binds to KEAP1 in the kelch domain and competes with NRF2 for KEAP1 binding. Therefore increased expression of P62 leads to stabilisation of NRF2 and increased expression of NRF2 gene targets (Komatsu *et al.*, 2010). Activators of P62 have the benefit of not only reducing oxidative stress but also activating autophagy through other P62 pathways that can aid in removing aggregated proteins in the cytoplasm. Trehalose has been shown to increase P62 leading to increased autophagy and increased expression of NRF2 regulated genes (Mizunoe *et al.*, 2018). Trehalose is currently in phase I clinical trials investigating its effect on AD (NCT04663854) as well as other diseases.

1.5.6. Apomorphine

Apomorphine is an electrophilic compound that occurs as two enantiomers R[-] and S[+] (from now on referred to as M102R and M102, respectively). M102R is a potent dopamine agonist currently used as a treatment of PD (Boyle and Ondo, 2015), whereas the S enantiomer, M102, lacks the dopamine activation (Sam and Verbeke, 1995). M102R was found in an *in vitro* screen that identified activation of NRF2 and both M102 and M102R are CNS penetrant (Mead *et al.*, 2013). M102 was investigated in a $SOD1^{G93A}$ mouse model where mice dosed with 5mg/kg M102 subcutaneously showed a significant slowing in the progression of disease indicated by increased rotarod performance and improved gait (Mead *et al.*, 2013). Despite this positive effect on disease progression, there was no effect on the overall survival of the mice when compared to vehicle dosed animals.

Comparison of the activity of M102 and M102R *in vivo* would be useful to identify which drug compound could potentially be explored further as a therapeutic for ALS patients. Since M102R is currently used in PD, the safety analysis profile in humans has already been completed, meaning that, if successful, M102R may be able to get to the clinic faster than M102.

From current in house data, it is thought that M102 may exhibit its effects through the metabolite oxoapomorphine (OXA), which is formed through auto oxidation of M102 (Auffret *et al.*, 2018). Investigation of OXA and its potential use as a therapeutic would be beneficial in order to understand the metabolism and mechanism of action of these drugs.

1.6. HSF1 pathway

As mentioned previously, electrophilic molecules are less specific when compared to protein-protein interaction molecules. Although this can be seen as a downside to a drug due to potential toxic off target effects, in the case of electrophiles there are numerous other pathways that can be altered through reactive cysteine molecules. These other pathways include activation of peroxisome proliferator-activator receptor y (PPARy), nuclear factor kB (NF-kB), peroxiredoxins (Prx) and heat shock factor 1 (HSF1) (Levonen *et al.*, 2014; O'Brien and Wendell, 2020). Although not all electrophiles will be able to activate all these pathways, if

M102 or M102R activate these pathways, there is more potential for neuroprotection through the pathways activated.

The heat shock response (HSR) was originally described from experiments in drosophila where heat shock proteins (HSPs) were first found after they were incubated at high temperatures. Since then, the HSR has been shown to have important cytoprotective roles and can be activated by various other cell stressors as well as heat (Dayalan Naidu *et al.*, 2015). Activation of a highly conserved transcription factor HSF1 activates many HSPs, including hsp40, hsp70 and hsp90, that act as molecular chaperones to aid correct folding of proteins, refold misfolded proteins or remove misfolded proteins (Hartl *et al.*, 2011) as well as activation of pathways involved in repressing apoptosis (Jacobs and Marnett, 2007).

Many neurodegenerative diseases are characterised by aggregates of proteins or misfolded proteins. Therefore activation of pathways such as HSP that act as chaperones to remove or refold misfolded proteins is an interesting target in these neurodegenerative diseases (Neef *et al.*, 2011).

In a cell model, overexpression of HSF1 protects against TDP-43 aggregates (Lin *et al.*, 2016). Another study showed that overexpression of a constitutively active form of HSF1 showed elimination of misfolded mutant SOD1 protein and extended survival of motor neurons (Batulan *et al.*, 2006). Overexpression of HSF1 in an ALS mouse model slows disease progression (Lin *et al.*, 2013) and arimoclomol, a HSP activator, slows disease progression in an ALS mouse model (Kieran *et al.*, 2004). It has been shown that riluzole, can increase levels of HSF1 and its downstream heat shock proteins (Yang *et al.*, 2008), which may contribute to the neuroprotective effects of riluzole. The levels of HSF1 protein have been shown to decrease over time in the spinal cords of $SOD1^{G93A}$ mice (Batulan *et al.*, 2006), suggesting dysregulation of the HSF1 pathway and reduced activity of HSPs as mice age. Together this suggests that upregulation of the HSF1 protein and downstream heat shock proteins may be neuroprotective.

In basal conditions HSF1 is located in the cytoplasm bound to Hsp90. Upon stressors, HSF1 moves into the nucleus where it trimerizes, binds to the heat shock element (HSE) upstream of a number of genes such as chaperones and is hyperphosphorylated (Vihervaara and

Sistonen, 2014). Each of the binding domains in the trimer binds to a HSE sequence individually, meaning there is a requirement for multiple HSE sequences in the promoter region of genes activated by HSF1 (Figure 1.7).

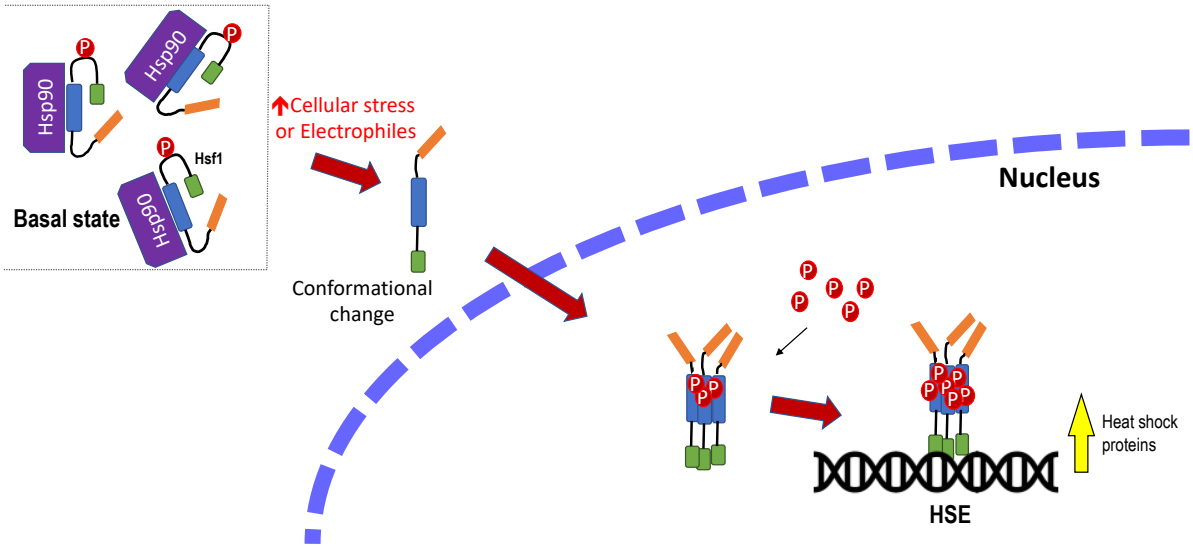

Figure 1.7: HSF1 pathway. In basal conditions HSF1 is sequestered in the cytoplasm by HSP90 and other heat shock proteins. Upon cellular stressors or in response to electrophiles, HSF1 undergoes conformational changes and translocates to the nucleus where it is hyper phosphorylated, forms trimers and binds to HSE in the promoter region of many heat shock proteins.

The mechanism of activation of HSF1 could be similar to NRF2 through the modification of cysteine residues. There could be benefits of activating the NRF2 and HSF1 pathways at the same time in ALS, as NRF2 activation could protect against oxidative stress and HSP response could help remove misfolded or aggregated proteins. This would allow one molecule to aid with multiple mechanisms causing degeneration of motor neurons in ALS, an approach which is looking increasingly popular compared to trying to hit one mechanism of the disease at a time.

1.7. Hypothesis

The hypothesis is that M102 and/or M102R activate both the NRF2 pathway and the HSF1 pathway and will slow disease progression in both SOD1 and TDP-43 mouse models demonstrating the potential to be used as therapeutic agents in ALS.

1.8. Aims of the project

The aims of the project are to:

1. Investigate the effects of M102 and M102R on the activation of NRF2-ARE system in vitro and compare it to known NRF2 activators including MMF and DMF, as well as comparison to an FDA approved ALS drug, Edaravone and HSF1 activator arimoclomol.
2. Investigate the effects of apomorphine enantiomers on the NRF2-ARE and HSF1 gene targets and regulation of downstream genes *in vivo*. This will initially involve investigating various doses of both M102 and M102R in wild type animals and analysing activation of Nrf2 and HSF1 gene targets by qPCR.
3. Extend the preclinical efficacy to models based on TDP-43 mutations and SOD1 mutations.
4. Find an optimal dose for either M102 or M102R that sufficiently activates the NRF2 and HSF1 pathways, and is well tolerated such that it can be translated into clinical trials.
5. Investigate the effects of the M102 auto oxidation product OXA and FDA approved ALS drug Edaravone in a SOD1 model.

2. Materials and Methods

2.1. Ethics statement

All studies on mice were carried out under a UK Home Office project licence by people that held the appropriate UK Home Office personal licence and had appropriate training for procedures. All work was carried out under the terms of the UK Animals (Scientific Procedures) Act 1986 and animals were housed and maintained in line with the Home Office Code of Practice for House and Care of Animals Used in Scientific Procedures.

2.2. Mice

Mice were housed in same sex groups of between 1 and 5 mice per cage. Each cage contained a plastic house, sawdust (Datesand) covering the floor and paper wool (Datesand) for bedding. The mice had ad libitum access to water and food (standard rodent diet 2018, Envigo). Temperatures in the rooms were maintained at 21°C with a 12 hour light/dark cycle (7am-7pm). Mice were identified through ear clips which were also collected for genotyping purposes.

2.2.1. WT mice

Wild-type mice used throughout were either C57BL/6J OlaHsd mice purchased from a supplier (Envigo) or non-transgenic (NT) mice from the $SOD1^{G93A}$ mouse colony but will be identified as part of each study.

2.2.2. $SOD1^{G93A}$ mice

The $SOD1^{G93A}$ C57BL/6 transgenic mice are bred in-house, NT females are bred with transgenic (T) males. To create this line B6SJL-Tg(SOD1-G93A)1Gur/J mice were backcrossed onto the C57BL/6J OlaHsd background for at least 20 generations. These mice have been extensively characterised in house and develop a progressive motor phenotype over the course of 160 days until they reach a humane endpoint (Mead *et al.*, 2011).

2.2.3. TDP-43^{Q331K} mice

TDP-43^{Q331K} C57BL/6NJ transgenic mice were obtained from the Jackson Laboratory (stock number 017933). The mice were originally on a C57BL/6NCrl background (Arnold *et al.*, 2013) but have been backcrossed onto a C57BL/6NJ background for a minimum of 4 generations

before being deposited at the Jackson Laboratory and characterised in-house up to 10 months of age. These mice have been extensively characterised in-house (Watkins *et al.*, 2021). The mice are transgenic for a myc-tagged full-length human TARDBP cDNA sequence with the Q311K mutation which is under the control of the mouse prion protein promoter to direct expression to the brain and spinal cord. The TDP-43^{Q331K} mutation is an ALS mutation found in patients. The mice develop an ALS and FTD phenotype over the course of 10 months (Watkins *et al.*, 2021).

2.3. Genotyping

Mice were ear clipped for identification and for genotyping purposes. DNA was extracted from the ear clips by adding 20µl of QuickExtract DNA Extraction Solution (Lucigen, QE09050) and incubating the clips at 65°C for 15 minutes followed by inactivating the enzyme by incubating the clips at 98°C for 2 minutes. PCR based genotyping was then used to show the presence of the transgene in the genomic DNA, the primers and protocol varied depending on which transgenic mice were being genotyped and are described below.

2.3.1. SOD1^{G93A}

To genotype the SOD1^{G93A} mice, a mix was made using 0.5µl of extracted DNA, 5µl nuclease free H_20, 2µl FIREPole (Solis Biodyne), 1µl each of the control *Il2* primers (I*l2* forward 5'-CTAGGCCACAGAATTGAAAGATCT-3', and *Il2* reverse 5'-GTAGGTGGAAATTCTAGCATCATC-3'), 0.25µl of the *SOD1* primers (*SOD1* forward 5'-CATCAGCCCTAATCCATCTGA-3', *SOD1* reverse 5'CGCGACTAACAATCAAAGTGA-3', Sigma-Aldrich). These were then run on a PCR machine (G-storm) with the following protocol: 94°C for 5 minutes, followed by 30 cycles of 94°C for 1 minute, 60°C for 45 seconds and 72°C for 30 seconds, followed by 72°C for 10 minutes (to allow for complete synthesis of strands) and then held at 15°C prior to storage.

2.3.2. TDP-43^{Q331K}

For the TDP-43^{Q331K} genotyping, a mix was made using 1µl of extracted DNA, 4µl of FIREPole (Solis Biodyne), 11µl of nuclease free H_20 and 1µl of each primer. The control *Il4* primers (*Il4* forward 5'-CTAGGCCACAGAATTGAAAGATCR-3' and *Il4* reverse 5'-GTAGGTGGAAATTCTAGCATCATCC-3') and *huTARDBP* primers (*huTARDBP* forward 5'-AGAGGTGTCCGGCTGGTAG-3' and *huTARDBP* reverse 5'-CCTGCACCATAAGAACTTCTCC-3').

These were run on a PCR machine (G-storm) with the following protocol: 94°C for 2 minutes, followed by 10 cycles of 94°C for 20 seconds, 65-50°C touchdown for 15 seconds and 68°C for 10 seconds. This was then followed by 28 cycles of the following: 94°C for 15 seconds, 50°C for 15 seconds and 72°C for 10 seconds. The final step was a final elongation step at 72°C for 2 minutes.

2.3.3. Agarose Gel

PCR reaction samples were run on an agarose gel to determine genotype. Agarose (Bioline, BIO-41025) was dissolved in 1xTAE buffer to create a 2% (w/v) agarose solution. This was heated until the agarose was completely dissolved and allowed to cool slightly. A 1μl volume of ethidium bromide (Sigma Life Science, 46067) per 100ml of solution of was added and the agarose solution was poured into a gel mould with the appropriate number of wells. Once set, the gel was placed in a gel tank filled with 1xTAE buffer so that the whole gel was submerged. A 4μl volume of hyper ladder 4 (Bioline) was added to the first well and 8μl of the genotyping sample was added to the wells. Gels were run at 120V for around 45 minutes and then imaged using a G:BOX UV transilluminator (Syngene) and analysed GeneSyn software (Syngene). For $SOD1^{G93A}$ genotyping, the control IL2 band is 324bp and the transgenic animals also have a band at 236bp, whereas non transgenic animals do not have this band at 236bp. For the $TDP\text{-}43^{Q331K}$ genotyping IL4 control band is at 324bp and the huTDP-43 band is at 228bp.

2.4. Formulation of compounds and dosing

All stocks of drugs were stored in a multipod system composed of a San Francisco storage pod and multipod controller (Roylan developments). The conditions within the storage pod were maintained at 0.5 PSI, <10% oxygen and <5% humidity to extend the life span of compounds by protecting them from oxygen and water. All vehicles were filter sterilized before mixing with drug to avoid contamination before dosing to mice.

S[+] apomorphine will be referred to in this thesis as M102 and R[-] apomorphine will be referred to as M102R. Oxo-apomorphine will be referred to in this thesis as OXA. The structure of M102, M102R and OXA are shown in Figure 2.1.

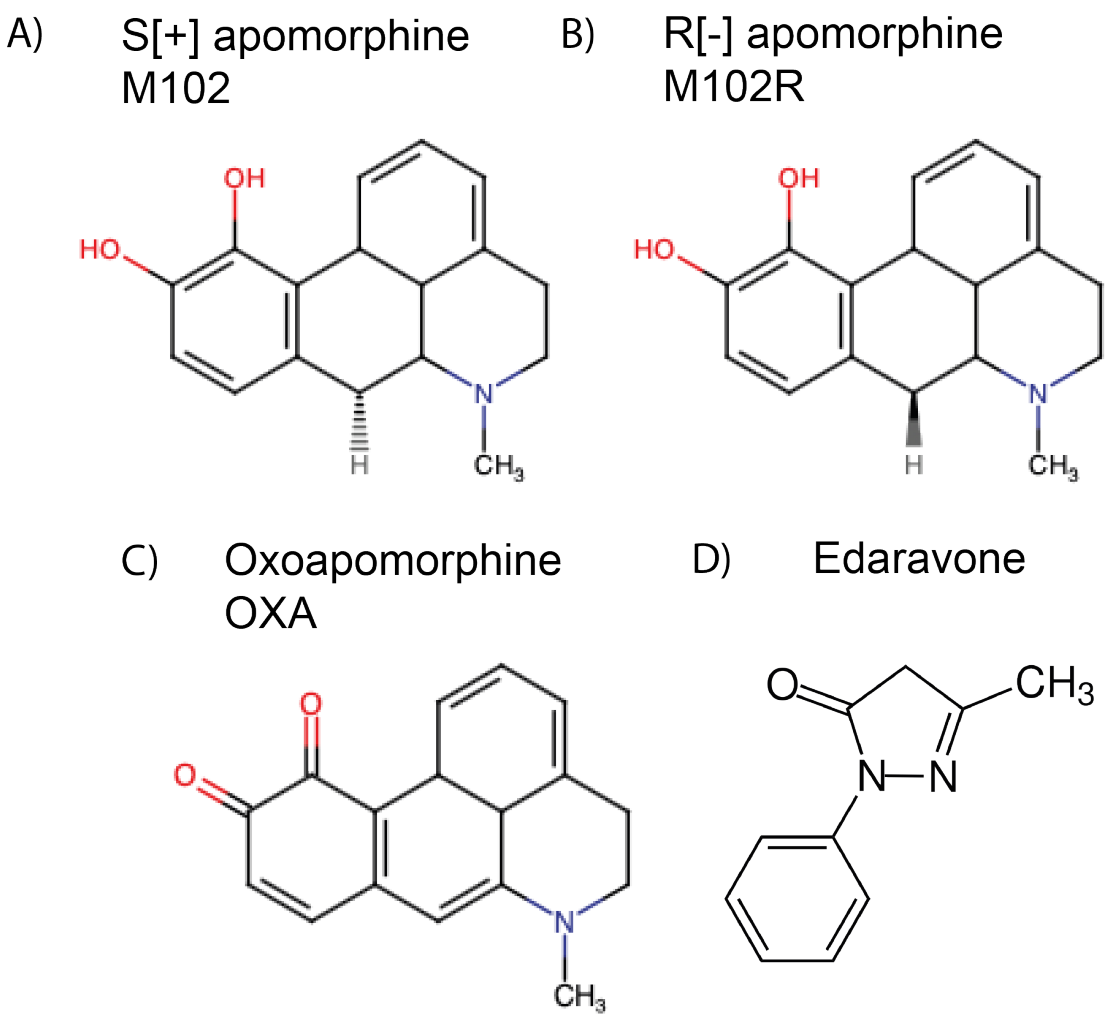

Figure 2.1: Structures of M102, M102R, OXA and Edaravone.

Where mice were dosed with any compound for the first time, at a higher dose or via a different dosing route, the lowest available dose was given first and mice were monitored continuously for 30 minutes and regularly for a few hours. Any adverse effects were noted during this period and planned doses were lowered if necessary to avoid adverse events.

2.4.1. M102 and M102R subcutaneous dosing

M102 or M102R was weighed out into bijous and kept away from light using aluminium foil. The compounds were diluted with vehicle before each day of dosing at the appropriate volume to make the desired concentration. Once mixed with vehicle, M102 or M102R was gently heated to allow the compound to fully dissolve before dosing. Once fully dissolved, the solution was kept in aluminium foil to protect from light and only loaded into the syringe directly before dosing. The most concentrated dose was created first, and all other doses were

made by diluting the most concentrated dose with more vehicle. A new aliquot of drug was used every day to provide fresh compound and prevent any degradation. Vehicle for both M102 and M102R subcutaneous dosing was 1% ascorbic acid (Sigma-Aldrich), 0.05% sodium metabisulfite (Sigma-Aldrich), 0.9% saline (NaCl) and adjusted to pH 3.5. Vehicle was filter sterilised and aliquoted into bijous in a tissue culture cabinet before use. This formulation was taken from stability assays which analysed the addition of antioxidants (Ang *et al.*, 2016).

M102 and M102R were dosed subcutaneously into the scruff of mice at 10ml/kg based on the daily weight of each mouse. When first dosed, mice were monitored for 2 hours after dosing and any adverse effects were recorded. When animals were dosed twice daily, they were dosed 4 hours apart and the new concentration was made from the most concentrated stock from the morning dosing.

2.4.2. M102 oral dosing

M102 was weighed out into bijous and protected from light as for subcutaneous dosing. The vehicle for M102 oral dosing was 10% (2-hydroxypropyl)-beta-cyclodextrin (HP-b-CD) and water which was filter sterilised. Just before dosing, M102 was diluted to 2.5mg/ml, 1.25mg/ml and 0.5mg/ml with vehicle. These were then dosed orally to mice at 10ml/kg using a metal gavage.

2.4.3. Vehicle for OXA

Stocks of OXA at concentrations of 25mg/ml or 50mg/ml were made with DMSO once a week. Just before dosing, the stock of OXA in DMSO was diluted 1 in 100 with sterile H_2O to the final concentration of 0.25mg/ml (2.5mg/kg) or 0.5mg/ml (5mg/kg). The DMSO stocks were made up fresh weekly during the dosing period and vortexed thoroughly before mixing with H_20. The two concentrations were made up separately in order to keep the final concentration of DMSO the same in both dose levels (1% DMSO). OXA was dosed subcutaneously at 10ml/kg based on the weight of mice.

2.4.4. Vehicle for Edaravone

Around 30mg of Edaravone was weighed out weekly and dissolved in 0.5ml of 1M NaOH and 8ml of H_20. The solution was then adjusted to a pH of 7 before being diluted to 1.5mg/ml

(15mg/kg) with 0.9% filter sterilised saline and stored protected from light. Mice were dosed intraperitoneally with 10ml/kg Edaravone daily.

2.5. Short term dosing study design

For the short-term dosing studies, different concentrations of M102 or M102R were dosed to mice of different genotypes and age for 7 consecutive days and tissue was collected either 6 or 24 hours after the final dose. M102 doses ranged from 0.5mg/kg to 10mg/kg once a day and included doses of 2.5mg/kg twice daily all dosed subcutaneously. M102R doses ranged from 0.5mg/kg to 5mg/kg subcutaneously once daily. Doses were chosen to determine a dose response for each compound. For each of the short term studies, mice of the correct genotype and age were randomised into the different dose groups using block randomisation (Sealed Envelope). Most of the studies were set up so that one mouse from each dose group started dosing on different days to assist with tissue collection as RNA was collected immediately after collection of tissue. In studies where mice were of a specific age, this was not always possible, but block randomisation ensured that not all animals of the same dose group were collected on the same day.

Tissue was collected by dosing mice with an overdose of pentobarbitone (2.5ml/kg) IP, and after loss of pedal reflex, blood was collected via cardiac puncture. Up to 0.4ml of blood was mixed with 1ml RNALater (Invitrogen, AM7020) and stored at -20°C. Spinal cord and brain were removed. Half of whole brain and upper spinal cord was snap frozen in liquid nitrogen and the other half of brain and lower spinal cord were homogenised in QIAzol (Qiagen) and RNA was extracted immediately following the protocol detailed in section 2.8.

2.6. TDP-43^{Q331K} study design

Female TDP-43^{Q331K} mice were dosed subcutaneously with vehicle or M102 at 5mg/kg once a day or 2.5mg/kg twice a day. The study was split into two cohorts, where one cohort was dosed from 25 days to 6 months of age (n=14) and the other cohort was dosed from 25 days until 3 months of age (n=6). Where mice were dosed twice per day, one dose was in the morning at around 9 am and the second dose was in the afternoon around 5pm.

For the 6-month cohort behavioural assessments including rotarod, electrophysiology, gait analysis and marble burying were carried out at different time points during the study. The 3-month cohort was designated for tissue analysis only.

Power analysis (G power version 3.0.3) was carried out on previous in-house data from this mouse model in order to determine the number of mice required to see a 20% improvement in rotarod performance. The number of mice required per group was 14 mice, so for the 6-month cohort the number of mice per group was 14 and for the 3 month cohort the number of mice per group was 6.

2.6.1. Dosing groups and randomisation

Female TDP-43^{Q331K} mice were block randomised into three different dose groups using a block randomisation to ensure that animals from the same litter were distributed throughout the different dose groups. (https://www.sealedenvelope.com/simple-randomiser/v1/lists).

The three different dose groups consisted of vehicle, 2.5mg/kg twice daily M102 and 5mg/kg once daily M102 all dosed subcutaneously. These doses were chosen based on the dose response experiments *in vivo*, which showed activation of Nrf2 at 5mg/kg. The 2.5mg/kg twice daily dose group was chosen due to the formulation and solubility of M102 at the time to see if two doses could be equivalent to one larger dose.

2.6.2. Weighing animals

Animals were weighed daily before dosing to determine quantity of dose. When being dosed, weight was rounded to the nearest gram, but weights were recorded to the nearest 0.1g.

2.6.3. Neuroscoring TDP-43^{Q331K} mice

Mice were neuroscored weekly from 16 weeks of age. Mice were held off the ground by the base of the tail to judge for the presence or absence of a tremor. Then mice were placed on the palm of a hand to judge for the presence and severity of a body tremor. Normal/no tremor (0), intermittent tremor (1), continuous tremor (2), full body convulsions (3). Mouse gait was analysed and scored as follows: normal (0), significant tremor (1), abnormal gait (2), severe 'waddle' (3).

Data were further analysed to detect time to reach a neuroscore of 2, by taking the age at which mice reached two consecutive neuroscores of 2 or more.

2.6.4. Accelerating rotarod test

Animals were rotarod tested once per week on an accelerated rotarod (ACCELER rota-rod for mice 7650, Jones & Roberts) from 40 days of age. Before the first test day, mice were trained on the rotarod for three consecutive days. The results of the training days were recorded but not analysed. For each test and training day, the mice were placed on the rotating beam of the rotarod and timed for how long they could remain on the beam as the speed increased from 4 to 40 rpm over the course of 5 minutes. On each day the mice completed two runs on the rotarod with a rest period in between of about 5 minutes. Analysis was carried out using Microsoft Excel and Graphpad Prism, using the maximum value from the two runs on each day.

2.6.5. Catwalk gait analysis

Gait analysis was carried out at 3 months and 6 months of age using the Catwalk gait analysis system (Noldus), which consists of a glass plate with a green LED inside that is internally reflected when mice place their paws on the surface. Mice walk over the plate and a camera from below can capture footprints from the mouse. The Catwalk software (Noldus version 7.1) can then analyse the footprints to give in-depth parameters to analyse gait.

On each test day, mice were put on the glass plate and 6 straight runs where the speed of the run is consistent were recorded. For analysis 3 runs of the 6 runs per mouse were annotated and analysed (Figure 2.2). The averages for each parameter from each run were calculated per mouse and then averages of the 8 mice per group were analysed using Microscoft Excel (Microsoft) and Graphpad Prism (version 9.1.2).

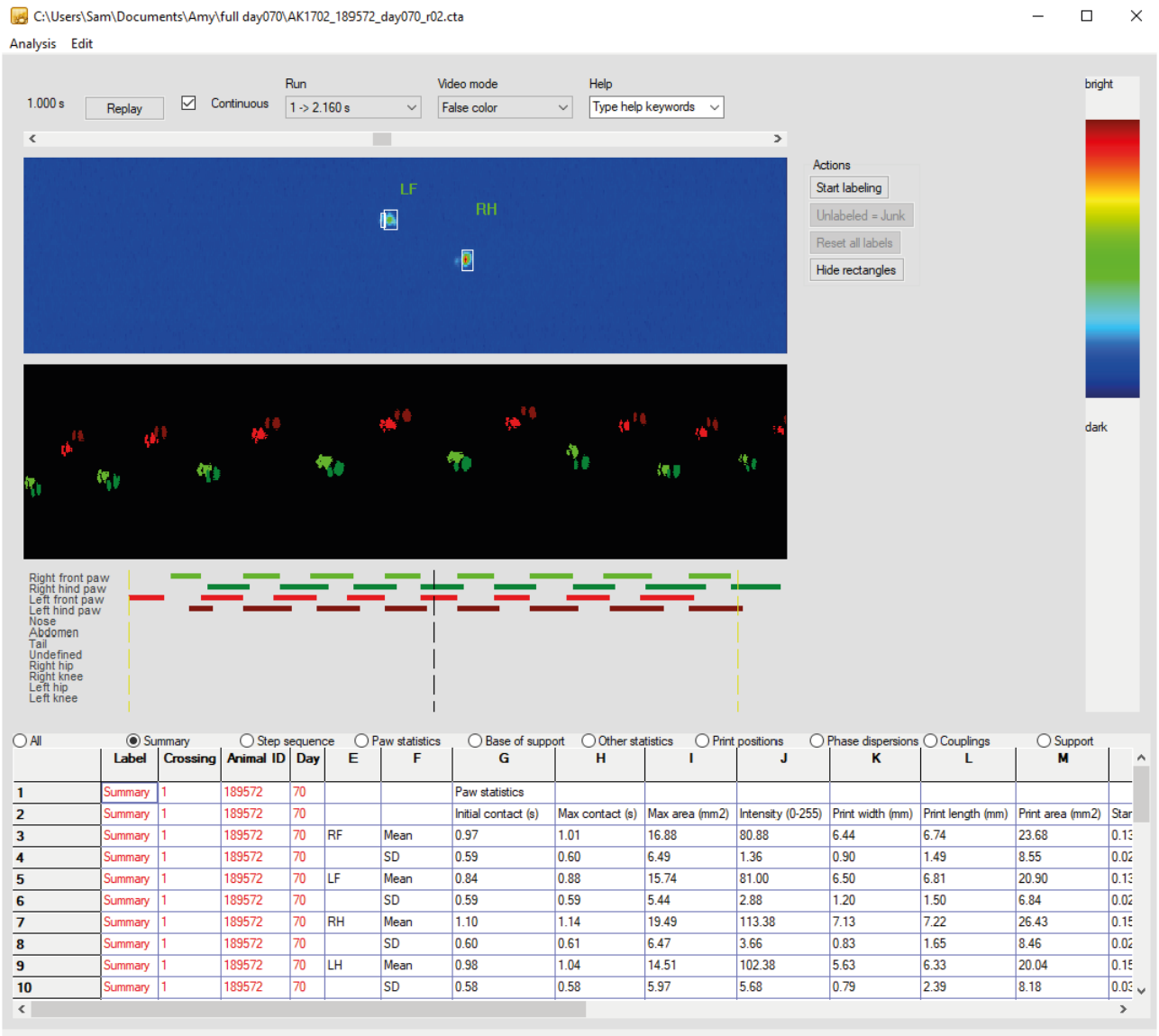

	Label	Crossing	Animal ID	Day	E	F	G	H	I	J	K	L	M	
1	Summary	1	189572	70			Paw statistics							
2	Summary	1	189572	70			Initial contact (s)	Max contact (s)	Max area (mm2)	Intensity (0-255)	Print width (mm)	Print length (mm)	Print area (mm2)	Star
3	Summary	1	189572	70	RF	Mean	0.97	1.01	16.88	80.88	6.44	6.74	23.68	0.13
4	Summary	1	189572	70		SD	0.59	0.60	6.49	1.36	0.90	1.49	8.55	0.02
5	Summary	1	189572	70	LF	Mean	0.84	0.88	15.74	81.00	6.50	6.81	20.90	0.13
6	Summary	1	189572	70		SD	0.59	0.59	5.44	2.88	1.20	1.50	6.84	0.02
7	Summary	1	189572	70	RH	Mean	1.10	1.14	19.49	113.38	7.13	7.22	26.43	0.15
8	Summary	1	189572	70		SD	0.60	0.61	6.47	3.66	0.83	1.65	8.46	0.02
9	Summary	1	189572	70	LH	Mean	0.98	1.04	14.51	102.38	5.63	6.33	20.04	0.15
10	Summary	1	189572	70		SD	0.58	0.58	5.97	5.68	0.79	2.39	8.18	0.03

Figure 2.2: Noldus catwalk gait analysis software version 7.1. Paws were manually labelled in the top blue panel, where paw position is shown and paw density is visualised on a sliding colour scale. The black panel in the middle shows all paw prints for the entire crossing to ensure correct labelling of left/right and fore/hind paws. Data were generated below for multiple gait parameters and later exported for further analysis.

2.6.6. Electrophysiology (CMAP and Repetitive Stimulation)

Electrophysiology was carried out at 6 weeks, 3 months and 6 months of age. Mice were anaesthetised with 5% isoflurane and 4L/min oxygen in an induction box. Mice were then maintained using a nose cone under 2% isoflurane and 0.5L/min oxygen. Isoflurane was adjusted as needed to keep the mouse maintained and breathing regularly. Once there was a loss of pedal reflex, the left hind limb was shaved using an electric razor and then fine fur was removed using hair removal cream (Veet). Ring electrodes were placed around the leg using

Ten20 nerve conductive paste (Weaver and Company) to ensure good contact with the skin, a grounding electrode (Ambu Neuroline) was placed in the base of the tail and a pair of twisted stimulating electrodes (Ambu Neuroline) were placed on the skin over the sciatic nerve. All recordings were made using a Dantec Keypoint Focus EMG system. A square input pulse with a 0.1ms duration was used to stimulate the hind limb. The compound muscle action potential (CMAP) amplitude was detected by the ring electrodes. The current started low (around 3mV) and was gradually increased until the CMAP amplitude did not increase further to ensure a supramaximal response (at around 7-8mV, Figure 2.3). CMAP analysis was analysed using Microsoft Excel and Graphpad Prism.

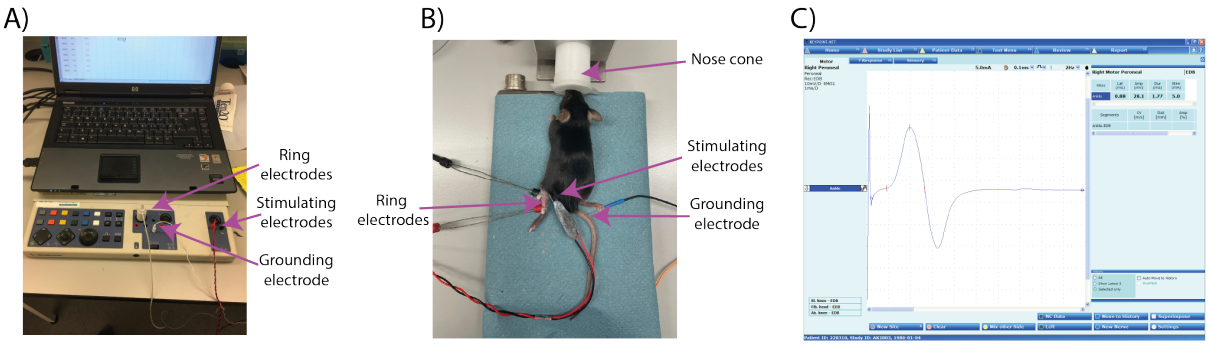

Figure 2.3: Set up EMG system for electrophysiology. A) Dantec Keypoint set up showing location of electrodes. B) A mouse under isoflurane anaesthesia from a nose cone showing the correct position of stimulating, ring and grounding electrodes to collect CMAP amplitude from the hind limb. C) An example of a standard CMAP trace from a mouse.

Repetitive stimulation used the same set up as for CMAP recording but used 10 stimuli at 10Hz to determine if the response declined (or fatigued) over time. The amplitude of each of the 10 stimuli was collected and analysed as percentage of first amplitude using Microsoft Excel and Graphpad Prism.

2.6.7. Marble burying

Marble burying was carried out at 6 months of age. Mice were placed in fresh cages which were 36 x 21 x 18.5cm (length x width x height) with an inch of sawdust at in the base. A total of 10 marbles were set up in two rows of 5 on top of the sawdust and one mouse was placed into the cage and left for 30 minutes. At the end of the 30 minutes, the mouse was removed carefully so the marbles were not disturbed and the number of marbles more than 2/3rds covered with sawdust were counted as buried (Figure 2.4).

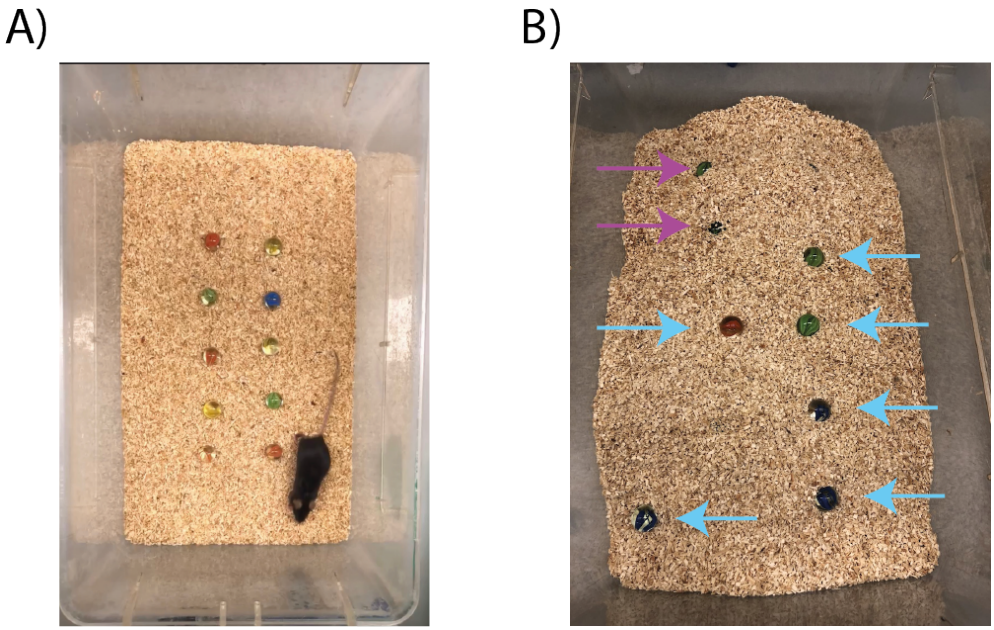

Figure 2.4: Marble burying set up and example of counting buried marbles. A) A set up of the marble burying behavioural test showing the placement of the 10 marbles in two rows of 5 and the size of the enclosure compared to a mouse. B) An example of a cage after 30 minutes. The purple arrows show marbles more than 2 thirds buried and the blue arrows show marbles that are not buried even though they have been moved from the original position.

2.6.8. Tissue collection

For the 3-month cohort (n=6 per group) and half of the 6-month cohort (n = 7 per group) were sacrificed and tissue was collected for analysis of RNA expression and protein levels. At the end of the study (3 or 6 months of age) animals were euthanised with an overdose (2.5ml/kg) of pentobarbitone. Once under deep anaesthesia, mice underwent cardiac puncture followed by removal of cortex and spinal cord. Whole blood, lower spinal cord and a quarter of the cortex were stored in RNALater (ThermoFisher) for RNA extraction, the rest of the tissue was snap frozen in liquid nitrogen. The remaining mice for the 6-month cohort (n = 7 per group) had tissue collected following perfusion for histological analysis. Mice were euthanised with an overdose (2.5ml/kg) of pentobarbitone. Once under deep anaesthesia, animals were perfused with 5ml of PBS followed by around 5 ml of 4% PFA. Brain and spinal cord were collected for IHC analysis and post fixed for 24 to 48 hours in 4% PFA before being transferred to PBS.

2.7. SOD1^{G93A} study design

Transgenic female SOD1^{G93A} mice were randomised into the 7 dosing groups using block randomisation (Sealed Envelope) to ensure animals from the same litter were separated into the different dosing groups. Female non transgenic mice from the SOD1^{G93A} colony were assigned to the vehicle WT group making sure they were from different litters and matched with T mice on the study. Animals were then dosed once daily from 25 days of age until 90 days of age, with a variety of behavioural tests carried out at various time points. There were 8 animals per dose group which was calculated using power analysis (G power version 3.1.9.2). Power analysis was based on 90% power to see a 14-day improvement in 20% rotarod decline in at least one dose group in an experiment with 7 dose groups. Effect size was determined using the average standard deviation of 20% rotarod decline in previous in-house studies using this mouse model (8.7) and mean effect levels that would replicate a 14-day improvement.

Transgenic female SOD1^{G93A} mice were dosed orally with vehicle (HP-b-CD), orally with M102 at 5mg/kg, 12.5mg/kg or 25mg/kg, subcutaneously with OXA at 2.5mg/kg or 5 mg/kg or Edaravone intraperitoneally at 15mg/kg on a two week on one week off cycle. There was also a group of NT SOD1^{G93A} mice dosed orally with vehicle. OXA groups were dosed subcutaneously to maximise exposure.

2.7.1. Weighing animals

Animals were weighed daily before dosing to determine amount of drug to dose.

2.7.2. Neuroscoring SOD1^{G93A} mice

Mice were neuroscored three times a week (Monday, Wednesday and Friday) from 60 days of age for signs of disease progression. Mice were held slightly off a surface by the base of the tail and were assessed for the presence or absence of a forelimb and hindlimb tremor. They were also assessed for a splay defect in both hindlimbs that is scored on a scale of absence of splay defect (0), mild defect (1), moderate defect (2), strong defect (3), paralysis of limb (4). Finally, they were also assessed on overall neuroscore, no defect (0), onset (0.5), abnormal gait (1), severe ‘waddle’ no dragging (1.5), dragging of one hind limb (2), paralysis of one hind limb (3). Onset is described as a splay defect and hind limb tremor when the mouse has a neuroscore of 0.5 for two consecutive scoring days.

2.7.3. Rotarod

Rotarod was carried out twice per week from 40 days of age. Before the first test day, mice were trained on the rotarod for 3 consecutive days. Rotarod testing and analysis is explained in 2.6.4.

2.7.4. Catwalk gait

Catwalk gait analysis was carried out at 70 and 85 days of age. This is described in 2.6.5.

2.7.5. Electrophysiology (CMAP and repetitive stim)

Electrophysiology analysis was carried out at 60 and 90 days of age. This is described in 2.6.6.

2.7.6. Tissue collection

At 90 days of age tissue was collected. For 4 mice per group tissue was collected via perfusion for histology and for the other 4 mice per group tissue was collected snap frozen or in RNA later. This is described in 2.6.8.

2.8. RNA extraction

RNA was extracted from lower spinal cord and cortex using the RNeasy lipid tissue mini kit (Qiagen, 74804) following the manufacturers protocol. Briefly tissue was homogenised in a small volume (150µl) of QIAzol (Qiagen) using a hand-held homogeniser in a fume hood. Once homogenised, the total volume of QIAzol was increased to 1ml. Samples were incubated at room temperature for 5 minutes after which 200µl of chloroform (Honeywell) was added, and samples were shaken vigorously for 15 seconds. Mixed samples were then incubated at room temperature for 3 minutes then centrifuged at 12,000g for 15 minutes at 4°C in a bench top microcentrifuge. The upper aqueous phase of the sample was transferred to a fresh labelled tube and 1 volume of 70% ethanol was added. Samples were vortexed and 700µl of sample was transferred to RNeasy mini spin columns attached to 2ml collection tubes. The samples were centrifuged at room temperature for 15 seconds at 13,000 rpm and the flow-through was discarded. The remainder of the sample was added to the spin columns, the samples were spun again and flow-through was discarded. A 700µl volume of RW1 buffer was added to the spin columns and these were spun at 13,000 rpm for 15 seconds. Flow-through was discarded. A 500µl volume of RPE buffer was added to the columns, which were spun and flow through

was discarded. A further 500µl of RPE buffer was added to the column and the samples were centrifuged for 2 minutes at 13,000 rpm. To further dry the membrane, the spin column was placed into a fresh 2ml tube and centrifuged at full speed for 1 minute. Finally, the column was placed in a fresh 1.5ml tube and 30µl of RNase-free water was added. These were centrifuged for 1 minute at 13,000 rpm and the flow-through was kept.

2.8.1. Quantification of RNA

Directly after extraction, RNA was quantified and checked for purity using a nanodrop ND-1000 spectrophotometer (Thermo Scientific) by measuring absorbance at 230, 260 and 280nM. This was achieved by blanking the machine with 1µl of RNase-free H_20 and then adding 1µl of sample RNA to the pedestal and measuring absorbance in the UV range to calculate RNA concentration as well as A260/280 and A260/230 ratios to check for purity of the sample. The A260/280 ratio determines if the RNA sample is contaminated by phenol or guanidine, which are found in the extraction solutions. A ratio above 2 is generally accepted to be pure, however ratios above 1.8 are acceptable to use. The A260/230 ratio is a secondary measure of RNA purity where the ideal ratio is around 2.

2.8.2. Precipitation of RNA

If for any reason the RNA concentrations were not enough for cDNA synthesis after extraction, samples were precipitated and diluted in a smaller volume of H_20. To start 0.1 volume of 3M sodium acetate and 3 volumes of ice cold 100% ethanol were added to the RNA sample and vortexed. This was stored at -20°C overnight (around 16 hours). The next day the samples were centrifuged at full speed (13000rpm) at 4°C for 30 minutes. The liquid was removed, and the pellet was washed with ice cold 75% ethanol twice with a 10 minute centrifuge at 4°C at full speed after each wash. All remaining ethanol was removed, and the pellet was left to air dry. It was then resuspended in an appropriate amount of H_20 to give the desired concentration.

2.9. cDNA synthesis

All water used in the synthesis of cDNA and throughout the qPCR protocol was diethylpyrocarbonate (DEPC) treated water. This was created by adding 1ml of DEPC (BioChemica) to 1L of water and autoclaving.

cDNA was synthesised from the RNA using the following method. Firstly, any potential DNA was digested from the samples using RNase-free DNase and DNase buffer (Roch Diagonstics, 04716728001). A 1µl volume of DNase and 1µl of 10x DNase buffer was added to 2000ng of RNA sample (total volume of 10µl). This was then incubated at 37°C for 10 minutes. The DNase was inactivated using 1µl of 25mM sterile DEPC treated EDTA (Amresco) and incubating at 75°C for 10 minutes.

A 1µl volume of DN6 (random hexamer primers, Sigma Aldrich) and 1µl deoxyribonucleotide triphosphates (dNTP, bioline, BIO-39053) were added to each reaction and these were incubated at 75°C for 5 minutes to denature the RNA. Samples were placed on ice immediately to prevent refolding of RNA and 2µl of DTT, 4µl 5x buffer and 1µl reverse transcriptase (RT) enzyme was added to all tubes (all Invitrogen, 28025-013). These were placed into a PCR machine (G-storm) and run on the following protocol: 25°C for 10 minutes, 42°C for 1 hour, 85°C for 5 minutes, 10°C infinite. Once the protocol has finished, 40µl of DEPC H_20 was added and cDNA was stored at -20°C.

2.10. Gene expression analysis

Genes chosen for expression analysis were downstream targets of the relevant transcription factors NRF2 and HSF1.

2.10.1. Primer design

Primers for qPCR were designed using primer3Plus software (https://primer3plus.com/cgi-bin/dev/primer3plus.cgi) and using the following settings:

- Product size: 100-200bp
- Primer size: Min=18, opt=18, max=24
- Primer Tm: min=58°C, opt=60°C, max=61°C, max tm difference=10°C
- Primer GC%: min=30, max=70
- Max poly-X=3
- Max3'self-complementarity=1

The template sequence for each mouse gene was the FASTA sequence for the mRNA for each target and was obtained from the NCBI website (https://www.ncbi.nlm.nih.gov). Potential primer pairs were run through the primer blast software (https://www.ncbi.nlm.nih.gov/tools/primer-blast/) in order to check for potential off target binding, to check that primers spanned exons and to find the product size to be identified on an agarose gel.

2.10.2. Primer optimisation

Multiple primer pair combinations were chosen for each target and each pair underwent a two-stage optimization protocol to identify primers that were specific and amplified cDNA and produced cycle threshold (cT) values proportional to the starting concentration of target in the sample. All primer optimisation was carried out on control cDNA from non-dosed mice unless otherwise stated. The first stage of primer optimisation consisted of differing concentrations of primers (10μM, 1μM, 0.5μM, 0.25μM and 0.125μM) with a constant concentration of cDNA, while the second stage of optimisation consisted of differing concentrations of cDNA (neat, ¼, 1/16, 1/64, 1/256) and constant concentrations of primers.

Primers were selected for the second stage of optimisation by analysis of melt peaks, amplification curves and correct amplicon size on the agarose gel. This was detected by a single band on an agarose gel at the correct size for the predicted product with no or minimal primer dimers, singular melt peaks that pass the background threshold limit and cT values that are between 20-30 cycles, where the NTC cT value is separated from the sample curves.

Primers that passed the second stage of primer optimisation were those that showed a good correlation (R^2>0.95) between the log starting concentration of cDNA and the cT value. Primers that passed both stages of optimisation and were used in this thesis are shown in Table 2.1. A complete list of gene targets and primers that were tested is found in the appendix.

Table 2.1: List of optimised mouse specific primers for qPCR. All primer pairs listed with gene ID and final concentrations used per well.

Gene name	Common name	Category	Pathway	Forward primer	Reverse primer	Product size (bp)	Gene ID	Concentration (μm)
Gapdh glyceraldehyde-3-phosphate dehydrogenase	*Gapdh*	Control	N/A	CATCACTGCCACCCAGAAGACTG	ATGCCAGTGAGCTTCCCGTTCAG	153	14433	0.5
Actin beta	*ß-actin*	Control	N/A	CATTGCTGACAGGATGCAGAAGG	TGCTGGAAGGTGGACAGTGAGG	138	11461	0.5
Glutamate-cycteine ligase, modifier subunit	*Gclm*	NRF2	Redox stress	TCCTGCTGTGTGATGCCACCAG	GCTTCCTGGAAACTTGCCTCAG	113	14630	0.25
Ppargc1a peroxisome proliferative activated receptor gamma coactivator 1 alpha	*Pgc1α*	NRF2	Mito biogenesis	GAATCAAGCCACTACAGACACCG	CATCCCTCTTGAGCCTTTCGTG	136	19017	0.25
DnaJ heat shock protein family (HSP40) member B1	*Dnajb1*	HSF1	Protein misfolding	TTCGACCGCTATGGAGAGGAAG	CCGAAGAACTCAGCAAACATGGC	131	81489	0.25
Heat shock protein 1A	*Hsp70 (Hspa1a)*	HSF1	Protein misfolding	ACAAGTCGGAGAACGTGCAGGA	GTTGTCCGAGTAGGTGGTGAAG	155	193740	0.25
NAD(P)H dehydrogenase quinone 1	*Nqo1*	NRF2	Redox stress	GCCGAACACAAGAAGCTGGAAG	GGCAAATCCTGCTACGAGCACT	120	18104	0.125
Nup62, nucleoporin 62	*Nup62*	Misc	Nucleocytoplasmic transport	ACACCTGCTTCTGGAGGAACAG	TTGGAGGTGCTGCCACTTGAGA	158	18226	0.5
Nuclear respiratory factor 1	*Nrf1*	NRF2	Mito biogenesis	CAACAGGGAAGAAACGGAAA	CCACATTCTCCAAAGGTGCT	210	18181	0.25
Glutathione S transferase pi 1	*Gstp1*	NRF2	Redox stress, glutathione	TGGAAGGAGGAGGTGGTTACCA	GGTAAAGGGTGAGGTCTCCATC	109	14870	1
Glutamate-cysteine ligase, catalytic subunit	*Gclc*	NRF2	Redox stress, glutathione	ACACCTGGATGATGCCAACGAG	CCTCCATTGGTCGGAACTCTAC	131	14629	0.125
Cytochrome c oxidase assembly protein 11	*Cox11*	NRF2	Redox stress	TGCTGCTATCCTGTGATGGT	AGGCCTATGTGGCAAACACTT	190	69802	0.125
Heat shock protein 8	*Hspa8*	HSF1	Protein misfolding	CCGATGAAGCTGTTGCCTATGG	CCAAGGGAAAGAGGAGTGACATC	112	15481	1

DnaJ heat shock protein family (Hsp40) member C6	*Dnajc6*	HSF1	Protein misfolding	TGCTAAGCCACCAGGTCAGGAT	CTGGATGTTCACAGCAGGAGTAC	136	72685	0.125
Heat shock protein 8	*Hspb8*	HSF1	Protein misfolding	CGTCAGCCTTGGTCCTTCT	GTTCGGTTCTCCCTCCCATC	128	80888	0.125
BCL2-associated athanogene 3	*Bag3*	NRF2/ HSF1	Autophagy	CCAGACAGATAAACAGTGTGGAC	GGAAGAGGATGAGCAGTCAGAG	124	29810	0.5
Discs large MAGUK scaffold protein 4	*Dlg4*	HSF1	Synapse maintenance	TTGACGCCAGCGACGAAG	CCAGTCCTTGGCCTTTAACCT	134	13385	0.25
Synapsin I	*Syn1*	HSF1	Synapse maintenance	TATGCCACTGCTGAGCCCTTCA	ATGGCAATCTGCTCAAGCATAGC	146	20964	0.125
Prostaglandin-endoperoxide synthase 2	*Ptgs2*	NRF2	Inflammation	GCGACATACTCAAGCAGGAGCA	AGTGGTAACCGCTCAGGTGTTG	132	19225	0.125
DnaJ heat shock protein family (Hsp40) member C5	*Dnajc5*	HSF1	Protein misfolding	GGACTGGACAAGAATGCAACCTC	CTTTTCGTGGCGTCTGTCAGGA	158	13002	0.5
Sequestosome 1	*Sqstm1*	NRF2	Autophagy	GCTCTTCGGAAGTCAGCAAACC	GCAGTTTCCCGACTCCATCTGT	128	18412	0.5
Eukaryotic translation elongation factor 2	*Eef2*	control	N/A	CCCAGTGCGTGTTTGACC	GCAGCATGTGGCAGTATCAG	174	13629	0.5
Heme oxygenase 1	*Hmox1*	NRF2	Redox stress	AGAACCAGCCTGAACTAGCC	CTGGACACCTGACCCTTCTG	161	15368	0.125
Tumor necrosis factor	*Tnf*	NRF2	Inflammation	AGCACAGAAAGCATGATCCG	GCCATTTGGGAACTTCTCATCC	198	21926	0.125
Oxidative stress induced growth inhibitor 1	*Osgin1*	NRF2	Redox stress	CGGTGACATCGCCCACTAC	GCTCGGACTTAGCCCACTC	107	71839	0.125
Glutathione reductase	*GSR*	NRF2	Redox stress, glutathione	AGGTGGTTGGCATTCACATG	TGGCAACTGTGTTGTCGAAG	111	14782	0.25

2.10.3. qPCR

Primers (Sigma-Aldrich) were diluted to 100μM with DEPC H_20. Primers were further diluted in the appropriate pairs to create primer mixes that contained both the forward and reverse primers at differing concentrations. 96 well qPCR plates (Bio-Rad, MLL9651) were capped using optical strip lids (Bio-Rad, TCS0803) and 384 well qPCR plates (Bio-Rad, HSP3865) were sealed with clear plate seals (Bio-Rad, MSB1001).

qPCR reactions were created with 1μl cDNA, 1μl primer mix (at appropriate dilution found from optimisation), 5μl Brilliant III Ultra-Fast SYBR® green qPCR master mix (Agilent technologies) and 3μl DEPC H_20 to make a total of 10μl per well. In non-template control (NTC) wells the 1μl of cDNA is replaced with 1ul of H_20. In wells where neat primer mixes are added, 1μl of forward and 1μl of reverse primers were added and only 2μl of H_20 was added.

Plates were run on the C1000 touch thermal cycler CFX96 (Bio-Rad) with the following protocol: Lid temp: 105°C, 95°C for 10 minutes, followed by 45 cycles of 95°C for 30 seconds, 60°C for 30 seconds and 72°C for 1 minutes with a plate read every cycle. After the amplification, the melt curve were was collected with 70 cycles of 95°C for 1 minute, 60°C for 30 seconds, and a ramp of 0.5°C per cycle starting at 60°C with a plate read every cycle.

Cycle threshold (cT) values, amplification curves and melt peaks were analysed and extracted using CFX Maestro software (Bio-Rad) and further analysed using Excel (Microsoft) and GraphPad Prism (version 9.1.2). Relative mRNA levels were detected by normalising to an endogenous control and normalisation to vehicle samples using the delta-delta cT method. The delta cT normalises the gene of interest to the housekeeping gene and is calculated from the cT of the gene of interest – cT of the housekeeping gene for the same animal. Delta-delta cT then normalises the data to the vehicle group and is calculated by subtracting the delta cT of the untreated sample from the treated sample. Relative gene expression is then calculated using 2^-(delta-delta cT).

For the qPCR plates that were run on the short-term study samples, it was set up so that there was one animal per group per plate, due to the number of animals per study. The animal samples that were on each plate were animals that had tissue collected on the same day from the block design. The results were analysed so that each of the targets was compared to

endogenous controls (*Gapdh, ß-actin* or *Eef2*) and so that each dosing level of M102 was compared to the vehicle on the sample plate. This means that the variability between vehicle samples was lost. Being laid out in this way allowed for 6 genes to be analysed per plate, with two endogenous controls, and a study of n=3 per group could be complete in 3 plates.

For qPCR plates that were run on the TDP-43^{Q331K} and SOD1^{G93A} studies, 384 well plates were used so that all the animals could be run simultaneously against multiple targets.

2.10.4. Agarose gel analysis

For the primer optimisation stages, the reactions from the qPCR were run on a 2% (W/V) agarose/1xTAE gel. A volume of 2µl of 5X loading dye (Bioline, BIO-37045) was added to each well and mixed and 4µl of hyper ladder 5 (Bioline, BIO-33057) was added to the first well and 10µl of sample was added to the preceding wells. The gels were run at 120V for 50 minutes and then imaged using a G:BOX chemiluminescent imager (Syngene).

2.10.5. Nanostring n counter

The NanoString is a technology that can detect exact quantities of specific mRNA directly from RNA samples using unique fluorescent barcodes and reporter probes. The Nanostring system uses reporter and capture probes for mRNA targets that are uniquely identifiably with molecular barcodes. The barcodes comprise a series of six fluorescent tags on each reporter probe. The probes are hybridised with RNA and then the complexes formed are captured on a surface before being imaged with a fluorescent microscope that is able to decode the fluorescent reporter tags (Geiss *et al.*, 2008). We ordered a custom kit which contained 36 mouse mRNA targets that we were interested in and three endogenous controls (Eef2, Tbp and Tada2b) (Table 2.2). The controls used for the Nanostring differed from the controls used in the qPCR analysis due to recommendations and suggestions from the Nanostring team for investigating a panel looking at neurological tissue. Each cartridge can run 12 samples, we had 4 cartridges and ran 47 separate samples.

Table 2.2: List of genes investigated on the NanoString using a custom design. The category column shows which transcription factor the target is expected to be modulated by.

Name	Gene	Gene ID (NCBI)	Category	Pathway
BCL2-associated athanogene 3	*Bag3*	29810	Nrf2/Hsf1	Autophagy
Brain Derived Neurotophic Factor	*Bdnf*	12064	Hsf1	Neurotrophic factor
Discs large MAGUK scaffold protein 4	*Dlg4*	13385	Hsf1	Synapse maintenance
DnaJ heat shock protein family (HSP40) member B1	*Dnajb1*	81489	Hsf1	Protein misfolding
DnaJ heat shock protein family (Hsp40) member B2	*Dnajb2*	56812	Hsf1	Protein misfolding
DnaJ heat shock protein family (Hsp40) member C5	*Dnajc5*	13002	Hsf1	Protein misfolding
DnaJ heat shock protein family (HSP40) member B1	*Dnajc6*	72685	Hsf1	Protein misfolding
Fas ligand (TNF superfamily, member 6)	*Fasl*	14103	Nrf2	Inflammation
Glutamate-cycteine ligase, catalytic subunit	*Gclc*	14629	Nrf2	Redox stress
Glutamate-cycteine ligase, modifier subunit	*Gclm*	14630	Nrf2	Redox stress
Glutathione S-transferase, pi 1	*Gstp1*	14870	Nrf2	Redox stress
Heme oxygenase 1	*Hmox1*	15368	Nrf2	Redox stress
Heat shock protein 90	*Hsp90*	15516	Hsf1	Protein misfolding
Heat shock protein 1A	*Hspa1a*	193740	Hsf1	Protein misfolding
Heat shock protein 8	*Hspa8*	15481	Hsf1	Protein misfolding
Heat shock protein 8	*Hspb8*	8088	Hsf1	Protein misfolding
Interleukin 12 beta	*Il12b*		Nrf2	Inflammation
Interleukin 1alpha	*Il1a*		Nrf2	Inflammation
Interleukin 1beta	*Il1b*	16176	Nrf2	Inflammation
Interleukin 6	*Il6*	16193	Nrf2	Inflammation
Nuclear factor, erythroid derived 2,-like 2	*Nfe2l2*	18024	Nrf2	Nrf2
Nitric oxide synthase 2, inducible	*Nos2*	18126	Nrf2	Inflammation
NAD(P)H dehydrogenase quinone 1	*Nqo1*	18104	Nrf2	Redox stress
Nuclear respiratory factor 1	*Nrf1*	18181	Nrf2	Mito biogenesis
Nucleoporin 54	*Nup54*	269113	Unknown	Nucleo/cyto transport
Nup62, nucleoporin 62	*Nup62*	18226	Unknown	Nucleo/cyto transport
Oxidative stress induced growth inhibitor 1	*Osgin 1*	71839	Nrf2	Redox stress
Oxidation resistance 1	*Oxr1*	170719	Misc	Redox stress
Ppargc1a peroxisome proliferative activated receptor gamma coactivator 1 alpha	*Ppargc1a*	19017	Nrf2	Mito biogenesis
Prostaglandin-endoperoxide synthase 2	*Ptgs2*	19225	Nrf2	Inflammation
Sequestosome 1	*Sqstm1*	18412	Nrf2	Autophagy
Synapsin I	*Syn1*	20964	Hsf1	Synapse maintenance
Tumor necrosis factor	*Tnf*	21926	Nrf2	Inflammation
TATA box binding protein	*Tbp*	21374	Control	N/A
Transcriptional adaptor 2B	*Tada2b*	231151	Control	N/A
Eukaryotic translation elongation factor 2	*Eef2*	13629	Control	N/A

The NanoString was run following manufacturers protocol and is a two-step process. Firstly, the hybridization reactions were set up to allow the reporter and capture probes to bind to the mRNA in the sample. A 70μl volume of hybridization buffer (NanoString Technologies) was added to the reporter probe set (NanoString Technologies) at room temperature. This was mixed by inverting as any harsh movement from vortexing or centrifugation may shear the probes. A volume of 8μl of this master mix was added to each of the hybridisation tubes followed by 5μl of RNA sample at 20ng/μl (100ng of RNA in total). Finally, 2μl of the capture probeset (NanoString Technologies) was added to each hybridization reaction. Tubes were mixed by inversion, briefly spun down and incubated at 65°C for 18 hours in a PCR machine (G-storm).

On the second day, the cartridge was brought to room temperature and samples were removed from the PCR machine and briefly spun down. A 15μl volume of hybridization buffer was added to each of the reaction, so the total volume was 30μl. This is then added onto the cartridge leaving an air bubble at the end, as suggested by the manufacturer. The cartridge was then loaded into the machine (nCounter SPRINT, NanoString technologies), the programme was then run. Data were extracted at the end of the programme and analysed using nSolver™ 4.0 software (NanoString Technologies). Within the software analysis, data were normalised to endogenous controls as well as internal negative and positive controls.

2.11. Tissue processing and embedding

Technical assistance for embedding and sectioning tissue was provided by Daniel Fillingham and Lynne Baxter. A 12mm section cantered on the lumbar enlargement was excised and cut in half from PFA fixed spinal cords. The two halves were embedded in the same paraffin wax block with the centre cut surface facing upwards. Sections were then cut using a microtome at a thickness of 10μm and placed onto glass slides in a serial manner. The first section was placed on slide one, the following section on slide 2 and so on for 5 slides, the 6^{th} section was placed back on slide one, this was repeated 4 times until there was a total of 8 sections per slide. The sections were 50μm apart due to the serial sectioning.

Paraffin was removed from the sections, and they were rehydrated by washing slides for 5 minutes in the following: 100% xylene twice, 100% ethanol, 95% ethanol, 70% ethanol and finally H_20.

2.11.1. GFAP and IBA1 staining

Once rehydrated, slides underwent antigen retrieval at pH9 using an antigen access unit (A. Menarini Diagnostics) for 30 minutes at 125°C with 20 psi. Slides were then cooled with H_20 and washed with PBS for 10 minutes. Slides were dried around the sections and 5% BSA with 0.25% triton was added to the slides and incubated for 20 minutes to block the sections.

After blocking, slides were dried again and primary antibodies were added at a 1 in 500 dilution in solution of 1% BSA with 0.25% triton in PBS. Primary antibodies were anti-GFAP raised in chicken (Abcam, ab4674) and anti-Iba1 raised in rabbit (GeneTex, GTX1000042). Slides were incubated with primary antibodies in the dark at 4°C overnight.

Slides were washed with 6 quick washes in PBS and then 3 x 10 minute washes in PBS. Secondary antibodies were used at a 1 in 1000 dilution and made up in a solution of 1% BSA in PBS. Secondary antibodies were 488 anti-chicken (Life Technologies, A11039) and 555 anti-rabbit (Thermo Fisher, A27039). Slides were dried and secondary antibody was added. Slides were then incubated for 1.5 hours at room temperature in the dark.

Slides were then washed 4 times in PBS for 10 minutes each time then placed in water for 5 minutes to remove salts. Slides were dried and mounted with hardset Vectashield with DAPI (Vector Laboratories) and cover slips. Slides were left to dry overnight and then stored at 4°C in the dark until they were imaged.

2.11.2. GFAP and Iba1 imaging

Fluorescent images of GFAP and Iba1 stained slides were captured using the INCELL 2000 (GE). Images were captured of ventral horns at 20x and 60x objective magnification using DAPI (excitation 350nm and emission 455nm), FITC (excitation 490nm and emission 525nm) and Cy3 (excitation 543nm and emission 605nm) filters.

2.11.3. GFAP and IBA1 analysis and macro

Captured images were analysed using ImageJ (version 1.52s). A macro was created to analyse the GFAP and Iba1 staining. The macro was designed using the protocol outlined in Healy *et al.* (Healy *et al.*, 2018) and optimised to work with the images captured on the INCELL 2000

(GE). The protocol uses methods to clean the image and then an autothreshold to identify the areas stained in the image. The macro was written to carry out the following on each of the 60X images:

- Duplicate the original image.
- Set measurements to redirect the analysis from the duplicate to the original image.
- Subtract background, rolling ball =50.
- Despeckle (removes noise).
- Set an autothreshold to “Li dark” using dark background and convert to a mask.
- Analyse particles with size 2μm-infinity.
- A step to save all images and analysis

Further analysis was carried out using Excel and Graphpad Prism using the output Excel sheets and parameters from the analyse particles analysis.

Composite images used for representative staining images were created by merging images from the three channels and maintaining the same contrast across each image so that they are comparable.

2.11.4. Nissl staining

Rehydrated sections were incubated in 0.1% cresyl violet solution for 15 minutes. Slides were then washed in H_20 and incubated in acetic acid for 4-8 seconds followed by 100% ethanol for 1 minute and 100% xylene for 1 minute. Sections were mounted using DPX mountant (Cellpath) and coverslips and left to dry. Slides were imaged using a nanozoomer digital slide scanner (Hamamatsu) and images were analysed using NDP.view 2 (Hamamatsu) software.

2.11.5. Motor neuron counting

Counting of motor neurons was performed blinded by Isaac Kirkland and the criteria for cells being counted as motor neurons were: cells with a cell body size greater than 20μm in any axis excluding processes; location in the spinal cord ventral horn; and the presence of a nucleus and nucleolus. Any sections that were torn or had been removed by any reason were excluded from analysis. A total of 2 slides per animal were Nissl stained and underwent motor neuron counting. This means a maximum of 16 sections were counted and 32 ventral horns.

The average number of neurons per ventral horn was calculated for each mouse and then for each dosing group.

2.12. Tissue culture

2.12.1. Cell reporter assay

For the ARE reporter assay ARE-TK-GFP and TK-GFP reporter Chinese hamster ovary (CHO) cells were used. These had already been established in the laboratory as stable cell lines expressing the reporter constructs given as a gift from William E. Fahl - McArdle Laboratory for Cancer Research, University of Wisconsin (Zhu and Fahl, 2001).

The TK-GFP construct consists of a 123bp thymidine kinase (TK) promoter upstream of pEGFP, while the ARE-TK-GFP contains of a 41bp of a synthesised GST ARE motif (TAGCTTGGAAATGACATTGCTAATCGTGACAAAGCAACTTT) upstream of the TK promoter (Mead *et al.*, 2013; Zhu and Fahl, 2001).

Cells were maintained in Dulbecco's Modification of Eagle's Medium (DMEM media (Lonza) with 4.5g/L glucose and L-glutamine without sodium pyruvate, Corning) with 10% Fetal Bovine Serum (FBS, BioSera) containing 1% 5000U Penicillin and 5000U Streptomysin (pen-strep BioWhittaker) (DMEM +/+) and 0.5mg/ml G418. Cells were grown in sterile Nunclon Delta Surface (ThermoScientific) petri dishes in an incubator (Sanyo) set at 37°C, 20% 0_2, 5% CO_2 and 95% humidity. Cells were split twice weekly into fresh dishes. When split, media was removed, and cells were carefully washed with PBS. Trypsin (Lonza) at 1X concentration was added to plates and incubated for 5 minutes at 37°C to detach the cells from the plates. Trypsin was neutralised with fresh media and cells were spun at 400g for 4 minutes to create a pellet. The pellet was resuspended in fresh media and mixed carefully to ensure an even distribution of cells. At this point cells could be counted if required or just split into fresh plates with appropriate amounts of fresh media (10ml total for a petri plate).

When used for the reporter assay, cells were grown in sterile 384 well cell culture microplates with clear bottoms (Greiner Bio-One) in DMEM +/+. Cells were counted and plated so there were 15,000 cells per well in 50µl of media. TK-GFP and ARE-TK-GFP cells were plated in alternate rows to try and limit plate effects.

Twenty-four hours after plating cells, the media was removed and 50µl per well of DMEM (Lonza) containing 1% pen-strep (Lonza) (+/- media) was added. Compounds were added at a range over concentrations across a 7-point concentration response curve with DMSO only as a control to the plate in triplicate using an Echo 550 liquid handler (Labcyte) from source plates with stock compound solutions in DMSO. Plates were then spun down and incubated for 24 hours.

After 24 hours, the plate was read on the Pherastar (BMG labtech) to measure GFP fluorescence with excitation wavelength of 485nm and emission recorded at 520nm using a 5x5 well scanning protocol. The gain was set so that the highest intensity well was 90% of maximum intensity. Data were extracted and analysed using Microsoft excel and Prism.

Compounds were prepared in DMSO at stock concentrations from 50mM to 0.5mM concentrations. The drugs run on the assay were: MMF, DMF, Edaravone, M102, M102R, Omaveloxolone, Arimoclomol maleate.

2.13. GSH-GSSG measurements

GSH and GSSG measurements were carried out by Dr Khoa Pham, University of Sheffield. Briefly, a total of 20 - 50 mg of brain cortex was used for the determination of both GSH and GSSG. Collected samples were extracted using a homogenizer in precipitating buffer (20mM NEM, 2% SSA and 2mM EDTA in 15% methanol) for 5 cycles (15 sec each). Samples were then incubated at room temperature for 1h to ensure that all reduced GSH was fully alkylated with NEM to form N-ethylsuccinimido-S-glutathione (ESG). Supernatants containing both GSE and GSSG were collected using centrifugation at 14,000 rpm for 10 min at 4^{o}C.

A High-Performance Liquid Chromatography (HPLC) U3000 (Dionex, Germany) coupled with a Lunar Omega 3 µm polar column C18 Å 100 x 2.1 mm (Phenomenex, UK) was used to clean up the sample as well as to separate GSE and GSSG. The system was operated at a flow rate of 0.2 mL/min with buffers A containing 0.1% formic acid and B consisting of 0.1% formic acid in 100% acetonitrile. A HPLC gradient was performed as follow: a linear gradient of 0–50% buffer B over 6 min, a second linear gradient of 50–95% Eluent B over 2 min, isocratic delivery of 95% Eluent B for 3 min, and a final wash with 100% buffer A for 5 min. The analytes eluted from the column was directly injected onto the Q-Trap.

The detection of GSE and GSSG was performed on a Q-Trap 4000 (Sciex, USA) operated at MRM modes with established parameters as follow: declustering potential, 40; focusing potential, 200; collision energy, 22 (GSE) or 32 (GSSG); entrance potential, 7.5; and collision cell exit potential, 18. Source and gas parameters for both compounds were: nebulizer gas, 8; curtain gas, 8; ion spray voltage, 4500; collision gas, 8; and temperature, 360 ◦ C. GSE and GSSG were monitored by their positive selected reaction monitoring (SRM) pairs using m/z 433>304 and m/z 613 > 355 respectively. The transition m/z 308 > 162 was also monitored for the presence of underivatized GSH. The quantitation of both GSE (corresponding to GSH) and GSSG was performed by comparing their MS signals to their standard curves.

2.14. Statistical Methods

The majority of the data analysed during this thesis were primarily analysed using Excel (Microsoft) and data were plotted on graphs and statistical analysis was carried out using GraphPad prism (version 9.1.2). Statistical analysis was carried out to compare the control of the experiment to the different variables (*e.g.* dose groups). Statistical levels were annotated with stars on graphs between significantly different groups with the following levels: * = $p<0.05$, ** = $p<0.01$, *** = $p<0.001$, **** = $p<0.0001$. Non-significant differences were not shown on graphs.

RT-qPCR data were initially analysed using CFX Maestro software (Bio-Rad) to assess melt peak and amplification data. For gene expression data two-way ANOVA with Dunnett's multiple comparisons were carried out between the mean of the vehicle group vs other dose groups. Mixed effect analysis with repeated measures with Dunnett's post-test multiple comparison was used for weight and rotarod data over time as some data points were missing at random. AUC analysis was analysed using one-way ANOVA with Dunnetts's multiple comparisons. Time to reach 10%, 20% and 30% decline was analysed using log-rank Mantel-Cox test.

Neuroscoring data were analysed using Kruskal-Wallis test with Dunn's multiple comparisons. Catwalk gait analysis data were analysed by two-way ANOVA with repeated measures and Dunnett's post-test. Change in CMAP data were analysed using one-way ANOVA with Dunnett's post-test. Marble burying data were analysed by Kruskal-Wallis with Dunn's post-test.

CMAP and repetitive stimulation data were analysed via two-way ANOVA with repeated measures and Sidak post-test, change in CMAP and change in repetitive stimulation data were analysed via one-way ANOVA with Dunnett's post-test.

Images of fluorescence staining of the lumbar spinal cords were captured on the INCELL. Images were analysed using ImageJ (version 1.5.2s) to generate data which were further analysed in Graphpad Prism (version 9.1.2). Fluorescence intensity was analysed using one-way ANOVA with Dunnett's multiple comparisons. Average MN counts were analysed using one-way ANOVA with Dunnett's multiple comparisons.

NanoString data were analysed initially using nSolver analysis software (NanoString), followed by analysis in Excel (Microsoft) and GraphPad Prism (version 1.5.2s).

3. Results: Dosing Studies and Gene Expression Analysis

3.1. Introduction

M102 was previously discovered to be an NRF2 activator through a high throughput *in vitro* screen using an ARE reporter cell line to identify compounds that can activate NRF2 and are also able to cross the BBB, to enable their use in ALS models and patients. In Mead *et al.* 2013, M102 is shown to be CNS penetrant and act via NRF2 *in vitro* to enhance expression of NRF2 targets and to also increase activation of NRF2 transcriptional targets in mouse CNS (Mead *et al.*, 2013).

M102R is currently used in the treatment of PD because of its potent dopamine receptor agonist activity (Boyle and Ondo, 2015). Exploring the NRF2 activity of M102R would allow potential repurposing of a drug that is already used in a clinical setting into other diseases that involved oxidative stress. M102 lacks the dopamine receptor agonist activity and is has mild dopamine receptor antagonist activity (van Hooft and Vijverberg, 1998).

Previously doses of 2.5mg/kg and 5mg/kg of M102 were explored in mice and dosed subcutaneously (Mead *et al.*, 2013), however a full dose response has not be done to find the optimal dose of M102 or M102R. Other NRF2 activators have shown a bell shaped dose response, with an optimal effect at a certain dose, but are less effective or even toxic at higher doses (Hybertson *et al.*, 2011). Doing a dose response with M102 and M102R would allow the identification of an optimal dose to pursue further.

There are other NRF2 activators that are currently being investigated pre clinically and in the clinic for many different diseases associated with oxidative stress (Robledinos-Antón *et al.*, 2019). Comparison of other NRF2 activators with M102 and M102R will give insight into the different potency of the molecules. NRF2 activators that were chosen to compare to M102 and M102R in an *in vitro* screen of NRF2 activation were DMF, MMF, Bardoxolone methyl and omaveloxolone. DMF is rapidly converted into MMF and both are electrophilic activators of NRF2 even though they interact with differing cysteine molecules on KEAP1 (Brennan *et al.*, 2015). Bardoxolone methyl (CDDO-me) is another electrophilic activator of NRF2 that is also able to inhibit NF-kB (Ahmad *et al.*, 2006; Liby *et al.*, 2005). Omaveloxolone has shown downstream activation of NRF2 targets in primates (Reisman *et al.*, 2019).

Alongside known NRF2 activators, Edaravone was also selected as it is an FDA approved treatment of ALS and has been shown to activate the NRF2 pathway (Shou *et al.*, 2019). Arimoclomol was also selected as it is a HSF1 activator that has shown neuroprotective effects in an ALS mouse model (Kieran *et al.*, 2004). This is a good comparator molecule to explore HSF1 activation.

Other electrophiles that activate NRF2 have the potential to activate other pathways, one of which is the HSF1 pathway which activates HSPs (Satoh *et al.*, 2011). Activation of HSF1 has shown to be neuroprotective (Lin *et al.*, 2013) so if M102 or M102R can activate HSF1 as well as NRF2, then this would be beneficial as a potential therapeutic in ALS. In the *in vivo* studies, we wanted to explore downstream markers of NRF2 expression alongside markers of HSF1 expression in order to investigate the mechanisms of M102 and M102R dosing as well as comparing doses to find an optimal dose that is potentially capable of activating both pathways in CNS tissue.

RT-qPCR analysis was used to do the majority of the gene expression from cortex and spinal cord tissue, however, this method can be time consuming and limits the number of genes that can be tested. The Nanostring n-counter analysis system is a higher throughput system that would allow analysis of multiple genes from many samples in less time. The Nanostring method allows the machine to count individual mRNA molecules without the need for reverse transcription or amplification that is required for traditional RT-qPCR. This means that there is less experimental error introduced compared to the multistep RT-qPCR. Nanostring also allows for multiple targets to be investigated at the same time in a high throughput manner and with little hands-on time compared to RT-qPCR. We wanted to compare the results from nanostring and RT-qPCR to see if it was beneficial to move to the newer nanostring method for analysing expression of genes.

NRF2 has been shown to cause activation and upregulation of genes involved in glutathione regulation (Harvey *et al.*, 2009). Glutathione has important roles in detoxification and in scavenging ROS, therefore has important roles in controlling the levels of oxidative stress (Lu, 2009). Reduced levels of GSH have been reported in cellular and mouse models of ALS, and reduction in GSH has been linked to increased levels of oxidative stress (Chi *et al.*, 2007).

Therefore, increasing levels of GSH, potentially through the activation if NRF2 is a potential pathway that could be targeted to help with neuroprotection in ALS (Kim, 2021). Alongside investigating glutathione synthesis genes via gene expression, we wanted to explore protein glutathione protein levels in the cortex of mice dosed with M102 to determine if the drug causes any difference in expression of reduced vs oxidised glutathione.

3.2. Aims

- To study the tolerability of dosing M102 and M102R short-term *in vivo*.
- To investigate the effects of M102 and M102R on the NRF2-ARE pathway and regulation of downstream genes *in vivo*.
- To investigate if M102 or M102R activate downstream markers of the HSF1 pathway *in vivo*.
- To compare effects of M102 and M102R *in vivo* and find the optimal dose that sufficiently activates the NRF2 and HSF1 pathways and is well tolerated that could be used in further preclinical studies to enable prediction of likely efficacious human doses with minimal toxicity.

3.3. NRF2-ARE reporter cell line

The NRF2-ARE reporter cell line was used to evaluate compounds to determine how effectively they activate the NRF2-ARE pathway *in vitro*. The aim was to compare the activity of M102 and M102R with other activators of NRF2, including compounds in late-stage clinical trials known to activate HSF1 (arimoclomol) and NRF2 (edaravone). There are two cell lines used for the assay (Zhu and Fahl, 2001). The reporter cell line has 4 ARE repeats upstream of a thymidine kinase (TK) promoter which gives low expression of a downstream eGFP construct under baseline conditions but enhanced expression in the presence of NRF2 activation (ARE-TK-GFP cells). A control cell line has the same TK promoter driving eGFP without upstream ARE elements (TK-GFP). Cells were plated in 384 well plates and compounds were added using acoustic dispensing (Echo 550, Labcyte) at a range of concentrations. The fluorescence was detected 24 hours after the addition of compounds using a plate reader following previous protocol (Mead *et al.*, 2013).

The results show a concentration-dependent increase in fluorescence detected in the ARE-TK-GFP cells, as expected (Table 3.1A). There was no significant increase of fluorescence in the

control cell line for any of the compounds (Table 3.1B). Bardoxolone Methyl (CDDO-me) and Omaveloxolone (RTA408) activate the pathway at much lower concentrations than the other compounds that were tested (Table 3.1A, Table 3.1). M102 was more efficacious than M102R, which has been seen before in this cell assay (Mead *et al.*, 2013). M102 had an EC50 of 2.5 x 10^{-5}M whereas M102R has an EC50 of 1.54 x 10^{-6}M.

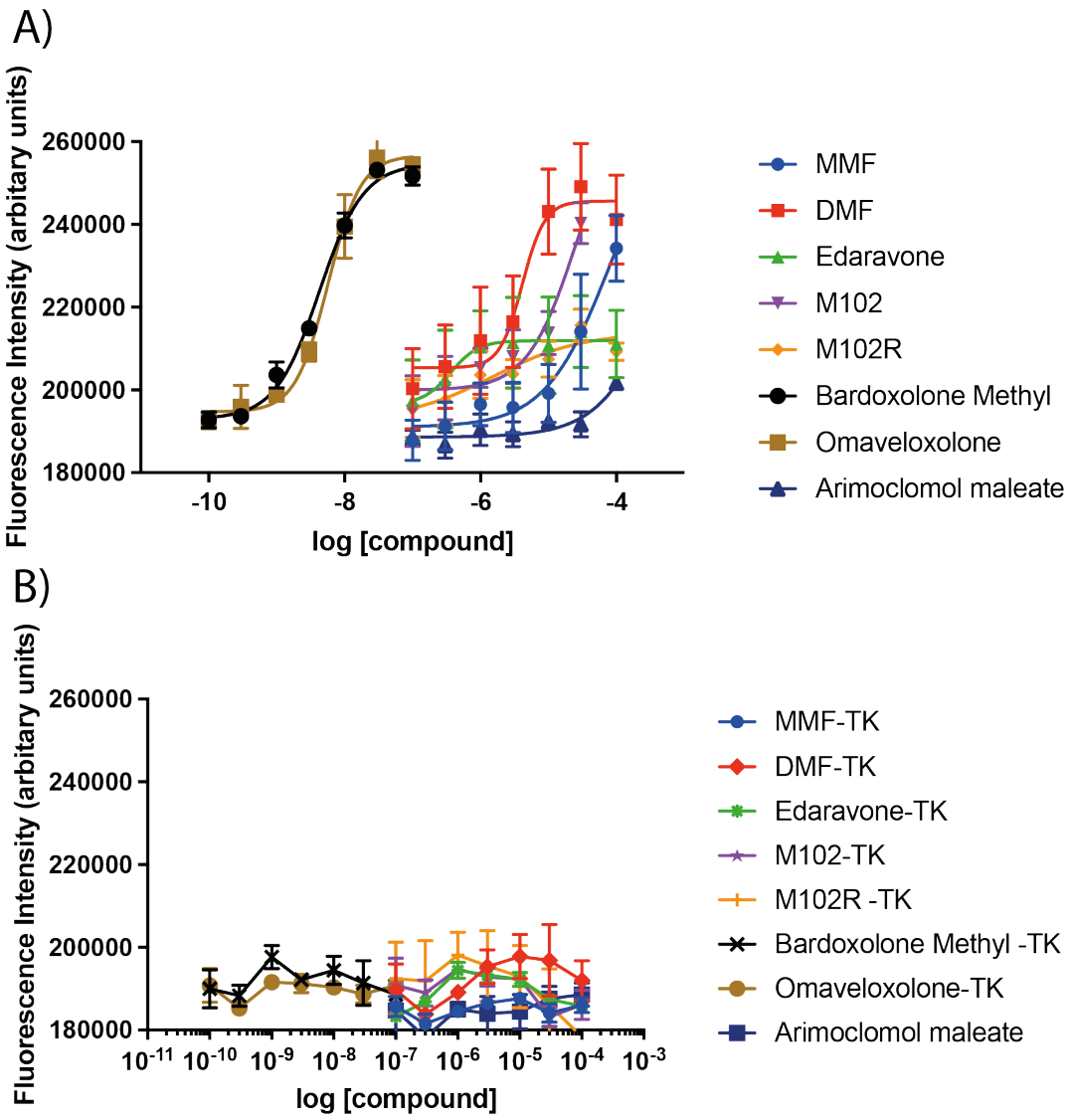

Figure 3.1: NRF2-ARE reporter cell line assay. The NRF2-ARE reporter cell lines comprises of two cell lines. A) Nrf2-ARE reporter cell line showing the fluorescence intensity of compounds against log of compound concentration (molar) shown as mean ± SD. The reporter cell line contains 4 ARE elements upstream if a TK promoter that expresses eGFP. There was a dose dependent increase in fluorescence for all compounds with Bardoxolone Methyl and Omaveloxolone being the most potent NRF2 activators. B) Control reporter cell line contains a TK promoter without ARE elements. There was no activation of GFP with compounds although some compounds showed toxicity at higher concentrations. N=3.

Table 3.1: EC_{50} values and increase in fluorescence of the ARE cell reporter assay EC_{50} determined through the midway point on a fitted curve for each compound. The change in fluorescence is determined by the change in fluorescence between the maximum and minimum detected for each compound. This is then shown as a percentage of the change seen in Omaveloxolone.

Compound	EC_{50} (M)	Change in fluorescence intensity as a percentage of Omaveloxolone (%)
MMF	8.18×10^{-5}	127.4
DMF	4.11×10^{-6}	65
Edaravone	3.65×10^{-7}	24.8
M102	2.50×10^{-5}	113
M102R	1.54×10^{-6}	34.3
Bardoxolone Methyl	4.26×10^{-9}	99.6
Omaveloxolone	5.72×10^{-9}	100.0
Arimoclomol maleate	6.01×10^{-4}	131.3

3.4. Method development

3.4.1. Selection of gene targets for gene expression analysis

Gene expression analysis is used throughout this thesis to study the effect that drugs are having on certain pathways in the CNS, specifically the spinal cord and cortex. This helps to determine if the drugs are activating the correct pathways in the tissue of interest. The main pathways that were explored were the NRF2 and HSF1 pathways so different genes that are downstream of these pathways were selected to be investigated. However, since NRF2 activates a wide range of targets, it was not possible to examine the level of every gene that could be changed by activation of NRF2 and so specific genes were selected. Some of the gene targets selected were well known downstream genes of the NRF2 pathway, such as *Hmox1*, *Nqo1* and *Osgin1* (Ma, 2013) and others were selected as we wanted to investigate certain specific pathways downstream of NRF2 such as inflammation (e.g. *Il6, Il1b, Fasl*) and autophagy (*Sqstm1* and *Bag3*) (Jiang *et al.*, 2015; Tang *et al.*, 2018). Downstream targets of HSF1 were also chosen such as *Hspa1a*, *Hspa8* and *Dnajc6* (Kovács *et al.*, 2019).

If the NRF2 or HSF1 targets were activated in vivo, there would be an expected increase in the mRNA levels of downstream targets. This would confirm that these pathways are being activated. However the duration of the increase in mRNA levels and the extent of the increase may be different due to different methods of regulation for each of the targets.

3.4.2. Optimization of primers

RT-qPCR analysis is a sensitive method of detection of mRNA levels with a sample, which is then normalised to a house keeping gene so that relative levels of gene expression can be determined. The RT-qPCR methodology uses conversion of RNA to cDNA, to which specific primers can then bind to the specific cDNA and these are amplified to detect the levels of original mRNA in the sample. The primers need to be specific enough to only bind to the target of interest and usually cover intron gaps to specifically bind mRNA sequences as opposed to any DNA that may be in the sample.

Primers were optimised in a two-stage process to ensure that they were amplifying a single specific target and that the cT values given were proportional to the amount of starting cDNA. The first stage of primer optimisation consisted of testing differing concentrations of primers (10μM, 1μM, 0.5uM, 0.25μM and 0.125μM) with a fixed amount of cDNA to determine the best combination that amplifies the target specifically with minimal primer dimer formation.

Primers that pass the first stage of optimisation move on to the second stage, which consists of differing dilutions of cDNA (neat, ¼, 1/16, 1/64, 1/256) and constant concentrations of primers to determine if the primers correctly amplify the target linearly, in proportion to the amount of starting cDNA.

Figure 3.2 shows an example of a primer pair that passed the two-stage optimisation (*Gapdh*). Panel A shows the amplification curves at different primer dilutions, the cT for the primer dilutions was much lower than for the non-template control (NTC) wells, indicating specific amplification of the target sequence. NTC wells contain all reagents for amplification of products apart from cDNA template. The NTC wells allow the identification of primer dimer formation or to detect the presence of contaminants in the reagents. Excessive creation of primer dimer can skew the quantification of product and therefore affect the relative mRNA expression calculated.

Melt curves calculate the melting temperature of products formed in the amplification. The melt curves are used to investigate the number of targets amplified by the primers with a single melt peak for a specific primer pair suggesting one product being formed (Figure 3.2B). The melt curve of the NTC is different to that of the wells with primers and was much lower in height, suggesting that these are amplifying a small amount of a different product, most likely due to primer dimer formation. The specificity is confirmed in the gel in Figure 3.2C where there was a single product at the expected size for the product of the PCR reaction and the suspected primer dimer band in the NTC and neat samples.

From the first stage of the primer optimisation, the 0.5μM concentration was chosen due to the single product, single melt peak and correct single product on the agarose gel. The amplification graph for the second stage of optimisation is shown in Figure 3.2D showing the results of different concentrations of cDNA with the primers at a concentration of 5μM. These are clearly separated as expected and when plotted as a standard curve for the log starting concentration of cDNA vs Ct there is a high R^2 value showing that the product is being detected in a linear fashion and is therefore able to be used to detect relative expression of the target in samples (Figure 3.2E). Figure 3.2F shows the resulting gel of the different concentrations of starting cDNA.

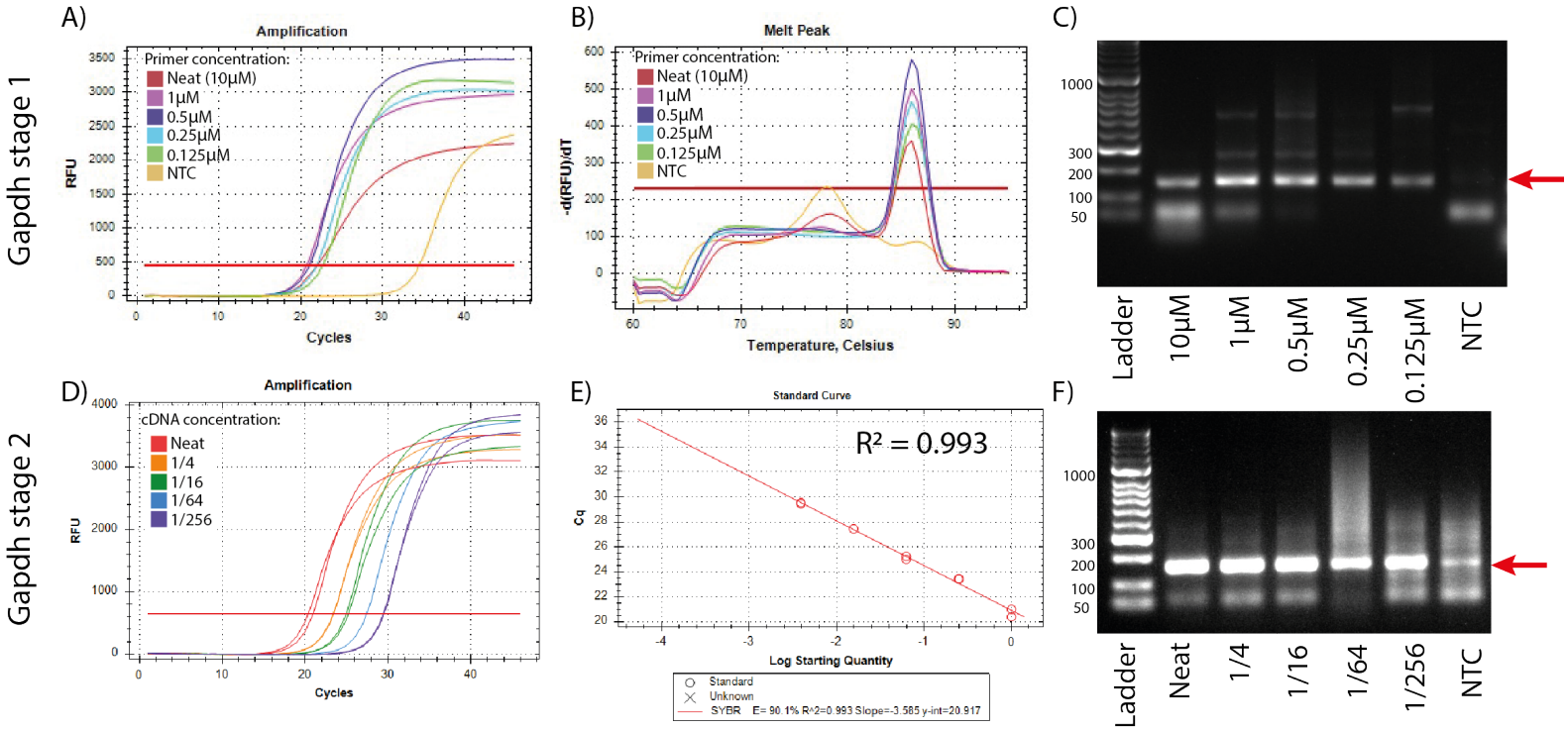

Figure 3.2: An example of a primer pair that passes the two-step primer optimisation protocol. A) *Gapdh* amplification curves from the first stage of primer optimisation as cycle number vs detected fluorescence for each primer concentration. B) From the same experiment the melt peaks for each primer concentration are shown. The non-template control (NTC) and neat primer concentrations have a melt peak suggesting primer dimer formation. C) Agarose electrophoresis of PCR products showing the bands at the different primer concentrations. D) Amplification curves for stage two of the primer optimisation protocol showing the amplification for different cDNA concentrations for stage 1 showing the expected band size for all primer concentrations and primer dimer formation in Neat and 0.5µM primer concentration. E) Standard curve of the log of the starting concentration of cDNA against Cq (Ct, cycle threshold) showing the linearity of the response and efficiency of 90.1%. F) An agarose gel showing the different cDNA concentrations against the Gapdh primers. Red arrow shows the size of expected product (156bp).

Figure 3.3 shows an example of a primer pair failing the two-stage primer optimisation. Similar to the *Gapdh* example, the melt peaks show the formation of a single product in the first stage, however there is not as much of a difference between the samples with cDNA and the NTC suggesting low abundance of the target, primer dimer formation or poor primer binding to the target (Figure 3.3A & B). From this first stage, the primer concentration of 1μM was selected as it showed one peak from the melt peak graph and the smallest cT on the amplification graph. Figure 3.3C shows the amplification curves of the different concentration of cDNA which shows very little difference between the different concentrations. This is shown in the standard curve where there is very little difference in the Ct for the different concentrations resulting in a very low R^2 score (0.138), suggesting that there is not a linear correlation between starting concentration of cDNA and amplification (Figure 3.3D). This is also backed up in the agarose gel, which shows multiple products (Figure 3.3E). This would make a bad primer pair as it would not be able to show the relative differences between the starting concentrations. The primer pairs used in the rest of the thesis for Osgin1 are from a different primer pair that passed this two-step process.

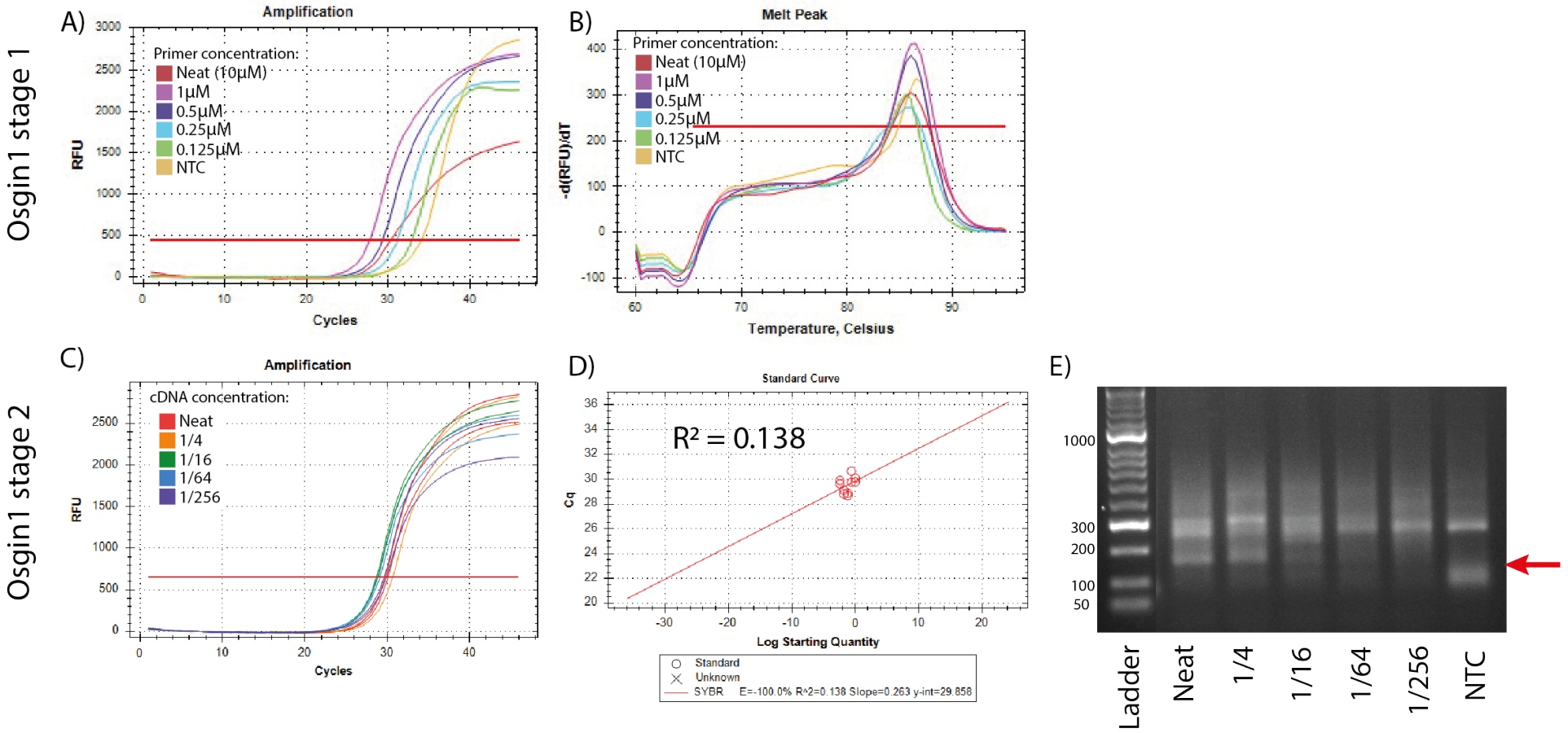

Figure 3.3: An example of a primer pair that fails the two-stage primer optimisation protocol. A) *Osgin1* amplification curves showing the different primer concentrations against control cDNA. B) Melt peak data showing a single product for most of the primer concentrations. C) Amplification curves for the second stage of the primer optimisation protocol showing the results for the different cDNA concentrations. D) Standard curve of the log of the starting concentration of cDNA against Cq (Ct, cycle threshold) showing a non-linear relationship between the two. E) An agarose gel showing the different cDNA concentrations against Osgin1 primers. Red arrow shows the size of expected product.

Multiple primer pairs were designed for each target to ensure at least one was suitable to take forward to the *in vivo* studies. Primers were designed using primer3 software, ncbi primer blast tool or taken from previous publications. A list of optimised primers is found in Table 2.1 and the full list of primer pairs tested is in the appendix (Section 8). In total, primers were designed for 35 different mRNA targets, with 83 primers being tested in total.

Primer pairs were originally tested on cDNA from a WT, control mouse cortex and spinal cord samples. Some of the primers that failed on the second stage of optimisation, could have failed due to the low abundance of target in the cDNA with lower cDNA concentrations being close to the non-template control and so skewing the R^2 value. For these primers, the lowest cDNA concentration was removed from the analysis, or the primers were tested on cDNA from other sources. Most of the primers were optimised using cDNA from a WT mouse, however cDNA from mouse cells lines or from transgenic $SOD1^{G93A}$ mice were also used for some targets, such as the inflammatory targets, that may be at low concentrations in the WT animals. Use of the cell line or transgenic $SOD1^{G93A}$ mouse cDNA showed that there was some variation between the cDNA abundance in these different samples which affected the R^2 value in the second stage of the optimisation.

3.4.3. Comparison of endogenous controls

To carry out the delta delta method of RT-qPCR analysis described in section 2.10.3, there needs to be a correct endogenous control gene (or genes) that the expression of targets can be compared with. Correct selection of endogenous controls is vital and can vary depending on tissue type, species, and analysis method. The three controls chosen to compare were *Gapdh*, *ß-actin* and *Eef2*. *Gapdh* and *ß-actin* are commonly used endogenous controls that are highly abundant in cells and *Eef2* was chosen based on previous publications showing that it is an appropriate control for mouse CNS tissue (Kouadjo *et al.*, 2007).

When the initial RT-qPCR experiments were carried out, multiple control genes were run as well as target genes in order to determine which controls were the most reliable. The results showed that at 6 hours post dose there was very little difference in expression in *Gapdh*, *ß-actin* and *Eef2* when the delta delta cT was normalised to *Gapdh* expression levels when animals were dosed with M102 (Figure 3.4). However, at 24 hours post dose there was a significant increase in ß-actin expression at all doses of M102 when compared to *Gapdh*,

whereas there was no significant difference in gene expression in *Eef2*, suggesting that *Gapdh* and *Eef2* are more comparable than *Gapdh* and *ß-actin*. Following on from this, all RT-qPCR results are shown as compared to *Gapdh*.

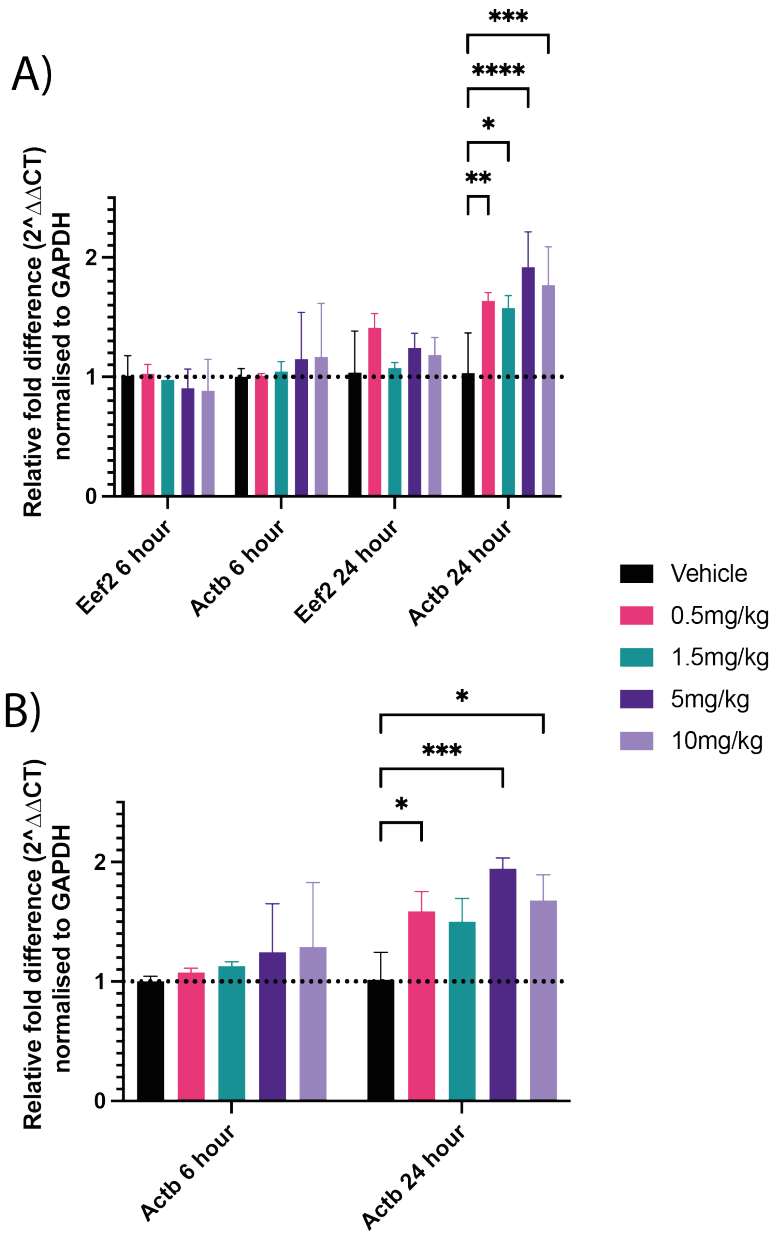

Figure 3.4: Comparison of endogenous controls *Gapdh, ß-actin* and *Eef2* in RT-qPCR following the administration of increasing doses of M102. Data shown as mean ± SD. Relative expression (using the delta delta cT method) of *ß-actin* and *Eef2* when compared to *Gapdh* in two different experiments where WT mice were dosed with M102 at differing concentrations. A) At 6 hours post dose, there was no difference between *Gapdh* and *ß-actin* or *Gapdh* and *Eef2*. At 24 hours post dose there was a significant and dose dependent increase in ß-actin expression when compared to *Gapdh*. B) Another experiment showing a similar increase in *ß-actin* expression at 24 hours post dose. Two-way ANOVA with Dunnett's multiple comparisons. (* = $p<0.05$, ** = $p<0.01$, *** = $p<0.001$, **** = $p<0.0001$).

3.5. M102R in WT mice at 6 hours and 24 hours post dose

We wanted to investigate dose response of M102R in WT mice by analysing the expression levels of NRF2 and HSF1 downstream targets in CNS tissue *in vivo*. We designed a short-term dosing study investigating different concentrations of M102R in WT mice. We were also able to investigate if there were any adverse effects of different doses of M102R and what the highest tolerated, or optimal, dose would be that could potentially be used as a therapeutic dose.

3.5.1. M102R in WT mice study design

WT mice were chosen initially to determine if M102R can activate target pathways *in vivo* in the CNS of mice in the absence of disease phenotype that may interfere or alter gene expression. The mice were block randomised into 8 different dosing groups and given the appropriate dose of M102R for 7 consecutive days (Table 3.2). Tissue was collected at 6 or 24 hours post final dose and there were 3 mice in each group for each dose and collection timepoint. The reasoning for having the two time points is to try and capture differential expression of multiple genes, as different transcripts may be present for different lengths of time after dosing. The 24-hour time point is equivalent to the trough level of gene expression as the animals are dosed every day. The 6-hour time point allows for more transient changes in genes to be detected. M102R has a short half-life and so mice were monitored after the first dose for at least 60 minutes to determine any adverse effects. Dosing for 7 consecutive days allows for an equilibrium to be created.

Table 3.2: M102R short term dose study in WT mice: study design showing dose levels and collection time points

mice	Age	Drug	Route of administration	Dose/Doses	Number of days dosing	n per group	Time point for collection
WT mice	10 weeks	M102R	SC	Vehicle	7	3	6 hours
			SC	0.5mg/kg			
			SC	1.5mg/kg			
			SC	5mg/kg			
			SC	Vehicle	7	3	24 hours
			SC	0.5mg/kg			
			SC	1.5mg/kg			
			SC	5mg/kg			

The study was designed in a block design so that each day one mouse from each group started dosing and in the following days, the next animal in each group was added. This was done for a couple of reasons. Firstly, it allowed for easier collection of tissue as RNA was extracted immediately from cortex and spinal cord samples, it meant that one animal per group per time point was collect so the maximum number of animals that were collected at one time point was 3. Secondly, dosing only one mouse per group on day one allowed better monitoring of any potential side effects that the animals might experience. Mice were dosed in their blocks generated from the block randomisation. Block randomisation accounts for variability that may be experienced on different days of dosing and means that tissue was collected from different groups on the same day (Festing, 2020). M102R is a dopamine agonist and so care was taken when choosing doses and monitoring the animals after dosing.

3.5.2. Observations from dosing M102R in WT mice

After 5 minutes of dosing at 0.5mg/kg M102R, an abnormal gait and slight straub tail was observed in the first mouse. The mouse dosed at 1.5mg/kg showed abnormal gait, straub tail and showed reduced provoked behaviour at 5 minutes post dose. At 5mg/kg at 5 minutes post dose similar effects were seen as seen at 1.5mg/kg but slightly more exaggerated and the mouse was slightly hunched. After 15 minutes mice dosed with 5mg/kg M102R showed a slight increase in provoked behaviour. All animals had fully recovered within 50 minutes of dosing. After three days of dosing animals dosed with 1.5mg/kg and 5mg/kg M102 seemed to be hyperactive 24 hours after dosing. Videos of the behaviours were captured at different time points post dose.

3.5.3. M102R in WT mice gene expression

cDNA was generated from the cortex RNA and then qPCR was carried out on the samples using the optimised primers. Because of the number of animals in the study, the qPCR plates were laid out so that there was one animal per group per plate and that the animals on each plate were the animals that were collected on the same day matching the block design. The data were analysed using the delta delta cT method as described in section 2.10.3 and all gene expression was compared to endogenous controls (*Gapdh* or *ß-actin*) and to the vehicle dose group. Because of the way the plates were laid out, the delta cT value from each plate was collected and then the delta delta cT was calculated from those and finally the relative gene expression.

There was no significant difference in *ß-actin* expression when compared to *Gapdh* (Figure 3.5), which is different to what is seen with M102 (discussed in 3.4.3). There was a significant increase in *Gclm* expression at 6 hours post dose with 1.5mg/kg M102R when compared to vehicle (P = 0.0281), however no difference was observed at 24 hours post dose (P = 0.8440). The relative expression level for *Hspa1a* was significantly higher than vehicle at 6 hours post dose for the 1.5mg/kg (P = 0.0189) and 5mg/kg (P = 0.0090) and at 24 hours for 1.5mg/kg (P = 0.0211) and 5mg/kg M102R (P = 0.0303, two-way ANOVA with Dunnett's multiple comparisons).

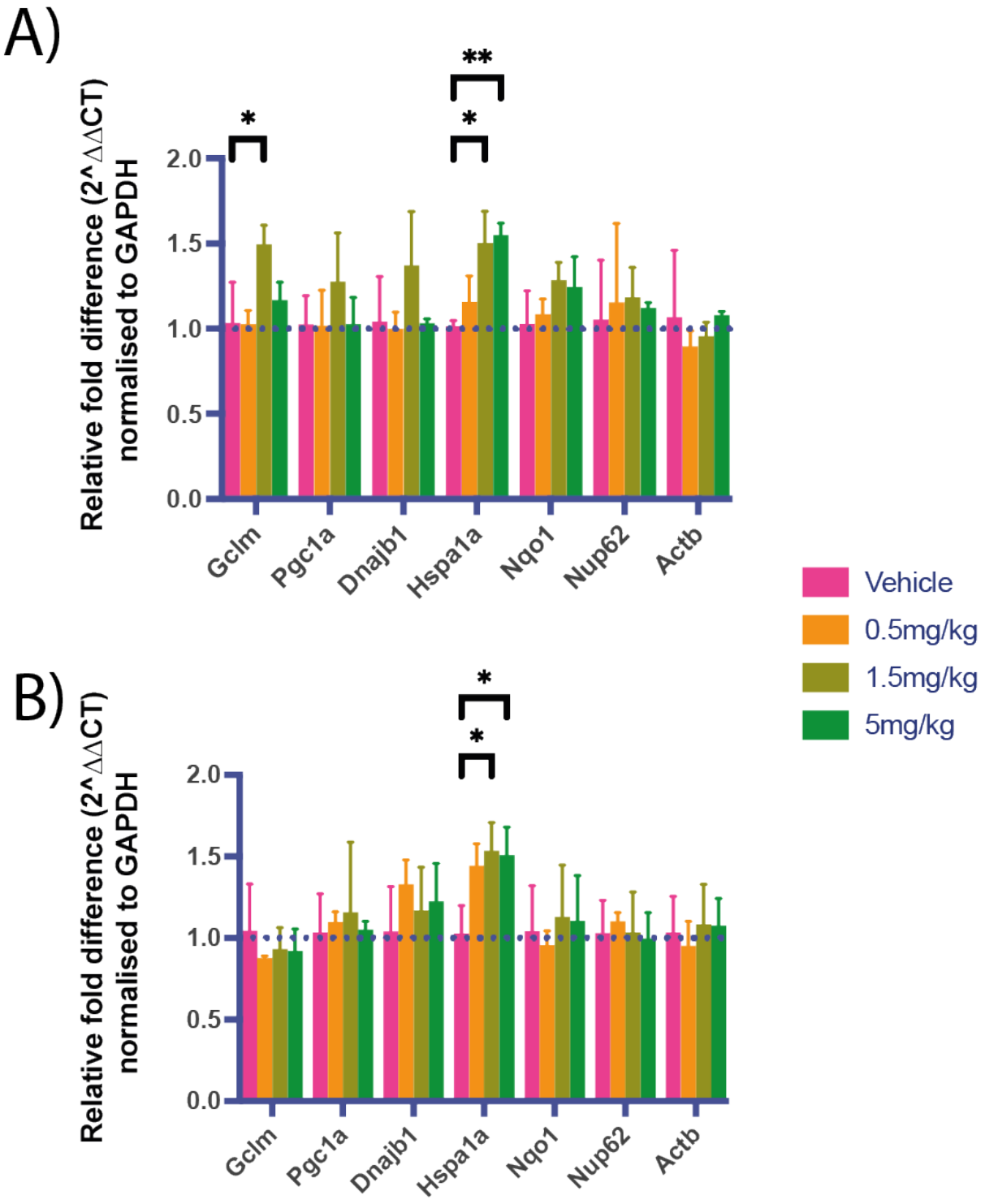

Figure 3.5: Relative expression of target genes in M102R dosed WT mice. Data shown as mean relative expression (using the delta delta cT method) ± SD from cortex samples for all dose levels M102R normalised to *Gapdh* at A) 6 hours and B) 24 hours post dose, n=3. There was a significant increase in *Gclm* expression at 1.5mg/kg M102 at 6 hours post dose and in *Hspa1a* expression at 1.5mg/kg and 5mg/kg at both 6 and 24 hours post dose. N=3, two-way ANOVA with Dunnett's multiple comparisons. (* = $p<0.05$, ** = $p<0.01$).

These data demonstrate NRF2 and HSF1 downstream gene target changes in the cortex of mice when dosed with M102R.

3.6. M102 in WT mice at 6 hours and 24 hours post dose

This study was designed similarly to the previous M102R study, but investigated the effects of M102 itself, the main compound of interest. The aim of this study was to define a dose response relationship for M102 on NRF2 and HSF1 pathway activation in the CNS and to identify a concentration of M102 that is well tolerated to take into future efficacy studies.

3.6.1. M102 in WT mice study design

WT NT female mice from the SOD1^{G93A} colony were block randomised into 10 different dosing groups (Table 3.3) and dosed for 7 consecutive days with the appropriate concentration of M102 followed by tissue collection at 6 hours or 24 hours post dose. This was done in a block design so that one animal per group is dosed on day one and then the second animal starts dosing on day 2 and so on until all animals were recruited, as with the previous M102R study. There were 3 animals per dose and timepoint. All animals were monitored for a minimum of 60 minutes following dosing on the first day to determine any adverse events.

Table 3.3: M102 in WT mice at 6 and 24 hours post dose study design showing dose levels of M102, mouse age, number of mice per group and collection time points.

mice	Age	Drug	Route of administration	Dose/Doses	n per group	Time point for collection
WT NT from SOD1 colony	29-50 days	M102	SC	Vehicle	3	6 hours
			SC	0.5mg/kg		
			SC	1.5mg/kg		
			SC	5mg/kg		
			SC	10mg/kg		
			SC	Vehicle	3	24 hours
			SC	0.5mg/kg		
			SC	1.5mg/kg		
			SC	5mg/kg		
			SC	10mg/kg		

3.6.2. M102 in WT mice observations from dosing

Originally the top dose of M102 was planned to be 15mg/kg. However, after dosing the first mouse on day one, it was lowered to 10mg/kg for this mouse and every other mouse in the highest dose group. This was due to adverse effects seen with the 15mg/kg M102 dose. On day one the mouse dosed at 15mg/kg showed decreased provoked behaviour and ataxia from 5 minutes post dose to 25 minutes post dose. At 25 minutes post dose the mouse was moving and exploring when provoked and at 30 minutes post dose there were no adverse effects. The following day the mouse was dosed at 10mg/kg and the mouse showed a milder transient reduction in provoked behaviour with no sign of ataxia and so this dose was taken forward for the remainder of the study.

3.6.3. M102 in WT mice gene expression

After 7 days of dosing, tissue was collected at 6 or 24 hours post dose and RNA was extracted from cortex and spinal cord. From cortex RNA, cDNA was synthesised, and qPCR was carried out using optimised primers for NRF2 and HSF1 gene targets. All qPCR was carried out in 96 well plates with one animal per group on the plate which allows for 8 different target mRNAs to be analysed per experiment. The data provided below for the relative gene expression have been combined from multiple qPCR experiments to show the gene targets for NRF2 and HSF1 together. Different NRF2 and HSF1 downstream targets were selected for each study as primers for new gene targets were being optimised alongside the experiments, meaning new targets were being added as the short-term *in vivo* experiments were being run. Limitations on the number of targets that could be run per RT-qPCR plate, alongside different numbers of groups and mice per group, also impacted the choice of which targets were selected for each experiment.

For NRF2 targets at 6 hours post dose there was a significant increase in *Nrf1* expression with 5mg/kg ($P < 0.0001$) and 10mg/kg ($P < 0.0001$) M102 when compared to vehicle (Figure 3.6A). There was also a significant increase in expression of *Hmox1* at 5mg/kg ($P = 0.0029$) and 10mg/kg ($P = 0.0030$) M102 when compared to vehicle.

At 24 hours post dose there was a significant increase in *Pgc1a* expression levels at 5mg/kg ($P = 0.0013$) and 10mg/kg ($P = 0.0044$) M102 when compared to vehicle (Figure 3.6B). There was a significant increase of *Nrf1* expression at 1.5mg/kg ($P = 0.0059$), 5mg/kg ($P = 0.0167$) and

10mg/kg (P = 0.0034) M102 when compared to vehicle. There was an increased expression of *Hmox1* at 1.5mg/kg (P <0.0001), 5mg/kg (P <0.0001) and 10mg/kg (P <0.0001) M102 when compared to vehicle.

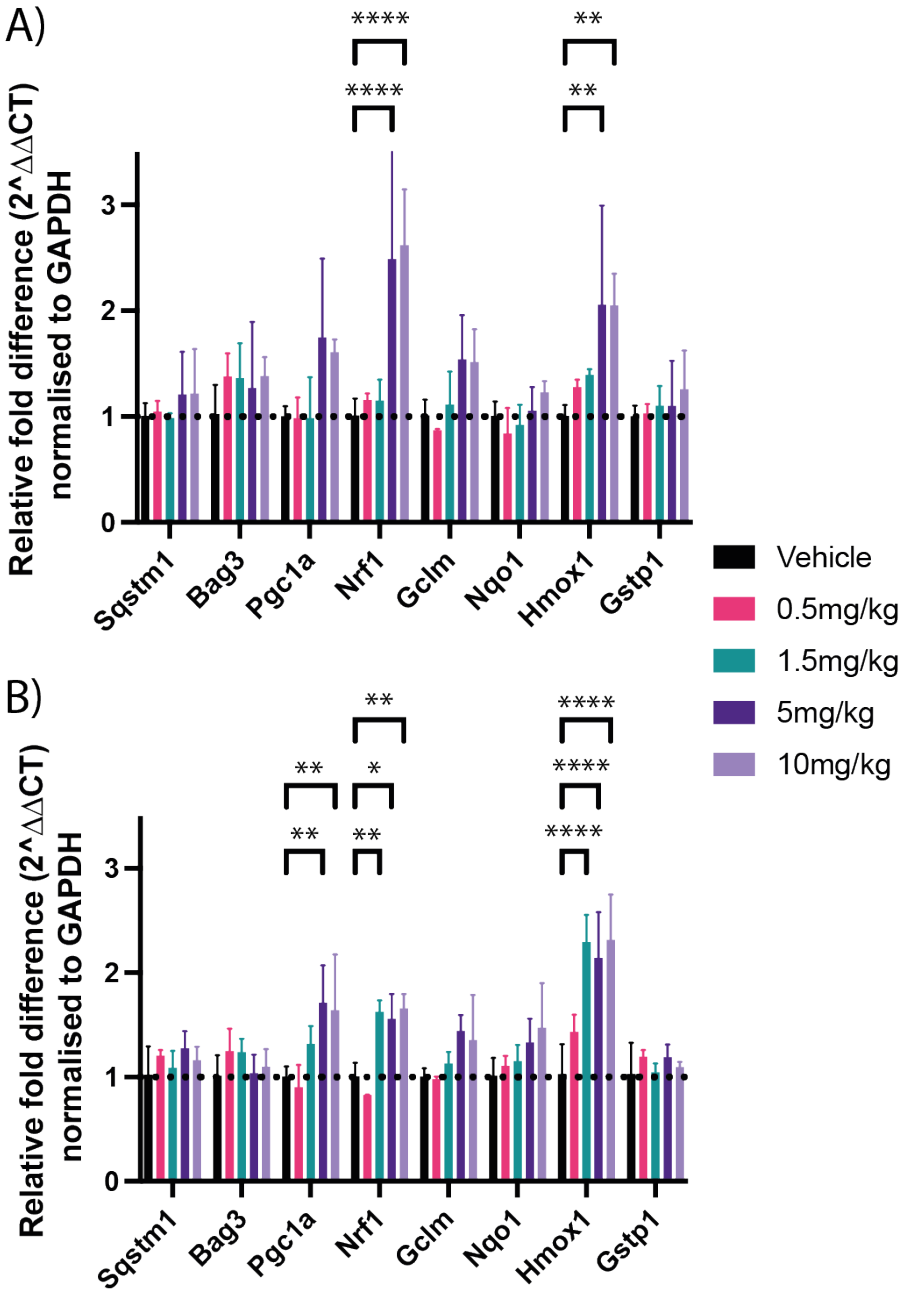

Figure 3.6: Relative expression of NRF2 target genes in the cortex tissue of WT mice dosed for 7 days with M102 at varying concentrations. Data shown as mean relative expression (using the delta delta cT method) relative to *Gapdh* and vehicle, plotted as mean ± SD. A) At 6 hours post dose there was a significant increase in *Nrf1* expression and *Hmox1* expression with 5 and 10mg/kg M102. B) At 24 hours post dose there was a significant increase in *Pgc1a* expression with 5 and 10mg/kg M102, in *Nrf1* at 1.5, 5 and 10mg/kg and *Hmox1* at 1.5, 5 and 10mg/kg. n = 3. Two-way ANOVA with Dunnett's multiple comparisons. (* = p<0.05, ** = p<0.01, *** = p<0.001, **** = p<0.0001).

Next HSF1 target genes were investigated. At 6 hours post dose there was a significant increase in *Hspa1a* expression in the 5mg/kg (P = 0.0058) and 10mg/kg (P = 0.0002) M102 dose groups when compared to vehicle (Figure 3.7A). At 10mg/kg M102 there was also a significant increase in the expression of *Dlg4* (P = 0.0101) and Syn1 (P = 0.0030) when compared to vehicle.

At 24 hours post dose there was a significant increase in *Hspa1a* expression with 1.5mg/kg (P = 0.0144), 5mg/kg (P <0.0001) and 10mg/kg (P = 0.0287) when compared to vehicle (Figure 3.7B). There was a significant increase in expression of *Hspa8* at 0.5mg/kg (P = 0.0208), 1.5mg/kg (P < 0.0001), 5mg/kg (P < 0.0001) and 10mg/kg (P < 0.0001) M102 when compared to vehicle.

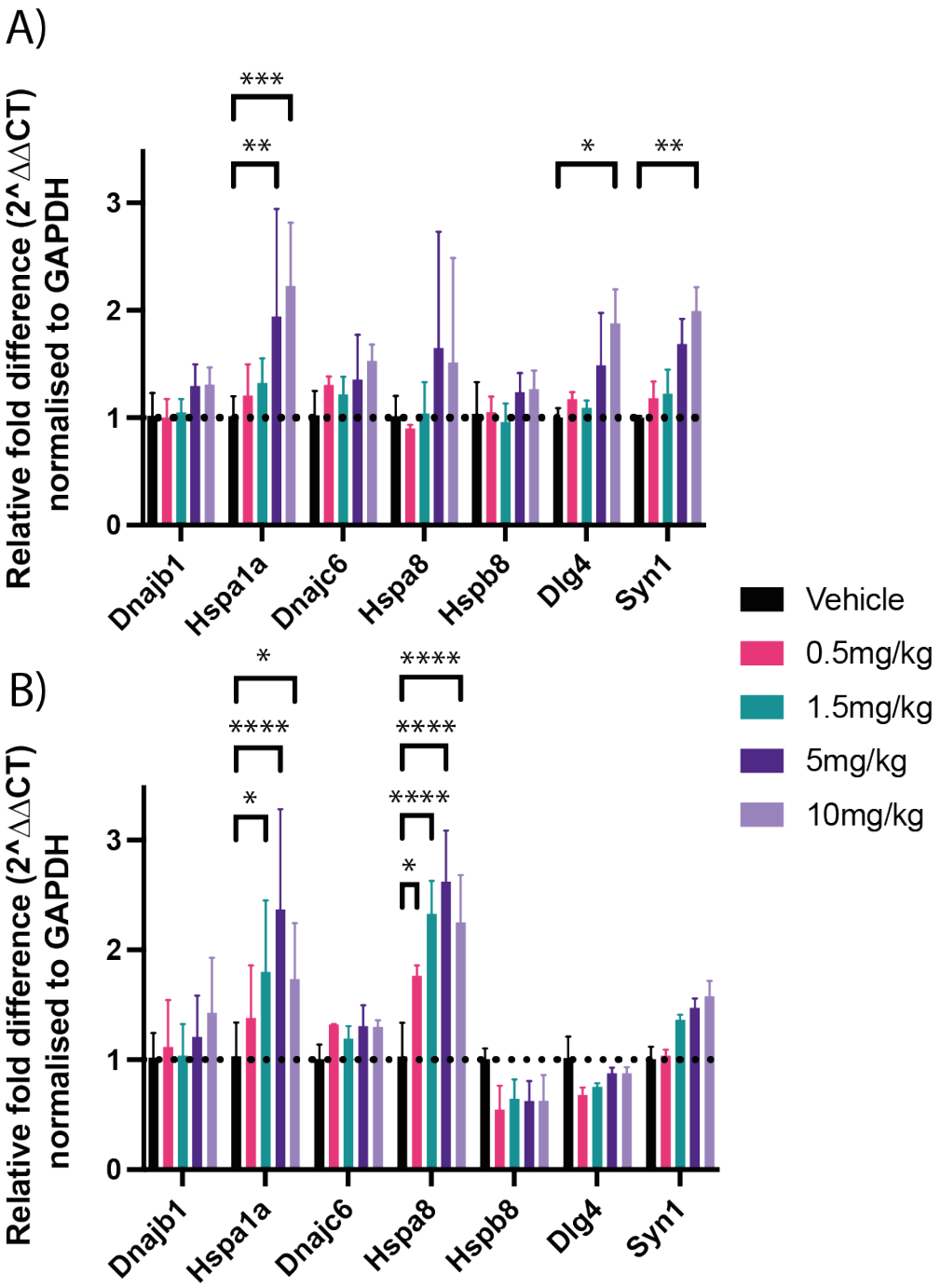

Figure 3.7: Relative expression of HSF1 target genes in the cortex tissue of WT mice dosed for 7 days with M102 at varying concentrations. Data shown as mean relative expression (using the delta delta cT method) ± SD. A) at 6 hours post dose there was a significant increase in the expression levels of *Hspa1a* at 5 and 10mg/kg M102 and a significant increase in both *Dlg4* and *Syn1* at 10mg/kg M102. B) at 24 hours post dose there was a significant increase in the expression of *Hspa1a* at 1.5, 5 and 10mg/kg and *Hspa8* at 0.5, 1.5, 5 and 10mg/kg M102. N = 3. Two-way ANOVA with Dunnett's multiple comparisons. (* = $p<0.05$, ** = $p<0.01$, *** = $p<0.001$, **** = $p<0.0001$).

These data show increased expression of NRF2 and HSF1 targets for the first time in the CNS of WT mice dosed with M012. Expression of genes shows a dose dependent response with increasing doses of M102.

3.6.4. GSH and GSSG measurements

To correlate the gene expression changes with downstream functional effects, glutathione measurements were made. NRF2 activation leads to increased transcription of glutathione synthesis genes and elevation of glutathione levels (Harvey *et al.*, 2009).

When tissue was collected, part of the cortex that was not used to isolate RNA was snap frozen. GSH and GSSG levels were determined from the snap frozen cortex tissue from mice dosed with vehicle, 5mg/kg and 10mg/kg M102 by Dr Khoa Pham using HPLC-MS. There was a significant increase in GSH levels at 24 hours post dose in both the 5mg/kg ($P = 0.0425$) and 10mg/kg ($P = 0.0292$) dose groups when compared to vehicle and at 6 hours post dose there was a significant decrease in GSSG levels in the 5mg/kg M102 dosed mice ($P = 0.0004$, Figure 3.8A & B).

In vehicle dosed animals, the ratio of GSH/GSSG was similar at 6 and 24 hours post dose, however at 5mg/kg there was a significant increase at 6 and 24 hours post dose ($P < 0.0001$ for 6 hours and $P = 0.0007$ for 24 hours). At 10mg/kg there was a significant increase in GSH/GSSG ratio at 24 hours ($P = 0.0008$) similar to that at 5mg/kg and no increase at 6 hours ($P = 0.9641$).

The increase in GSH/GSSG ratio shows mechanistic target engagement of NRF2 activation in the CNS, validating the increase in NRF2 targets seen by RT-qPCR.

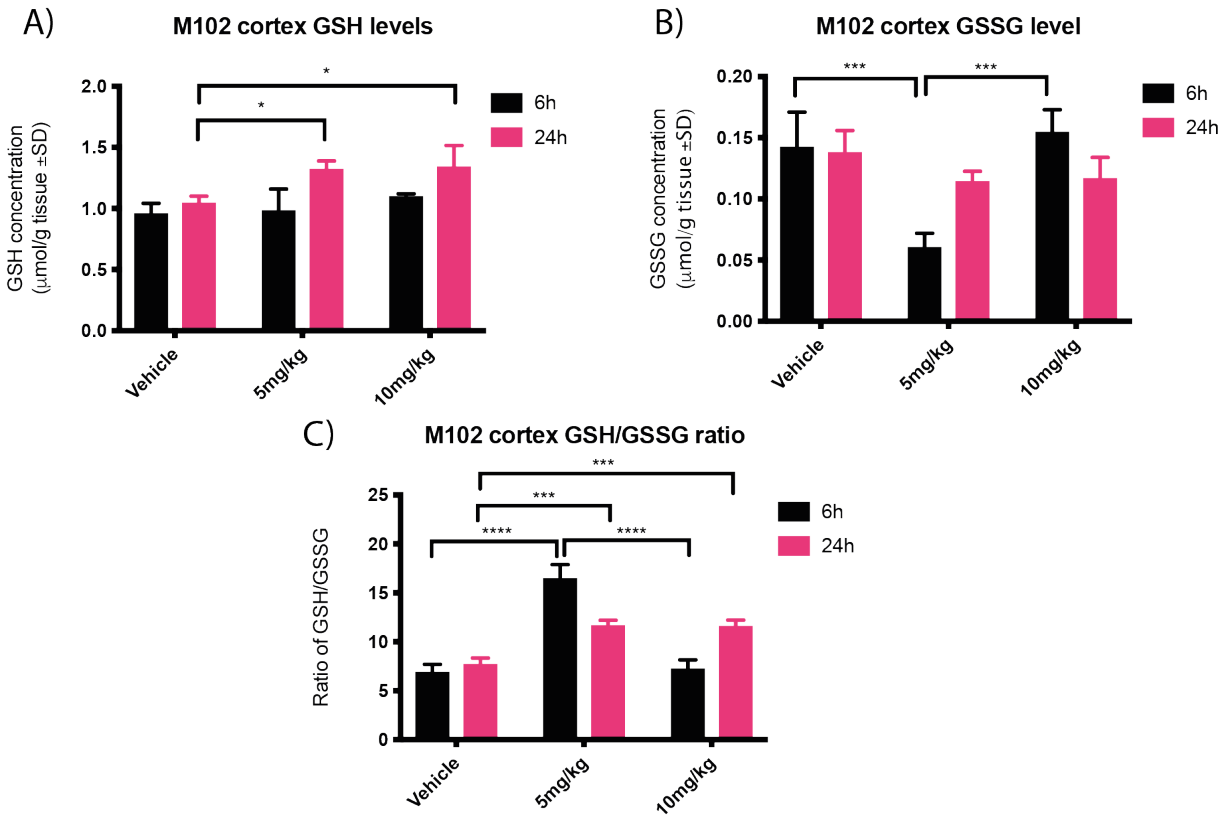

Figure 3.8: GSH and GSSG measurements from cortex samples of mice dosed for 7 days with M102 at 5mg/kg and 10mg/kg. Levels (µmol/g) of GSG and GSSG plotted as mean +/- SD for vehicle, 5mg/kg and 10mg/kg cortex samples at 6 hours and 24 hours post dose n=3. A) There was a significant increase in GSH levels at 5mg/kg and 10mg/kg at 24 hours post dose while levels at 6 hours post dose remain stable. B) Mean levels of Levels of GSSG were significantly reduced at 5mg/kg at 6 hours post dose when compared to vehicle. GSSG levels at 10mg/kg remained stable. C) The ratio of GSH/GSSG showed a significant increase at 6 hours post dose in the 5mg/kg samples, however in the 10mg/kg samples the ratio is similar to the vehicle samples. There was a significant increase in GSH/GSSG levels at 24 hours post dose in the 5mg/kg and 10mg/kg samples when compared to vehicle. (*p<0.05, ***p<0.001 ,****p<0.0001) two-way ANOVA with Sidak's multiple comparisons.

3.7. M102 in SOD1^{G93A} mice at an intermediate stage of disease 24 hours post dose

We next wanted to look at the effect of M102 as an NRF2 and HSF1 activator in the SOD1^{G93A} mouse model of ALS (Mead *et al.*, 2011). For this we used older animals that were between 112 and 116 days of age at the start of dosing, which is at an intermediate stage of disease. At this time point, mice have a substantial disease phenotype including an altered gait and weight loss, but no paralysis.

3.7.1. M102 in SOD1^{G93A} mice at an intermediate stage of disease study design

Animals were block randomised into 5 different dose groups, with 4 animals per group (Table 3.4). The 0.5mg/kg M102 dose level was removed as there was a limit on the number of animals available at the time of dosing and to increase the number of animals from 3 to 4 per group. The time point selected was 24 hours post dose as significant gene expression changes had been seen at this time point in WT mice.

The study was run in the same block design as the previous studies where one animal from each group was dosed on day one and then another was added on day 2 and so on until all animals were recruited. Animals were dosed for 7 consecutive days and tissue was collected 24 hours post final dose. Tissue was analysed at 24 hours as a compromise timepoint when the most robust changes in gene expression were seen.

Table 3.4: M102 in aged SOD1^{G93A} mice at 24 hours post dose showing dose levels of M102, mouse age, number of mice per group and collection time points.

mice	Age	Drug	Route of administration	Dose/Doses	n per group	Time point for collection
SOD1^{G93A}	113-116 days (Intermediate stage of disease)	M102	SC	Vehicle	4	24 hours only
			SC	1.5mg/kg		
			SC	5mg/kg		
			SC	10mg/kg		

3.7.2. M102 in SOD1^{G93A} mice at an intermediate stage of disease observations from dosing

Animals were monitored after the first dose. Mice dosed with 10mg/kg M102 showed slowing transient reduction in provoked behaviour but no severe adverse effects.

3.7.3. M102 in SOD1^{G93A} mice at an intermediate stage of disease gene expression

After 7 days of dosing, tissue was collected, and RT-qPCR was carried out on cortex samples using a range of optimised primers for downstream targets of NRF2 and HSF1 pathways. A sample of the WT vehicle from a previous study was run alongside the samples to get an idea

of the difference between the SOD1^{G93A} animals and a WT animal in terms of gene expression of the target genes.

Within the NRF2 target genes, there was a significantly higher expression level of *Pgc1a* (P = 0.0006), *Nqo1* (P = 0.0022) and *Hmox* (P = 0.0162) in the WT vehicle animals when compared to the SOD1^{G93A} vehicle (Figure 3.9A).

There was a significant increase in expression of *Hmox* in the 1.5mg/kg (P = 0.0188), 5mg/kg (P = 0.0388) and 10mg/kg (P = 0.0162) M102 dosed mice when compared to vehicle. There was no significant difference in expression with any of the M102 dosed groups when compared to vehicle of *Sqstm*, *Bag3, Pgc1a, Nrf1, Gclm. Nqo1* or *Gstp1*.

Within the HSF1 gene targets, there was a significantly higher expression level of *Dnajb1* (P <0.0001) and *Hspa1a* (P < 0.0001) in the WT vehicle group when compared to the SOD1^{G93A} vehicle group (Figure 3.9B).

There was an increase in *Hspa1a* in the 1.5mg/kg (P = 0.0064), 5mg/kg (P = 0.0052) and 10mg/kg (P = 0.0007) M102 dosed groups when compared to vehicle. There was no significant difference in the expression levels of *Dnajb1, Dnajc6, Hspa8, Hspb8, Dlg4* or *Syn1* between any of the M102 dosed groups and vehicle.

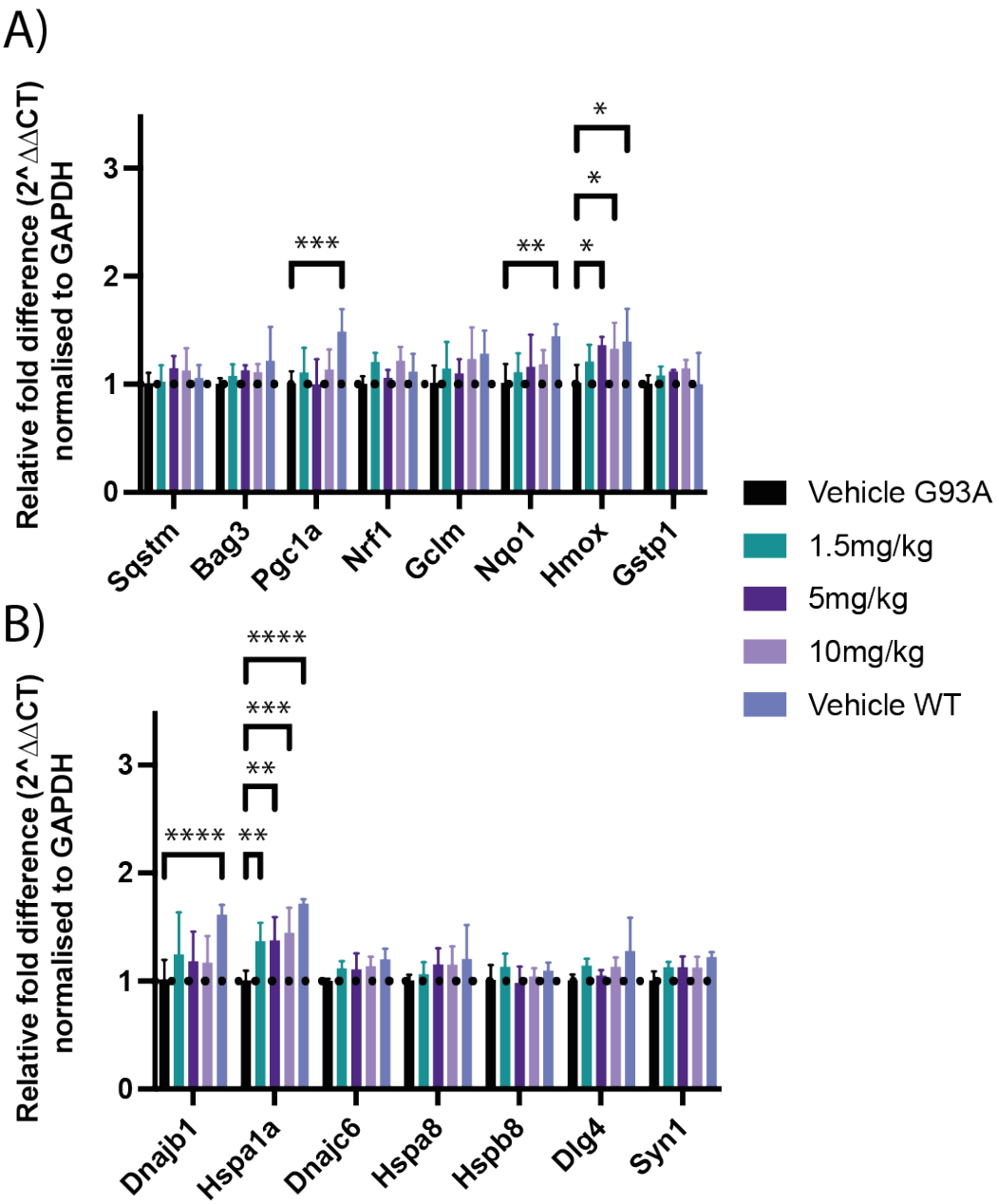

Figure 3.9: Relative expression of NRF2 and HSF1 targets in cortex tissue of SOD1^{G93A} mice at an intermediate stage of disease at 24 hours post final dose with M102 at varying concentrations. Data shown as relative expression (using the delta delta cT method) ± SD. A) Within the NRF2 targets, the WT vehicle animals showed significantly more expression of *Pgc1a*, *Nqo1* and *Hmox* when compared to the SOD1^{G93A} vehicle mice. There was also a significant increase in *Hmox* expression with 5mg/kg and 10mg/kg M102 when compared to vehicle. B) Within the HSF1 targets, the WT vehicle animals showed significantly higher expression of *Dnajb1* and *Hspa1a* when compared to the SOD1^{G93A} vehicle mice. There was a significant increase in Hspa1a expression of the 1.5mg/kg, 5mg/kg and 10mg/kg M102 dosed groups when compared to vehicle. N= 4, two-way ANOVA with Dunnett's multiple comparisons. (* = $p<0.05$, ** = $p<0.01$, *** = $p<0.001$, **** = $p<0.0001$).

These data demonstrate changes in NRF2 and HSF1 downstream targets in a mouse model of ALS at an intermediate stage of disease. These changes are significant but show a lower fold changes to targets compared to WT mice, with fewer targets being upregulated.

3.8. M102 in SOD1^{G93A} mice at an early and intermediate stage of disease 6 hours post dose

The previous study investigated the effects of M102 on cortex gene expression in SOD1^{G93A} mice at an intermediate stage of disease at 24 hours post dose. There were not as many changes in gene expression as were seen in the WT animals when dosed with M102 and it has been documented that the NRF2 pathway is dysregulated in ALS (Sarlette *et al.*, 2008). We wanted to explore if the gene expression changes occurred at a more transient timepoint (6 hours post dose) than 24 hours and to compare the differences between early disease stage (60 days) and intermediate stage (110 days) in SOD1^{G93A} mice, to determine if stage of disease influenced the capability of M102 to activate NRF2-directed transcription. At 60 days of age, mice have loss of motor neurons and perform worse on rotarod, but do not have visible signs of disease.

3.8.1. M102 in SOD1^{G93A} mice at an early and intermediate stage of disease study design

Mice were block randomised within their age categories and split into 5 different dosing groups (Table 3.5 and Table 3.6). The dosing group of 2.5mg/kg twice daily was added due to the conversion to the human subcutaneous dose level. At the time the predicted level of the mouse 5mg/kg dose to humans and the formulation of M102 shows that the volume would be too large to give in one subcutaneous injection. Therefore, this group has been added so that we can investigate the difference between 5mg/kg once daily and 2.5mg/kg twice daily. The two doses were given approximately 4 hours apart.

The difference between this study and previous studies is that the animals were not all dosed in a block design with one animal per dose group being dosed on the first day and more being added on subsequent days. This was due to the age of available animals not being as close as previous studies. The animals were therefore dosed in groups when they neared either 110 or 60 days, however they were block randomised as closely as possible and different dose

levels were collected on the same days, rather than all the animals from one dose group being collected on the same day. Animals were dosed for 7 consecutive days and tissue was collected at 6 hours post the first dose of the day. There were 3 animals per group.

Table 3.5: M102 in SOD1^{G93A} mice at an intermediate stage of disease showing dose levels of M102, mouse age, number of mice per group and collection time points.

mice	Age	Drug	Route of administration	Dose/Doses	n per group	Time point for collection
SOD1^{G93A}	110 days (intermediate stage of disease)	M102	SC	Vehicle	3	6 hours
			SC	1.5mg/kg		
			SC	2.5mg/kg twice daily		
			SC	5mg/kg		
			SC	10mg/kg		

Table 3.6: M102 in SOD1^{G93A} mice at an early stage of disease showing dose levels of M102, mouse age, number of mice per group and collection time points.

mice	Age	Drug	Route of administration	Dose/Doses	n per group	Time point for collection
SOD1^{G93A}	60 days (early stage of disease)	M102	SC	Vehicle	3	6 hours
			SC	1.5mg/kg		
			SC	2.5mg/kg twice daily		
			SC	5mg/kg		
			SC	10mg/kg		

3.8.2. M102 in SOD1^{G93A} mice at an early and intermediate stage of disease observations from dosing

It is known that M102R can cause injection site reactions in patients, related to its pharmacological effect (Poltawski *et al.*, 2008). We had not noted a particular issue during our previous studies but in this study a more extensive assessment of injection site reactions was performed. This involved shaving the mice to enable a close evaluation of injection site reactions. Some of the mice, developed inflammation and redness around the injection site. This was caused not only by the injection but also the animals scratching around the injection site. Similar issues were observed in vehicle dosed animals.

3.8.3. M102 in SOD1^{G93A} mice at an early and intermediate stage of disease gene expression

After 7 days of dosing, tissue was collected, and RNA was extracted from cortex and spinal cord. RT-qPCR was carried out on cortex samples using a range of optimised primers. Not all of the primers were carried out on this study, so the data set is currently incomplete. The first primers used were selected to cover NRF2 and HSF1 targets that have previously been upregulated with M102 dosing.

In the 60-day old animals, there was a significant increase in gene expression of *Hspa1a* in the 2.5mg/kg twice daily (P = 0.0066), 5mg/kg (P <0.0001) and 10mg/kg (P <0.0001) M102 dose groups when compared to vehicle (Figure 3.10A). There was no significant difference in the other NRF2 or HSF1 targets investigated with M102 dosing.

In the 110-day old animals, there was a significant increase in *Hspa1a* expression in the 1.5mg/kg (P = 0.0174), 2.5mg/kg twice daily (P <0.0001), 5mg/kg (P <0.0001) and 10mg/kg (P = 0.0373) M102 dose groups when compared to vehicle (Figure 3.10B). There was no significant difference in the gene expression of *Gclm, Hmox1, Nrf1, Hspa8* or *Syn1*.

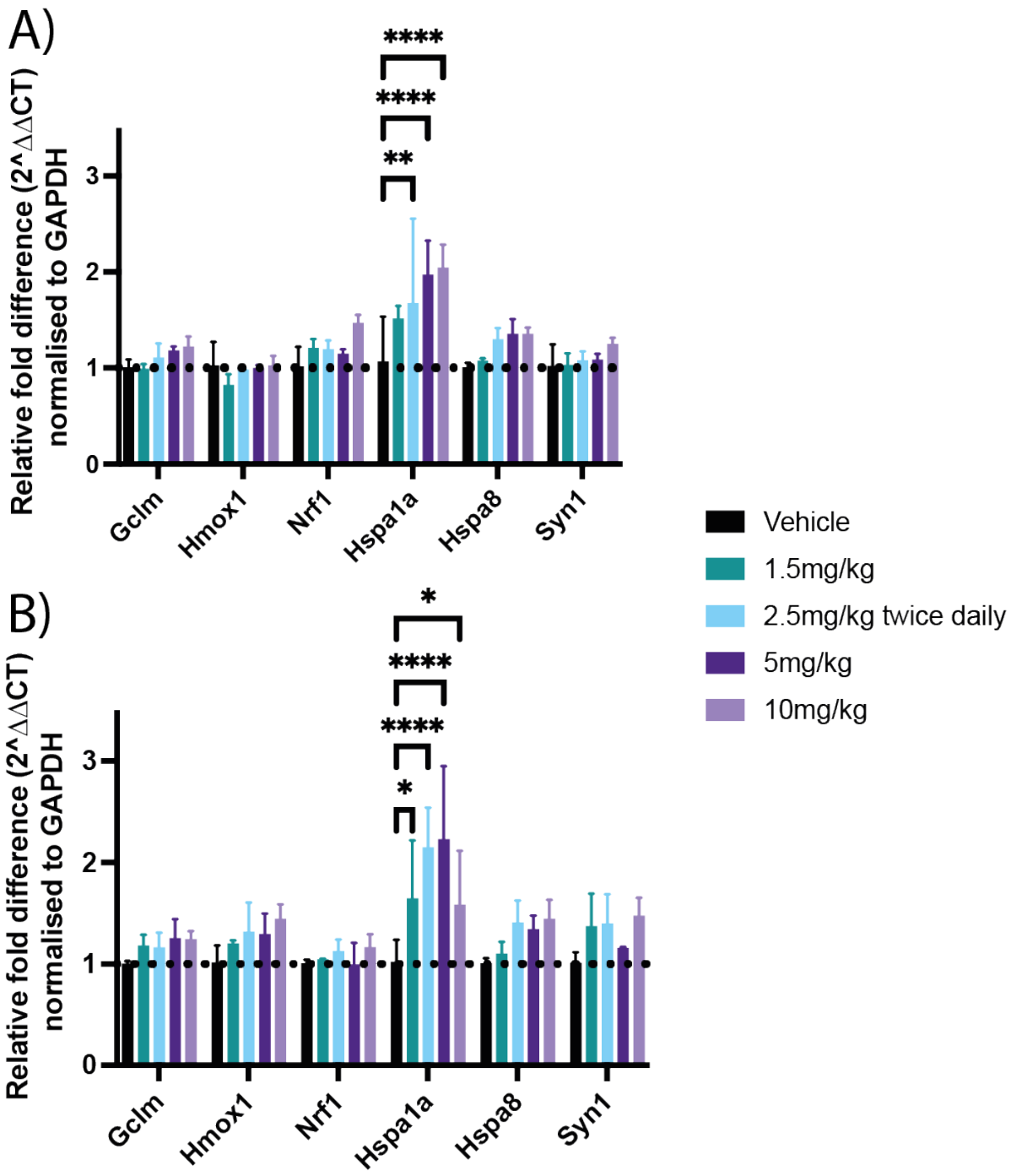

Figure 3.10: Relative expression in the cortex of SOD1^{G93A} mice at an early and intermediate stage of disease at 6 hours post dose with M102 at varying concentrations. Data shown as relative expression (using the delta delta cT method) ± SD. A) SOD1^{G93A} animals at 60 days of age showed a significant increase in relative expression of *Hspa1a* at 2.5mg/kg twice daily, 5mg/kg and 10mg/kg M102 when compared to vehicle. B) SOD1^{G93A} animals at 110 days of age showed a significant increase in expression of *Hspa1a* in the 1.5mg/kg, 2.5mg/kg twice daily, 5 mg/kg and 10mg/kg M102 dose groups when compared to vehicle. N = 3, two-way ANOVA with Dunnett's multiple comparisons. Carried out by Alex Danielle. (* = p<0.05, ** = p<0.01, *** = p<0.001, **** = p<0.0001).

These data show that there is activation of HSF1 targets in a mouse model of ALS at both an early and intermediate stage of disease.

3.9. Nanostring RNA quantification

RT-qPCR is a process involving multiple steps, including generation of cDNA and amplification of products, which could lead to increased experimental error. RT-qPCR also requires a lot of hands on time and is low throughput for targets. We wanted to explore alternative methods that would allow us to analyse the activity of larger arrays of gene targets at a higher throughput scale using either custom arrays or targeted arrays. The Nanostring n-counter system allows the analysis of larger arrays and the analysis uses counts of RNA molecules directly by using unique fluorescent barcodes rather than relying on amplification (Geiss *et al.*, 2008). Using the Nanostring n-counter also allowed the expansion into inflammatory targets and potentially other pathways that M102 may interact with. We first wanted to use the Nanostring n-counter to look at a variety of NRF2 and HSF1 target genes and validate the system against the results seen in RT-qPCR

RNA from the previous short-term dose studies was analysed using a custom array of probes for a list of defined targets. Due to the desire to compare across multiple experiments and the limitation on the number of samples that could be run, only certain dose groups were analysed. The samples that were run were: the vehicle, 5mg/kg and 10mg/kg dose groups for the WT mice at 6 hours post-dose; vehicle and 10mg/kg for the 110 $SOD1^{G93A}$ animals at 24 hours post-dose and all of the dose groups for the 60 and 110 day old $SOD1^{G93A}$ animals at 6 hours post dose. The results were analysed based on relative change from vehicle for each of the experiments.

The Nanostring results showed mild gene expression changes in the NRF2 and HSF1 gene targets in all the samples that were run (Figure 3.11). There is a clear distinction in the expression of genes between the intermediate stage disease and early stage disease $SOD1^{G93A}$ animals with many of the targets being increased in the young animals but decreased in the older animals, such as Hmox1 which is upregulated in the early stage disease animals but downregulated in the intermediate stage disease animals when compared to vehicle. This is expected as shown with the qPCR data, we were not able to activate the NRF2 pathway as

effectively in the later stages of disease. This is also backed up by research showing that the NRF2 pathway is dysfunctional in ALS (Mimoto *et al.*, 2012).

The changes in NRF2 and HSF1 targets seem to vary in the WT animals, with some canonical NRF2 activation such as *Osgin1, Nqo1* and *Gclm* being downregulated in the WT animals after M102 dosing. It would be expected that the canonical NRF2 downstream targets would be upregulated in the WT animals as M102 activates the NRF2 pathway (Mead *et al.*, 2013). However, different downstream targets could be activated at different time points after activation of the pathway.

The most substantial changes in gene expression are seen in the inflammatory targets. There was a decrease in expression of *Il1a*, *Il12b* and *Nos2* in the 110-day old $SOD1^{G93A}$ mice which are not seen in the younger 60-day old mice.

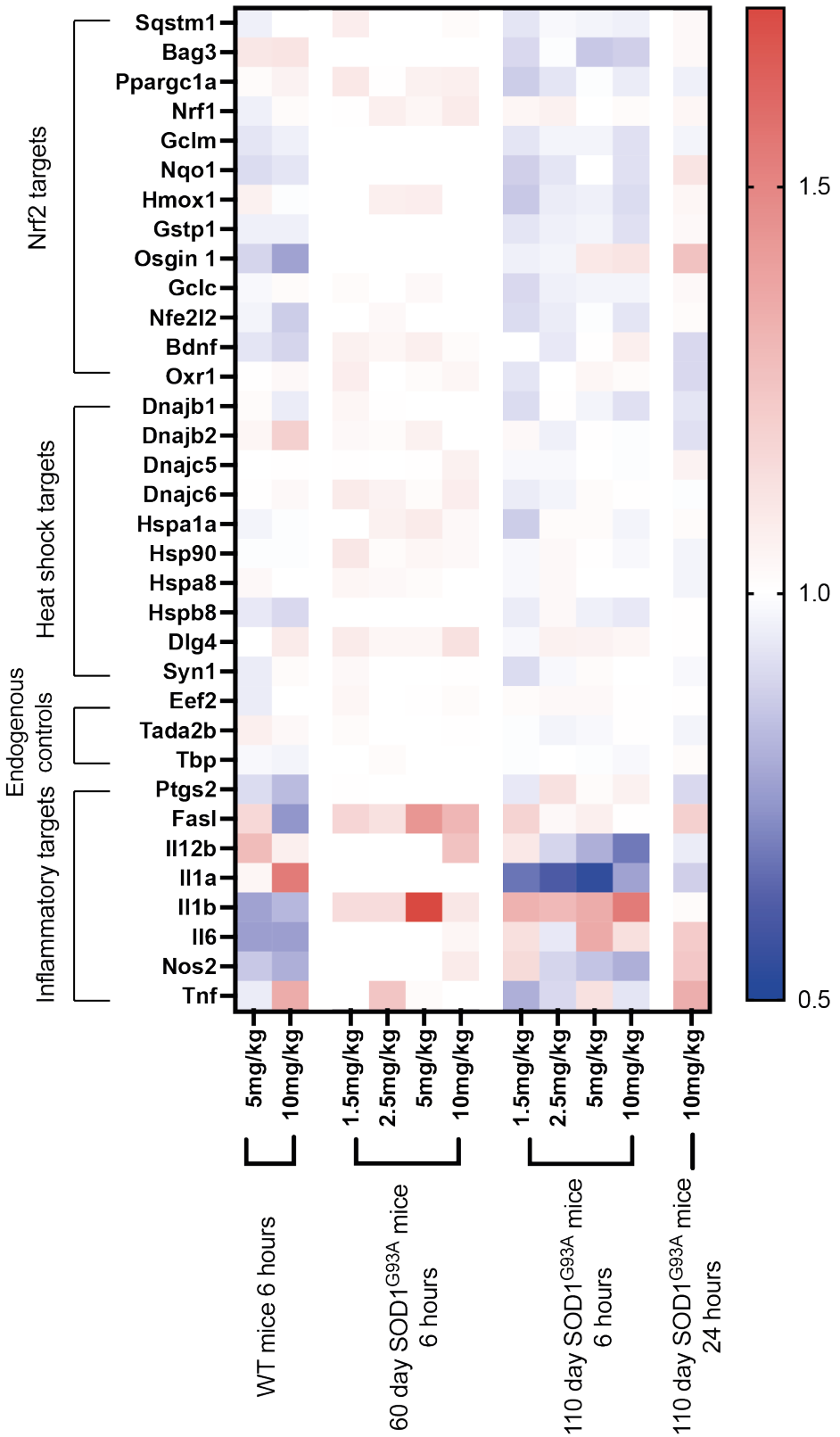

Figure 3.11: Expression levels of target RNA in samples from the different seven day dose studies. Data are normalised to three endogenous controls and each group is shown as relative RNA expression change compared to the vehicle within the same experiment. N = 3-4 mice per group.

3.9.1. NanoString vs RT-qPCR analysis

There was a difference in expression of genes when calculated through the NanoString and via qPCR. To determine if these were significantly different the log_2 of the NanoString ratio data were plotted against the Log_2 of the relative expression of the qPCR data to determine if there is a correlation between the two methods. The results plotted were the mean ratios per group when normalised to the appropriate vehicle.

Figure 3.12 shows the correlation between the two assays for 15 genes that were run on both assays. The results showed that a few of the genes are highly correlated between the two assays, such as *Bag3* (R^2 = 0.9150), *Dnajc6* (R^2 = 0.9903) and *Hspb8* (R^2 = 0.9301). *Bag3* and *Dnajc6* were positively correlated, suggesting that increased expression was detected using both methods, whereas *Hspb8* is negatively correlated, suggesting that expression of *Hspb8* is not similar between the two assays.

There are also examples of genes which are not highly correlated such as *Gclm* (R^2 = 0.0763), *Gstp1* (R^2 = 0.0480), *Hmox1* (R^2 = 0.0005), *Hspa1a* (R^2 = 0.0773), *Hspa8* (R^2 = 0.0707) and *Syn1* (R^2 = 0.0261), suggesting that the assays did not agree in gene expression of these genes.

It was concluded that although NanoString enabled expanded and more rapid analysis of gene expression that it did not correlate well with the gold standard of RT-qPCR for those genes that were run in both assays so was not taken forward into other experiments presented in this thesis.

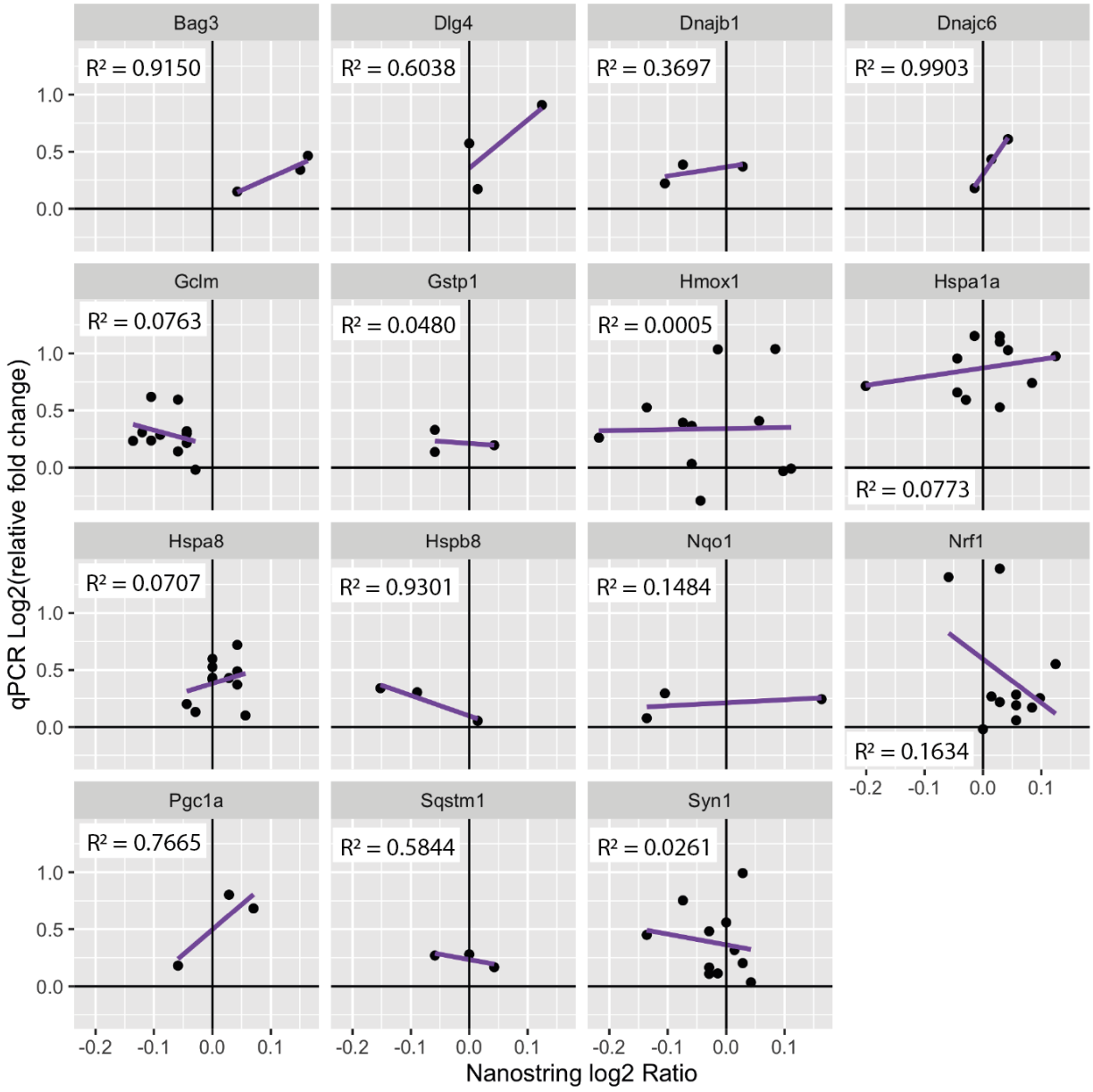

Figure 3.12: Comparison of NanoString and qPCR analysis of genes. Data shown as the log2 ratio of the NanoString data vs the log2 of the relative fold change seen in qPCR. Individual points are the values per group vs vehicle. Data sets included are those run on the NanoString vs the appropriate gene in qPCR. Purple line shows regression line.

3.10. Discussion

3.10.1. Endogenous controls

It was discovered that *Gapdh* and *Eef2* were the most appropriate endogenous controls to use for the RT-qPCR data. *ß-actin* was shown to increase in expression when compared to *Gapdh* at 24 hours post dose when animals were dosed with M102, making it an inappropriate control to compare relative changes in gene expression of target genes. The expression

changes in *ß-actin* are dose dependent, suggesting that M102 may have an effect on the levels of *ß-actin*.

3.10.2. ARE reporter cell line data show M102 is more efficacious than M102R

Data from the ARE reporter cell assay show that the EC_{50} for M102 $2.5x10^{-5}$ M is and for M102R is $1.54x10^{-6}$ M. These data suggest that M102R is more efficacious than M102, however the fitting of the curve for analysis of EC50 is difficult for M102R. Looking at the change in induction, M102 is much higher and is more similar to Omaveloxolone than M102R, suggesting that M102 is more efficacious than M102R, which has been seen previously in this cell assay (Mead *et al.*, 2013). Although the reason for this higher potency of M102 is unknown, it could be that M102 is more easily oxidised than M102R to create a more reactive metabolite. Another reason could be a differential binding interaction with areas of KEAP1 surrounding reactive cysteine residues, which would influence the interaction. This has been seen with another electrophilic NRF2 activator Bardoxolone methyl, where non-covalent interactions with the BTB domain of KEAP1 close to C151 increase activity of the interaction with the cysteine (Cleasby *et al.*, 2014).

3.10.3. Observations from dosing of M102 and M102R

Observations from mice dosed with M102R showed evidence of dopamine agonism as mice showed classic signs of dopamine agonism including hyperactivity (S. Wang *et al.*, 2013). The dopamine agonist response activity of M102R been well documented and is the reason that M102R is used as a treatment for PD (Boyle and Ondo, 2015). We also observed a mild straub tail reaction in the doses we used in this project which is typical of apomorphine dosing (Bilbey *et al.*, 1960). The straub tail reaction is where the mice hold their tails straight and perpendicular to the floor and it has been linked to dopamine receptor activation (Zarrindast *et al.*, 1993).

M102R is shown to be a dopamine receptor agonist and to increase locomotor activity in mice but M102 has been shown to be a dopamine receptor antagonist (van Hooft and Vijverberg, 1998). From the dosing studies it was observed that animals dosed with M102R showed increased activity and there was mild ataxia in animals dosed with M102 at 15mg/kg along with subdued behaviour.

The skin irritation seen on the mice dosed with M102 seems to be from a combination of injection site inflammation exacerbated by animals scratching the injection site. This irritation has been shown with subcutaneous dosing of apomorphine in patients with PD (Poltawski *et al.*, 2008). Irritation varies between patients and also varied between mice, however the severity of the scars formed on the mice never reached a stage where it was negatively impacting the mice.

3.10.4. Activation of NRF2 and HSF1 pathways is greater with M102 than M102R *in vivo*

From the first few studies, we saw that there was a greater upregulation of NRF2 and HSF1 downstream targets with M102 when compared with M102R. This may be due to the increased NRF2 activation potency of M102 when compared to M102R, which was seen in the cell assay. M102 was also able to be dosed at higher doses than M102R as seen by the adverse event profile of both compounds which likely is reflected in the dopamine agonist activity of M102R. Due to the lack of dopamine agonism of M102, it was previously chosen for testing in the $SOD1^{G93A}$ mouse model (Mead *et al.*, 2013) and these studies confirmed the validity of this selection.

3.10.5. M102 activation of NRF2 and HSF1 downstream targets is greater in WT animals than in an ALS mouse model

In the WT animals dosed with M102, there was evidence of activation of the HSF1 pathway as downstream markers such as *Hspa1a, Hspa8, Dlg4* and *Syn1* levels are elevated with dosing of M102 when compared to vehicle dosed animals at 6 and 24 hours post dose. *Hspa1a, Hspa8* and *Dnajc6* are important chaperones for refolding of proteins or targeting misfolded proteins to autophagy (Cristofani *et al.*, 2017). These are interesting targets in ALS due to the misfolding of TDP-43, SOD1 or FUS proteins that are present in ALS cases (Ross and Poirier, 2004).

The relative fold change in the activation of genes in the intermediate stage disease $SOD1^{G93A}$ animals compared to the WT animals is lower, even though the animals are on the same background and from the same colony of mice (summarised in Table 3.7). This could be due to a variety of reasons such as the NRF2 pathway being harder to activate in these animals as it is potentially dysfunctional in ALS (Mimoto *et al.*, 2012). However, the 60-day old early disease stage $SOD1^{G93A}$ mice also had limited activation of NRF2 gene targets, suggesting the difference in activation may not be entirely down to progression of the disease. The $SOD1^{G93A}$

animals at 60 days of age don't have visible signs of disease, but they have a reduction in rotarod performance and loss of motor neurons so the NRF2 pathway could already be disrupted and harder to alter at this age.

Table 3.7: Summary of upregulation of NRF2 and HSF1 targets from cortex tissue from short term dosing studies. Yes = upregulation of gene compared to control, no= no change in expression, N/A = not carried out.

Gene		Wild type mice		SOD1^{G93A} animals		
				Early disease	Intermediate	
		6h	24h	6h	6h	24h
Nrf2 targets	Sqstm1	no	no	N/A	N/A	no
	Bag3	no	no	N/A	N/A	no
	Pgc1a	no	yes	N/A	N/A	no
	Nrf1	yes	yes	no	no	no
	Gclm	no	no	no	no	no
	Nqo1	no	no	N/A	N/A	no
	Hmox1	yes	yes	no	no	yes
	Gstp1	no	no	N/A	N/A	no
HSF1 targets	Dnajb1	no	no	N/A	N/A	no
	Hspa1a	yes	yes	yes	yes	yes
	Dnajc6	no	no	N/A	N/A	no
	Hspa8	no	yes	no	no	no
	Hspb8	no	no	N/A	N/A	no
	Dlg4	yes	no	N/A	N/A	no
	Syn1	yes	no	no	no	no

When NRF2 activators are tested in the SOD1^{G93A} model, it is quite often seen that they have an effect earlier on the disease progression, such as an improved rotarod score and a delay in onset of disease symptoms, however it is much harder to alter the later stages of the disease and many compounds do not show extended survival, such as M102 in Mead *et al*. 2013 (Mead *et al.*, 2013). It may be harder to regulate this stage of disease because progression is so rapid but it may also reflect differential activation of the Nrf2 pathway. However, one study showed an increase in survival in a SOD1^{G93A} mouse model using CDDO ethylamide and CDDO trifluorethylamide (Neymotin *et al.*, 2011). Some electrophilic NRF2 activators have the ability to activate other pathways, and the activation of other pathways may help with neuroprotection at later stages of disease progression when NRF2 activity may be dysregulated.

As well as cortex tissue analysis, there was RT-qPCR analysis of expression changes in the spinal cord tissue for WT mice. However, these data were a lot more variable, potentially due to the lower yield of RNA from the spinal cord (data not shown). The hypothesis is that the activation in cortex and spinal cord should be similar, however this is still being investigated.

3.10.6. Inflammatory targets

We wanted to explore the effects of NRF2 activation on inflammatory targets, such as *Il6* and *Il1b*. NRF2 has been shown to have anti-inflammatory properties through the suppression of proinflammatory cytokines (Kobayashi *et al.*, 2016), which could potentially ameliorate the neuroinflammation that is seen in ALS (Komine and Yamanaka, 2015). However optimising primers for RT-qPCR for inflammatory targets has proved to be difficult. Multiple primers were designed for the inflammatory targets however they mostly failed on the second stage of optimisation. This may be due to the low abundance of inflammatory targets in cortex from both WT and $SOD1^{G93A}$ mice. In cDNA from cell samples the inflammatory primers worked well (data not shown), suggesting an abundance issue in cDNA from mouse cortex tissue.

3.10.7. NanoString data

The NanoString system offers many advantages over qPCR analysis, such as the ability to test a larger number of genes at a time, using RNA rather than converting RNA to cDNA and thus reducing variability by limiting the number of steps and the amount of hands-on time required to generate results. NanoString data are given as actual number of RNA molecules and are therefore directly quantitative and claimed to be more sensitive and robust than RT-qPCR methods that use PCR amplification of cDNA products for one gene normalised to a house keeping gene. Fewer steps also reduce variability from human error or inaccuracies across multiple different qPCR plates.

The NanoString data produced were normalised to three endogenous control genes (*Eef2, Tada2b* and *Tbp*) and then a ratio was formed to show gene expression between the M102 dose groups and the vehicle for each of the experiments. Unfortunately, there was very little correlation between the fold changes seen in the NanoString vs RT-qPCR when looking at NRF2 and HSF1 targets. Looking at the correlation between the NanoString and RT-qPCR data in terms of gene expression showed a range of results, with some genes showing good positive correlation between the two assays and most of the genes showing minimal or poor

correlation between the assays (Figure 3.12). There could be several reasons for this lack of correlation between the genes, such as the sensitivity of both assays or differences in the probes used for the targets between the two assays, meaning that they were targeted to different variants of the same gene. This poor correlation between the gene expression on the NanoString and via traditional RT-qPCR has also been seen in other studies (Adam *et al.*, 2016; Bergbower *et al.*, 2020; Prokopec *et al.*, 2013), suggesting that the two methods do not show relative gene expression changes equally. Prokopec *et al.* show that the NanoString results correlated with microarray and open array results and not as well with RT-qPCR results (Prokopec *et al.*, 2013).

It has been suggested that the poor correlation could be due to the abundance of target RNA in the samples (Bergbower *et al.*, 2020) and the NanoString offers the ability to look at the raw counts of targets per gene of interest. There are very low raw counts for quite a few of the targets that we investigated, however there was no correlation between the raw counts and the correlation seen between NanoString and qPCR.

Unfortunately, due to the lack of optimised inflammatory targets primers, I am unable to make comparisons between the RT-qPCR and NanoString for these, which were the genes with the most significantly different gene expressions from the NanoString analysis. However, the raw count values for a large number of inflammatory targets were very low, suggesting that it may be abundance issues making it difficult to optimise inflammatory primers via RT-qPCR.

It has been shown that NRF2 can inhibit the transcription of pro inflammatory cytokines such as *Il6* and *Il1b* in a mechanism that is independent of AREs (Kobayashi *et al.*, 2016). From NanoString data, there were decreases in *Il6* and *Il1b* expression in WT mice dosed with M102, but an increase in these targets in the $SOD1^{G93A}$ mice at the intermediate stage of disease. Although these results need to be investigated more, the changes in these proinflammatory targets are interesting. The difference in the data between our study and Kobayashi *et al.* could be due to cell type. In Kobayashi *et al.* they focused on macrophages (Kobayashi *et al.*, 2016), whereas our data was on cortex tissue, which contains a variety of different cell types that could express cytokines in different levels.

3.10.8. GSH/GSSG measurements

Glutathione levels in tissue are a good indicator of the reducing power of the cells, a high amount of reduced glutathione is able to remove reactive oxygen species and therefore prevent the damage they can cause (Lu, 2009). The results of the GSH and GSSG measurements show an increase in the GSH/GSSG ratio suggesting more reducing power in the cells. The results also suggest there is no further benefit of dosing at 10mg/kg M102 over the 5mg/kg M102 dose. This was only carried out on the two highest doses of M102 in the WT mice and it would be interesting to see the effect on glutathione levels in other doses of M102 and also within the $SOD1^{G93A}$ model of mice in order to compare the changes that have already been found.

NRF2 activates a number of genes involved in glutathione synthesis and maintenance, such as *Gclm, Gclc* and *GSR* (Harvey *et al.*, 2009). Improvement in the GSH/GSSG in the cortex suggests activation of these genes, potentially through NRF2 activation, thus validating a downstream effect of NRF2 activation. Although we saw an increase in *Gclm* expression with M102R, there was no significant increase with M102 dosing, but further analysis would be required to explore more GSH synthesis and maintenance targets as there are many involved that are regulated by NRF2.

Glutathione can be imaged by MRS in the cortex of humans with fairly high accuracy (Anton *et al.*, 2022). Glutathione, as well as other metabolites, can also be imaged in mice under anaesthesia (Hsu *et al.*, 2021). The ability to detect changes in both patients and animals in real time and at multiple timepoints allows the ability for GSH levels to be used as a translatable biomarker for the activation of drug effects. This would be extremely valuable in future clinical trials to measure target engagement.

4. Results: M102 administration in TDP-43^{Q331K} mice

4.1. Introduction

Previously I have shown that M102 activated NRF2 directed transcription *in vitro* and NRF2 and HSF1 transcription factors *in vivo*. Importantly I have shown that these pathways were activated in the CNS, which is the tissue of interest in ALS and shows that M102 is able to cross the blood brain barrier.

M102 has previously been dosed in the SOD1^{G93A} mouse model of ALS after first being identified as an NRF2 activator (Mead *et al.*, 2013). This previous study showed that mice dosed once daily subcutaneously with M102 at 5mg/kg had a slowing of early rotarod decline and an improvement in forelimb and hindlimb stride length when compared to vehicle dosed mice (Mead *et al.*, 2013). Tissue analysis showed increased muscle innervation in the gastrocnemius muscle of the M102 dosed group when compared to the vehicle group and M102 caused a reduction in oxidised glutathione levels in the spinal cord (Mead *et al.*, 2013). These data suggest that the M102 at 5mg/kg dosed subcutaneously can slow disease progression in the SOD1^{G93A} mouse model by increasing levels of NRF2 regulated genes (*e.g. Hmox1* and *Nqo1*) in the CNS and leading to a reduction in oxidative stress shown by the reduction in oxidised glutathione. However, there was no increase in survival of mice when compared to vehicle. These promising results suggest that M102 may be able to relieve symptoms in patients with ALS, however this need to be investigated further to determine if the effect is robust.

Having *in vivo* data from multiple mouse models of ALS is beneficial to better understand the action of M102 and to determine if it has efficacy in multiple different mouse models, which may give it a better chance of translating to ALS in humans. This is particularly important because of the lack of translation historically between the SOD1^{G93A} mouse model and human disease, as discussed previously (Scott *et al.*, 2008). For these reasons we decided to test M102 in a second mouse model of ALS.

The mouse model we used is a transgenic TDP-43^{Q331K} model. These TDP-43^{Q331K} mice were obtained from the Jackson Laboratory (stock number 017933), where they were deposited by Arnold *et al.* on a C57BL/6Ncrl background (Arnold *et al.*, 2013). The TDP-43^{Q331K} transgenic

mouse model has been backcrossed onto a C57BL/6NJ background and extensively characterised in house (Watkins *et al.*, 2021). From this in house analysis and previous characterisation, the model shows ALS and FTD phenotypes that develop over time. The phenotype of the TDP-43^{Q331K} mice is milder than in the SOD1^{G93A} mice and they do not reach an end point based on severity of disease but do develop a progressive motor and cognitive phenotype. Based on previous data it is possible to determine differences between WT and transgenic mice in many behavioural assays, such as a reduction in rotarod performance and increased unsteadiness of gait in transgenic mice up to 6 months of age (Watkins *et al.*, 2021) (Figure 1.3). The TDP-43^{Q331K} mouse model may be more representative of ALS patients due to the milder phenotype and the overlap of ALS and FTD features, which is observed in patients, as well as the fact that SOD1^{G93A} mice may only represent a small number of patients with SOD1 mutations.

ALS and FTD overlap clinically and share genetic mutations such as *C9ORF72, FUS* and *SQSTM1* as well as TDP-43 pathology (Abramzon *et al.*, 2020). TDP-43 inclusions are found in almost all cases of ALS and about half of FTD cases. A knock-in TDP-43^{Q331K} model has shown cognitive defects that align with FTD phenotypes as well as motor defects that can be attributed to ALS phenotypes (White *et al.*, 2019). White *et al.* showed a decrease in brain volume in areas equivalent to the temporal lobe, neuron loss in the entorhinal cortex as opposed to the motor cortex, as well as significant weight gain, which could be attributed to the hyperphagia seen in FTD patients (White *et al.*, 2019). These mice have also been shown to have apathy-like behaviour and perseveration, showing cognitive decline of these mice compared to NT litter mates (Kim *et al.*, 2020). Our in-house analysis has shown that, similar to the knock-in mice, the TDP-43^{Q331K} mice have increased weight gain indicative of an FTD phenotype (Watkins *et al.*, 2021).

Many transgenic mouse models rely on overexpression of the target gene or mutated target gene, and it has been shown that overexpression of TDP-43 (WT and mutant) in mice causes ALS phenotypes in a dose dependent way (Wils *et al.*, 2010). Loss of TDP-43 in mice has also been shown to cause a neurodegeneration phenotype (Iguchi *et al.*, 2013). Together this shows that both gain, and loss of TDP-43 function causes motor neuron degeneration in mice, suggesting correct regulation of TDP-43 is vital for correct neuron functioning.

The TDP-43^{Q331K} model used in this project matches TDP-43 transgene expression to endogenous mouse expression of TDP-43, with the mice expressing human TDP-43 mRNA levels of between 1 and 1.5x that of endogenous mouse levels in neuronal tissue (Arnold *et al.*, 2013). The in-house characterisation of the model showed that the TDP-43^{Q331K} mice had increased expression of human *TDP-43^{Q331K}* mRNA in cortex (<3 fold), spinal cord (2 fold) and hindlimb muscle (4 fold) when compared to the TDP-43^{WT} mice and a reduction in endogenous mouse *Tardbp* mRNA (Watkins *et al.*, 2021). This increase in TDP-43 levels could be dependent on the Q331K mutation causing dysregulation of TDP-43 and the decrease in mouse TDP-43 could be due to autoregulation of TDP-43. We have the equivalent colony of WT human TDP-43 mice, which are good controls for the TDP-43^{Q331K} mice. These WT mice also have equivalent human TDP-43 levels compared to controls and show no signs of motor degeneration seen in the TDP-43^{Q331K} model, demonstrating that endogenous levels of WT TDP-43 in the mouse model does not cause neurodegeneration and the phenotype seen in the TDP-43^{Q331K} mice is due to the Q331K mutation in TDP-43.

There are several different tests that can be carried out to follow disease progression and assess the impact of therapeutics in mouse models, one of which is examining motor unit function using electrophysiology. Electrophysiology is used as part of the diagnosis process and to track progression of ALS in patients (de Carvalho *et al.*, 2008). Studies have shown that electrophysiological measures in humans correlated with clinical severity and motor function (Arnold *et al.*, 2014), making it a powerful tool in clinical trials to monitor progression of ALS. Use of electrophysiological techniques in animal models of neurodegenerative disease has increased and has now become a robust measurement to follow disease progression and monitor drug treatments *in vivo* due to the ability to carry out repeated measurements in the same mice over time. The advantage of electrophysiology measurements in mice is that they are able to detect early changes in disease progression before the onset of symptoms appear in behavioural assays (Mancuso *et al.*, 2011). Due to the translatability of the technique from mouse models to humans, it has the potential to speed up drug development in terms of translation from animal models to human clinical trials (Arnold *et al.*, 2015), something that is much needed in ALS research (Scott *et al.*, 2008).

In this study we measured compound muscle action potential (CMAP) amplitude as a measure of the output of motor units in the hind limb of mice. We chose to use surface ring electrodes

rather than needle electrodes due to the consistency of ring electrode recordings, however this technique will miss differences within individual muscles as it is a measure of the combined muscles in the hind limb (Arnold *et al.*, 2015). We also investigated repetitive nerve stimulation (RNS), which uses 10 pulses of 10Hz and determines the difference in CMAP amplitude over all 10 stimuli. RNS is used in ALS and other neurodegenerative disorders to test the function of neuromuscular junctions, with healthy neurons and muscles producing no decrease in CMAP amplitude over the 10 stimuli and ALS patients showing a decrease in CMAP amplitude over the quick repetitive stimulations (Fu *et al.*, 2019).

Another test used to test progression of disease is marble burying. Marble burying is a test that involved placing individual mice in fresh cages with marbles and counting the number of marbles buried after 30 minutes (Deacon, 2006). Previously marble burying has been used as a screening procedure for anxiolytics due to the defensive digging behaviour observed in mice in response to aversive stimuli, and a reduction in burying behaviour was correlated with a reduction in anxiety (Broekkamp *et al.*, 1986). However, whether mice are burying marbles due to anxiety and aversive behaviour has been debated. Digging behaviour has been observed in mice to non-aversive stimuli such as food pellets, and mice have been shown to not actively avoid marbles when given the opportunity to (Thomas *et al.*, 2009). Marble burying also corelated poorly with other anxiety measures in mice and may be more of a measure of intrinsic digging behaviour rather than anxiety (de Brouwer *et al.*, 2019; Thomas *et al.*, 2009). In the knock-in TDP-43^{Q331K} mouse model, there was a reduction of marble burying behaviour when compared to WT mice, which was attributed to cognitive impairment and linked to the FTD phenotype seen in these mice (White *et al.*, 2019). The transgenic TDP-43^{Q331K} mice show levels of reduced activity and apathy, so we used marble burying as a measure of normal exploratory behaviour to determine if this was altered in M102 dosed mice when compared to vehicle.

4.2. Aims

- To investigate the pharmacology and efficacy of M102 in the TDP-43^{Q331K} ALS mouse model.
- To compare M102 dosed at 2.5mg/kg twice per day vs 5mg/kg once per day with respect to efficacy.

4.3. Study design

At the point of starting this study, M102 was difficult to formulate for subcutaneous dosing to humans and the human equivalent of the mouse 5mg/kg dose at the time would mean that the volume would be too large to inject into humans. Therefore, two dose levels were chosen to be dosed to the mice: 2.5mg/kg twice a day and 5mg/kg once a day. This was chosen to compare the efficacy and tolerability of a twice daily dose compared to the once daily dose so that if the formulation could not be improved it may be possible to dose patients twice per day.

Dosing twice a day vs once a day will lead to different concentration time profiles of M102 in the target CNS tissues. Two smaller doses will lead to smaller Cmax but potentially the same AUC (Tuntland *et al.*, 2014). Since we know that M102 has a short half-life, it may be more beneficial to dose twice per day as then there will be activation of NRF2 and HSF1 pathways at multiple points during a 24-hour period. However, because of the lower dose, and therefore lower Cmax, it may be difficult to reach the concentration of drug required in the CNS to activate the transcription factors and have beneficial effects on the progression of disease.

Transgenic female TDP-43^{Q331K} mice were dosed from 25 days of age until 6 months of age based on the previous in-house data that show a difference in behavioural analysis of NT and transgenic mice at this time point. Based on power analysis, there were 14 mice assigned to each group, which gives power to detect changes in rotarod, neuroscoring, weight and catwalk parameters (Watkins *et al.*, 2021). Mice were assigned to dosing groups via block randomisation to separate litter mates throughout the dose groups to distribute the source of variability that comes from different litters. The dosing groups were vehicle, M102 2.5mg/kg twice daily and M102 5mg/kg once daily subcutaneously injected.

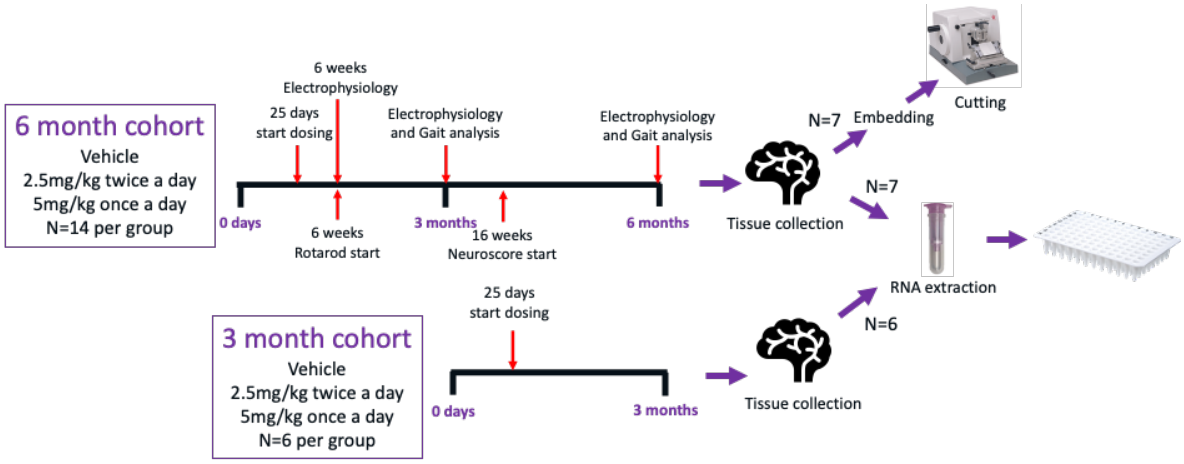

Figure 4.1: Study design and timeline for the M102 dose study in TDP-43^{Q331K} mice, showing timepoints of behavioural testing and an overview of tissue analysis.

Various behavioural tests were carried out throughout the study (Figure 4.1) based on the progression of the disease and previous characterisation (Figure 1.3). Rotarod was carried out once per week from 40 days of age and neuroscoring was carried out weekly from 16 weeks of age. Gait analysis was carried out at 3 and 6 months of age using the Catwalk gait analysis system (Noldus). Electrophysiology was carried out at 6 weeks, 3 months and 6 months of age to determine CMAP and repetitive stimulation in the hind limbs. Marble burying was carried out at 6 months of age. These time points were chosen based on previous data (Watkins *et al.*, 2021).

Tissue collected at the end of the study was split into collecting half of the mice per group snap frozen for RT-qPCR and protein analysis and half of the mice per group through fixation for staining analysis. Brain and spinal cord were collected and gene expression analysis of downstream targets of the NRF2 and HSF1 pathways were explored in cortex tissue to show target engagement and activation of these pathways in target tissue. Histological analysis included glial staining to determine activity of astrocytes and microglia, and staining of neurons to detect loss of motor neurons and if M102 is able to slow this loss.

A satellite cohort of mice (n=6 per group) were dosed from 25 days of age until 3 months of age for tissue collection and analysis and did not undergo behavioural analysis. Tissue was collected snap frozen for qPCR and protein analysis at 3 months of age.

4.4. Results

4.4.1. Mouse weights 6-month cohort

Mouse weight was recorded daily with dosing to calculate dose volume and to determine if there was an effect of M102 when compared to the vehicle group. In the 6-month cohort, mice were weighed daily before dosing from 25 days of age until 6 months of age. Transgenic TDP-43^{Q331K} mice gain significantly more weight than WT or NT mice over the course of their life and become significantly heavier than NT animals. This has previously been shown to be associated with increased food intake in these mice (Previous in-house data). In this study there was a significant decrease in weight in the M102 2.5mg/kg twice daily dosed mice when compared to vehicle dosed mice towards the end of the study (Figure 4.2). At the end of the study at 177 days of age, M102 2.5mg/kg twice daily dosed animals weighed 23.2 ± 1.9g whereas vehicle animals weighed 25.3 ± 2.3g (P = 0.0316). There was no significant difference at 177 days between the M102 5mg/kg (24.5 ± 1.6g) dosed mice when compared to vehicle dosed mice (P = 0.4911, mixed-effect analysis with repeated measures and Dunnett multiple comparison test).

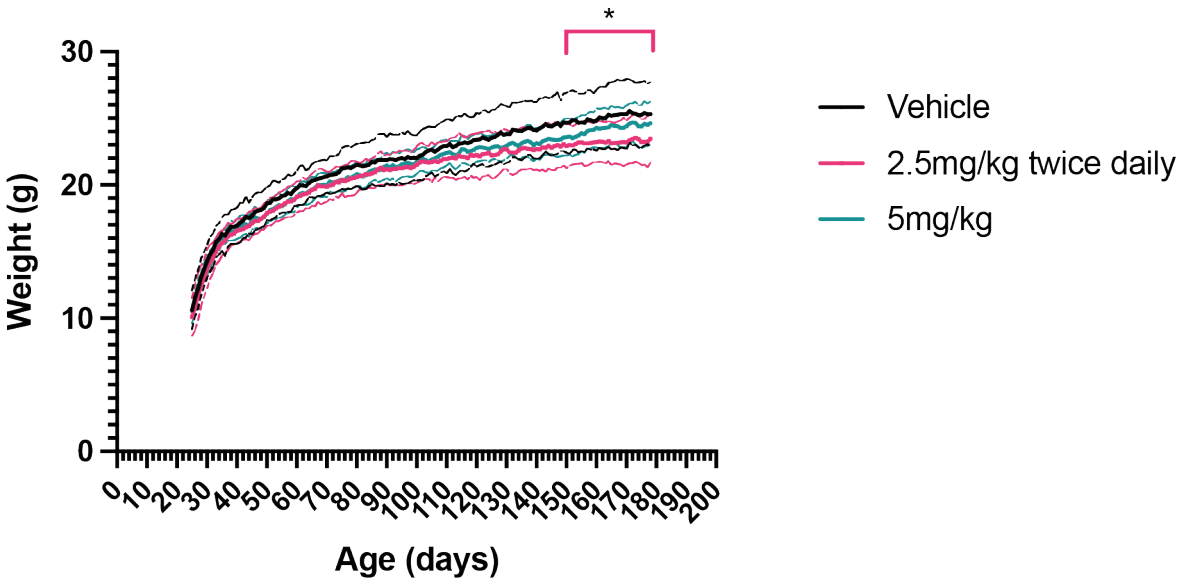

Figure 4.2: Weight of the 6-month cohort of TDP-43^{Q331K} mice dosed with vehicle, M102 2.5mg/kg twice daily or M102 5mg/kg once daily over the study. Weight was measured daily before dosing with vehicle, 2.5mg/kg M102 twice daily or M102 5mg/kg once daily. The solid line shows the mean of the group and the dotted lines show the ± SD. There was a significant decrease in weight in the M102 2.5mg/kg dosed group when compared to the vehicle dosed group from 157 days onwards. N=13-14 per group, mixed measures analysis with repeated measures (* = p<0.05).

Weight was also evaluated by area under the curve (AUC) analysis. AUC of the 6-month cohort weight showed a significant decrease in weight for both M102 dose groups when compared to vehicle (Figure 4.3). The AUC for M102 2.5mg/kg was 3156 ± 12 g x days vs 3321 ± 16 g x days for vehicle ($P < 0.0001$) and for M102 5mg/kg was 3219 ± 9 g x days vs vehicle ($P < 0.0001$).

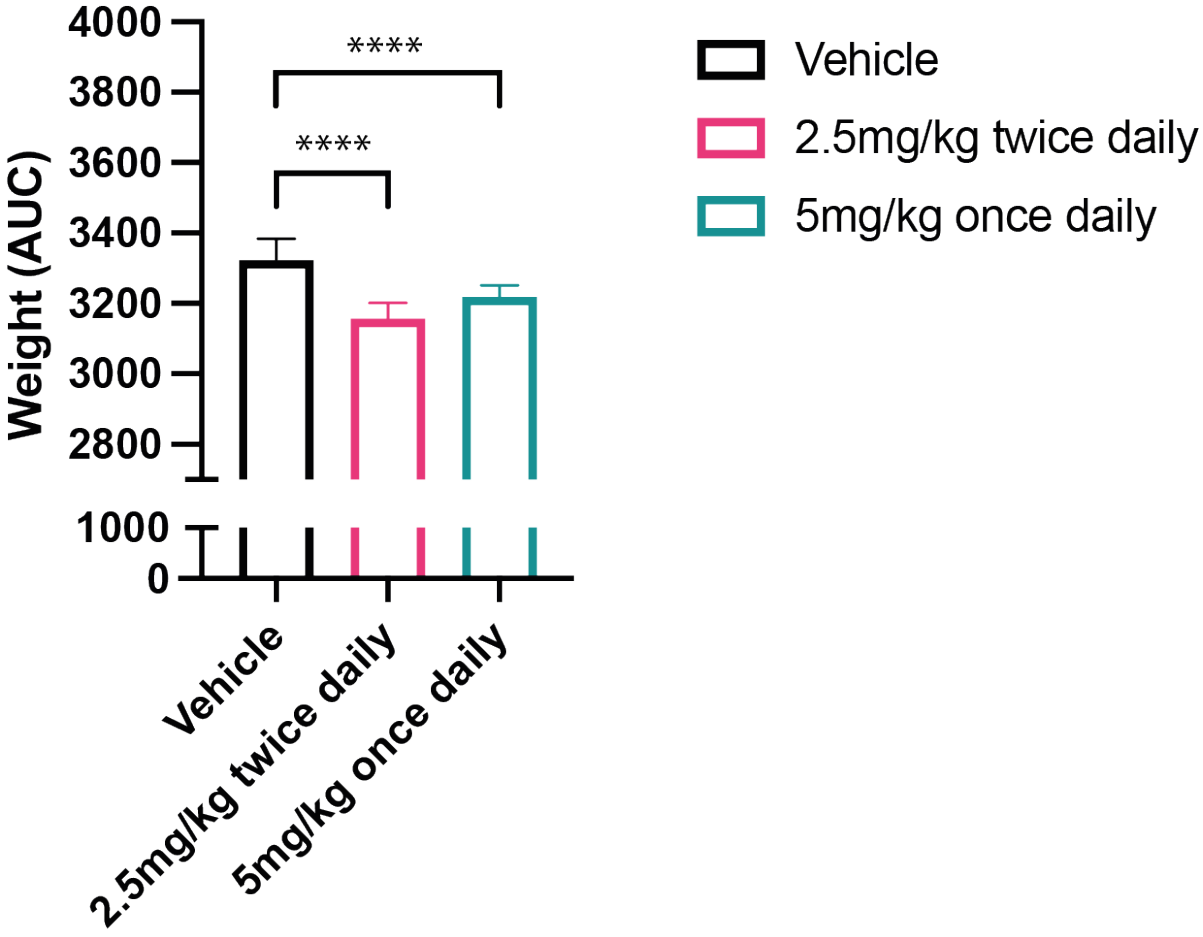

Figure 4.3: AUC analysis of weight of the TDP-43^{Q331K} 6-month cohort dosed with M102. Area under the curve (AUC) analysis of weight shown as mean ± SD. There was a significant decrease in AUC for weight in both of the M102 dosed groups when compared to the vehicle dosed group. N = 13 – 14 per group. One-way ANOVA with Dunnett's multiple comparisons, **** = $p<0.0001$

4.4.2. Mouse weights 3-month cohort

In the 3-month cohort, mice were weighed daily before dosing from 25 days until 3 months of age (Figure 4.4). There was no significant difference between either of the M102 dosed groups when compared to the vehicle dosed group (two-way ANOVA with repeated measures).

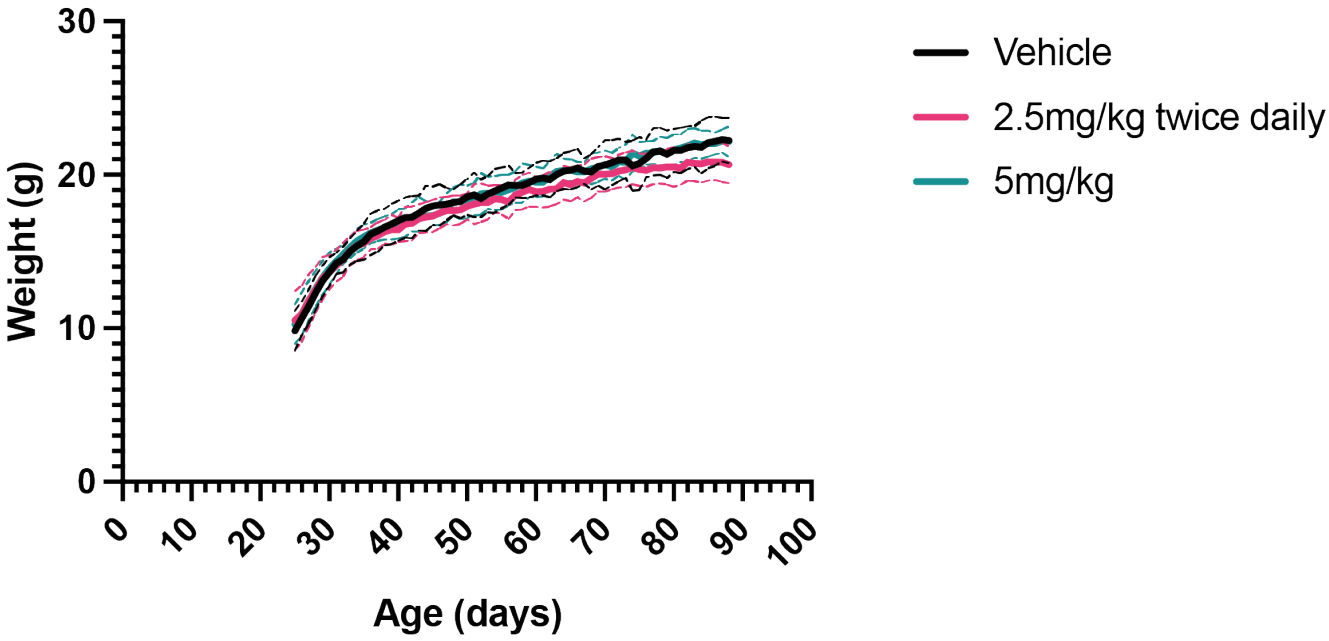

Figure 4.4: Weight of the 3-month cohort of TDP-43^{Q331K} mice dosed with vehicle, M102 2.5mg/kg twice daily and M102 5mg/kg once daily. Weight was measured daily before dosing. The solid line shows the mean of the group and the dotted lines show the ± SD. No significant difference was seen between the M102 dosed groups and vehicle dose group (n=6 per group, mixed effect analysis with repeated measures).

AUC analysis showed a significant decrease in weight between the M102 2.5mg/kg twice daily dosed group vs vehicle with values of 1136 ± 6 SEM and 1171 ± 7 SEM respectively (Figure 4.5, P = 0.006, one-way ANOVA with Dunnett's multiple comparisons). There is no significant difference between the M102 5mg/kg and vehicle dosed groups (P = 0.9909).

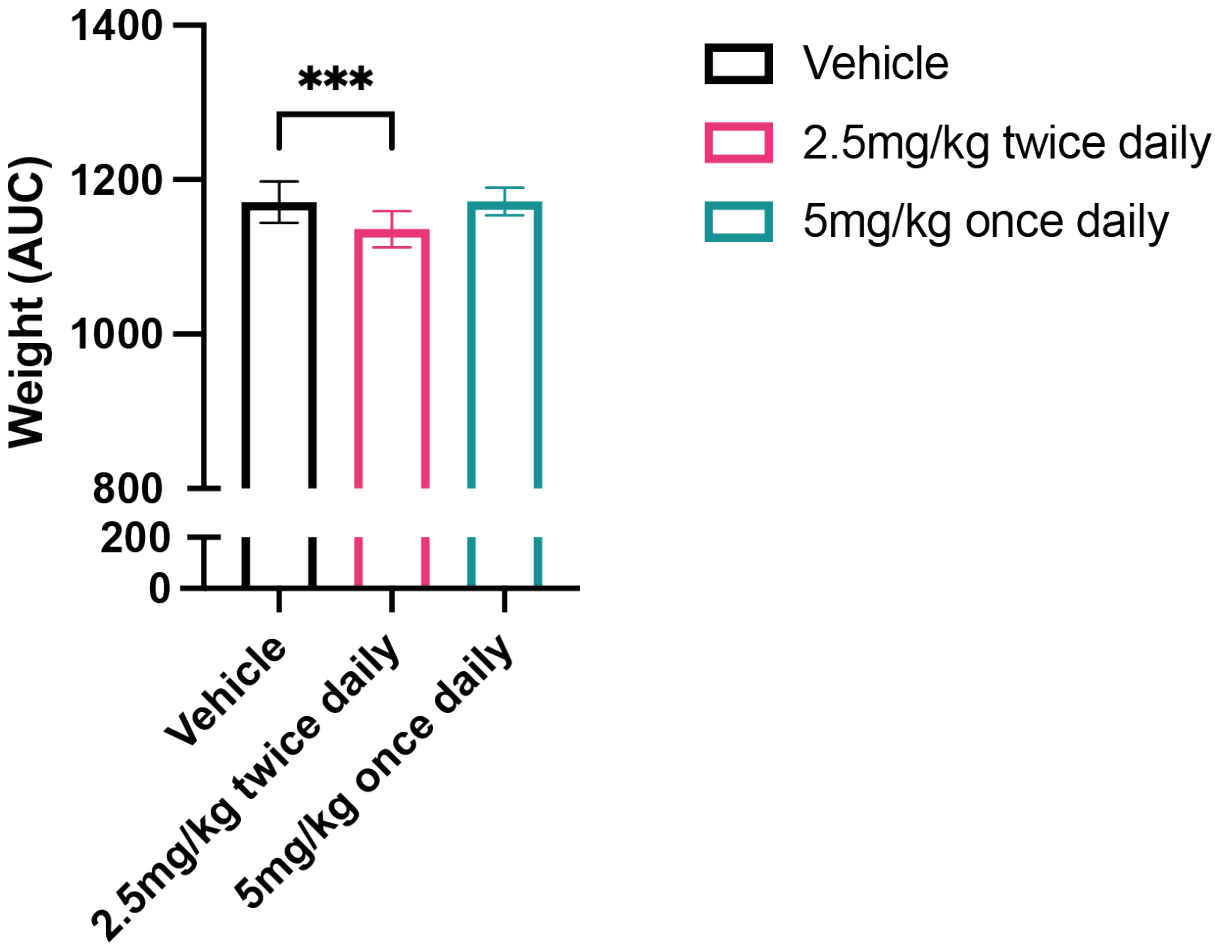

Figure 4.5: AUC analysis of the weights of the 3-month TDP-43^{Q331K} cohort. Area under the curve (AUC) analysis of body weight shown as mean ± SD. There was a significant decrease in area under the curve (AUC) of the M102 2.5mg/kg dosed group when compared to the vehicle group. N = 13 – 14 per group. One-way ANOVA with Dunnett's multiple comparisons, *** = p<0.001.

4.4.3. Rotarod

Motor function and coordination of mice were analysed using the accelerating rotarod test to determine if M102 can improve rotarod performance over time. Mice were tested on the rotarod once a week from 40 days of age until the end of the study. Rotarod is a measure of motor function and coordination as mice must balance on the beam and keep up with the increasing speed for the duration of the test. However, it could also be a measure of apathy as mice could fall due to lack of motivation to continue. The TDP-43^{Q331K} transgenic mice perform significantly worse on the rotarod as time progresses, whereas the NT mice can stay at the maximum 300 seconds up to 6 months of age. Overall, there was no significant

difference between the dose groups in rotarod performance over time (Figure 4.6, overall P = 0.3826, mixed-effect analysis with repeated measures and Dunnett's post-test).

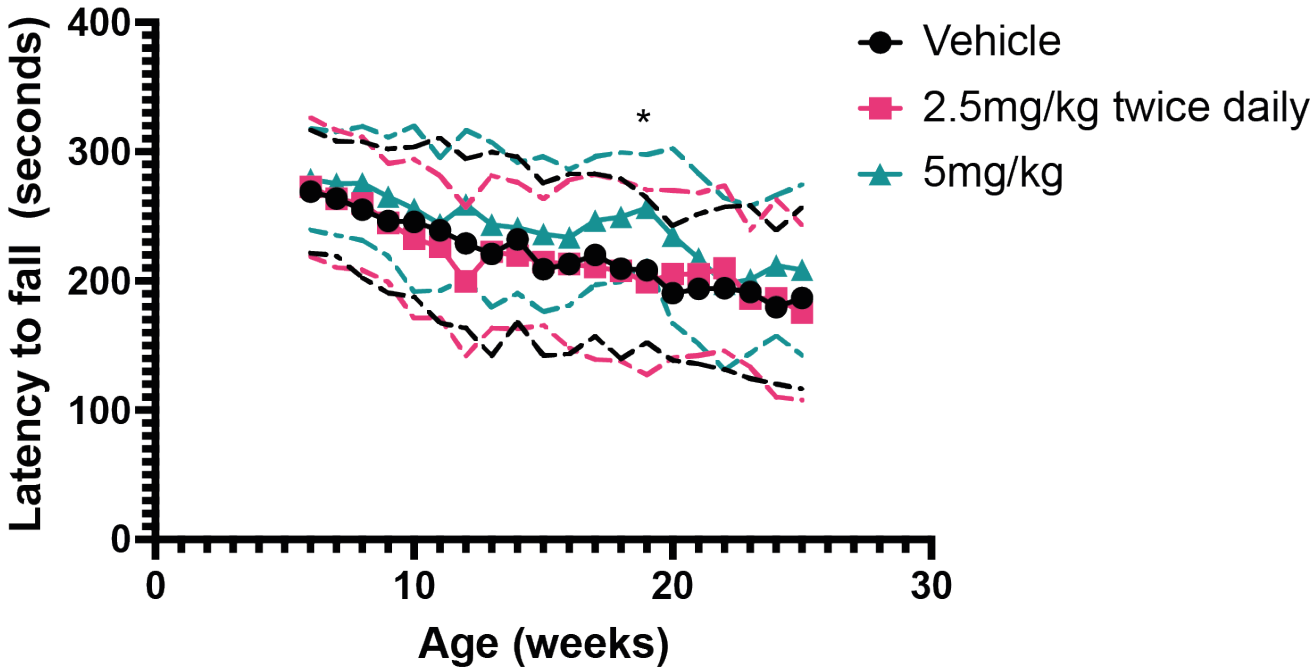

Figure 4.6: Rotarod performance of TDP-43^{Q331K} mice over the course of the study shown as latency to fall in seconds. Mean shown as individual points and dotted lines represent ± SD. Overall there was no significant difference between the vehicle and either of the M102 dosed groups in terms of rotarod performance. N = 13-14 per group. Mixed-effects analysis with repeated measures and Dunnett's post-test multiple comparisons (* = p<0.05).

For the SOD1^{G93A} mouse model we typically look at the age at which mice reach 20% decline in rotarod performance. In the TDP-43^{Q331K} model this type of analysis has not been previously explored, so analysis was carried out to see the age of the mice when they reach 10%, 20% and 30% decline in rotarod performance. There was no significant difference in time to reach 10%, 20% or 30% decline between either of the M102 dosed groups and the vehicle dose group (Figure 4.7, Log-rank Mantel-Cox test).

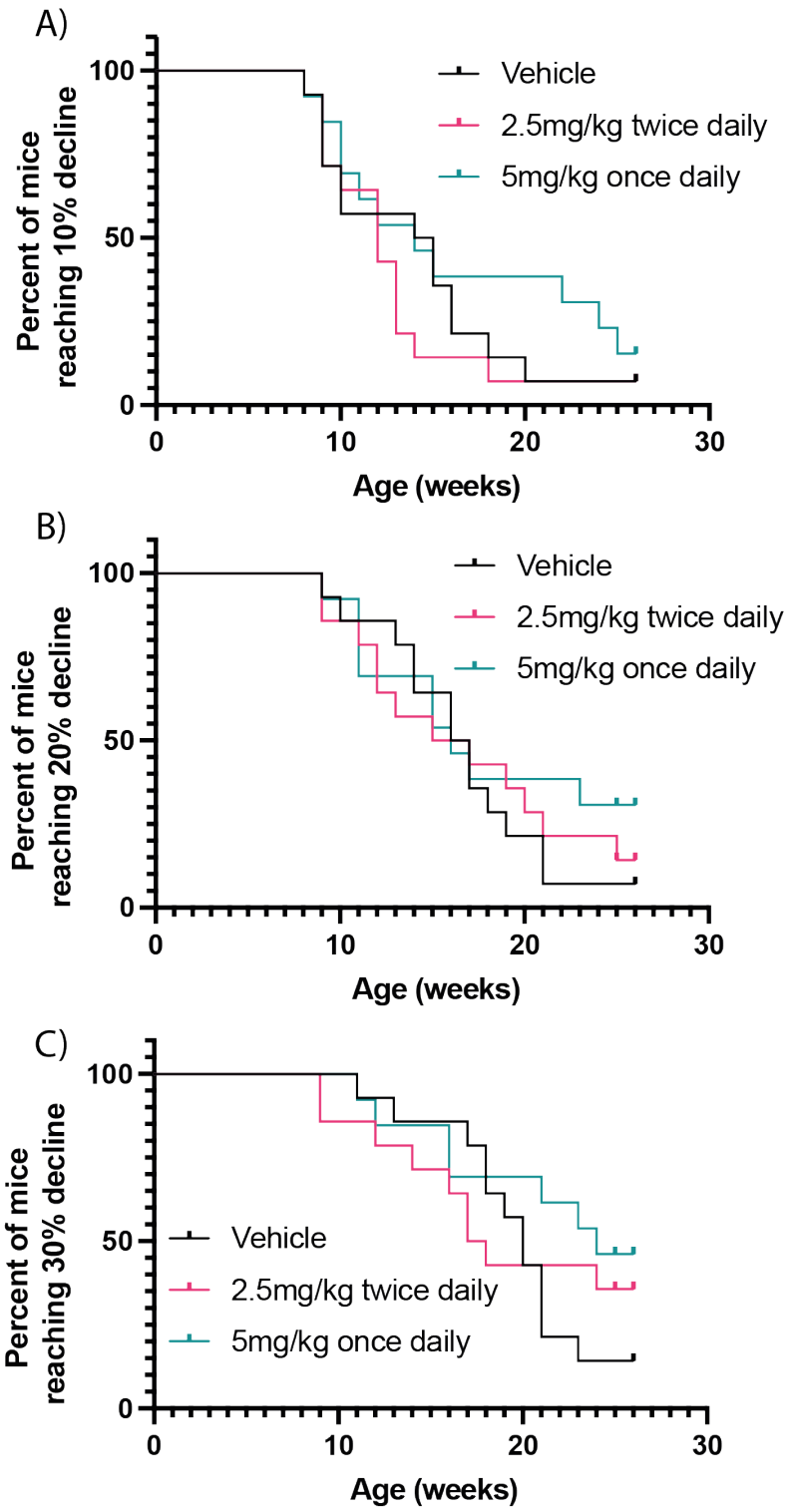

Figure 4.7: Time to reach 10, 20 and 30% decline in rotarod performance in TDP-43^{Q331K} mice dosed with vehicle, 2.5mg/kg M102 twice daily and 5mg/kg once daily. Plotted as survival analysis. Time to reach A) 10% rotarod decline (P = 0.3599), B) 20% rotarod decline (P = 0.5947), C) 30% rotarod decline (P = 0.3518). There was no significant difference between the vehicle or M102 dosed groups at any of the time points. N = 13-14 per group. Log-rank Mantel-Cox test.

Area under the curve analysis also showed no significant difference in rotarod performance between the M102 dosed groups and the vehicle dosed group. Values for vehicle, M102 2.5mg/kg and 5 mg/kg were 4171 ± 192.3 s x day, 4132 ± 188.2 s x day and 4589 ± 170.2 s x day, respectively (Figure 4.8).

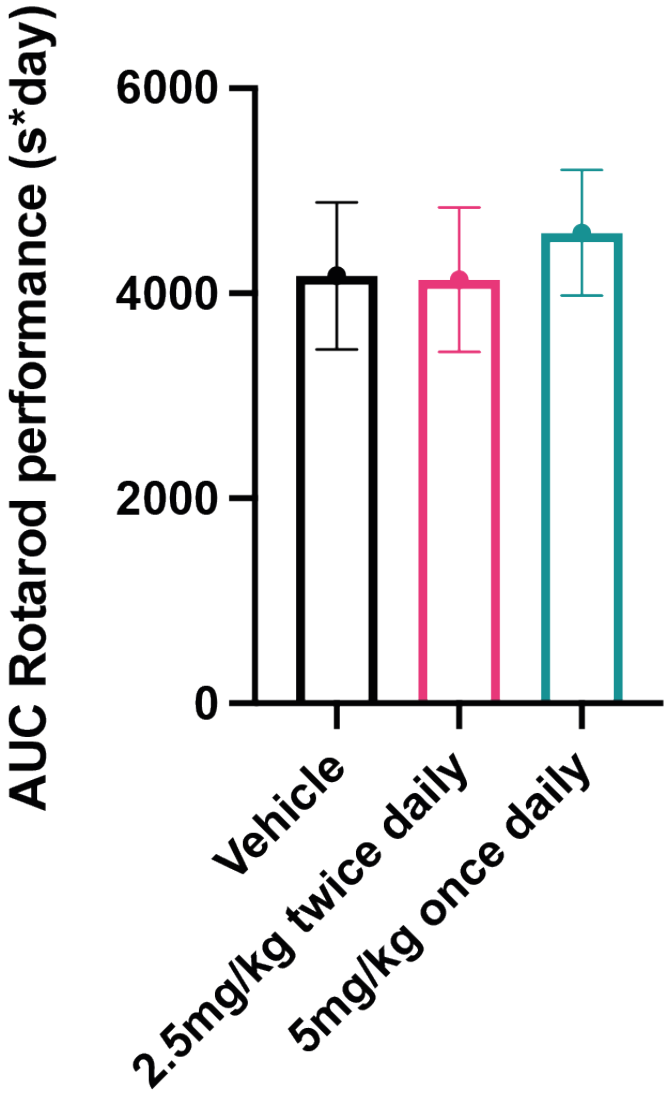

Figure 4.8: AUC of rotarod performance. Area under the curve (AUC) of rotarod performance shown as mean ± SD. No significant difference was seen in AUC rotarod performance. N = 13 – 14 per group One-way ANOVA with Dunnett's multiple comparisons.

4.4.4. Neuroscore

Neuroscoring was carried out weekly from 16 weeks of age to determine if M102 has an effect on progression of visible signs of disease in the TDP-43^{Q331K} mice. TDP-43^{Q331K} transgenic mice develop a tremor and an abnormal gait over time that can be recorded using a set scoring system. For overall tremor and neuroscore, all groups increased in score overtime as expected

with the model (Figure 4.9A and B). The neuroscore data were analysed to show age at which mice reached a neuroscore of 2 for 2 consecutive scores (Figure 4.9C). There was no significant difference between the groups in the time to reach a neuroscore of 2 (P = 0.7594, Kruskal-Wallis test with Dunn's multiple comparisons, n = 13 – 14 per group).

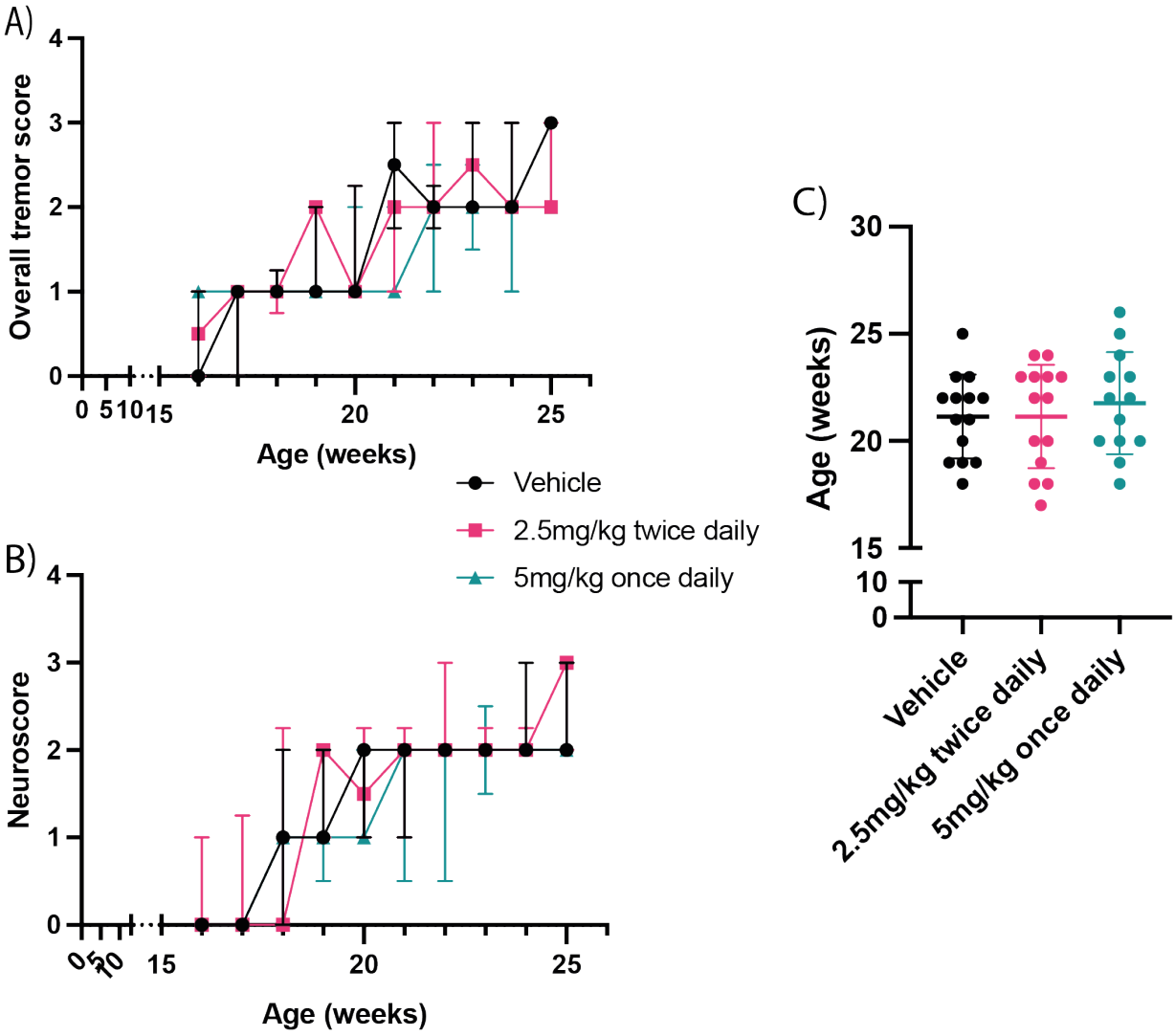

Figure 4.9: Tremor and neuroscore scores over time and time to reach a neuroscore of 2 in the TDP-43^{Q331K} mice. A and B) scores over time shown as median ± IQR. C) Time to reach a neuroscore of 2 showed no difference between dose groups (P = 0.7594, Kruskal-Wallis test with Dunn's multiple comparisons, n = 13 – 14 per group).

4.4.5. Catwalk gait analysis

Catwalk gait analysis was carried out at 3 and 6 months of age on 8 mice per group. The gait analysis provides many different parameters linked to gait which can be compared between the three dose groups to determine if M102 influences gait when compared to vehicle dosed animals. The parameters shown below are the most appropriate to compare based on previous analysis with the TDP-43^{Q331K} model that show differences between T and NT mice at these timepoints (Watkins *et al.*, 2021).

Stand time is the amount of time in the swing cycle that the paws are on the ground. This increased between 3 and 6 months of age for all dose groups for both forelimb and hindlimbs as this makes the gait steadier (Figure 4.11A and B). Vehicle mice have a hindlimb stand time of 0.17 ± 0.03 seconds at 3 months and 0.21 ± 0.04 seconds at 6 months of age. There was a significant increase in the M102 2.5mg/kg vs vehicle at 3 months of age for forelimb stand time, however there was no longer a significant difference at 6 months of age. At 3 months of age the forelimb stand time is 0.14 ± 0.02 seconds for vehicle mice and 0.18 ± 0.05 seconds for M102 2.5mg/kg mice (P = 0.0488, one-way ANOVA with Dunnett's post-test).

Stride length is a measure of distance between each paw and when a mouse places the same paw down again. For the vehicle dosed group this remained steady between 3 and 6 months of age for forelimb and hindlimb, however for both M102 dosed groups this increased in the same time frame (Figure 4.10C and D). The differences between the dose groups at either time point were not significantly different. For vehicle hindlimb stride length was 55.0 ± 5.3mm at 3 months and 55.3 ± 5.3mm at 6 months whereas for the M102 2.5mg/kg twice daily and M102 5mg/kg once daily groups the stride length at 3 months was 53.8 ± 3.2mm and 53.4 ± 3.0mm, respectively, and for 6 months was 56.1 ± 4.4mm and 57.3 ± 4.5mm, respectively.

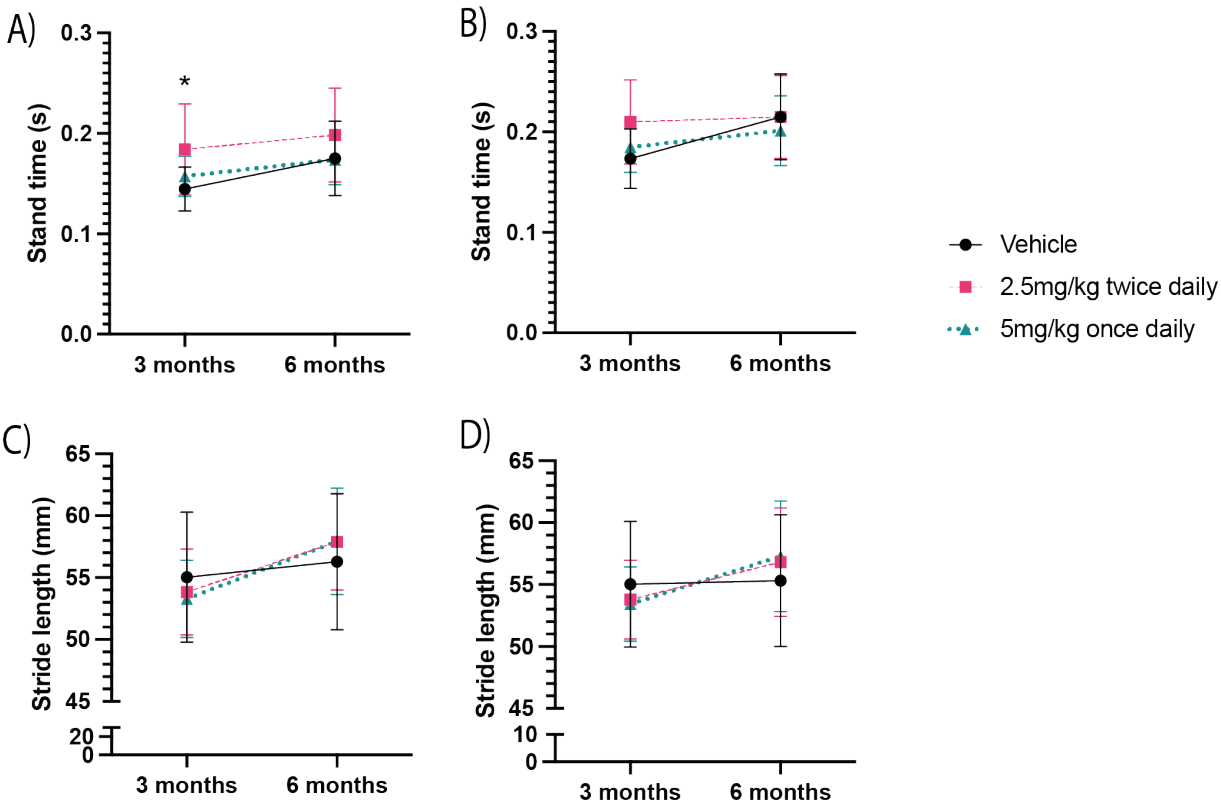

Figure 4.10: gait analysis parameters showing stand time and stride length. Shown as mean ± SD for each group. A) forelimb and B) hindlimb stand time shows the average time in seconds of the forelimbs or hindlimbs on the surface during the step cycle. There was a significant increase in stand time in the M102 2.5mg/kg dose group when compared to vehicle at 3 months of age (P = 0.0488). C) Forelimb and D) hindlimb stride length, which showed the average distance from the placement of the same paw in a step cycle. There was no significant difference between the groups at any time points for forelimb or hindlimb stride length. N = 8 per group. Two-way ANOVA with repeated measures and Dunnett's post-test (* = p<0.05).

Swing speed is the speed at which the limb is being moved and is calculated from the distance between each step (stride length) and the time spent to place it down again (swing time). There was no significant difference in swing speed in either forelimb or hindlimb (Figure 4.11E and F). Duty cycle is a measure of stand time as a percentage of the full step cycle. The forelimb and hindlimb duty cycle increased between 3 and 6 months of age for the vehicle dosed group as expected from the model, as animals spend more time with paws on the ground to stabilise their gait. Both of the M102 dosed groups remained steady between 3 months and 6 months of age, however the differences between the groups at either time point are not statistically significant (Figure 4.11G and H).

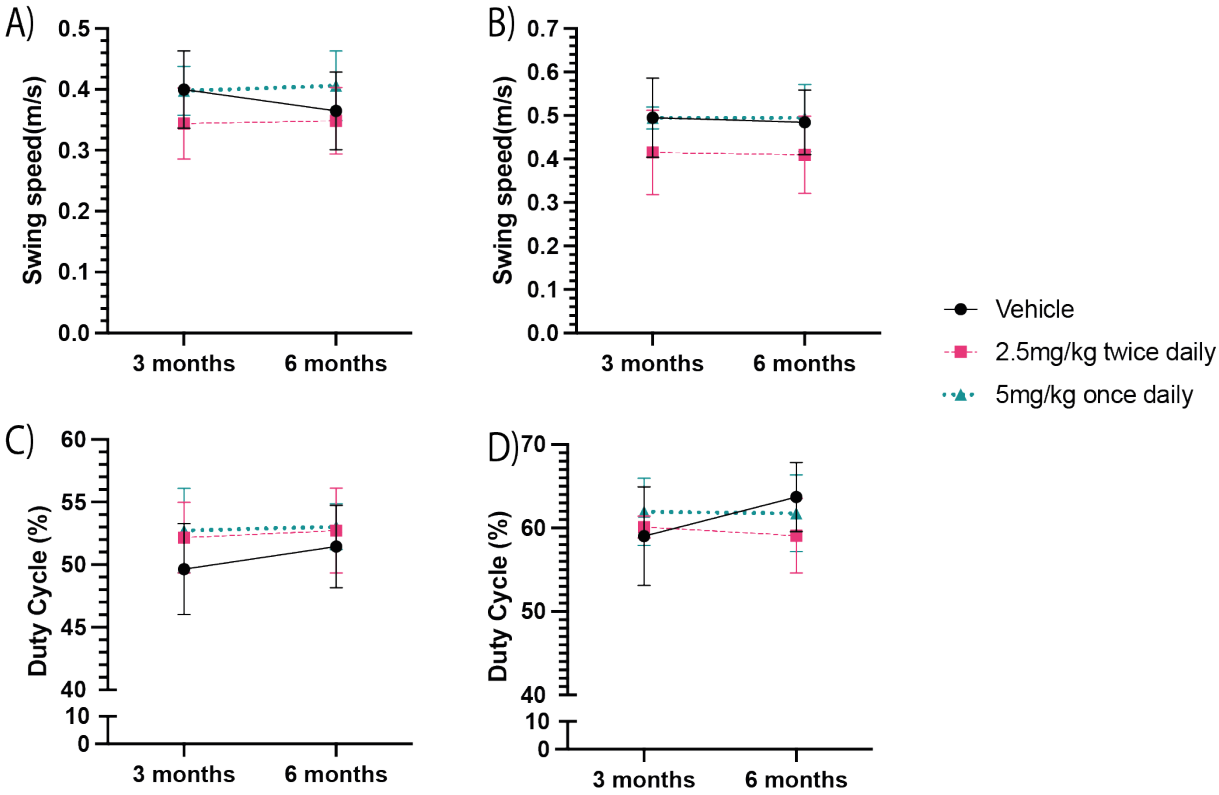

Figure 4.11: Gait analysis parameters showing stride pattern. Shown as mean ± SD for each group. A) Forelimb and B) hindlimb swing speed showed no significant difference between the dose groups. C) forelimb and D) hindlimb duty cycle, expressing the time spent standing as a percentage of the step cycle showed no significant difference between the dose groups at either time point, however the trend between 3 and 6 months of age looks better in the M102 dosed animals when compared to the vehicle dosed animals. N = 8 per group. Two-way ANOVA with repeated measures and Dunnett's post-test (* = $p<0.05$).

Base of support (BOS) is a measure of the distance between the two forelimbs or two hindlimbs and as expected from the model this increased between 3 and 6 months of age for all the dose groups and there was no significant difference between vehicle and M102 dosed mice at either of the time points (Figure 4.12A and B).

An indicator of unsteady gait is the amount of time spent on either diagonal (opposite) legs or 3 paws at once. WT animals tend to spend most of the time on diagonal paws and limited time on 3 paws. However, as animals develop motor phenotypes and their gait gets increasingly unsteady, they tend to spend less time on diagonal legs and more time on 3 paws as this offers

more stability. As expected, the vehicle dosed animals followed this trend and spent less time on diagonal paws and more time on 3 paws between 3 and 6 months of age (Figure 4.12C and D). However, both M102 dosed groups do not follow this trend and stayed fairly stable between 3 and 6 months of age.

Duration is the time taken for the mice to complete the full run from the start to the end of the recording area on the catwalk. WT animals tend to move quickly, whereas mice with motor phenotypes or reduced motivation may take longer to complete the run and show an increased duration. There was no significant difference between either M102 dose groups and vehicle at 3 or 6 months of age (Figure 4.12E).

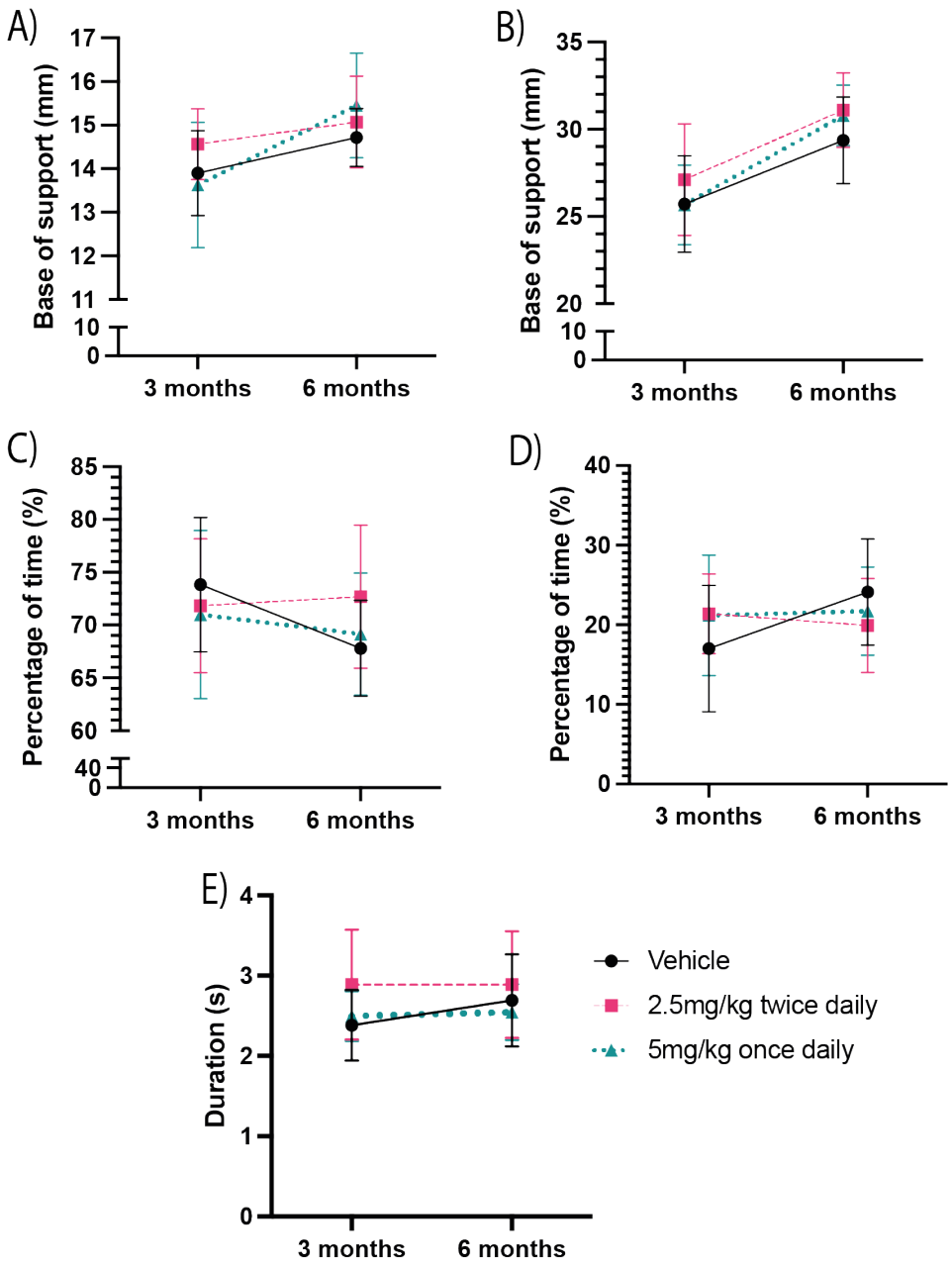

Figure 4.12: Gait analysis showing base of support, percentage of time on diagonal paws and 3 paws, and duration of run a measure of gait steadiness in animal. Shown as mean ± SD for each group. A) forelimb and B) hindlimb base of support (BOS) showed an increase over time but there was no significant difference between dose groups. Percentage of time spent on C) diagonal paws and D) 3 paws showed increased need for support of vehicle animals between the two time points but no significant difference between the dose groups. E) Duration of the run showed no significant difference between the groups. N = 8 per group. Two-way ANOVA with repeated measures and Dunnett's post-test (* = $p<0.05$).

Although the changes at the individual time points were not significant, the trend of the M102 dosed mice between the two time points is interesting as it opposes the trend observed in the vehicle dosed animals and suggests an improvement in gait parameters. To investigate this further the percentage change from 3 to 6 months was calculated for each animal taking 3 months as a baseline. The change in forelimb and hindlimb base of support between 3 and 6 months of age was not significantly different between the dose groups (Figure 4.13A and B). There was a significant improvement in the percentage of time spent on diagonal paws in the M102 2.5mg/kg group when compared to the vehicle dosed group (Figure 4.13C). The M102 2.5mg/kg group had a 0.86 ± 5.59% increase vs the vehicle group with -6.03 ± 3.97% decrease in time spent on diagonal paws between 3 and 6 months of age ($P = 0.0241$, one-way ANOVA with Dunnetts post-test). The M102 2.5mg/kg dose group also had a decrease in time spent on 3 paws compared to the vehicle dosed animals which showed an increase of time spent on 3 paws between 3 and 6 months of age (Figure 4.13D). This difference was -1.47 ± 5.63% change in time spent on 3 paws between 3 and 6 months of age for the M102 2.5mg/kg group vs 7.11 ± 9.01% for the vehicle group ($P = 0.0299$, one-way ANOVA with Dunnett's post-test). There was no significant difference between the groups in the change in percentage of time spent on 4 paws between 3 and 6 months of age (Figure 4.13E).

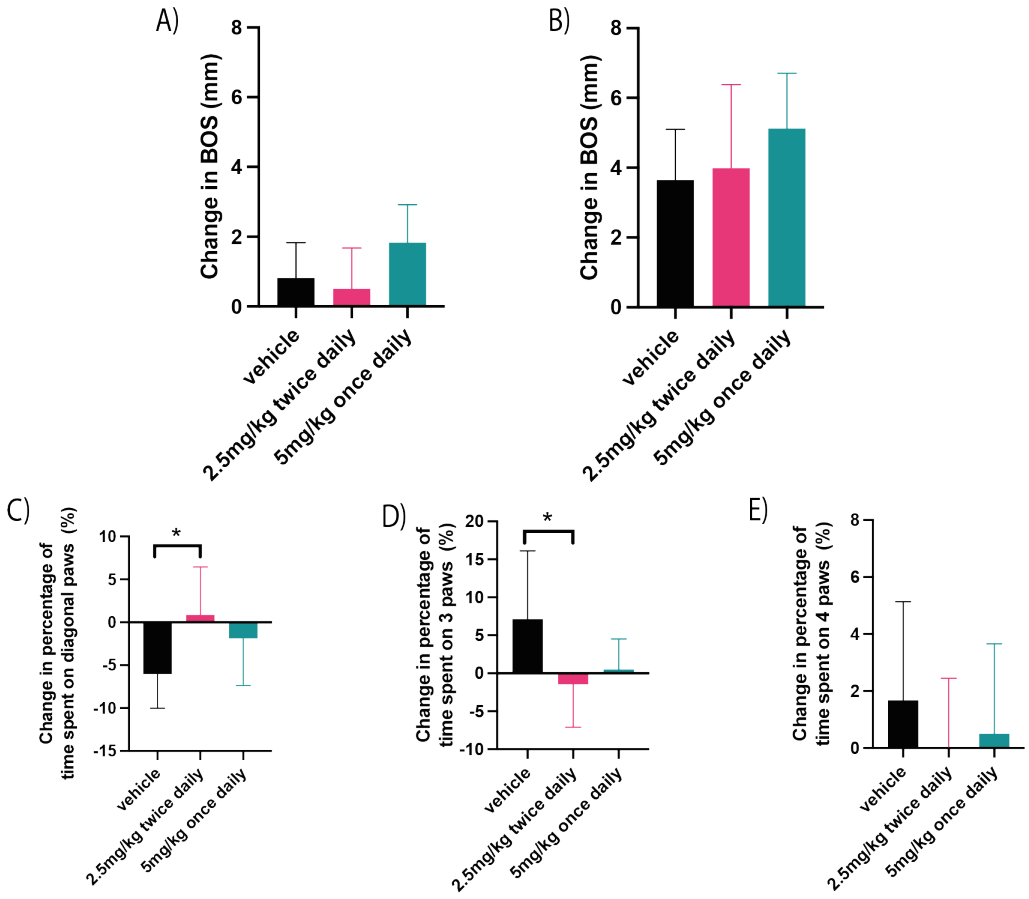

Figure 4.13: Change between 3 and 6 months of age of gait parameters linked with gait stability. Change in A) forelimb and B) hindlimb base of support (BOS) between 3 and 6 months of age showing an increase in BOS but no significant difference between the dose groups. C) The change in the percentage of time spent on diagonal paws showed a significant difference between the M102 2.5mg/kg dosed group and the vehicle dosed group. The vehicle mice spent less time on diagonal paws whereas the M102 2.5mg/kg group spent more time on diagonal paws between 3 and 6 months of age. D) The change in the percentage of time spent on 3 paws between 3 and 6 months of age showed a significant difference between the vehicle and M102 2.5mg/kg dose group where the vehicle animals are spending more time on 3 paws than the M102 2.5mg/kg dose groups. E) The change in time spent on 4 paws between 3 and 6 months of age showed no significant difference between the dose groups. N = 7 – 8 per group. One-way ANOVA with Dunnett's post-test. (* = $p<0.05$)

4.4.6. Electrophysiology

Electrophysiology is carried out in humans to diagnose different muscular or nervous system diseases and track their progression (de Carvalho *et al.*, 2008). Here we investigated CMAP amplitude, which is equivalent to the number of functional motor axons within the hind limb of mice. Repetitive stimulation looks at the fatigue in the response to multiple quick stimulations to assess functionality of neuromuscular junctions.

We carried out CMAP and repetitive stimulation analysis at 6 weeks, 3 months, and 6 months of age to compare the overall function of motor axons in the different dose groups and to compare the change in CMAP over time in the TDP-43^{Q331K} model.

4.4.6.1. Compound Muscle Action Potential (CMAP)

At 6 weeks of age there was no significant difference between the M102 dose groups and vehicle in CMAP amplitude (Figure 4.14). At three months of age there was a significant decrease in the 5mg/kg M102 dose group CMAP amplitude when compared to vehicle (27.3 ± 6.2mV for M102 5mg/kg vs 33.7 ± 5.2mV for vehicle, p = 0.0084). At 6 months of age there was a significant increase in CMAP amplitude of both M102 dosed groups when compared to the vehicle dose group. The mean CMAP amplitude for M102 5mg/kg dosed animals was 33.6 ± 4.6mV vs 26.8 ± 7.3mV for vehicle dosed animals (P = 0.0140) and CMAP for the M102 2.5mg/kg dose group is 35.7 ± 6.5mV (P = 0.0006 when compared to vehicle, two-way ANOVA with repeated measures and Sidaks multiple comparisons).

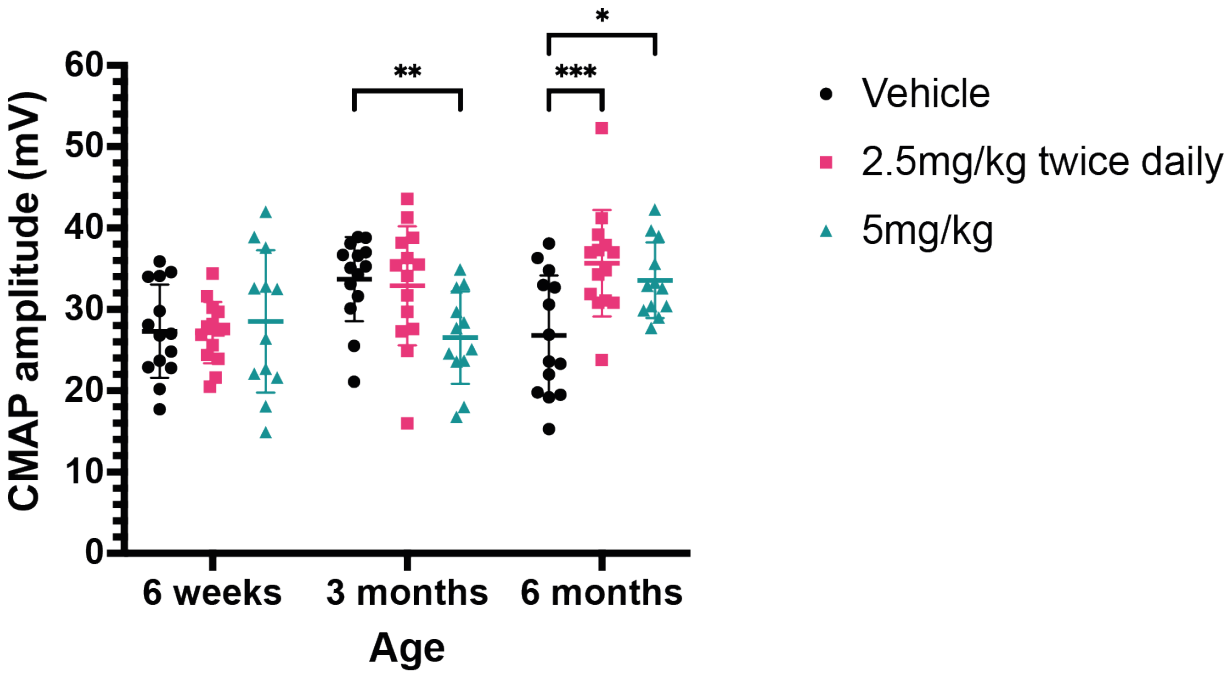

Figure 4.14: Compound muscle action potential (CMAP) amplitude of TDP-43^{Q331K} mice dosed with vehicle, M102 2.5mg/kg twice daily or M102 5mg/kg once daily. Individual values shown as well as mean ± SD. At 3 months of age there was a significant decrease in CMAP amplitude in the M102 5mg/kg dose group when compared to the vehicle dosed group. At 6 months of age there was a significant increase in CMAP amplitude in both M102 dosed group when compared to the vehicle dose group. N= 13-14 per group. Two-way ANOVA with repeated measures and Sidak post test (* = p<0.05, ** = p<0.01, *** = p<0.001, **** = p<0.0001).

As well as analysing the individual CMAP values, further analysis was carried out to compare between the time points in terms of change in CMAP amplitude and percentage change in CMAP amplitude. To carry this out, the difference between CMAP amplitude at 6 weeks and 6 months and the difference between CMAP amplitude at 3 months and 6 months was calculated as a change in mV and as a percentage change for each mouse and then averaged for the different groups.

The results from the analysis showing change in CMAP amplitude from 6 weeks to 6 months showed a significant increase in CMAP amplitude in the M102 2.5mg/kg dosed group when compared to the vehicle dosed group (Figure 4.15A and B). The change is 8.54 ± 6.51mV for M102 2.5mg/kg dosed mice vs -0.52 ± 8.05mV for vehicle dosed mice (P = 0.0051) or in

percentages 131.5 ± 24.1% for M102 2.5mg/kg dosed mice vs 98.1 ± 27.0% for vehicle dosed mice (P = 0.0010, one-way ANOVA with Dunnett post-test).

In the comparison from 3 months to 6 months of age, there was a significant increase in the change of CMAP in both M102 groups when compared to the vehicle dosed groups (Figure 4.15C and D). The change is -6.24 ± 9.97mV for vehicle vs 2.79 ± 8.77mV for M102 2.5mg/kg (P = 0.0068 when compared to vehicle) vs 7.04 ± 6.39mV for M102 5mg/kg (P = 0.0002 when compared to vehicle). In percentages these changes are 79.4 ± 21.9% for vehicle vs 108.5 ± 19.9% for M102 2.5mg/kg (P = 0.0008 compared to vehicle) vs 122.9 ± 17.0% for M102 5mg/kg (P <0.0001 when compared to vehicle, one-way ANOVA with Dunnett post-test).

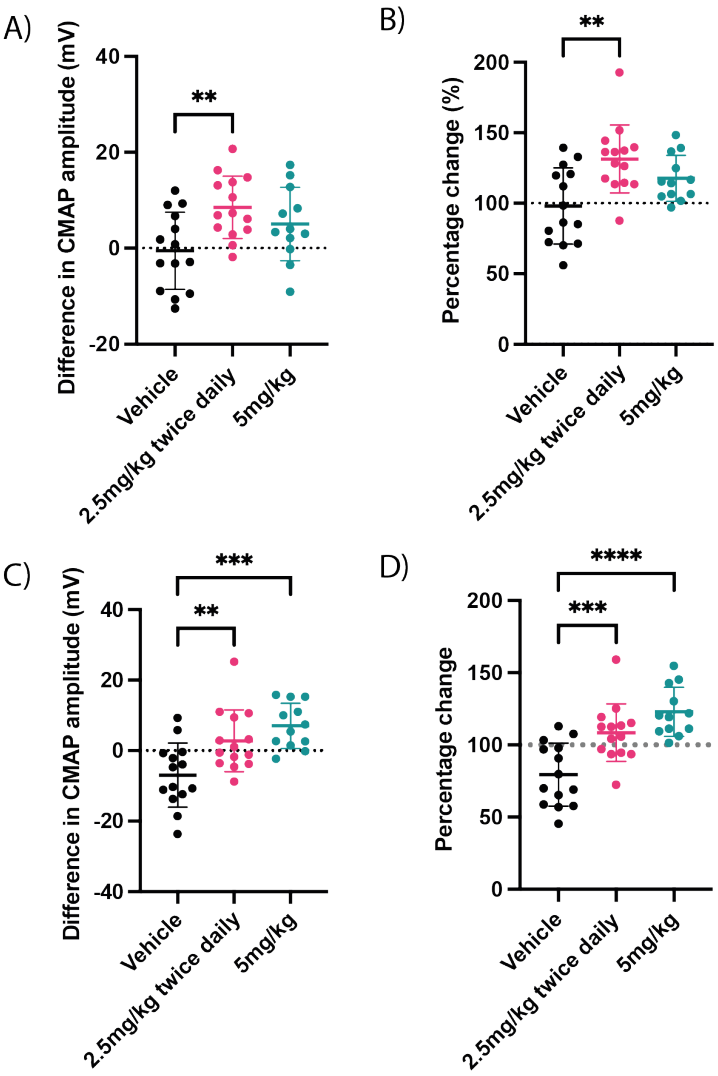

Figure 4.15: Analysis in change in CMAP amplitude between different time points in TDP-43^{Q331K} mice dosed with vehicle and M102 shown as mV change and percentage change. A) Change in CMAP amplitude from 6 weeks to 6 months of age in TDP-43^{Q331K} mice dosed with vehicle or M102 at 2.5mg/kg once daily or 5mg/kg twice daily. There was a significant increase in the 2.5mg/kg M102 dosed group when compared to vehicle (P = 0.0051). B) Change in CMAP amplitude from 6 weeks to 6 months expressed as percentage change showed a significant increase in M102 2.5mg/kg dosed mice compared to vehicle dosed mice (P = 0.0010). C) Change in CMAP amplitude between 3 months to 6 months of age showed a significant increase in the change in CMAP in M102 2.5mg/kg vs vehicle dosed animals (P=0.0068) and M102 5mg/kg vs vehicle dosed animals (P = 0.0002). D) Change in CMAP amplitude between 3 and 6 months of age shown as percentage change. There was a significant increase in change in CMAP in M102 2.5mg/kg vs vehicle dosed animals (P = 0.0008) and also in M102 5mg/kg vs vehicle dosed animals (P < 0.0001). N = 13-14 per group. One-way ANOVA with Dunnett post-test (** = p<0.01, *** = p<0.001, **** = p<0.0001).

4.4.6.2. Repetitive stimulation

TDP-43^{Q331K} transgenic mice have been shown previously to have a reduction in CMAP amplitude over 10 repetitive 10Hz stimulations when compared to non-transgenic animals. Repetitive stimulation is a good marker of neuromuscular function and was carried out at 6 weeks, 3 months and 6 months of age immediately after collecting the recordings for CMAP amplitude to determine if M102 has an effect in TDP-43^{Q331K} mice. Animals received 10 pulses at 10hz and the results are shown as the CMAP amplitude as a percentage of the first stimulus.

At 6 weeks of age, there was no overall significant difference between the vehicle dosed and either of the M102 dosed groups in terms of repetitive stimulation (Figure 4.16A, overall P = 0.0831, two-way ANOVA with repeated measures and Dunnett multiple comparison).

At 3 months of age there was no significant difference in the repetitive stimulation between either of the M102 dosed groups or the vehicle dosed groups (Figure 4.16B, two-way ANOVA with repeated measures and Dunnett multiple comparison).

At 6 months of age there was an overall significant increase in the repetitive stimulation amplitudes when compared to the vehicle dosed groups (Figure 4.16C, overall P = 0.0268). The 5th and 7th stimuli were also significantly increased in the M102 2.5mg/kg dosed group when compared to the vehicle dosed group. At the 5th stimulus the vehicle dosed animals has an average of 93.4 ± 3.5% of first stimulus whereas the M102 2.5mg/kg animals had an average of 96.5 ± 2.86% of first stimulus (P = 0.0334) and at the 7th stimulus the vehicle animals had an average of 93.4 ± 4.1% of first stimuli vs 96.4 ±2.4% of first stimulus for the M102 2.5mg/kg dosed mice (P = 0.0470, two-way ANOVA with repeated measures and Dunnett multiple comparison).

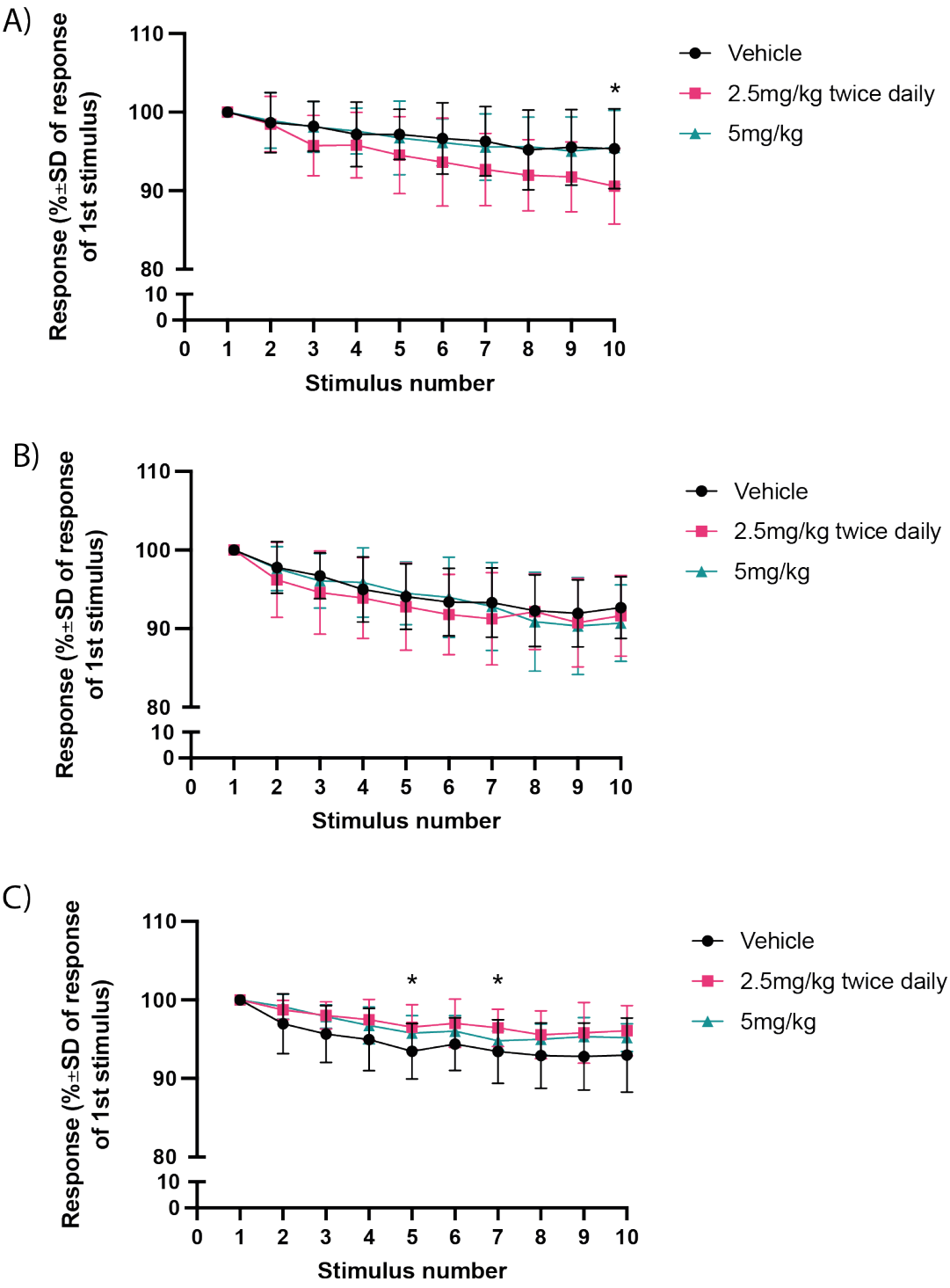

Figure 4.16: Repetitive stimulation at 10Hz of TDP-43^{Q331K} animals dosed with vehicle, M102 2.5mg/kg twice daily or M102 5mg/kg once daily at 6 weeks, 3 months and 6 months of age. Data are shown as percentage of first stimulus mean ± SD. Repetitive stimulation at: A) 6 weeks; B) 3 months and C) 6 months of age. N= 12 -14 per group. There was an overall significant improvement in the 6 month repetitive stimulation in the M102 groups when compared to vehicle (P=0.0268). Two-way ANOVA with repeated measures and Dunnett multiple comparison (* = $p<0.05$).

Repetitive stimulation can also be analysed as the change in amplitude between the 1st and 10th stimulus. For each animal the percentage change from the 1st to the 10th stimulus was recorded and these were averaged for the dose groups. There was no significant difference between the vehicle and either of the M102 dosed groups at 6 weeks (M102 2.5 mg/kg P= 0.0518, M102 5mg/kg P =0.7535) or 3 months of age (M102 2.5mg/kg P= 0.7856, M102 5mg/kg P = 0.4511), but there was a significant reduction in the loss of CMAP amplitude in the M102 2.5mg/kg dose group when compared to vehicle (P= 0.0471) (Figure 4.17, ordinary one-way ANOVA with Dunnett's multiple comparisons, n = 12 – 14 per group).

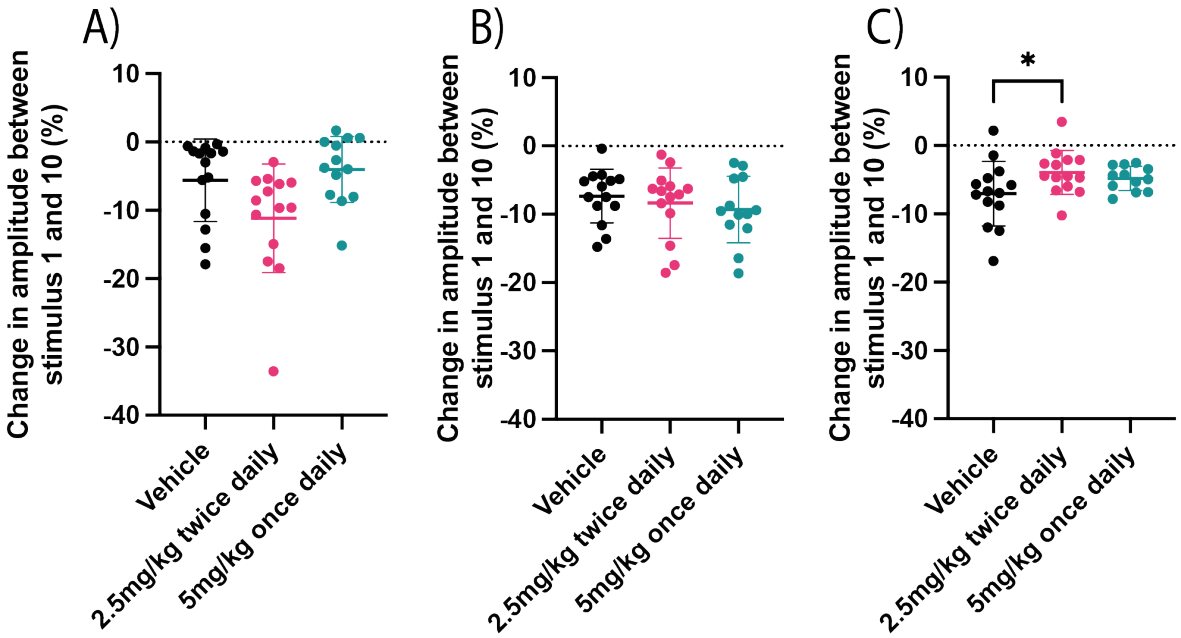

Figure 4.17: Percentage change in amplitude between stimulus 1 and 10 at 6 weeks, 3 months and 6 months of age. Data shown as individual values with mean ± SD. The change in CMAP amplitude between the 1st and 10th stimulus at: A) 6 weeks of age; B) 3 months of age and C) 6 months of age. There was a significant increase in the difference in CMAP amplitude at 6 months of age in the M102 2.5mg/kg twice daily dosed group when compared to vehicle. N = 12-14 per group. One-way ANOVA with Dunnett's multiple comparisons (* = p<0.05).

4.4.7. Marble burying

To analyse potential differences in innate digging and exploratory behaviour between the different dose groups, the marble burying test was carried out in the mice at 6 months of age. A set of 10 marbles was set out in a fresh cage and after 30 minutes the number of marbles buried out of 10 was counted. The transgenic TDP-43^{Q331K} mice bury fewer marbles than WT or NT mice and we wanted to investigate if dosing with M102 could impact on the number of

marbles buried by TDP-43^{Q331K} mice. There was no significant difference in number of marbles buried between the dose groups (Figure 4.18, P = 0.2674 Kruskal-Wallis with Dunn's post-test, n = 11- 14 per group).

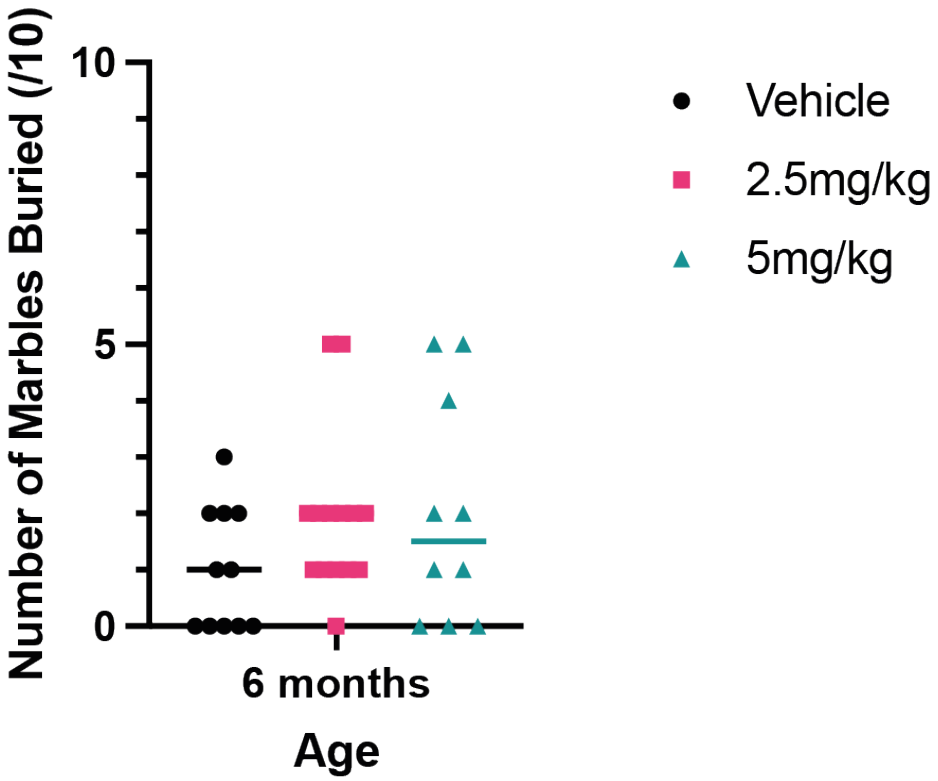

Figure 4.18: Marble burying of TDP-43^{Q331K} mice dosed with vehicle or M102 at 2.5mg/kg twice daily or 5mg/kg once daily. Data shown as individual values and median. The was no significant difference was seen between dose groups. P = 0.2674 Kruskal-Wallis with Dunn's post-test, n = 11 – 14 per group.

4.4.8. RTqPCR analysis 3 months

Quantitative RT-qPCR analysis following reverse transcription was carried out to compare levels of mRNA transcripts of downstream targets of NRF2 and HSF1 between the different dose groups to determine the effect of M102 on NRF2 and HSF1 transcriptional targets *in vivo*. RNA was collected from cortex and lower spinal cord immediately after collection of tissue for the 3-month cohort mice. RNA was converted into cDNA and then qPCR analysis was carried out on target genes using optimised primers. Data are reported as relative to *Gapdh* housekeeper and relative to the vehicle group.

The relative gene expression change in the cortex showed significantly increased gene expression in several downstream targets of NRF2 and HSF1 (Figure 4.19A). In the M102 2.5mg/kg twice daily dose group the following targets were significantly upregulated when compared to the vehicle dosed group: *Nqo1* (P = 0.0011), *Osgin1* (P = 0.0102) and *GSR* (P = 0.0005). In the M102 5mg/kg dosed group the following targets were significantly upregulated: *Sqstm1* (P = 0.0251), *Nqo1* (P = 0.0067), *Gsr* (P < 0.0001) and *Hspa1a* (P <0.0001).

For the same set of genes analysed, there was no significant differences in gene expression in the lower spinal cord tissue (Figure 4.19B).

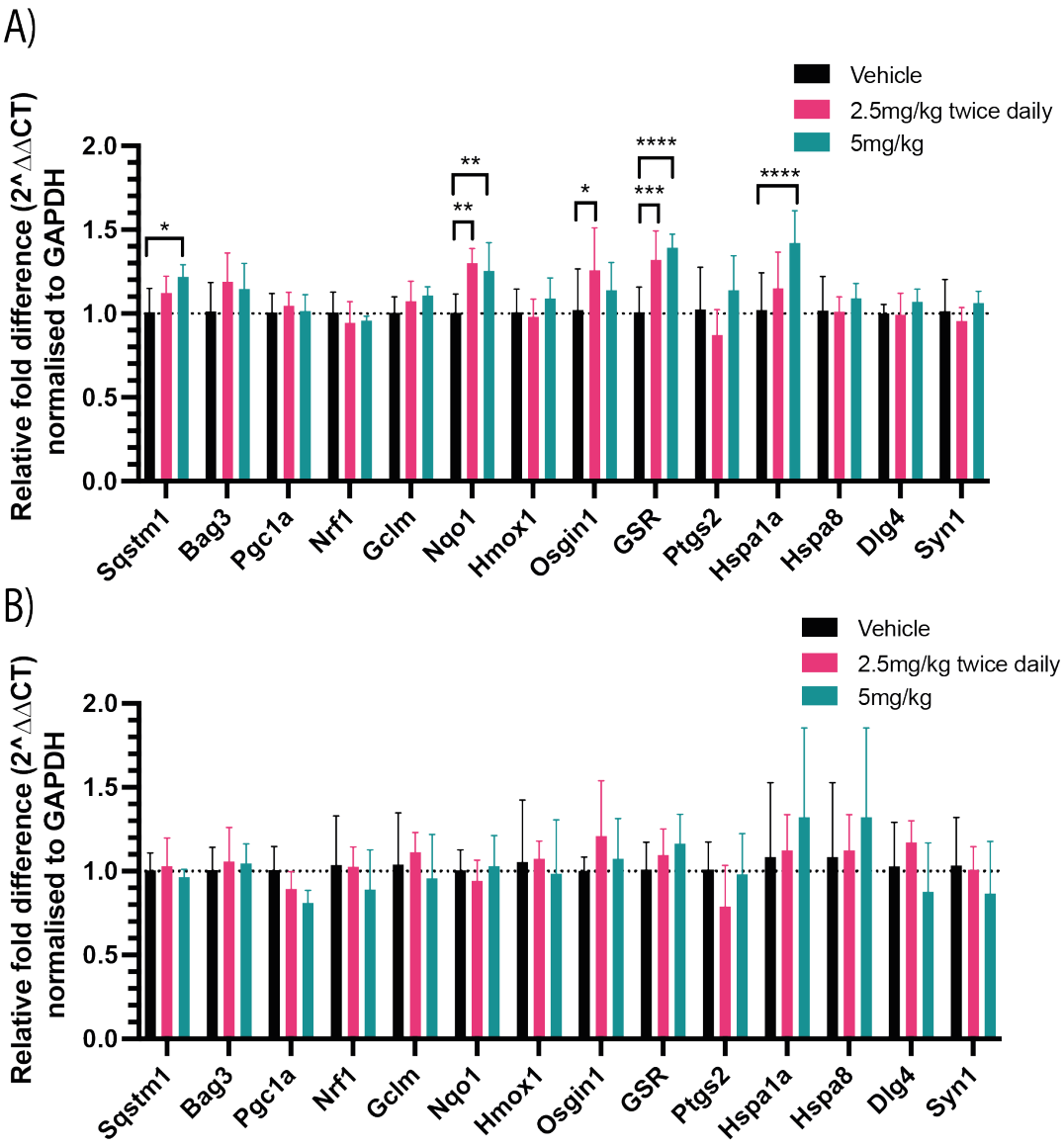

Figure 4.19: Relative expression of target genes in 3 month old TDP-43^{Q331K} mice. Shown as mean expression (using the delta delta cT method) ± SD. A) Relative gene expression from 3-month old cortex tissue. There were significant increases in the gene expression of *sqstm1, Nqo1, Osgin1, Gsr* and *Hspa1a* in M102 dosed mice compared to vehicle. B) Relative gene expression from 3-month old spinal cord tissue showed no significant difference between M102 dosed groups and the vehicle group. N = 6 per group. Two-way ANOVA with Dunnett's multiple comparisons. (* = p<0.05, ** = p<0.01, *** = p<0.001, **** = p<0.0001)

4.4.9. RT-qPCR analysis 6 months

The tissue collected at 6 months of age was stored in RNALater before RNA was extracted, cDNA was synthesised and RT-qPCR was run for a number of gene targets. Relative expression of Hspa1a was increased in both M102 dosed groups at 6 months of age when compared to

vehicle (P<0.0001 for both groups, Figure 4.20A). There was also a significant decrease in *Osgin1* in the M102 2.5mg/kg dose group when compared to vehicle (P = 0.0147).

The spinal cord RT-qPCR data at 6 months also showed a significant increase in *Hspa1a* expression in the M102 5mg/kg dose group (P = 0.0054, Figure 4.20B).

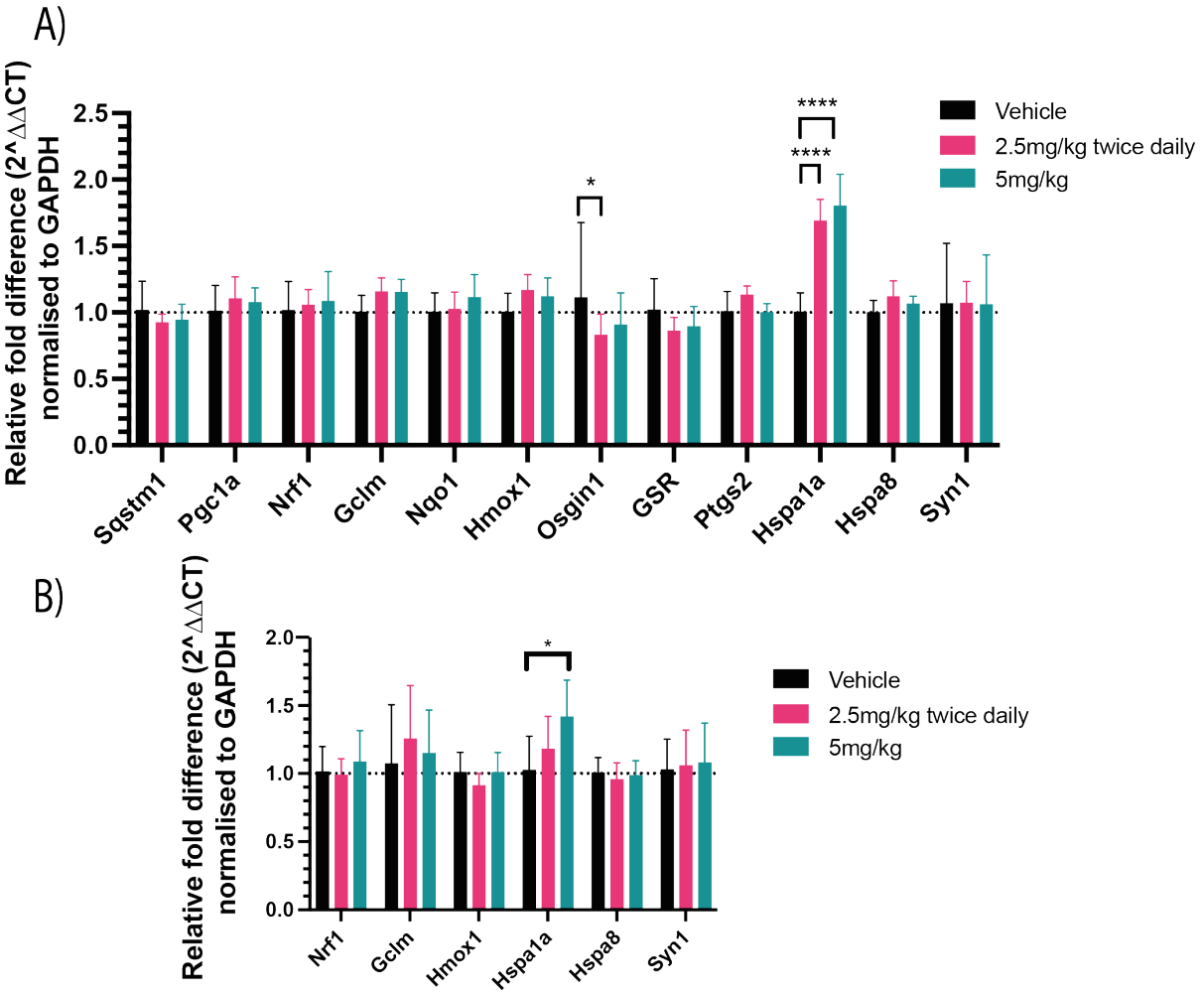

Figure 4.20: Relative expression of target genes in 6 month old TDP-43^{Q331K} mice. Shown as mean expression (using the delta delta cT method) ± SD. A) Relative gene expression from 6-month old cortex tissue. There were significant increases in the gene expression of *Hspa1a* in M102 dosed mice compared to vehicle and a significant decrease in Osgin1. B) Relative gene expression from 6-month old spinal cord tissue showed significant increase in *Hspa1a* in M102 5mg/kg once daily dosed mice compared to vehicle. N = 7 per group. Two-way ANOVA with Dunnett's multiple comparisons. (* = p<0.05, ** = p<0.01, *** = p<0.001, **** = p<0.0001)

4.4.10. GFAP and IBA1 staining

Staining of lumbar spinal cords was carried out to determine changes in astrocyte and microglia activity in the CNS in M102 dosed animals when compared to vehicle dosed animals. Lumbar spinal cords were embedded in paraffin wax and sections were cut and placed serially on slides. Staining of sections was achieved through co-staining with GFAP and Iba1 antibodies and DAPI staining was added in the mounting step. The different channels of images taken at 60X magnification of the ventral horns were analysed in ImageJ to determine percentage area coverage, integrated density, and circularity. Between 5 and 15 ventral horns were analysed per animal and 5 to 7 animals per group were analysed.

Representative image of staining from each of the dose groups shows the 60X images with the individual channel staining and the composite of all staining for ventral horns of the lumbar spinal cords (Figure 4.21A). There was no significant difference in GFAP staining in terms of percentage area coverage by staining or integrated density of staining (Figure 4.21B and C). There was also no significant difference in the percentage area coverage of Iba1 staining or integrated density of Iba1 staining between the different dose groups (Figure 4.21D and E). Circularity of Iba1 staining was analysed to determine the activation status of microglia, however there was no significant difference in the circularity of the Iba1 staining between dose groups (Figure 4.21F, one-way ANOVA with Dunnett's post-test).

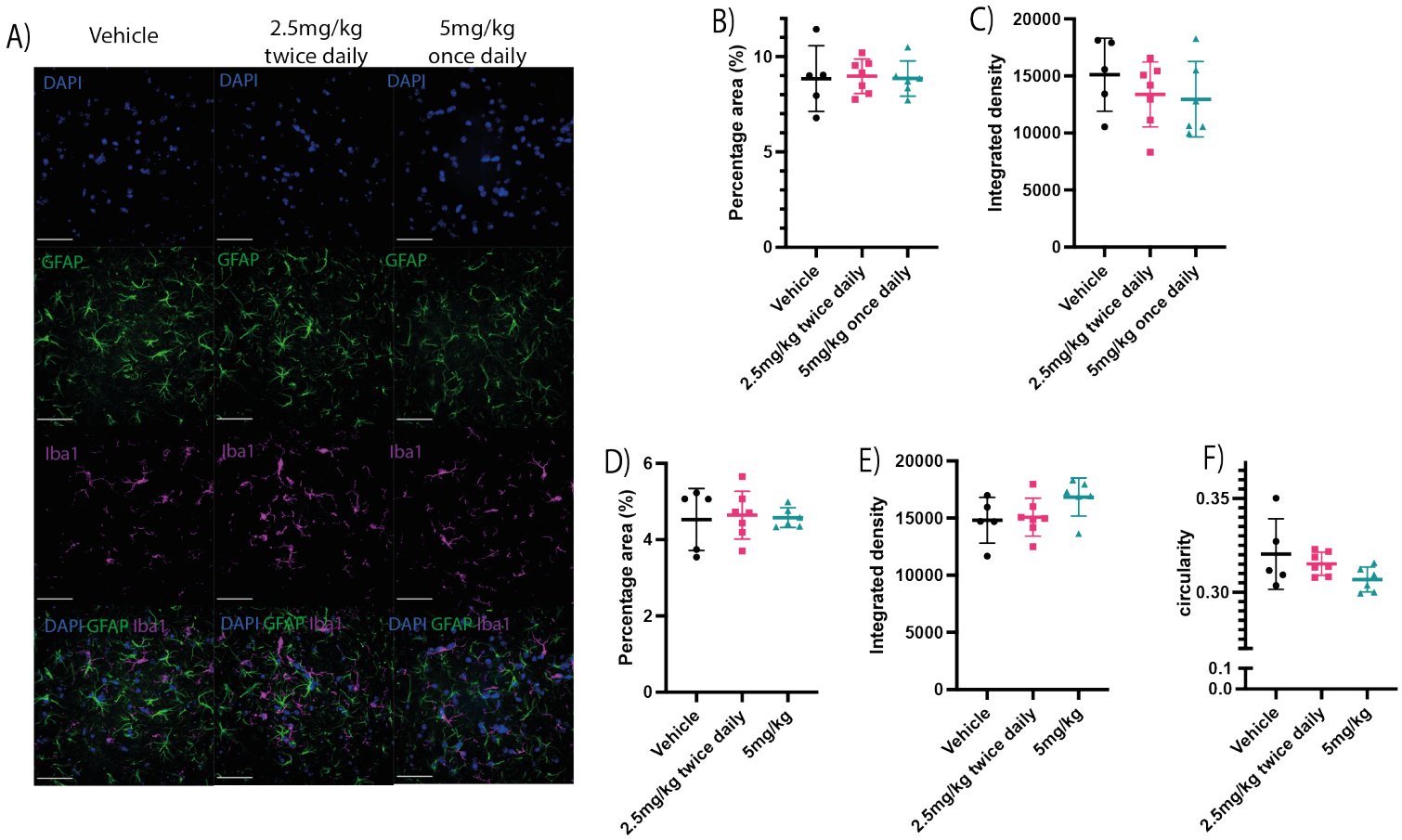

Figure 4.21: Immunohistochemical staining of lumbar spinal cord for astrocytes (GFAP) and microglia (Iba1) of TDP-43^{Q331K} mice dosed with vehicle and M102. A) Representative images of lumbar spinal cord from 6 month old mice showing individual and composite images for staining with DAPI, GFAP and Iba1. Scale bar = 50μm. Graphs shown as individual values, mean ± SD. B) GFAP percentage area staining. C) GFAP integrated density. D) Percentage area staining of Iba1. E) Integrated density of Iba1 staining. F) circularity of Iba1 staining. There was no significant difference was seen between the groups in GFAP or Iba1 staining of lumbar spinal cords (one-way ANOVA with Dunnett's multiple comparisons, n = 5 – 7 mice per group).

4.4.11. Nissl staining

Lumbar spinal cord sections were stained for Nissl to aid counting of alpha motor neurons in order to determine if the number of motor neurons was affected by treatment of M102. Sections were stained with creysl violet solution to stain Nissl substance, which is found in the cytoplasm of motor neurons. Motor neurons were counted from ventral horns using an optimised system to correctly identify α-motor neurons. We assessed the number of motor neurons to determine if M102 affected the loss of motor neurons. The TDP-43^{Q331K} mouse model has been shown to have significant loss of motor neurons in the lumbar spinal cord at 10 months of age when compared to NT mice, however this loss starts at 2 months of age and progresses over time (Arnold *et al.*, 2013).

There was no significant difference in the average number of motor neurons per ventral horn between the different dose groups (Figure 4.22). Average number of motor neurons per ventral horn was 21.4 ± 4.8 for vehicle mice, 18.0 ± 5.5 for M102 2.5mg/kg twice daily dosed mice (P = 0.3961 compared to vehicle, one-way ANOVA with Dunnett's multiple comparisons), and 17.8 ± 4.8 for M102 5mg/kg once daily dosed mice (P = 0.3892 compared to vehicle, one-way ANOVA with Dunnett's multiple comparisons).

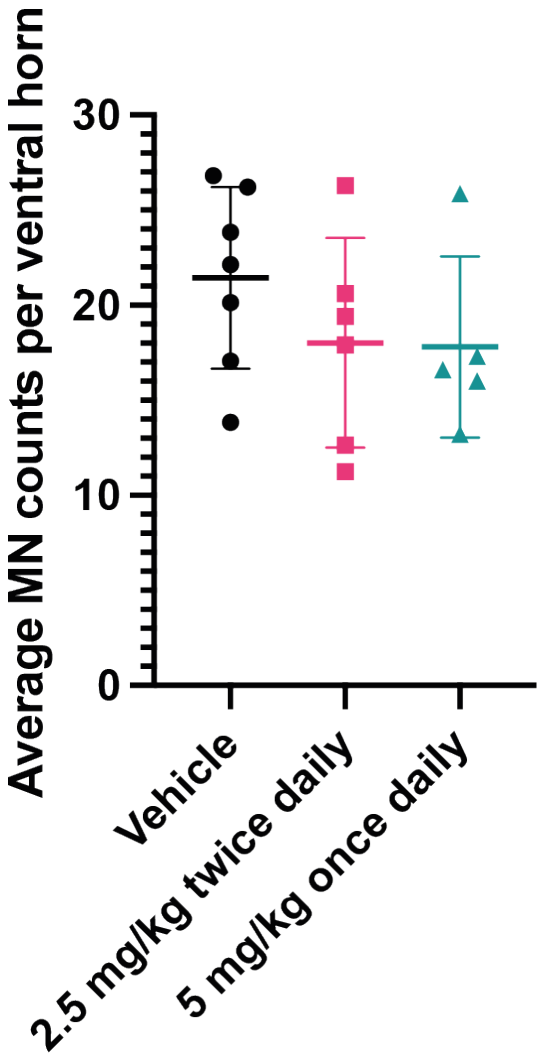

Figure 4.22: Motor neuron counts from ventral horn of lumbar spinal cords of TDP-43^{Q331K} mice dosed with M102. Data shown as individual values with mean ± SD. There was no significant difference in the average motor neuron number per ventral horn between the different dose group. One-way ANOVA with Dunnett's multiple comparisons. N = 5 – 7 mice per group.

4.5. Discussion

4.5.1. Motor function phenotypes

The TDP-43^{Q331K} mouse model shows a variety of behavioural phenotypes that show loss of motor function or motor coordination as part of the ALS phenotype (Watkins *et al.*, 2021).

4.5.1.1. Rotarod

Rotarod is a robust measurement of the motor function and coordination of animals and has been used in multiple mouse models of neurodegenerative diseases to track disease

progression and determine differences made by different potential treatments (Weydt *et al.*, 2003). Rotarod performance for the TDP-43^{Q331K} mice declines over the progression of the disease (Watkins *et al.*, 2021) and this study was powered to see a 20% improvement in rotarod performance with a therapeutic compound.

As expected from the mouse model, all the dose groups see a decline in rotarod performance over time, however there is no overall significant difference between the dose groups. AUC analysis also confirms no overall significant difference between dose groups.

Analysis carried out regularly in the SOD1^{G93A} mouse model looks at age at which animals reach a 20% decline in rotarod performance and has been a robust analysis to compare between different dose groups. However, this has not been analysed in the TDP-43^{Q331K} mouse model previously. Similar analysis of a time to reach a 10, 20 and 30% decline of rotarod performance, showed no significant difference between the dose groups at any time point. A trend for an increase in age for 30% decline in performance was seen however a later timepoint may have been needed as some animals did not reach the endpoint.

Reduction in rotarod performance could be due to a difference in weight between the dose groups, however in previous studies, when corrected for the increased weight of the transgenic mice compared to NT, there is still a significant decline in rotarod performance (Watkins *et al.*, 2021). Reduction may also be due to apathy in the model and lack of motivation to continue. However, M102 showed no significant improvement in rotarod over the course of dosing.

4.5.1.2. Neuroscore

Neuroscoring is carried out weekly and the age at which mice reached a neuroscore of 2 is a marker of disease progression in these mice as the disease phenotype is a lot milder than that seen in the SOD1^{G93A} mice. There is no significant difference found in this onset marker between the different dose groups indicating that M102 did not influence observable progression of disease. However, neuroscoring is a very subjective recording of disease progression and may not be as sensitive as other methods. To combat this, the same observer carried out the neuroscoring as much as possible over the course of the study. It was also

carried out once weekly and so changes in animals may have been missed between these time points.

4.5.1.3. Gait

Gait analysis allows the detection of gait abnormalities and defects and using the Catwalk gait analysis system we can analyse multiple different parameters regarding gait in the mice. Gait parameters analysed in this study are parameters used previously to distinguish transgenic vs non transgenic TDP-43^{Q331K} mice and are mostly focused on gait unsteadiness.

Although there were very few significant differences between the M102 dosed group and the vehicle group in the parameters chosen for this study, the difference between the two time points is very interesting and shows some significant improvement for the M102 dosed mice. For this model, the time spent on diagonal paws goes down over time and the animals spent a higher percentage of time on 3 and 4 paws for more support. This is shown in the vehicle dosed group for all these parameters. However, the M102 dosed mice do not follow this same trend and the change between 3 and 6 months of age is significantly improved in the M102 2.5mg/kg dose group when compared to vehicle.

Overall, the gait analysis shows significant improvement over time in parameters linked to gait steadiness in the M102 2.5mg/kg dose group when compared to the vehicle dose group suggesting that M102 has an impact on gait of TDP-43^{Q331K} mice.

Gait in mice is complex, and the way I have analysed the data is similar to how we have analysed it previously forelimb and hindlimb, however, in some ALS patients there is evidence that unsteady gait is happening through discrepancy between the left and right hand side of the body. It may be worth reanalysing the data to compare left and right rather than forelimb and hindlimb to see if there is a difference between the groups.

4.5.1.4. Electrophysiology

CMAP is a measure of the number of functional motor axons in the hindlimb of the mice. As expected from the model, the vehicle dosed TDP-43^{Q331K} mice had a consistent CMAP of around 28mV over the different time points. From previous data collected from these mice, transgenic and WT animals have a CMAP amplitude of around 25-30mV at 4 weeks of age.

However, at 3- and 6-months of age WT and NT animals have CMAP amplitude of around 50mV whereas the CMAP for transgenic TDP-43^{Q331K} animals stays around 25-30mV (Keerie *et al.*, 2021). For these experiments we used ring electrodes as shown in Figure 2.3. CMAP measurements using ring electrodes have been shown to have less variability when compared to needle electrode, although needle electrodes have the advantage of being able to isolate specific muscles as opposed to all of the muscles in the hind limb (Arnold *et al.*, 2015).

At 6 weeks of age there was no significant difference between the CMAP amplitude between the different dose groups. This is what was expected as it is an early timepoint in terms of disease progression and acts as a baseline reading. At 3 months of age there was a significant decrease in the M102 5mg/kg dose group when compared to vehicle. However, the result for 3 months at the vehicle dosed group looks unusual, as the CMAP for these mice tends to stay steady for the course of the disease (Keerie *et al.*, 2021).

At 6 months of age there was a significant increase in both M102 groups when compared to vehicle and a significant increase in CMAP from 6 weeks to 6 months of age for the M102 2.5mg/kg dosed group when compared to the change in vehicle over the same time point. This suggests that M102 causes improvement in functional motor axons in the TDP-43^{Q331K} mouse model.

Repetitive stimulation uses 10 pulses at 10Hz using the input needed to create the maximal CMAP amplitude and uses the difference in CMAP amplitude between the stimuli to judge the performance of the NMJs (Fu *et al.*, 2019). Healthy mice should show no, or little, change in CMAP amplitude over the 10 pulses, but mice and patients with ALS show a decrease in CMAP amplitude following repetitive stimulation.

The repetitive stimulation data show a slight decrease in the M102 dosed group compared to vehicle at 6 weeks of age, however this was not significant and could be to do with the difficulty to gain reliable repetitive CMAPs in mice of this age. For 6 months of age there was a significant improvement in the M102 2.5mg/kg twice daily dose group when compared to vehicle in terms of repetitive stimulation. This improvement is shown both in the 10-stimulation trace and in the difference between the 1st and 10th stimulus. This suggests that the improvement we see in the CMAP at 6 months is also reflected in the RNS stimulation and

suggests an improvement in functional motor axons and NMJ activity at this time point in the 2.5mg/kg dosed group.

4.5.2. FTD phenotypes

As well as the motor phenotypes described in the TDP-43^{Q331K} transgenic mouse model, there are FTD phenotypes such as apathy, reduction of activity, lack of cognitive function and increased weight gain seen in this model (Kim *et al.*, 2020; Watkins *et al.*, 2020; White *et al.*, 2019).

4.5.2.1. Weight

Weight is an easy and robust measurement of the health of mice and is indicative of disease progression in many disease models of ALS. Usually in ALS mouse models, mice lose weight as the disease progress similar to ALS patients who become hypermetabolic and lose weight due to problems with swallowing, reduced appetite or loss of muscle mass (Wang *et al.*, 2021). The transgenic TDP-43^{Q331K} mice used for this study gain significantly more weight when compared to NT littermates which is more suggestive of an FTD phenotype where patients become hyperoral and have elevated BMI (Ahmed *et al.*, 2016). A TDP-43^{Q331K} knock-in mouse line has been shown to gain weight and eat more than WT mice and NT littermates (White *et al.*, 2018), and our analysis of our in-house transgenic model has also shown similar weight gain with age (Watkins *et al.*, 2021). Also the knock-in mice have been shown to be less active on running wheels than WT mice (Watkins *et al.*, 2020), which could contribute to the weight increase seen in the mice and may be due to the increased apathy seen in the model (Kim *et al.*, 2020).

There was a significant decrease in weight in both M102 groups when compared to the vehicle group. This decrease in weight could be indicative of an improvement in the FTD-like phenotype in these mice.

There was no significant difference in weight between the groups at 3-months of age, which is in line with the 6-month data as the significant difference did not develop until nearer the 6-month time point. AUC analysis shows a significant decrease in weight of the M102 2.5mg/kg dosed group when compared to vehicle and no difference in the 5mg/kg dosed

group. This suggests that the reduction in weight gain starts earlier in the M102 2.5mg/kg dose group, which could be indicative of better activity of M102 in this dose group.

Weight can also be affected by stress, and dosing can add significant stress to the animals. The twice daily dose group are being dosed twice as often as the once daily group and this increased stress could be part of the weight loss. If I were to run an experiment with twice daily dosing vs once daily dosing again, I would have the once daily group and vehicle group have a vehicle dose in the afternoon so that all mice were being dosed an equal number of times.

4.5.2.2. Marble Burying

Marble burying has been suggested in the past to reflect anxiety-like behaviours (Broekkamp *et al.*, 1986). However it has more recently been shown to be linked with innate repetitive digging behaviour and normal exploratory behaviour rather than directly related to anxiety (Thomas *et al.*, 2009). Marble burying behaviour is tightly linked to mouse strain. Our transgenic TDP-43^{Q331K} mice have previously been shown to bury fewer marbles than non-transgenic mice at 6 months of age (in-house data) and it has also been shown that knock-in TDP-43^{Q331K} mice also bury fewer marbles (White *et al.*, 2018).

The reduction of marble burying behaviour in the transgenic TDP-43^{Q331K} mice may be due to reduced activity related to apathy, i.e. a lack of desire to explore a new environment a feature of human FTD (Radakovic *et al.*, 2016). Indeed TDP-43^{Q331K} mice on some occasions fell asleep in the marble burying cages within the 30 minutes of the test duration rather than exploring a new environment as mice would typically do. This lack of activity could be due to lack of motivation in these mice which may be linked to the reduced cognitive function of these mice through the FTD phenotype.

There was no significant difference between the M102 dosed groups and the vehicle dosed group in the number of marbles buried, suggesting that M102 does not have an effect on activity levels. Using running wheels in home cages may be another more sensitive way to see changes in activity between dosed mice and vehicle mice as it shows voluntary running in the mice rather than the forced activity of rotarod assessment. The TDP-43^{Q331K} transgenic mice have been shown to have reduced running time and reduced running distance each night

when compared to WT mice (in house data) and the knock-in male and female mice have also been shown to have this behaviour (Watkins *et al.*, 2020; White *et al.*, 2018). However, adding running wheels means housing animals individually for the duration of the study. Reduction in activity could be linked with motor decline as seen in the SOD1^{G93A} mouse model as it correlates with reduction in rotarod performance (Bennett *et al.*, 2014). However, as described previously reduction in activity could also be due to lack of motivation, which would be interesting to explore in these mice.

Another measure that could be used to compare activity would be an open field test (Seibenhener and Wooten, 2015). Mice are free to run in a square space for 10 minutes while being recorded by a camera and analysis will show distance run but can also compare time spent in the middle of the space compared to at the edges, which is linked to anxiety like behaviour. Anxiety like behaviour or lack of fear could also be linked to FTD phenotypes in mice.

4.5.2.3. Observations of TDP-43^{Q331K} mice

I believe the TDP-43^{Q331K} mice have a prominent FTD phenotype after working with them for a few years and comparing them to other mice I have worked with. They lack motivation and have reduced activity, this is shown in other studies through running wheel analysis but is also very easy to see when handling the mice as they are far calmer and more relaxed as they get older. Whether this is through regular dosing and handling can be debated, but regular dosing of other mice strains does not lead to the same level of calmness in my opinion. This information, combined with the mice often falling asleep in marble burying cages and not running as often or as enthusiastically on the catwalk (often needing more encouragement to collect the required six continuous runs) leads me to believe the FTD phenotype is as prominent as the motor defects seen in these mice. Although all of this is anecdotal evidence, previous studies in male TDP-43^{Q331K} knock in mice note the reduction of volume in the hippocampus compared to NT and significant loss of parvalbumin-positive (PV+) interneurons (Lin *et al.*, 2020), which may be linked to cognitive decline. Also, White *et al.* showed that the in TDP-43^{Q331K} knock in mice had impairments in memory and executive dysfunction that they believed representative of what is seen in FTD patients, alongside the defects in motor function (White *et al.*, 2018). Taking all this information together indicates that the FTD

phenotype is prominent in this TDP-43^{Q331K} model, and it would be beneficial to develop behavioural techniques to better distinguish differences in cognition in this model.

4.5.3. Tissue analysis

4.5.3.1. Spinal cord Nissl staining and glial staining

Staining of lumbar spinal cords with Iba1 and GFAP showed no significant change in intensity of staining or percentage area of staining between vehicle or either M102 dosed groups suggesting that M102 gives no benefit to activation of microglia or astrocytes. Previous work on this transgenic model showed increased staining of Iba1 and GFAP in transgenic mice compared to non-transgenic litter mates suggesting an increase in microgliosis and astrogliosis at 10 months of age. In this study, the staining was carried out at 6 months of age and therefore there may not have been a significant increase in either staining at this time point when compared to 10 months of age. However, it may also be that M102 does not affect astrocytes or microglia in the spinal cord.

Nissl staining was also carried out in order to count motor neuron number in the lumbar spinal cord; however, no difference in motor neuron number was observed in the ventral horns of the M102 dosed mice when compared to vehicle. Previous studies in the TDP-43^{Q331K} knock-in mice did not report any differences between motor neuron number or morphology at 5 months of age (White *et al.*, 2018), suggesting that these mice do not lose motor neurons over time as seen in the SOD1^{G93A} model (Gurney *et al.*, 1994). However, work in the original transgenic model showed significant loss of neurons at 10 months of age, with the loss starting as early as 2 months of age (Arnold *et al.*, 2013).

The significant improvement in CMAP of the 2.5mg/kg and 5mg/kg dose groups is not reflected in an increase in the number of motor neurons in the lumbar spinal cord. CMAP is, however, not directly correlated to number of motor neurons but functional innervation of muscles. This suggests that the treated mice have improved innervation of muscle. Further work is needed to fully understand the protective mechanism, such as analysis of NMJ innervation.

So far, staining has only been carried out on lumbar spinal cords. Due to the FTD phenotype seen in these mice, it would also be interesting to investigate differences in the brains of the

mice. Specifically, staining of microglia, astrocytes and neurons in the brain would be useful to calculate if there is a difference between NT and T mice in terms of number of neurons or amount of neuroinflammation in the brains of mice and then determine if that is different in the M102 dosed mice. It has been shown previously that the brains of TDP-43^{Q331K} mice are smaller in volume when compared to NT mice and that there is increased microglia staining in the frontal cortex, entorhinal cortex and visual cortex (Lin *et al.*, 2020). Brains from 10-month-old TDP-43^{Q331K} and NT mice have been sectioned and are currently being stained for microglia, astrocytes and neurons in order to determine if there is a difference. Once the method has been developed for staining and analysis, this can be carried out on brains from this dosing study to see whether M102 influences inflammation or number of neurons.

4.5.3.2. RT-qPCR analysis

Quantitative RT-qPCR was carried out on cDNA derived from CNS tissue on a range of gene targets of NRF2 and HSF1 using primers that have previously been optimised. The results show that at 3 months of age several NRF2 and HSF1 target genes are upregulated in the M102 dosed groups within the cortex tissue when compared to the vehicle dosed groups, however at 6 months of age only the HSF1 targets are upregulated with no significant change in NRF2 targets. Tissue was collected at the same time point post final dose, so this was not an effect of different time points of tissue collection. The only difference in the collection of the tissue was that the 3-month cohort tissue was collected, and RNA was extracted immediately whereas the 6-month-old tissue was stored in RNALater at -20°C and RNA was extracted using the same method but later. There are pros and cons of both methods. RNALater has been shown to keep RNA stable in tissue and produce the same results from later RNA extraction.

The difference between mRNA expression at the 3-month and 6-month time point may be due to the difficulty in activating the NRF2 pathway later in disease progression, which I have demonstrated in the shorter-term dosing studies in SOD1^{G93A} mice. NRF2 pathway dysregulation has been documented previously in patients (Sarlette *et al.*, 2008), cellular models (Kirby *et al.*, 2005), and mouse models (Mimoto *et al.*, 2012) of ALS.

Mimoto *et al*. showed increases in NRF2 in the spinal cord of SOD1^{G93A} mice as they aged, with smaller percentage increases of downstream targets, suggesting an impairment of the pathway with NRF2 increases not being correlated to the response downstream (Mimoto *et*

al., 2012). In a SOD1 cellular model, Kirby *et al.* showed a significant decrease in NRF2 levels and linked this with decreases in multiple downstream NRF2 targets involved in antioxidant pathways (Kirby *et al.*, 2005). There was also evidence of upregulation of proteins suggested to be negative regulators of the ARE. Upregulation of negative regulators of ARE genes could have a significant impact on the activation of these genes using M102.

RNA binding proteins have also been implicated to affect the KEAP1/NRF2 pathway, with RBM45 being shown to stabilise KEAP1 and therefore reduce NRF2 activity (Bakkar *et al.*, 2015). Another RNA binding protein, hnRNPK, has been shown to bind to NRF2 target transcripts and potentially aiding with NRF2 signalling. However, in TDP-43 mutant cells, hnRNPK is mislocalised and therefore the activation of downstream targets is dysregulated (Moujalled *et al.*, 2017). The involvement of RNA binding proteins and other regulatory proteins in NRF2 signalling makes the pathway more complex, and the dysregulation of these pathways in ALS models may make it increasingly difficult to increase downstream targets of NRF2 with increased NRF2 activation alone.

Hspa1a is upregulated in cortex and spinal cord at 3 months and 6 months of age, which suggests that the improvements seen in CMAP, weight and gait may be due to the activation in HSF1 rather than NRF2. This may be especially true at later stages of disease, as NRF2 downstream targets are not activated and the NRF2 pathway is dysregulated.

Some but not all NRF2 targets are upregulated in cortex tissue, which may be due to the timepoint at which we collected the mice. NRF2 target genes will be upregulated for variable lengths of time after activation of NRF2 due to differing stability and regulation of mRNA transcripts. All the tissue for RT-qPCR was collected 24 hours post dose where we had previously seen upregulation of NRF2 and HSF1 targets in WT and $SOD1^{G93A}$ mice, however there may be different time points more suited to seeing upregulation of specific NRF2 targets. Ideally, we would have been able to collect tissue at multiple time-points and compare them to each other, however, to keep the number of mice per timepoint as high as possible for greater statistical power, we opted for one timepoint in this study for tissue collection.

Although the cortex tissue showed significant changes in expression of NRF2 and HSF1 target genes, the spinal cord data did not show these significant changes. Many genes show similar

trends in the spinal cord when compared to cortex tissue. This could be because the spinal cord data are more variable than the cortex tissue data. Although the qPCR experiment was normalised at the cDNA synthesis step and normalisation occurs to compare to endogenous control genes, the RNA concentration of spinal cord tissue was lower than that of cortex tissue after RNA extraction, which may have increased the variability between animals.

Given more time, it would have been advantageous to have explored more gene targets. Inflammatory gene transcripts would be extremely interesting to compare between vehicle and M102 dosed animals as NRF2 has the ability to activate anti-inflammatory mechanisms (Kobayashi *et al.*, 2016). However, it has been challenging to optimise inflammatory markers for qPCR in cortex tissue of animals due to the low level of inflammatory markers in WT animals. More work is required to optimise these primers using animals that we know have elevated inflammatory responses so that they can be used on this tissue to compare. As an alternative approach, astrocyte and microglial staining was carried out on lumbar spinal cords to detect signs of inflammation. Since electrophiles also activate other pathways, it would be great to explore a wider range of targets from pathways such as NF-kB.

4.5.4. Comparisons to the Mead *et al*. 2013 $SOD1^{G93A}$ study

M102 has previously been dosed in a $SOD1^{G93A}$ study at 5mg/kg subcutaneously (Mead *et al.*, 2013). In the study by Mead *et al.* there were significant improvements in rotarod performance, fore and hind-limb stride length, and an increase in muscle innervation of M102 dosed mice when compared to vehicle dosed mice. However, no significant improvement in survival was detected.

In the TDP-43^{Q331K} study we dosed at the same dose level (5mg/kg) as well as the split dose of 2.5mg/kg twice daily. In the previous study subcutaneous dosing of M102 contained DMSO (Mead *et al.*, 2013), whereas the formulation of M102 in this TDP-43^{Q331K} study was modified and the DMSO was removed and was instead formulated in a solution of saline, ascorbic acid and sodium metabisulfite. This change was made for a couple of reasons, firstly to remove the need for DMSO which could affect the mice. The second reason was to formulate M102 with antioxidants as M102 has been shown to readily oxidise in solution and the intension was to prevent this before dosing. The ongoing hypothesis is that M102 is oxidised to a more active

electrophile (oxo-apomorphine) *in vivo* which is better able to activate NRF2 and HSF1, so we wanted to make sure that we are injecting M102 specifically rather than the oxidised form.

Although in the TDP-43^{Q331K} subcutaneous study there was no difference in the stride length or rotarod performance between the M102 and vehicle dosed groups, there was a significant difference in CMAP, which suggests that there is an improvement in muscle innervation. There was also a significant impact on some gait parameters, and although these are not the same as in the SOD1 model, they suggest a similar improvement on overall gait stability with M102 dosing.

4.5.5. Conclusions

The most significant improvements in weight, CMAP and gait were seen in the M102 2.5mg/kg twice daily dosed group over the M102 5mg/kg once daily dosed group. This suggests that giving M102 twice daily has a superior neuroprotective effect. Taking these data and the data from the previous study with M102 in SOD1^{G93A} mice (Mead *et al.*, 2013) together suggests that M102 is tolerated in mouse models and is able to improve progression of disease in two different mouse models of ALS.

Due to the interest and exploration of NRF2 activators, coupled with the promising results from HSF1 activation in ALS, as well as our results in a TDP-43^{Q331K} mouse model, there is potential promise for M102 to have a positive effect on disease progression in ALS patients.

5. Results: M102 in SOD1^{G93A} mice

5.1. Introduction

After the promising results seen with subcutaneous dosing of M102 in TDP-43^{Q331K} mouse model where there were significant improvements in weight, CMAP and gait, we decided to look at M102 again in the SOD1^{G93A} mouse model. The main aim was to investigate oral dosing of M102, as that is the proposed dosing route for clinical studies. Oral dosing is the most common way of dosing in patients and is easy to administer which makes compliance of oral dosing higher than other methods of dosing (Alqahtani *et al.*, 2021). We wanted to investigate if orally dosed M102 was able to impact on the progression of disease in the SOD1^{G93A} mouse model. Another aim was to investigate the potential of the oxidised form of M102, oxo-apomorphine (OXA) in this model and compare the effects to M102. The final aim was to investigate the action of edaravone in the mouse model as it is a newly approved treatment for ALS patients, edaravone, and we wanted to compare any effect on the model with M102.

The SOD1^{G93A} mouse model is the "gold standard" mouse model of disease. It was the first ALS mouse model generated (Gurney *et al.*, 1994) and it has been the most commonly used mouse model for ALS (Ittner *et al.*, 2015). This original model (Gurney *et al.*, 1994) has been back crossed onto a C57BL/6J OlaHsd background and extensively characterised in house and shows a robust and reproducible progression of disease (Mead *et al.*, 2011). In this model, mice develop motor defects that progress over time and can be picked up through behavioural assays, such as rotarod and catwalk, and loss of motor neurons and inflammation of CNS that can be seen at various time points throughout the progression of disease determined by tissue analysis.

SOD1^{G93A} mice reach an end-stage of disease and have to be humanely culled at around 140 days old due to significant weight loss or impairment of the righting reflex (Mead *et al.*, 2011). End-stage studies allow differences in life span to be determined, which can be useful to see if a treatment has the potential to extend lifespan in patients, however this causes significant distress to the animals due to the severe disease phenotype. Because of the robustness of the model, studies can be terminated at an earlier timepoint than end-stage of disease and differences in therapeutic approaches can be identified through behavioural tests and tissue analysis (Mead *et al.*, 2011). This means that the mice remain at a less severe stage of disease

by the end of the study, which is beneficial to the 3R's, while still providing useful information on the efficacy and mechanisms of action of therapeutic compounds.

There has been a lack of translation from ALS mouse models to patients in clinical trials, especially in end-stage studies showing extension of life-span in mice, but the compounds do not show this extension in patients (Scott *et al.*, 2008). Having positive data from M102 effects in two mouse models, where the studies have been sufficiently powered and randomised, will increase confidence in M102 and its potential to treat patients with ALS.

M102 has been dosed subcutaneously previously in the $SOD1^{G93A}$ model where there were improvements seen in rotarod performance and gait parameters as well as improvements in glutathione levels and evidence of activation of Nrf2 targets in spinal cord tissue (Mead *et al.*, 2013). The aim of this current experiment was to explore oral dosing of M102 in the model and compare the data with historical subcutaneous data, as the route of administration can influence the exposure and therefore efficacy of compounds (Steinmetz and Spack, 2009).

OXA is a putative active metabolite of M102, with the ability to activate the NRF2 pathway. The addition of OXA to the study was to investigate the tolerability of OXA and its potential effects in the $SOD1^{G93A}$ mouse model. The results of OXA can then also be compared with the effects of M102. The current theory is that M102 can target specific tissue by being oxidised at sites within areas of high oxidative stress and therefore it is able to preferentially exert its effects in tissue experiencing higher levels of oxidative stress. However, we do not know the point at which M102 converts to OXA in the body. In the previous $TDP\text{-}43^{Q331K}$ study where M102 was injected subcutaneously, antioxidants were added to the formulation to ensure the compound dosed was M102 and not OXA.

The final aim of the study was to replicate the effects seen in previous mouse studies of edaravone in the $SOD1^{G93A}$ model and compare the potential effects with M102. Edaravone, has been recently approved for use in ALS patients by the FDA (Cruz, 2018) and is thought to exert its neuroprotective effects by acting on oxidative stress, although the complete mechanism of action is still currently unknown. It has been shown recently that edaravone activates the NRF2 pathway and this may contribute to the neuroprotective effects (Shou *et al.*, 2019). Edaravone was selected for the study because of its known anti-oxidant properties

and due to its reported positive effect in mouse models (Ito *et al.*, 2008) and clinical trials (Jiménez-Villegas *et al.*, 2021), which makes it a good comparator for M102.

5.2. Aims

- To investigate the pharmacology and efficacy of orally dosed M102 in the SOD1^{G93A} ALS mouse model.
- To investigate the pharmacology and efficacy of subcutaneously dosed OXA in the SOD1^{G93A} ALS mouse model and compare the effects to M102.
- To replicate the effects of edaravone in the SOD1^{G93A} ALS mouse model and compare the effects to those observed M102.

5.3. Study Design

Transgenic female mice were block randomised into the 7 different dose groups and dosed from 25 days until 90 days of age (Table 5.1). The end time point is based on the previous data that have shown significant differences in a number of behavioural parameters and tissue analysis between T and NT mice at this age point without the need to take animals to a point of disease where they will undergo substantial distress (Mead *et al.*, 2011). Rotarod testing was carried out twice per week from 40 days of age and neuroscoring was carried out thrice per week from 60 days of age. Electrophysiology was carried out at 60 days and 90 days of age with catwalk gait analysis on 70 and 85 days of age (Figure 5.1). All of the time points were based on progression of the model and previous characterisation (Figure 1.2).

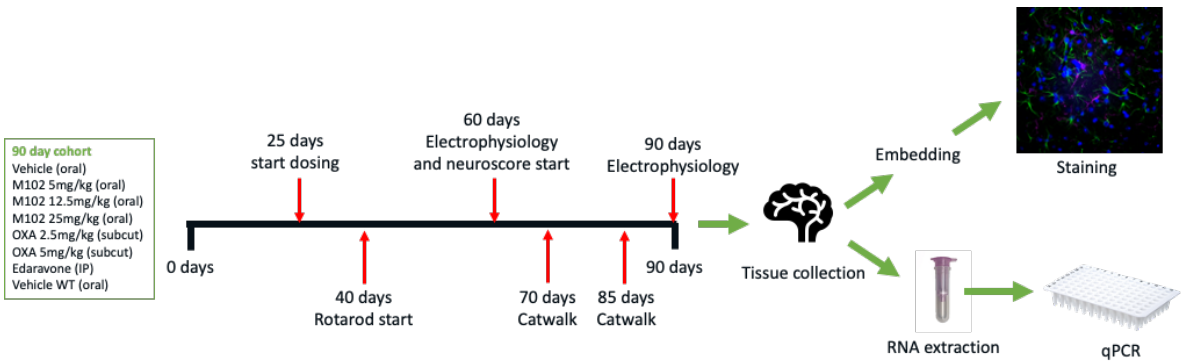

Figure 5.1: Study design for the SOD1^{G93A} mouse model study showing time points for behavioural test and tissue analysis.

Table 5.1: A summary of dose groups, dose quantities and route of dosing for the groups in the SOD1^{G93A} study

Group	Genotype	Substance	Dose	Dose route	N per group
1	WT C57Bl/6	Vehicle	-	oral	8
2	SOD1^{G93A}	Vehicle	-	oral	8
3	SOD1^{G93A}	M102	5mg/kg/day	oral	8
4	SOD1^{G93A}	M102	12.5mg/kg/day	oral	8
5	SOD1^{G93A}	M102	25mg/kg/day	oral	8
6	SOD1^{G93A}	OXA	2.5mg/kg/day	subcutaneous	8
7	SOD1^{G93A}	OXA	5mg/kg/day	subcutaneous	8
8	SOD1^{G93A}	Edaravone	15mg/kg/day (2 week on/off cycle)	intraperitoneal	8

The study was powered to have 90% confidence to see a two-week delay in 20% rotarod decline in at least 1 group out of the 7 groups. The power analysis was carried out using the average standard deviation in rotarod performance from previous in-house SOD1^{G93A} studies. The results of the power analysis showed that the number of animals per group to meet these criteria is 8. Half of the animals had tissue collected for gene expression analysis and protein analysis and therefore underwent a snap freezing protocol, whereas the other half of the animals had tissue collected for histology and therefore were PFA perfused at the end of the study.

The study was designed to explore multiple drugs within the same study using the same vehicle group, reducing the need for multiple vehicle groups, and therefore reducing the number of animals required for the study. Because the main objective of the study was to investigate orally dosed M102 in the SOD1^{G93A} mice, the vehicle animals were dosed orally using a gavage needle with 10% (2-Hydroxypropyl)-β-cyclodextrin (HP-ß-CD) as this is the vehicle used for the M102 formulation. The doses of M102 were selected based on the data showing that 25mg/kg dosed orally has the same bioavailability as 5mg/kg dosed subcutaneously. M102 has previously been dosed orally in short term mouse studies with no adverse effects but has not been dosed orally for an extended period.

The investigation of OXA was the secondary aim of the study. As OXA has not previously been dosed in mice before, this was dosed via subcutaneous injection as oral bioavailability studies have not yet been carried out. The dose levels selected for OXA were chosen based on assumptions that absorption would be similar to M102 in mice, although we were expecting the drug to be more potent.

The final aim of the study was to explore the effects of edaravone. Because of the similarities in mechanisms that edaravone and M102 potentially act upon, and the fact edaravone has been successful in the clinic, makes edaravone a good comparator to M102. As well as comparisons of behavioural tests, comparison of gene expression in tissue will give more details on whether the same pathways are activated with edaravone and M102 dosing. In the clinic edaravone is treated in a two week on and two week off regime, so we followed this for dosing in the mice. However, humans are given edaravone intravenously (Abe *et al.*, 2017), whereas animal studies routinely dose edaravone intraperitoneally (Baba *et al.*, 2016; Ito *et al.*, 2008). The dose level of 15mg/kg was selected as this is the dose that has previously been shown to have beneficial effects in a SOD1 mouse model (Ito *et al.*, 2008).

A group of non-transgenic $SOD1^{G93A}$ (WT) mice were recruited from the same litters as T mice and dosed orally with vehicle from 25 days to 90 days of age. These animals were to compare with the transgenic $SOD1^{G93A}$ mice on the behavioural parameters and tissue analysis, especially for the electrophysiology data, as this has not been carried out extensively in this mouse model in-house previously.

Because of the design of the study and the aims, the data were analysed with each of the compounds compared with $SOD1^{G93A}$ vehicle separately from each other.

5.4. Results

5.4.1. Formulation of compounds

M102 was dosed orally for this study using 10 % HP-ß-CD in purified water. HP-ß-CD is a well-tolerated commonly used cyclodextrin that increases the solubility of organic compounds. Cyclodextrins are composed of chains of glucose that form a circular structure with a hydrophobic interior that can form complexes with hydrophobic compounds (Gould and Scott, 2005).

Since we did not have PK data for OXA, we chose subcutaneous dosing to avoid potential issues with oral bioavailability, however after sonication, heating and vortexing OXA would not go into solution with 10% HP-ß-CD.

Another common vehicle for oral dosing solutions is to use a suspension in a viscous solution such as methyl cellulose (MC). However, OXA quickly fell out of suspension making it difficult to dose consistently. Instead OXA was diluted in pure DMSO at 50mg/ml or 25mg/ml and diluted 1 in 100 before dosing with sterilised water to create 0.5mg/ml and 0.25mg/ml which are needed for doses of 5mg/kg and 2.5mg/kg when dosed at 10ml/kg. OXA was easily dissolvable in the DMSO, and when diluted 1 in 100 with water would form a fine suspension which maintained long enough to enable consistent dosing. The final concentration of DMSO is 1% w/v. Edaravone was formulated as described (Baba *et al.*, 2016) and was prepared once per week.

A)

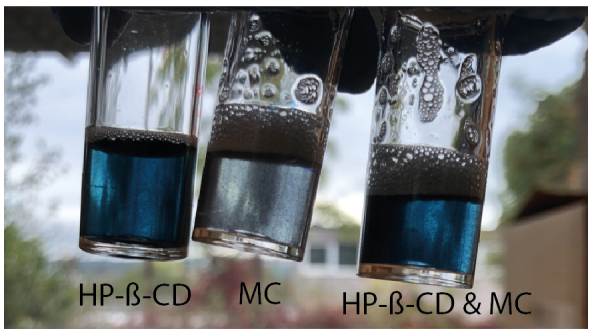

B)

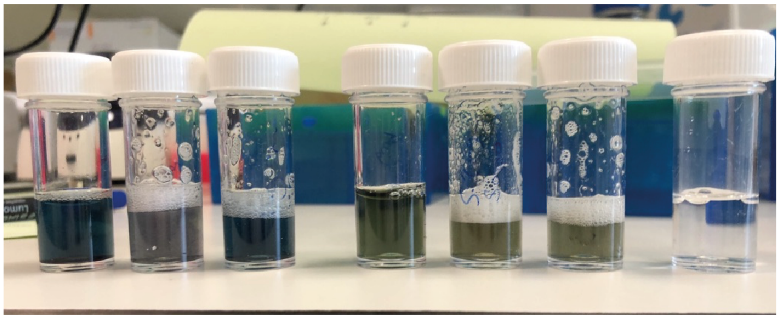

Figure 5.2: Formulation of M102, OXA and edaravone for dosing. A) OXA formulated in HP-ß-CD, methyl cellulose (MC) and both HP-ß-CD and MC at a concentration of 0.5mg/ml, which was the highest concentration used in the study. In all of the formulations OXA particles can be seen in the solution and OXA fell out of suspension easily. B) 1 = 0.5mg/ml OXA HP-ß-CD, 2 = 0.5mg/ml OXA MC, 3 = 0.5mg/ml OXA HP-ß-CD and MC, 4 = 2.5mg/kg M102 HP-ß-CD, 5 = 2.5mg/ml M102 MC, 6 = 2.5mg/ml M102 HP-ß-CD and MC, 7 = 1.5mg/ml Edaravone. OXA was not soluble in any of the above formulations at a concentration of 0.5mg/ml. M102 is soluble in all the solutions at 2.5mg/ml.

5.4.2. Tolerability

Mice were monitored closely when first dosed to assess any adverse effects of dosing. This was particularly important for OXA as it has previously not been dosed in mice. Mice were also checked daily before and after dosing in case there were any adverse effects that can accumulate over time. Animals were monitored for extreme changes in weight, changes in behaviour or any signs of distress, such as piloerection or pinched features.

No adverse effects were seen in any of the dose groups during the study. There was slight scarring of skin around the injection site of mice dosed subcutaneously with OXA but this is an

expected effect from long term daily subcutaneous injections and previously seen with apopmorphine injections (Poltawski *et al.*, 2008).

5.4.3. Mouse weights

The weight of mice was recorded before each daily dose to determine the dose volumes and to assess the effect of treatment on weight. All dose groups quickly put on weight at the start of the study as expected as the mice are still growing and this plateaus from around 40 days of age. There was no significant difference in weight in any of the M102 dosed groups when compared to $SOD1^{G93A}$ vehicle over the course of the study (Figure 5.3a, overall P = 0.5020, mixed-effect analysis with Dunnett's multiple comparisons).

There was no significant difference in weight in either of the OXA dosed groups when compared to $SOD1^{G93A}$ vehicle (Figure 5.3b, overall P = 0.3582, mixed effect analysis with Dunnett's multiple comparisons).

There was no significant difference between the edaravone group or WT vehicle group when compared to the $SOD1^{G93A}$ vehicle group (Figure 5.3c, overall P = 0.1853, mixed effect analysis with Dunnett's multiple comparisons).

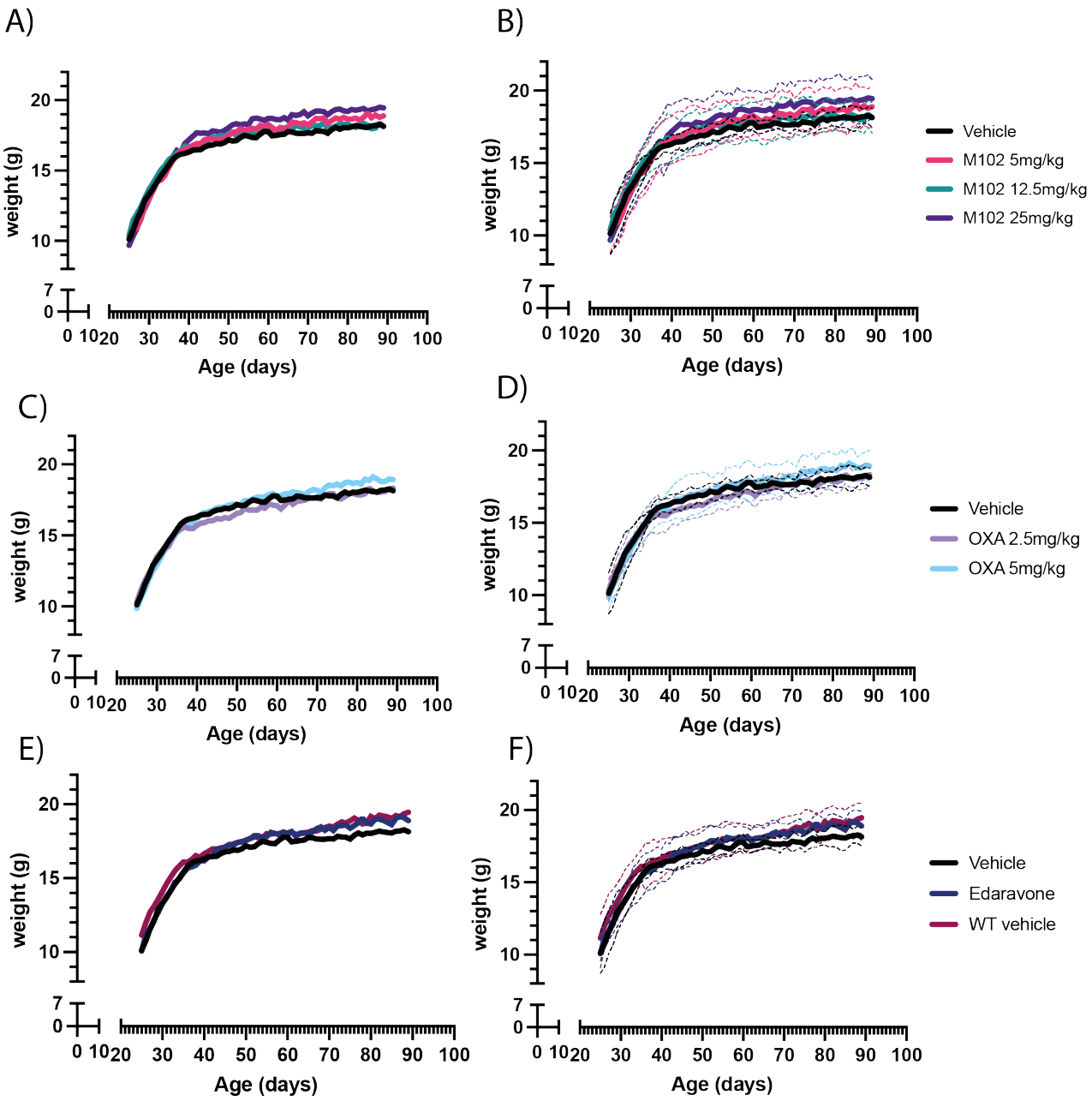

Figure 5.3: Mouse weights over time for animals dosed with M102, OXA and edaravone Solid line shows the mean of the group and the dotted lines show ± SD. Data shown as mean and mean ± SD for clarity of data. A) Mean and B) mean ± SD of daily weights over time of vehicle and M102 at 5mg/kg, 12.5mg/kg and 25mg/kg. C) mean and D) mean ± SD of daily weights over time of vehicle and OXA at 2.5mg/kg and 5mg/kg. E) Mean and F) mean ± SD of daily weights over time for vehicle, edaravone and WT vehicle. There was no significant difference in any of the dose groups when compared to vehicle. N=8 per group, mixed effect analysis with Dunnett's multiple comparisons.

AUC analysis of weight over the duration of the study showed significant increases in weight for M102 5mg/kg, M102 25mg/kg, edaravone and WT mice when compared to SOD1^{G93A}

vehicle dosed mice (Figure 5.4a & c, one-way ANOVA with Dunnett's multiple comparisons). There was no significant difference in the 12.5mg/kg M102 or any of the OXA groups when compared to SOD1^{G93A} vehicle (Figure 5.4a & b). The AUC for the vehicle group was 1070 ± 4.0 g x days vs 1096 ± 8 g x days for the M102 5mg/kg dosed group (P = 0.0328 vs vehicle), 1089 ± 6.9 g x days for M102 12.5mg/kg (P = 0.1896 vs vehicle), 1126 ± 8.7 for M102 25mg/kg g x days (P <0.0001 vs vehicle), 1053 ±4.9 g x days for OXA 2.5mg/kg (P = 0.2857 vs vehicle), 1086 ± 6.1 g x days for OXA 5mg/kg (P = 0.3446 vs vehicle), 1098 ± 5.4 g x days for Edaravone (P = 0.0183 vs vehicle), and 1114 ± 6.3 for WT vehicle g x days (P <0.0001 vs vehicle).

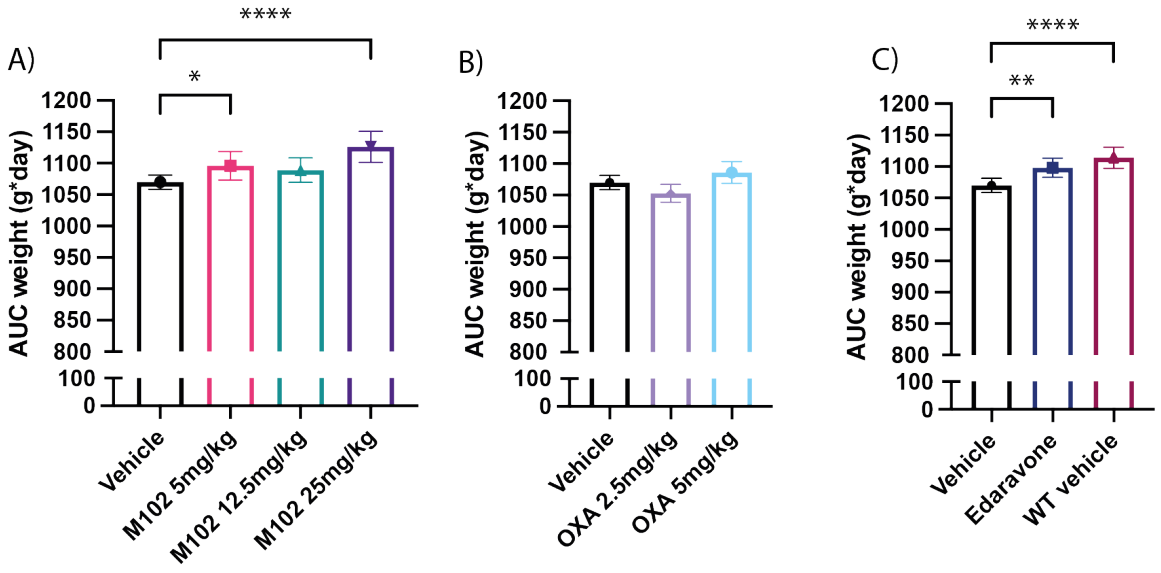

Figure 5.4: Area under the curve analysis of mouse weight from 25 days until 90 days of age. Area under the curve (AUC) analysis of weight shown as mean ± SD. A) M102 and vehicle dosed groups weight AUC. B) OXA and vehicle dosed groups weight AUC. C) Edaravone dosed group and WT vehicle vs vehicle weight AUC. There was a significant increase in weight in the M102 5mg/kg and 25mg/kg, edaravone and WT vehicle groups when compared to the vehicle group. N = 8 per group. One-way ANOVA with Dunnett's multiple comparisons (* = p<0.05, ** = p<0.01, *** = p<0.001, **** = p<0.0001).

5.4.4. Rotarod

Rotarod is a good indicator of motor function and coordination and has been previously shown to be an early indicator of disease in SOD1^{G93A} mice (Mead *et al.*, 2011). Mice were tested on the rotarod twice per week to determine how long they could remain on the equipment and the time taken to fall off (latency to fall) was recorded. As expected from the model, the rotarod performance of the mice decreased over time for all the SOD1^{G93A} transgenic mice whereas WT mice continued to run for the maximum amount of time allowed for the duration of the study (Figure 5.5c).

Overall, there was no significant difference between the M102 dosed groups when compared to SOD1^{G93A} vehicle in terms of rotarod performance (Figure 5.5a, overall P = 0.8397, two-way ANOVA with Dunnett's multiple comparisons).

There was a significant reduction in rotarod performance of the OXA 5mg/kg group when compared to SOD1^{G93A} vehicle (Figure 5.5b, overall P = 0.0166, two-way ANOVA with Dunnett's multiple comparisons). There was no significant difference of the OXA 2.5mg/kg group when compared to vehicle.

The WT group performed significantly better over the course of the study than the SOD1^{G93A} vehicle group as expected (Figure 5.5c, overall P = 0.0041, two-way ANOVA with Dunnett's multiple comparisons). There was no significant difference between the edaravone group and the vehicle group in terms of rotarod performance.

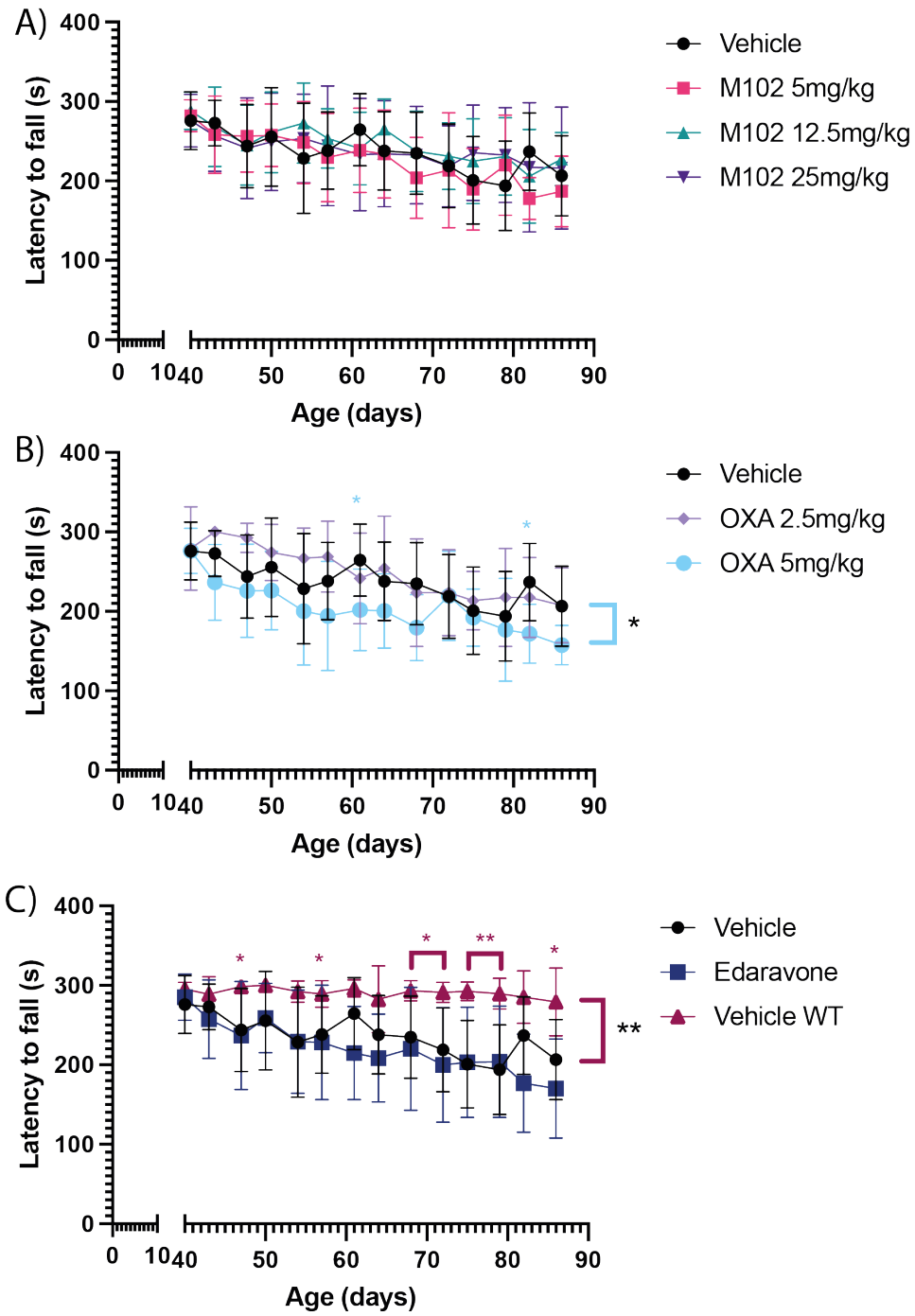

Figure 5.5: Rotarod performance of SOD1^{G93A} mice shown as latency to fall in seconds. Mean shown as individual points and error bars show ± SD. A) Rotarod performance over time of the vehicle, 5mg/kg M102, 12.5mg/kg M102 and 25mg/kg M102 dose groups. B) Rotarod performance over time for vehicle, 2.5mg/kg OXA and 5mg/kg OXA dose groups. C) Rotarod performance over time for vehicle, edaravone and WT vehicle dose groups. N = 8 per group. Two-way ANOVA with Dunnett's multiple comparison's (* = p<0.05, ** = p<0.01, *** = p<0.001, **** = p<0.0001).

Typically for the SOD1^{G93A} mouse model, rotarod performance can be analysed as age to reach 20% decline in performance (Mead *et al.*, 2011). This is calculated as the time it takes for animals to reach a 20% decline in rotarod performance compared to the best performance from their first two test runs. The WT animals did not reach 20% decline in rotarod performance as they continued to perform at 100% for the duration of the study, which was expected. There was no significant difference in the age at which mice reach 20% decline in rotarod performance in any of the M102, OXA or edaravone dose groups when compared to SOD1^{G93A} vehicle (Figure 5.6A, B & C).

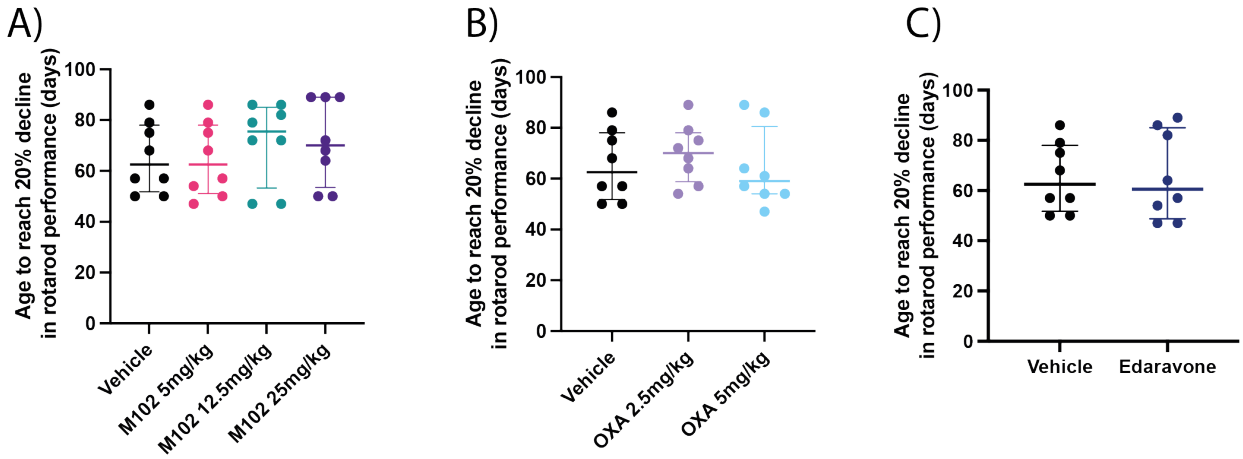

Figure 5.6: Time taken to reach 20% decline in rotarod performance in SOD1^{G93A} mice. Individual animals plotted and median ± IQR. Age to reach 20% decline in rotarod performance for A) M102 dosed groups, B) OXA dosed groups, C) edaravone dosed group. N = 8 per group. Kruskal-Wallis test with Dunn's multiple comparison).

AUC analysis showed a significant difference between the SOD1^{G93A} vehicle and WT vehicle animals as expected from the model, with the WT animals performing significantly better than vehicle dosed mice (Figure 5.7c, P = 0.0054, one-way ANOVA with Dunnett's multiple comparisons). SOD1^{G93A} vehicle AUC was 10835 ± 475 vs 13395 ± 194 for WT animals.

There was no significant difference in rotarod performance AUC between the SOD1^{G93A} vehicle dosed group and any other dose group. The AUC (mean ± SEM) of the SOD1^{G93A} vehicle group was 10835 ± 475 s x day vs 10440 ± 468 s x day for M102 5mg/kg (P = 0.8941 vs SOD1^{G93A} vehicle), 11284 ± 432 s x day for M102 12.5mg/kg (P = 0.8552 vs SOD1^{G93A} vehicle), 10929 ± 579 s x day for M102 25mg/kg (P = 0.9982 vs SOD1^{G93A} vehicle), 11421 ± 444 s x day for OXA

2.5mg/kg (P = 0.5841 vs SOD1^{G93A} vehicle), 9305 ± 469 s x day for OXA 5mg/kg (P = 0.0607 vs SOD1^{G93A} vehicle), and 10108 ± 582 s x day for edaravone (P = 0.4423 vs SOD1^{G93A} vehicle, one-way ANOVA with Dunnett's multiple comparisons).

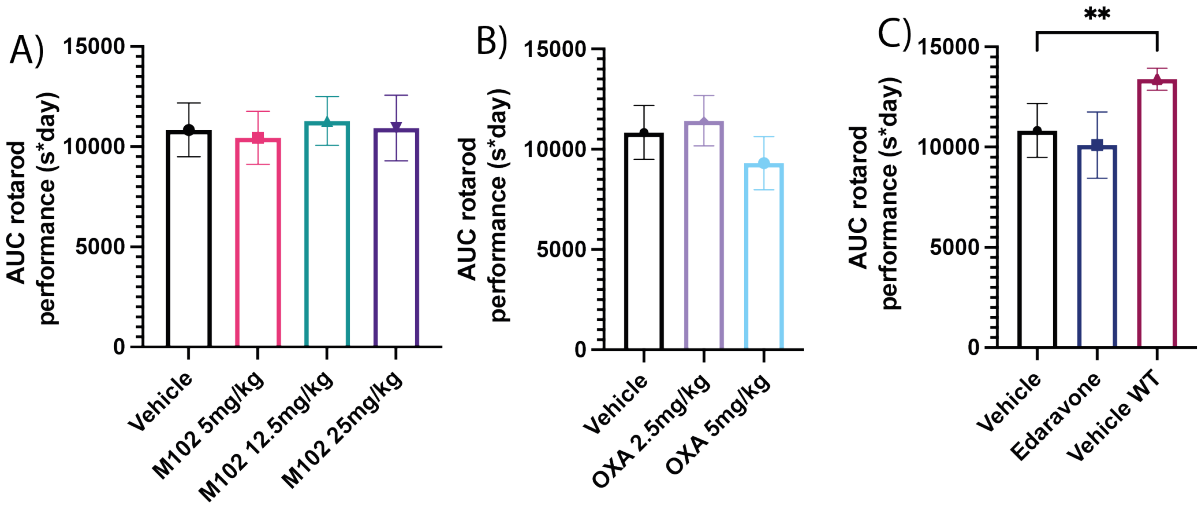

Figure 5.7: AUC of rotarod performance of SOD1^{G93A} mice. Area under the curve (AUC) analysis of rotarod performance shown as mean ± SD. N = 8 per group. A) M102 dosed groups vs vehicle rotarod AUC. B) OXA dosed groups vs vehicle rotarod AUC. C) Edaravone dosed group and WT vehicle vs vehicle rotarod AUC. There was a significant difference in rotarod performance of WT mice when compared to vehicle mice. There was no difference in rotarod performance between any of the dose groups and vehicle. One-way ANOVA with Dunnett's multiple comparison's (** = p<0.01).

5.4.5. Neuroscore

Mice were neuroscored three times per week (Monday, Wednesday, Friday) to determine onset of visible signs of disease, characterised by a splay defect and presence of a hind-limb tremor for at least two consecutive scores. There was no significant difference between the SOD1^{G93A} vehicle dosed group and the 5mg/kg M102 group (P = 0.7711), or the 12.5mg/kg M102 group (P = 0.2162) or the 25mg/kg M102 dose group (P = 0.3479, Figure 5.8A, one-way ANOVA with Dunnett's multiple comparison's). There was a significant decrease in age of onset of the 5mg/kg OXA group when compared with SOD1^{G93A} vehicle (P = 0.0284) but no significant difference with the 2.5mg/kg OXA group (P = 0.3977, Figure 5.8B). There was a significant decrease in the age of onset of edaravone dosed animals when compared to

SOD1^{G93A} vehicle (P = 0.0283, Figure 5.8C, unpaired t-test). WT animals were not included in this analysis as they did not reach onset for the duration of the study, as expected.

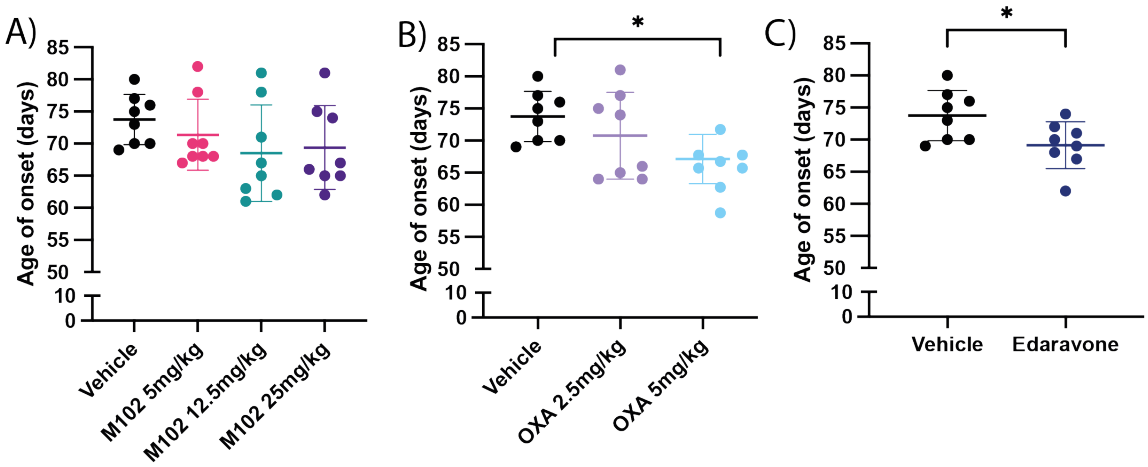

Figure 5.8: Age of onset for SOD1^{G93A} mice. The age at which mice reached onset of disease shown as individual animals with mean ± SD for A) M102 dose groups, B) OXA dosed groups and C) edaravone. There is a significant decrease in age of onset of OXA at 5mg/kg and edaravone when compared to vehicle. N = 8 per group. One-way ANOVA with Dunnett's multiple comparisons for A and B, unpaired t-test for C. (* = p<0.05)

5.4.6. Gait analysis

Gait analysis was carried out at 70 and 84 days of age using the catwalk gait analysis system (Noldus). Gait of SOD1^{G93A} mice changes over time due to neuromuscular degeneration and gait analysis was carried out to determine if any of the treatments improved gait parameters. The time points were selected based on previous characterisation data that showed significant differences between T and NT SOD1^{G93A} animals at these time points (Mead *et al.*, 2011).

Many parameters are collected for gait analysis, and I have just shown percentage of time on diagonal paws and stride length here. There was no difference between SOD1^{G93A} vehicle and WT vehicle in almost all parameters, meaning there was no window to see any potential therapeutic effects. There are more parameters of gait in the appendix.

The percentage of time spent on diagonal (2 paws) throughout the step cycle can give an indication of the steadiness of the gait in animals as mice would need more feet on the ground

as they get increasingly unstable in their gait. There was no difference between M102 dosed, OXA dosed, edaravone dosed or WT vehicle mice when compared to SOD1^{G93A} vehicle mice in percentage of time spent on diagonal paws (Figure 5.9A, C & G).

Stride length is the distance between the same paw being placed during walking in mm. There was no significant difference in hindlimb stride length between M102 dosed, OXA dosed, edaravone dosed or WT vehicle animals when compared to SOD1^{G93A} vehicle at either time point (Figure 5.9B, D & F).

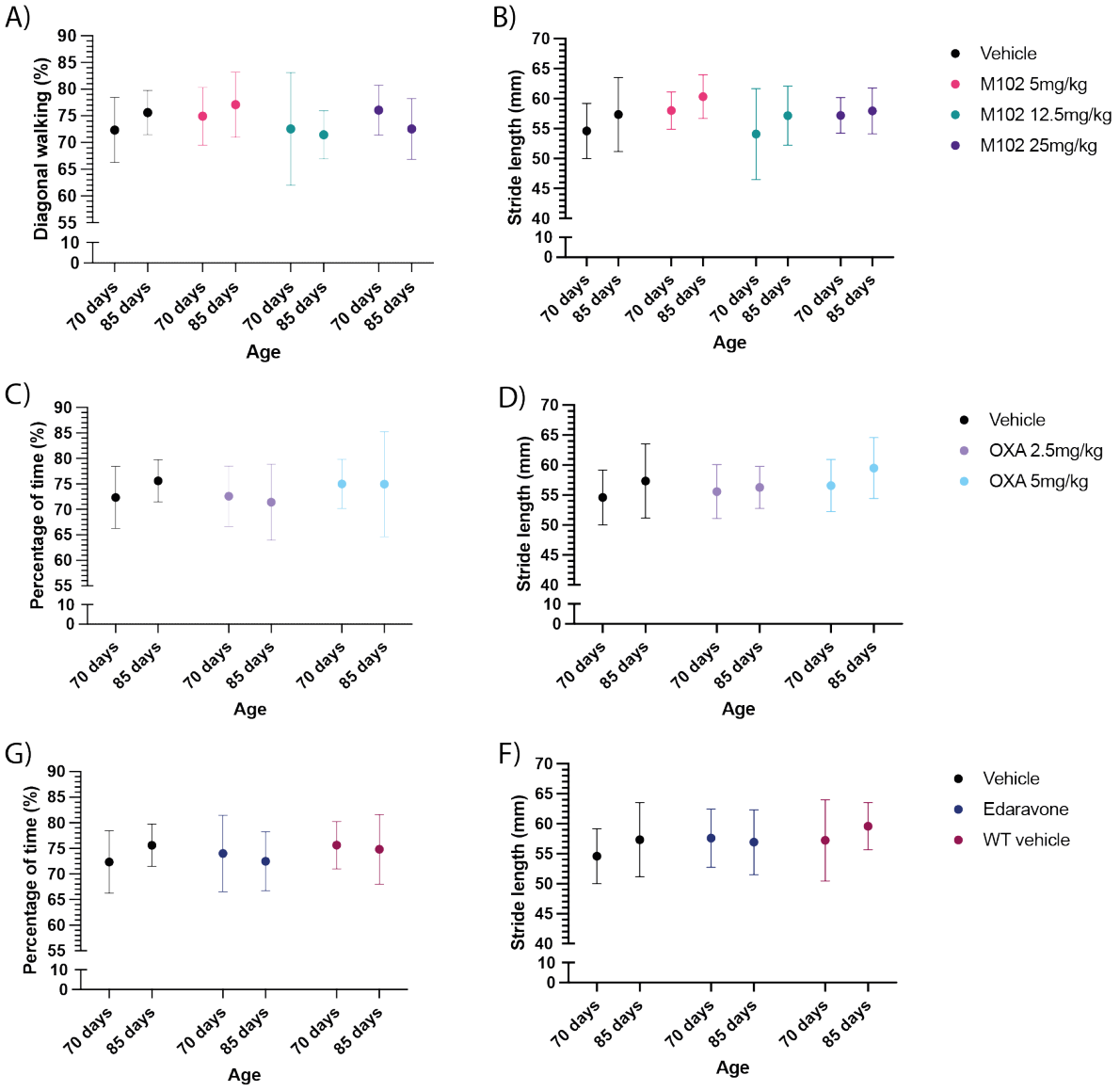

Figure 5.9: Percentage of time on diagonal paws and hindlimb stride length from gait analysis. Data shown as mean ± SD. Percentage of time spent on diagonal paws is the percentage of time that two paws are on the ground and stride length is the distance in mm between the previous paw placement and the same paw in a step cycle. A) time on diagonal paws and B) hindlimb stride length at 70 and 85 days for M102 and vehicle dosed groups. C) percentage of time on diagonal paws and D) hindlimb stride length of OXA and vehicle dosed groups. E) percentage of time on diagonal paws and F) hindlimb stride length of WT vehicle, edaravone and vehicle dosed animals. N = 8 per group. Two-way ANOVA with Dunnett's multiple comparison's.

5.4.7. Electrophysiology

5.4.7.1. Compound Muscle Action Potential (CMAP)

CMAP recordings were collected at 60 and 90 days of age to determine if the treatments had an effect on the motor units in the hind limb. CMAP measures the total functional output of the motor units in the hind limb following supramaximal stimulation of the sciatic nerve (Harrigan *et al.*, 2019). Electrophysiology has been carried out in SOD1 mouse and rat models previously and has shown a decrease in CMAP amplitude over progression of disease as animals become weaker (Harrigan *et al.*, 2019; Leermakers *et al.*, 2021; Mancuso *et al.*, 2011).

At 60 days of age there was no significant difference between any of the M102 dosed groups when compared to $SOD1^{G93A}$ vehicle (Figure 5.10A). However, at 90 days of age there was a significant increase in CMAP amplitude of the M102 25mg/kg dosed group when compared to the $SOD1^{G93A}$ vehicle dosed group (Figure 5.10B, 17.9 ± 4.7mV for M102 25mg/kg vs 12.9 ± 3.5mV for $SOD1^{G93A}$ vehicle, P = 0.0413, one-way ANOVA with Dunnett's multiple comparison) but not in the other M102 groups.

At 60 and 90 days of age there was no significant difference in CMAP amplitude between either of the OXA dosed groups and the $SOD1^{G93A}$ vehicle group (Figure 5.10C & D, one-way ANOVA with Dunnett's multiple comparisons).

The WT vehicle mice had a significantly higher CMAP when compared to $SOD1^{G93A}$ vehicle animals at both 60 and 90 days as expected (Figure 5.10E & F). At 60 days the WT vehicle average CMAP amplitude was 29.8 ± 9.8mV vs 15.7 ± 5.1mV for the $SOD1^{G93A}$ vehicle group (P = 0.0013) and for 90 days the WT average CMAP amplitude is 37.4 ± 6.7mV vs 12.9 ± 3.5mV for the $SOD1^{G93A}$ vehicle animals (P < 0.0001 one-way ANOVA with Dunnett's multiple comparisons). There was no significant difference between the $SOD1^{G93A}$ vehicle and edaravone groups at 60 or 90 days of age (Figure 5.10E & F).

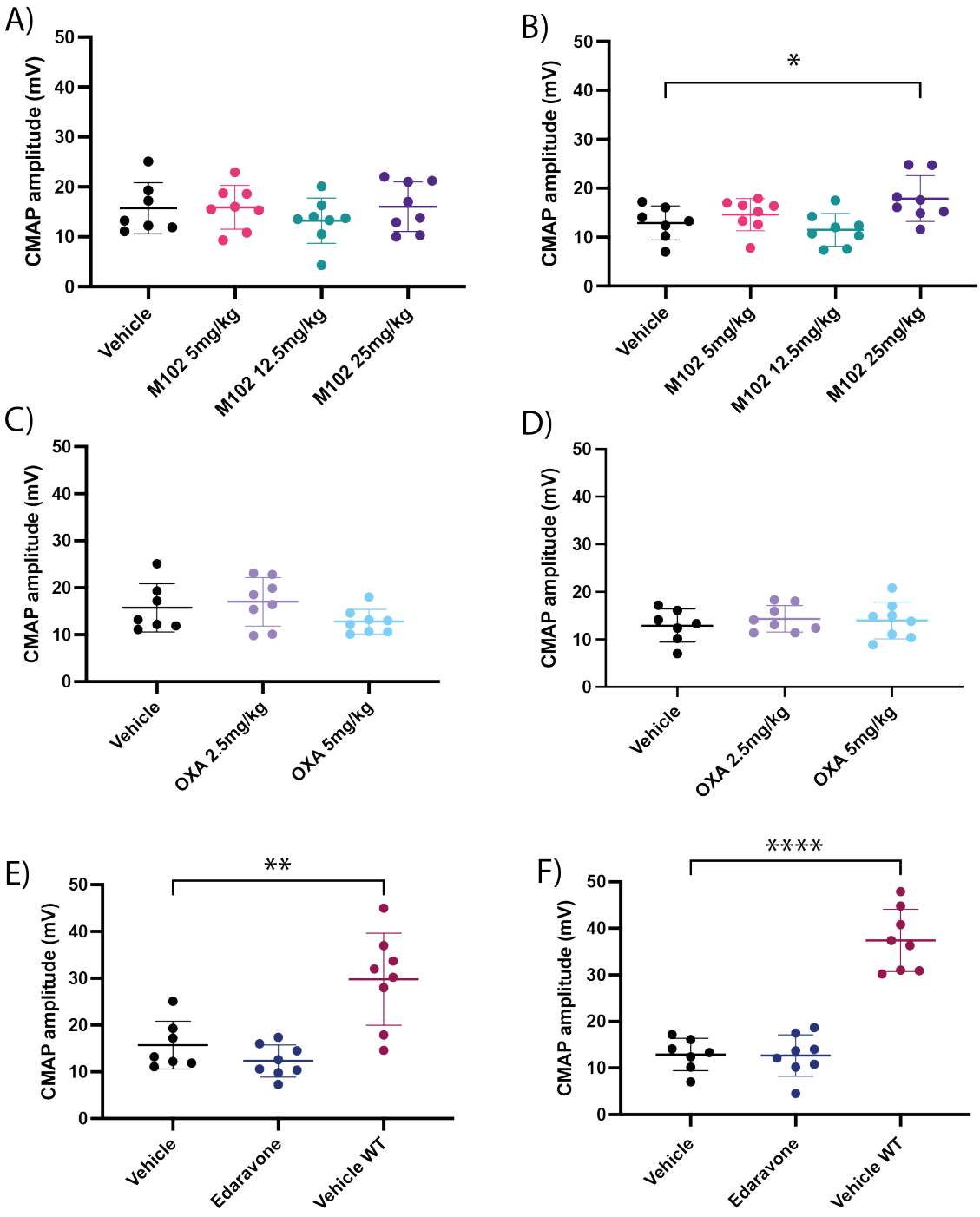

Figure 5.10: Compound muscle action potential (CMAP) amplitude of SOD1^{G93A} mice dosed with vehicle, M102, OXA and edaravone. Data shown as individual values as well as mean ± SD. CMAP of A) M102 dosed groups vs vehicle at 60 days, B) M102 dosed groups vs vehicle at 90 days, C) OXA dosed groups at 60 days, D) OXA dosed groups at 90 days, E) Edaravone and WT vehicle groups vs vehicle at 60 days, and F) Edaravone and WT vehicle vs vehicle at 90 days. N = 7 – 8 per group. One-way ANOVA with Dunnett's multiple comparisons (* = p<0.05, ** = p<0.01, *** = p<0.001, **** = p<0.0001).

An important factor is the change in CMAP amplitude between the two time points as it can give valuable insights into the impact of treatment on functional axon loss in individual mice across the groups. Change in CMAP amplitude over time has been linked to survival in humans (Yu *et al.*, 2020).

SOD1^{G93A} vehicle dosed animals showed a reduction in CMAP at 90 days compared to 60 days as shown by the -2.8 ± 3.1mV average decrease in CMAP amplitude (Figure 5.11), indicating functional axon loss in hind-limb through the disease course as would be expected.

There were no significant differences in CMAP amplitude change in any of the M102 dose groups when compared to SOD1^{G93A} vehicle. However, there was a dose dependent trend in the data, with the highest dose of M102 giving improvements in CMAP amplitude compared to the reduction in amplitude seen in the vehicle dosed mice (Figure 5.11A). The change in CMAP for vehicle, 5mg/kg M102, 12.5mg/kg M102 and 25mg/kg M102 was -2.8 ± 3.1mV, -1.3 ± 2.7mV (P = 0.7853 vs vehicle), -1.7 ± 4.8mV (P = 0.8964 vs vehicle) and 1.8 ± 4.4mV (P =0.0684 vs vehicle), respectively.

There was no significant difference between the change in CMAP amplitude between the OXA dosed groups and the SOD1^{G93A} vehicle dosed groups (Figure 5.11B). Although there was no significant difference between the dose groups, like with M102, there seems to be a slight improvement in CMAP amplitude that looks dose dependent, and the highest dose of OXA improves CMAP amplitude between the two time points compared to the vehicle group which decreases in amplitude. The average change in CMAP amplitude for vehicle, 2.5mg/kg OXA and 5mg/kg OXA was -2.8 ± 3.0mV, -2.7 ± 6.5mV and 1.2 ± 3.7mV, respectively.

There was a significant difference in the change in CMAP amplitude of WT mice when compared to SOD1^{G93A} vehicle where the WT animals have an increased CMAP between the two time points (Figure 5.11C). WT mice had an average change in CMAP amplitude of 7.6 ± 10.5mV (39.4 ± 54.8%) vs -2.8 ± 3.1 (-15.9 ± 17.9%) in SOD1^{G93A} vehicle mice.

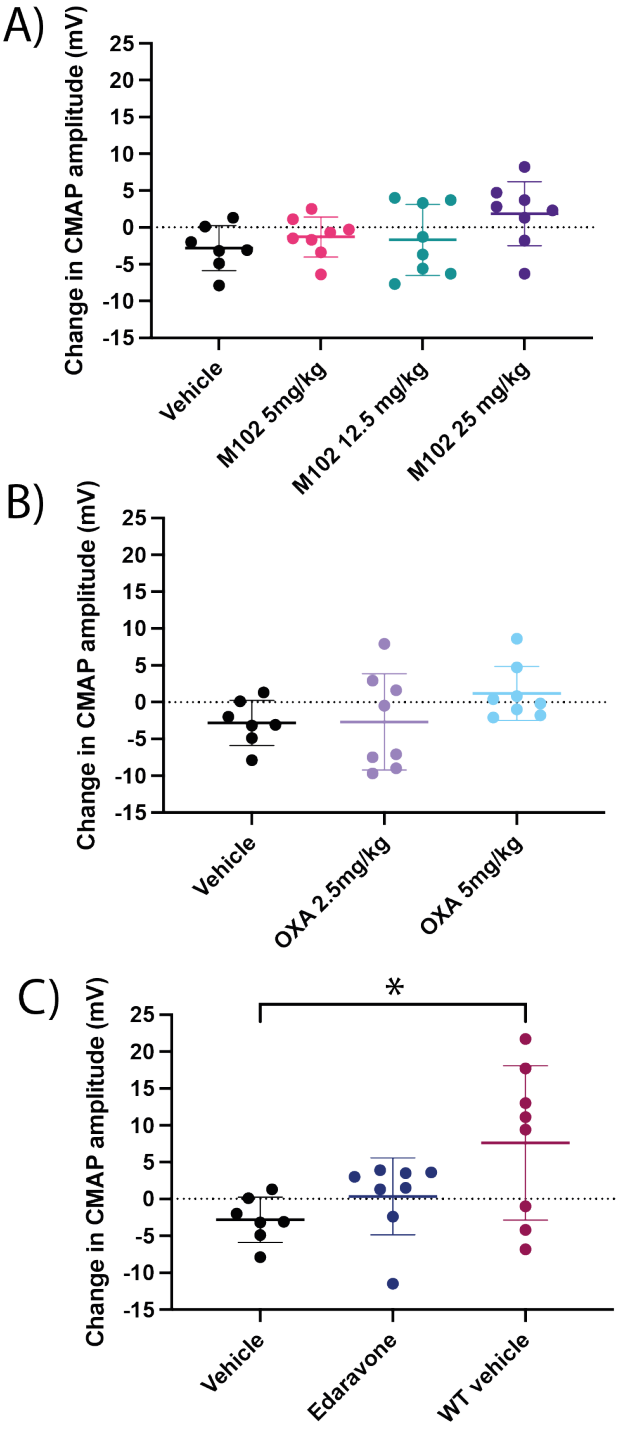

Figure 5.11: Change in CMAP amplitude between 60 and 90 days of SOD1^{G93A} mice dosed with M102, OXA and edaravone. Results are shown as individual values with mean ± SD. Dotted line shows no change or no percentage change. A) The effect of M102 on change in CMAP amplitude. B) The effect of OXA on change in CMAP amplitude. C) The effect of edaravone alongside WT mice in change in CMAP amplitude. (* = p<0.05, ** = p<0.01, *** = p<0.001, **** = p<0.0001).

5.4.7.2. Repetitive stimulation

Repetitive stimulation looks at the CMAP amplitude over 10 pulses at 10Hz. This is routinely measured in ALS patients to evaluate the function of NMJs (Fu *et al.*, 2019; Iwanami *et al.*, 2011). In ALS patients, the CMAP amplitude decreases over 10 repetitive stimulations, as opposed to remaining constant in healthy patients, which shows fatigability of the response to stimuli in ALS patients (Alanazy *et al.*, 2017).

There was no significant difference between M102 dosed animals and $SOD1^{G93A}$ vehicle at 60 or 90 days of age (Figure 5.12A & B). By the 10^{th} stimulus, the average percentage when compared to the 1^{st} stimulus at 60 days was 93.7 ± 5.7% for $SOD1^{G93A}$ vehicle, 88.8 ± 4.9% for 5mg/kg M102, 89.4 ± 8.6% for 12.5mg/kg M102 and 90.1 ± 10.1% for 25mg/kg M102. At 90 days the 10^{th} stimulus was 93.2 ± 7.3% for $SOD1^{G93A}$ vehicle, 87.8 ± 5.8% for 5mg/kg M102, 89.5% ± 6.7% for 12.5mg/kg and 90.6 ± 12.1% for 25mg/kg M102 in terms of percentage of 1^{st} stimulus.

There was no significant difference between OXA dosed groups and $SOD1^{G93A}$ vehicle at 60 or 90 days of age (Figure 5.12C & D). The CMAP amplitude as a percentage of the first dose at the 10^{th} stimulus at 60 days of age for $SOD1^{G93A}$ vehicle, 2.5mg/kg OXA and 5mg/kg OXA was 93.7 ± 5.7%, 93.2 ± 8.1% and 78.9 ± 29.3%, respectively. For 90 days of age the percentage at the 10^{th} stimulus was 93.2 ± 7.3%, 87.0 ± 5.3% and 91.5 ± 4.3% for vehicle, 2.5mg/kg OXA and 5mg/kg OXA respectively.

There was no significant difference between edaravone dosed mice or WT mice when compared to $SOD1^{G93A}$ vehicle dosed mice at 60 or 90 days of age (Figure 5.12E & F). By the 10^{th} stimulus at 60 days, the CMAP amplitude as a percentage of the 1^{st} stimulus was 93.7 ± 5.7%, 92.5 ± 5.9% and 95.8 ± 6.6% for vehicle, edaravone and WT vehicle, respectively. At 90 days the 10^{th} stimulus was 93.2 ± 7.3%, 87.9 ± 7.7% and 97.2 ± 3.6% for $SOD1^{G93A}$ vehicle, edaravone and WT vehicle respectively.

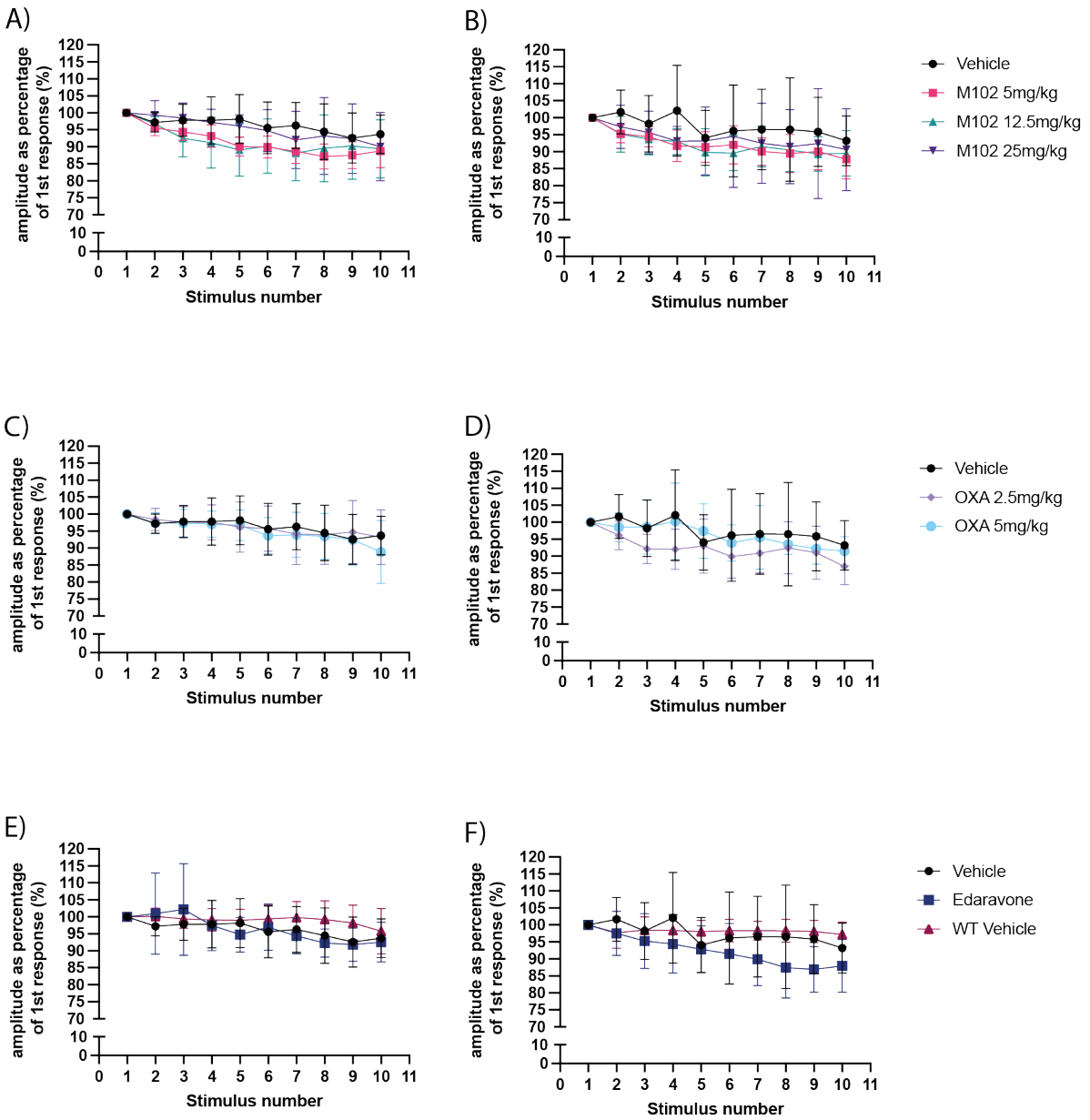

Figure 5.12: Repetitive stimulation at 10Hz of SOD1^{G93A} animals. Data are shown as percentage of the first stimulus mean ± SD. Relative percentage of CMAP amplitude after repetitive stimulation of M102 dosed mice at A) 60 days of age and B) 90 days of age. OXA dosed mice at C) 60 days of age and D) 90 days of age. Edaravone dosed and WT mice at E) 60 days of age and F) 90 days of age. N = 7 - 8 per group. Two-way ANOVA with repeated measures and Dunnett's multiple comparisons.

Another way of analysing repetitive stimulation data is to look at the change in CMAP amplitude between the 1st and 10th stimuli. These data show no significant difference between

the change in amplitude between the 1st and 10th stimulus for any of the groups when compared to SOD1^{G93A} vehicle (Figure 5.13).

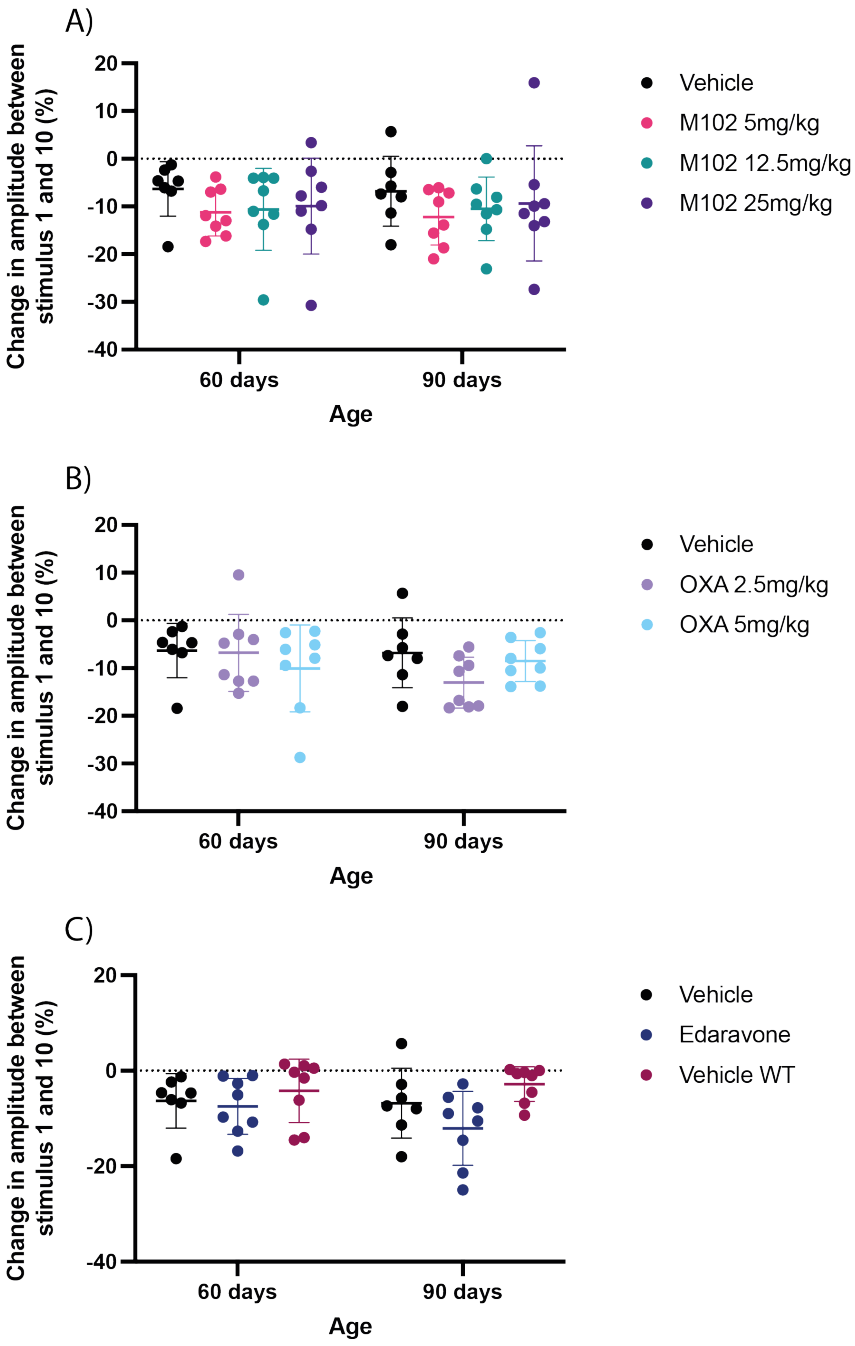

Figure 5.13: Percentage change in amplitude between stimulus 1 and 10 at 60 days and 90 days of age. Data shown as individual values with mean ± SD. N = 7 – 8 per group. There is no significant change in the percentage change in amplitude between the 1st and 10th stimulus in any of the dose groups when compared to vehicle. Two-way ANOVA with Dunnett's multiple comparisons.

5.4.8. qPCR analysis

RT qPCR analysis was carried out at the end of the study to compare the mRNA expression levels of NRF2 and HSF1 targets in the cortex and spinal cord. cDNA was synthesised from RNA and then RT qPCR was carried out using optimised primers. Data were analysed to show gene expression relative to a *Gapdh* endogenous control and compared to vehicle. Downstream targets of NRF2 (*Nqo1*, *Gsr* and *Osgin1*) and HSF1 (*Hspa1a*) were selected as targets shown in previous studies to be upregulated by M102.

There was no significant difference in gene expression level of *Nqo1*, *Gsr*, *Hspa1a* or *Osgin1* between any of the M102 dose groups and SOD1^{G93A} vehicle (Figure 5.14A), or any of the OXA dosed groups and SOD1^{G93A} vehicle (Figure 5.14B) or the edaravone dose group and SOD1^{G93A} vehicle (Figure 5.14C).

The relative gene expression analysis showed significantly more *Nqo1* in the WT vehicle dosed mice compared to the SOD1^{G93A} vehicle dosed mice (Figure 5.14C, P = 0.0015). The other gene targets showed no significant difference between WT vehicle and SOD1^{G93A} vehicle dosed groups.

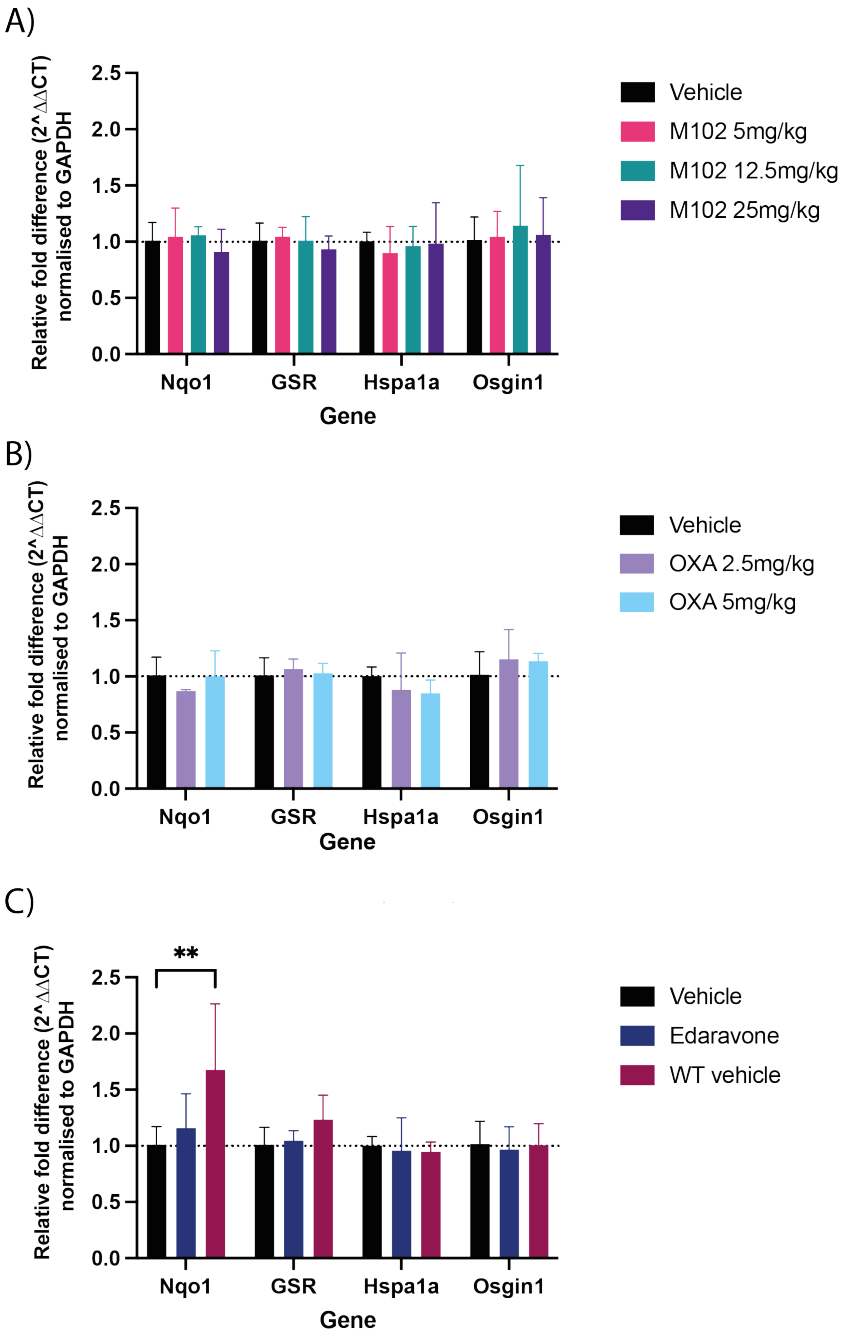

Figure 5.14: Relative expression of target genes in 90 day old cortex tissue from SOD1^{G93A} mice. Data shown as mean relative expression (using the delta delta cT method) ± SD. A) M102 dosed groups, B) OXA dosed groups, C) Edaravone and WT groups. There is significantly more *Nqo1* in WT vehicle mice than SOD1^{G93A} vehicle mice. N = 3 – 4 per group. There was no significant difference in any of the dose groups when compared to vehicle in *Nqo1*, *Gsr*, *Hspa1a* or *Osgin1* gene targets. Two-way ANOVA with Dunnett's multiple comparisons (** = $p<0.01$).

RT-qPCR analysis was also carried out on lower spinal cord from the same animals to investigate gene expression. None of the M102 dose groups showed a significant difference in the expression levels of *Nqo1, Gsr, Hspa1a* or *Osgin1* when compared to $SOD1^{G93A}$ vehicle (Figure 5.15A).

OXA at 2.5mg/kg showed significant decrease in *Osgin1* when compared to $SOD1^{G93A}$ vehicle (Figure 5.15B, P = 0.0204, two-way ANOVA with Dunnett's multiple comparisons), but not at 5mg/kg (P = 0.4542).

The WT animals had significantly lower levels of *Hspa1a* and *Osgin1* when compared to the $SOD1^{G93A}$ vehicle animals (Figure 5.15C, P = 0.0049 for Hspa1a and P = 0.0033 for Osgin1).

The edaravone dosed group showed a significant reduction in *Hspa1a* gene expression when compared to $SOD1^{G93A}$ vehicle (Figure 5.15C, P = 0.0429).

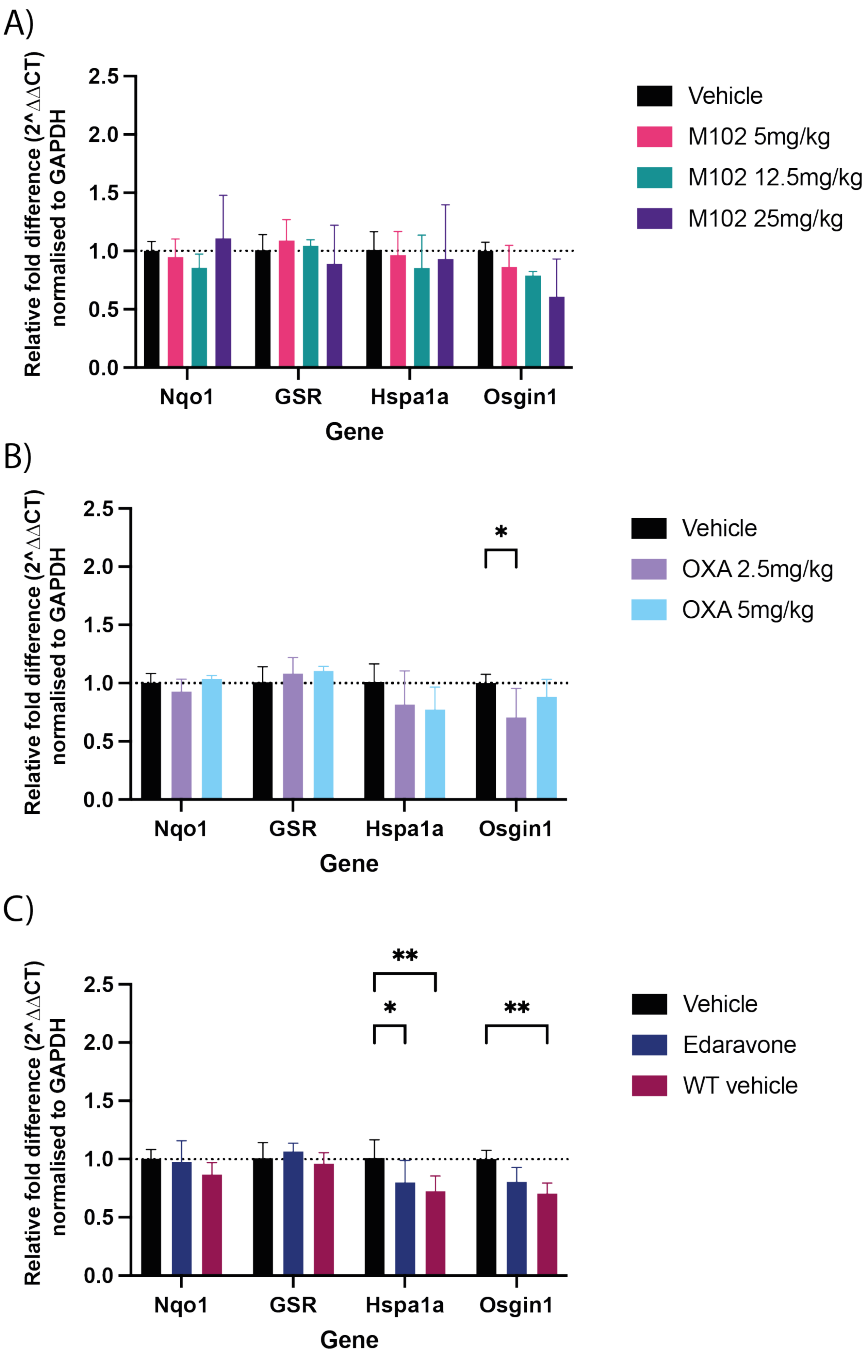

Figure 5.15: Relative expression of target genes in 90 day old from lower spinal cord tissue from SOD1^{G93A} mice. Data shown as relative expression (using the delta delta cT method) ± SD. A) M102 dosed groups, B) OXA dosed groups, C) Edaravone and WT groups. There is a significant decrease in osgin1 in 2.5mg/kg OXA dosed mice when compared to vehicle. There is a significant decrease in *Hspa1a* in edaravone treated mice when compared to vehicle. The WT mice had significantly less *Hspa1a* and *Osgin1* when compared to the vehicle dosed mice. N = 3 – 4 per group. There was no significant difference in any of the dose groups when compared to vehicle in Nqo1, GSR, Hspa1a or Osgin1 gene targets. Two-way ANOVA with Dunnett's multiple comparisons (* = $p<0.05$, ** = $p<0.01$).

5.5. Oral vs subcutaneous dosing of M102

5.5.1. Study design

In order to compare the oral and subcutaneous dosing of M102 directly a short-term dosing study was set up where M102 was dosed subcutaneously or orally for seven consecutive days before tissue was collected at 6 or 24 hours post dose (Table 5.2). Brain and spinal cord were collected and RNA was extracted immediately. cDNA was generated from RNA and RT-qPCR was carried out on a number of targets.

Table 5.2: M102 oral vs subcutaneous dosing study design showing dose levels and collection time points

Mice	Age	Drug	route of administration	Dose	Number of days dosing	n per group	Time point for collection
SOD1^{G93A} mice	100 days	M102	oral	Vehicle	7	5	6 hours
			SC	5mg/kg			
			oral	25mg/kg			
			oral	Vehicle	7	5	24 hours
			SC	5mg/kg			
			oral	25mg/kg			

5.5.2. Oral vs subcutaneous Results

At 6 hours post dose there was a significant increase in *Sqstm1* (P = 0.127) and *Hspa1a* (0.0211) expression for the 5mg/kg subcutaneous dose when compared to vehicle (Figure 5.16A). There was also a significant increase in *Hspa1a* in the 25mg/kg oral group when compared to vehicle (P = 0.0101). There was no significant difference in expression of any genes at 24 hours post dose (Figure 5.16B).

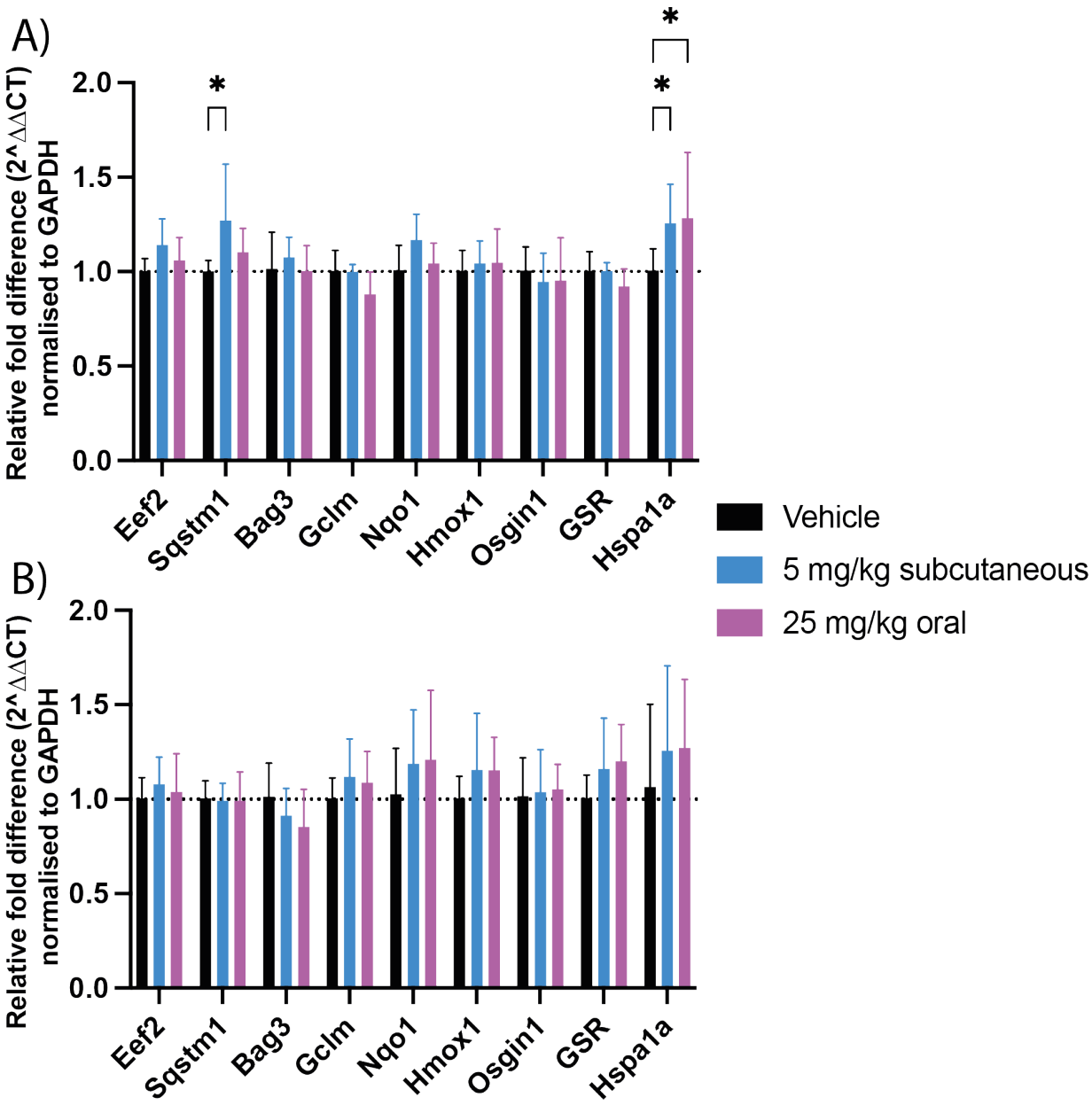

Figure 5.16: Expression at 6 and 24 hours post dose in cortex tissue in SOD1^{G93A} mice dosed with M102 subcutaneous and orally. Data shown as relative expression (using the delta-delta cT method) plotted as mean ± SD. A) 6 hours post dose. There was a significant increase in *Sqstm1* and *Hspa1a* with 5mg/kg subcutaneous dosed M102 and a significant increase in *Hspa1a* with 25mg/kg orally dosed M102. B) At 24 hours post dose there was no significant difference in expression with either oral or subcutaneously dosed M102. N= 3-5 per group. Two-way ANOVA with Dunnett's multiple comparisons (* = $p<0.05$).

This work is currently ongoing and more targets will be explored to gain a better understanding of the difference between the subcutaneous and oral dosing.

5.6. Discussion

5.6.1. Study design

The study was designed to primarily investigate the effects of orally dosed M102 on the disease progression in a SOD1^{G93A} mouse model of disease. The secondary aims of the study were to investigate the effects of OXA, a likely active metabolite of M102 with greater *in vitro* potency and to evaluate the effects of a recent FDA approved drug edaravone, which acts on one of the main pathways targeted by M102, namely oxidative stress. We wanted to investigate oral dosing of M102 as previously it has only been tested in SOD1^{G93A} and TDP-43^{Q331K} mouse models using subcutaneous delivery and calculations based on likely dosing scaling to human studies indicated that the volumes would be too large for SC dosing and therefore oral dosing was preferable. PK data indicates that oral dosing at 25mg/kg gave a similar exposure profile to 5mg/kg SC dosing. When translating from preclinical to clinical studies it is preferable to use the intended route of administration to confirm efficacy and side effect profile.

Since this was the most critical part of the study, the vehicle was also orally dosed. OXA was dosed subcutaneously as we did not have the PK data available to confirm its oral bioavailability. Edaravone is approved for IV dosing in humans, but this is an impractical route for mouse and so the intraperitoneal route was selected, as in previously published papers (Baba *et al.*, 2016; Ito *et al.*, 2008). Edaravone was dosed at 15mg/kg based on previous mouse studies that have shown this dose level to be effective in a SOD1^{G93A} mouse model (Ito *et al.*, 2008) and formulated edaravone as described previously (Baba *et al.*, 2016; Ito *et al.*, 2008). Edaravone is dosed IV in patients, following a two week on/off regime. In the current study, edaravone was dosed in a 2 week on/off dosing regimen in order to mimic the dosing in patients with ALS (Cruz, 2018), although it was dosed intraperitoneally.

Cyclodextrins are commonly used to increase the solubility and stability of compounds, especially those with low solubility in water, and HP-ß-CD is well tolerated orally when given to mice with little effect when dosed at levels such as in this study (Gould and Scott, 2005). HP-ß-CD has been shown to have antioxidant activity in a rat model of chronic renal failure (Anraku *et al.*, 2016), and Zimmer *et al.* showed anti-inflammatory effects of HP-ß-CD in a mouse model of atherosclerosis (Zimmer *et al.*, 2016). The dosages of HP-ß-CD in these studies ranges from 0.25g/kg and 2g/kg daily, whereas the dosing of 10% HP-ß-CD in the SOD1^{G93A}

study equates to a dose of 1g/kg, which is within the range of these previous studies where they see antioxidant and anti-inflammatory effects. However, these were just peripheral studies and did not look at anti-inflammatory effects in the CNS. Whether there is an effect of HP-ß-CD on inflammation or oxidation should not affect the study because the vehicle and M102 mice are both receiving HP-ß-CD at the same concentration and so any difference seen will still be M102 driven.

5.6.2. SOD1^{G93A} mouse model shift

Data from this study indicate that the SOD1^{G93A} mouse model disease course is delayed in terms of disease progression from when the mice were originally generated in Mead *et al.* 2011 (Mead *et al.*, 2011). To compare the potential differences, the vehicle dosed from multiple studies is shown in Table 5.3.

Table 5.3: Table of various readouts from previous data on the SOD1^{G93A} model and more recent data. Mead *et al.* data from Mead *et al.* 2011. M102 study is this current study described in the thesis. Drug A study is a study that recruited mice from the colony immediately preceding the start of the M102 study. Data from Mead *et al.* show only female data. Nd = not determined.

Study	Onset (age in days)		Survival (age in days)		Rotarod (age at 20% reduction)	
	Mean	SD	Mean	SD	Mean	SD
Mead *et al*. trial 1	74.8	4.7	nd	nd	47.6	4
Mead *et al.* trial 2	nd	nd	134	5.4	44.6	2.2
Mead *et al.* trial 3	74.2	4.6	144.7	5.3	nd	nd
Mead *et al.* trial 4	76.3	2.9	142.7	3.9	60.7	9.1
Mead *et al.* trial 5	74.4	2.5	142	3.1	57	7.5
Mead *et al.* trial 6	68.5	3.5	136.5	0.7	46.7	3.5
M102 study	73.75	3.9	nd	nd	65.25	13.8
Drug A study	80.33	7.7	168	12.8	nd	nd

For the current study described in this thesis the average age for 20% rotarod decline was 65.25 ± 13.75 days for the vehicle dosed group and in the Mead *et al.* paper there were a few different studies where the average age of 20% decline in rotarod performance for female mice ranged from 44.6 ± 2.2 to 60.7 ± 9.1 days (Table 5.3). The age of 20% rotarod decline in the current study occurs later than previously observed in this model with a greater variance also observed. This study was powered based on the standard deviation from previous rotarod data and the power analysis was carried out assuming the average standard deviation from the original studies which was 8.7 not 13.8 observed in the present study. Importantly the group size of 8 used in this study is underpowered and may not detect small but relevant differences between groups.

From this current study, the average age of onset was 73.75 ± 3.9 days for the vehicle group compared to that of the Mead *et al.* paper they carried out a few different trials and the average age of onset for female mice ranges from 68.5 ± 3.5 days to 76.3 ± 2.9 days (Table 5.3). The results for age of onset in the present study are consistent with the results seen previously in this model. This suggests that age of onset has not altered as part of the changing progression of the $SOD1^{G93A}$, however further investigation could confirm if this model has a slowed motor decline at the early stages. However, age of onset is based on neuroscoring data which are subjective and the different researchers carrying out the scoring may score the mice slightly differently. The physical aspects of MN degeneration usually occur before visible signs of disease (Feeney *et al.*, 2001).

Although the present study did not follow the mice through to end-stage of disease, the 'Drug A' study was recruited just before the current study. Vehicle mice from the 'Drug A' study had an increase in time to reach end-stage disease compared to previous studies. The vehicle group of the recent $SOD1^{G93A}$ study had an average end-stage of 168 ± 12.8 days, whereas the end-stage in the Mead *et al*. paper had a few studies that ranged from 134 ± 5.4 and 144.7 ± 5.3 days of age (Table 5.3).

Taken together all these data suggest that the mouse model phenotype has shifted over time. The biggest differences seen are the lack of the sharp decline in rotarod that was previously observed before visible onset of disease (Mead *et al.*, 2013) and the increased age of end-stage disease.

In the Mead *et al.* 2013 paper, the main difference between M102 and vehicle animals was the improvement in the sharp early decline as shown by the time to reach 20% decline (Mead *et al.*, 2013). Due to this difference in rotarod performance between older and newer studies, and the increased variation between the mice, the current study may have been underpowered for changes in rotarod performance.

Gait analysis has also been significantly affected by the shift in the model phenotype. There is no detectable difference between WT vehicle and $SOD1^{G93A}$ vehicle in most of the parameters relating to gait that have previously been shown to be important in this mouse model at our selected time points, such as stride length (Figure 5.9) (Mead *et al.*, 2013), support on diagonal

limbs and forelimb stand time (Mead *et al.*, 2011). Due to the lack of difference between WT vehicle and SOD1^{G93A} vehicle in gait parameters, there is no window to see a therapeutic effect of compounds on gait in the model before 90 days of age. Although there was no difference in any of the parameters in gait analysis between M102, OXA or edaravone groups, because of the lack of difference between WT vehicle and SOD1^{G93A} vehicle, small changes may have been undetected.

The change in the progression of the disease could be due to a change in the copy number of the SOD1^{G93A} gene. The original model, developed by Gurney *et al.* (Gurney *et al.*, 1994) had 18 copies of the human transgene, including the endogenous promoter, in tandem inserted into the mouse genome. This was later increased to 25 copies (Gurney, 1997). It has previously been shown that the severity of disease progression in a mouse model of SOD is related to the copy number of the SOD1 gene (Chiu *et al.*, 1995). Smaller changes can also happen over time, where copies of the human SOD1 gene are lost between generations because of intra locus recombination during meiosis (Gurney, 1997), which although rare, does happen occasionally in breeding colonies leading to longer survival (Alexander *et al.*, 2004).

The SOD1^{G93A} model differs between laboratories, with some mice living longer than others, even with the same copy number (Heiman-Patterson *et al.*, 2011). This difference is mostly due to the genetic back ground that the mice are on (Heiman-Patterson *et al.*, 2011). However, genetic drift tends to happen over time in in-bred mouse colonies (Taft *et al.*, 2006), which could lead to other changes in the genome that affect the progression of the disease. The COVID lockdown could have also had an effect, as the number of breeding animals was decreased and the colony went through a genetic bottle neck, which could have increased the probability of genetic changes (Taft *et al.*, 2006). Changes in methylation of DNA in and around the transgene could also alter transgene levels (Whitelaw *et al.*, 2001; Zhou *et al.*, 2014). Studies are currently underway to investigate these possibilities by using qPCR to detect transgene level (Alexander *et al.*, 2004) and nanopore technology to detect methylation changes (Simpson *et al.*, 2017).

Although there is a shift in the model, there are still some parameters which show a significant difference between the WT vehicle and SOD1^{G93A} vehicle animals, such as weight, CMAP and onset of visible signs of disease. Therefore, although there is a change in the model, there are

still some tests where a therapeutic effect would be able to be detected. As expected, WT animals are significantly heavier than the SOD1^{G93A} vehicle group at later stages of the study confirmed in the AUC analysis.

CMAP is the summation of the depolarisation within muscle fibres in the hindlimb of mice, therefore CMAP amplitude represents the functional motor units (Harrigan *et al.*, 2019). There is a good separation of CMAP between WT and SOD1^{G93A} vehicle animals, especially at 90 days of age and this could be used to separate transgenic vs non transgenic mice. The WT mice also have a significant difference in the change in CMAP between 60 and 90 days of age, suggesting that between these time points the mice are gaining motor function, probably due to increased weight or muscle gain during this time, whereas the T animals do not have this increase.

The SOD1^{G93A} vehicle animals have a decline in CMAP amplitude between 60 and 90 days of age, as seen in other SOD1 mouse models (Harrigan *et al.*, 2019; Leermakers *et al.*, 2021; Mancuso *et al.*, 2011). We know in this model that at 90 days of age there is significant loss of motor neurons in the ventral horn of the spinal cord (Ciervo *et al.*, 2021) as well as loss of muscle volume (Mead *et al.*, 2011), which we assumed would be linked to a reduction in CMAP. CMAP amplitude is not directly correlated with the loss of motor neurons and instead represents motor unit function. Due to compensatory mechanisms by motor neurons after denervation, such as collateral sprouting, CMAP may remain constant even if motor neuron numbers are decreasing (Arnold *et al.*, 2015). From other papers looking at CMAP there is a large decrease in CMAP amplitude over the progression of the disease and at 60 days the CMAP of the mice is higher than in this study (Mancuso *et al.*, 2014). However, background strain has an effect on the CMAP of the mice (Mancuso *et al.*, 2012) and many other papers use needle electrodes rather than ring electrodes. The advantage of needle electrodes is the ability to isolate and test the CMAP of individual muscles in the hindlimb rather than ring electrodes that show the summation of motor output in the whole hind limb. The advantage of ring electrodes is that they have shown to be more reproducible, there is less variability between users and there are no needles inserted into the hindlimb of the mice as the stimulating electrodes are just placed on the skin (Arnold *et al.*, 2015).

We have not previously studied CMAP analysis on this in-house model so it cannot be determined if CMAP amplitude has been affected by the shift in the model at these timepoints, but the significant difference in the SOD1^{G93A} vehicle and the WT animals allows the potential to detect therapeutic effects.

Ultimately, the shift in the SOD1 model does not impact any potential differences detected between compound dosed or vehicle dosed animals in this study as all mice were recruited and dosed over the same period and therefore the animals are comparable. One problem could be that the transgenic male breeders have different copy numbers to each other, leading to different copy numbers of the mice recruited. This could be the reason for the increased variability in the data from this study. However, since animals were block randomised into the different dose groups, this should spread the variability of the mice between the groups. Another problem is that the time points selected may not be optimal for investigating some behavioural parameters as the disease now progresses at a different rate, as shown by the catwalk data. Investigation is ongoing into understanding the changes that have occurred in the breeding colony. Once we can accurately detect the copy number of the SOD1^{G93A} mice, we will be able to select breeders again with the closest copy number to the original line and remove any mice that have lost copies of the transgene. Moving forward the progression of disease may be slightly different in the SOD1^{G93A} colony until changes are made to breeders or even after the problem has been corrected. This means careful consideration will need to be put into place regarding design of new studies and that power analysis is based on recent standard deviation values from recent studies.

5.6.3. Oral M102 effects on SOD1^{G93A} mice

The main aim of the study was to determine if orally dosed M102 had an effect on disease progression in a SOD1^{G93A} mouse model of ALS. Three doses were chosen to potentially see a dose response, with the top dose of 25mg/kg being equivalent in exposure to 5mg/kg subcutaneous dose of M102.

There was a significant increase in weight of the 5mg/kg and 25mg/kg M102 dose groups compared to SOD1^{G93A} vehicle. This indicates reduced atrophy and is supported by findings on electrophysiology. There was a significant improvement in CMAP amplitude for the M102 25mg/kg dose group when compared to vehicle at 90 days of age, suggesting M102 has a

positive impact on motor units in SOD1^{G93A} mice. There is a dose response in the M102 dosed groups in change in CMAP amplitude, with the SOD1^{G93A} vehicle showing a decline in CMAP over time through to 25mg/kg M102 where there is a slight improvement in CMAP from 60 to 90 days. This suggests a dose response in M102 activity on CMAP, where higher doses of M102 not only slow the loss of function seen in the model, but actively aid with motor unit function.

Although there was an improvement in CMAP with M102 dosing, this did not translate to an improvement in rotarod performance. This could be because of the shift in the model, which could mask small changes in rotarod performance at the earlier stages of disease, or it may be that rotarod changes would now be seen at a later timepoint, beyond the timepoints in this study.

Spinal cords have been fixed, embedded, and sectioned and are currently being stained with Nissl, to determine the number of motor neurons. CMAP amplitude does not directly correlate with motor neuron number as compensatory mechanisms occur after denervation (Gordon *et al.*, 2004). Comparison of motor neuron numbers between the groups will help to determine if the effects of improvement of CMAP are due to the preservation of MNs. Staining with GFAP and Iba1 to compare the level of astrocytes and microglia activity in the ventral horns is also currently being carried out to compare neuroinflammation in the ventral horns between the dose groups. An improvement to the study would have been to collect muscle weights from hind limbs to see if there was a difference in muscle mass between the groups.

Gene expression analysis was carried out on cDNA from cortex and spinal cord tissue using RT-qPCR and optimised primers. Analysis of gene expression from cortex tissue showed no significant difference in expression levels of *Nqo1, GSR, Hspa1a* or *Osgin1* between the M102 dosed groups when compared to vehicle, suggesting no change in these gene targets after continued treatment with the different compounds. The lack of upregulation of NRF2 targets in the cortex could be due to the difficulty in activating the NRF2 pathway later in disease progression, that I have previously shown in a short term PKPD study and has been discussed previously (section 4.5.3.2). The NRF2 pathway is known to be dysregulated in ALS patients (Sarlette *et al.*, 2008) and mouse models of ALS (Mimoto *et al.*, 2012), meaning that it could be more difficult to activate this pathway later in disease progression.

5.6.4. Oral vs subcutaneous M102 in SOD1^{G93A} mice

As mentioned previously, Mead et al. carried out a study with M102 subcutaneous dosing in 2013 where there were significant improvements in age to reach 20% rotarod decline, forelimb and hindlimb stride length and percentage of innervated NMJs (Mead *et al.*, 2013). Because of the shift in the model, we were unable to see an advantage of M102 in rotarod performance and gait parameters, however the ages at which there were significant improvement in stride length were older than 90s days. In the current study we did not investigate NMJ structure through staining, however, we performed repetitive stimulation and investigated the reduction in CMAP amplitude over multiple repeated stimuli, which is often used to measure NMJ function (Fu *et al.*, 2019). There was no significant difference between the repetitive stimulation data of M102 and SOD1^{G93A} vehicle. However, there was also no significant difference between SOD1^{G93A} vehicle and WT vehicle, which may mean at the time points chosen there was not significant loss of CMAP after multiple stimulations in the model.

The Mead *et al.* 2013 study also found a significant reduction in oxidised glutathione levels (Mead *et al.*, 2013), this is something we can explore further in our study by examining more mRNA targets by RT-qPCR and through mass spectrometry, which has been carried out on the cortex tissue of short term studies (section 3.6.4). We are also in the process of optimising MRI techniques on anaesthetised mice to get readings of glutathione levels *in vivo* at multiple timepoints. This would allow us to track the levels through the progression of the disease as well as with treatment, with the view of translating this to humans as a biomarker for clinical studies.

Because the studies were carried out at different times with different sets of mice, it is difficult to directly compare the difference between orally dosed M102 and subcutaneously dosed M102. A small short term study was carried out to directly compare the effects of oral and subcutaneous dosing of M102 on the downstream targets of NRF2 and HSF1 pathways. Increases were seen in a HSF1 target gene at 6 hours post dose with both oral and subcutaneous doses of M102, with the subcutaneous dose also showing an increase in *Sqstm1* at 6 hours. However, there were no changes seen at 24 hours post dose in cortex tissue. This data shows the difficulty in activation of the NRF2 pathways at intermediate stage of disease.

More analysis is required to form a conclusion about the difference between the two routes of dosing. More targets are currently being explored from cDNA from this study.

Together the information from both M102 SOD1^{G93A} studies shows that M102 has a positive impact on the progression of disease in this mouse model, suggesting it could potentially have beneficial effects in ALS patients.

5.6.5. OXA in SOD1^{G93A} mice

In this study, we wanted to compare the effects of OXA, the oxidised form of M102, with the effects of M102 in the mouse model. OXA had no significant effect on weight however, there was a significant decrease in rotarod performance of the OXA 5mg/kg group, but not 2.5mg/kg when compared to vehicle (Figure 5.5B). This suggests that OXA at 5mg/kg was having a negative effect on motor performance of SOD1^{G93A} mice which may be dose dependent. Although the overall decrease in rotarod performance was significant there was no change in the age to reach 20% decline in performance. OXA at 5mg/kg also has a negative effect on age of disease onset. Together with the decline in rotarod performance data, this suggests that OXA at 5mg/kg is negatively impacting the mice and causing a faster decline in motor phenotype when compared to the SOD1^{G93A} vehicle group. Although this suggests that OXA at 5mg/kg accelerated the disease, it could be that at this dose level the mice were experiencing some adverse effects that may have affected their ability to perform motor function tests. There was no significant difference in CMAP of the OXA group when compared to SOD1^{G93A} vehicle (Figure 5.10), however tissue analysis is currently underway to determine the number of motor neurons in the lumbar spinal cord to compare between the dose groups.

There are no results in this study showing that subcutaneous dosing of OXA has a positive impact on disease progression in this model.

5.6.6. Edaravone in SOD1^{G93A} mice

Edaravone is a newly FDA approved treatment for ALS, however has previously been used to treat ischaemic stroke (Takei *et al.*, 2017). Edaravone acts as a free radical scavenger, exerting its neuroprotective effects through reducing oxidative stress, which makes it an ideal comparator for M102, as the mechanisms of action are similar.

Edaravone was dosed intraperitoneally rather than intravenously, which is the dose route currently for humans due to the previous use for ischaemic stroke, although an oral formulation is currently being developed (Hyung *et al.*, 2018). The intraperitoneal dose route is typical of edaravone studies in rodents (Baba *et al.*, 2016; Ito *et al.*, 2008), although typically they are dosed continuously rather for 2 weeks on/off in mouse models.

In this study there was a significant increase in weight of the edaravone dosed mice when compared to $SOD1^{G93A}$ vehicle, suggesting a beneficial effect on disease progression. However, there was no significant difference in rotarod performance or CMAP and a significant decline in age of onset. Overall, this suggests that although there is a significant positive impact on weight, there is no benefit of edaravone in the motor phenotype in these mice, in comparison to M102 which has shown an overall positive effect on multiple disease parameters.

The RT-qPCR data showed no significant difference in gene expression in the cortex and a significant reduction of Hspa1a in the spinal cord tissue when compared to vehicle. This suggests that edaravone does not activate the NRF2 or HSF1 pathways, however, there was also no significant difference in M102 dosing on these gene targets, so it may be due to NRF2 dysregulation discussed earlier. There was a limited number of targets investigated in this study, and ideally more targets would be investigated. Previous studies investigating edaravone in mice have suggested improvements in GSH/GSSG levels in the hippocampus (Baba *et al.*, 2016), so investigation of more mRNA targets that regulate glutathione would be valuable to explore in cortex tissue. Glutathione levels could also be investigated using mass spectrometry as we have previously shown to compare edaravone effects with M102.

In a previous study investigating edaravone in $SOD1^{G93A}$ mouse model Ito *et al.* showed improvement in body weight, rotarod and grip strength, as well as increased numbers of motor neurons in lumbar spinal cord (Ito *et al.*, 2008). However, despite these significant improvements, there was no extension of survival of these mice. In the current study, although we saw the improvement in weight, we did not see any benefit in terms of rotarod performance, however due to changes in the model, an effect could be masked. Tissue analysis has yet to be completed on lumbar spinal cords, however this will be carried out to analyse the number of motor neurons in each dose group.

There were some differences between the Ito *et al*. study and our study but the major difference is the dosing regimen. In the Ito *et al.* study, they dosed the animals every day from the day they got to disease onset, defined as leg tremor or failure of 15 rpm rotarod, whereas our study employed dosing from 25 days of age in a 2 week on/off schedule (Ito *et al.*, 2008). Dosing from disease onset mimics clinic dosing, as patients can only be dosed from signs of disease onset and may be more representative of dosing in patients. However, our schedule was to mimic dosing of edaravone in the clinic also as patients have a break currently. These differences in dosing may have caused the differences we see in the effect of edaravone on disease progression. Dosing pre-symptomatically could have a potential detrimental effect on glia, as early on in disease glia are protective and become destructive later on, so modifying them at an early stage may not be beneficial (Liao *et al.*, 2012).

5.6.7. Outcome and future work

The overall outcome of this study is that the 25mg/kg oral dose of M102 was able to improve weight and CMAP in the $SOD1^{G93A}$ mouse model, showing that M102 can improve progression of disease in a $SOD1^{G93A}$ mouse model. This suggests that the oral dose route of M102 is a promising dose route, however more work is currently being carried out to directly compare the subcutaneous and oral dosing routes.

OXA at 2.5mg/kg and 5mg/kg dosed subcutaneously did not have any impact on motor function in this model. In fact, the 5mg/kg dose of OXA significantly decreased rotarod performance when compared to vehicle mice and decreased the age of visible symptom onset of these mice. Although this suggests that OXA at this dose accelerated disease progression, it could be that at this dose level the mice were experiencing some adverse effects that may have affected their ability to perform motor function tests, which was not detectable visually. From the results of this study, there are no data to suggest that OXA can impact positively on progression of ALS. However, as this is the first study with OXA, further investigation is required to investigate mechanisms of action and bioavailability of OXA *in vivo* to determine if the dose levels were correct and whether OXA was entering the CNS as assumed for the study. The formulation of OXA could also be explored in order to optimise the dose route for best delivery.

Although previous studies have shown positive effects of edaravone in the mouse model (Ito *et al.*, 2008), we were unable to replicate this, except for the improvement in body weight. Further investigation into the dosing schedule of edaravone would be useful to identify if this was responsible for the differences observed in the two studies.

6. Discussion

The aim of this thesis was to investigate the potential of M102 to activate the NRF2 and HSF1 pathways in the CNS of mice and whether it has potential neuroprotective properties that could be beneficial in ALS patients. The discovery of HSF1 pathway activation with M102 is novel and activation of this pathway has been shown to have neuroprotective effects (Batulan *et al.*, 2006). The ability for M102 to activate multiple neuroprotective pathways in the CNS makes it a promising drug candidate for use in ALS, since targeting just one mechanistic pathway has so far failed to produce beneficial therapeutic compounds in ALS. The positive effects of M102 in two different mouse models of ALS, gives confidence that this can be beneficial for patients.

6.1. Comparisons to other NRF2 activators

Due to the potential of the NRF2 pathway in the progression of ALS, there have been a few NRF2 activators that have been tested in animal models of ALS and in clinical trials (Jiménez-Villegas *et al.*, 2021). Edaravone has been shown to have protective effects in animal models of ALS (Aoki *et al.*, 2011; Ito *et al.*, 2008) and in a specific subset of patients (Abe *et al.*, 2017). Following these clinical trials, edaravone is now approved for ALS in Japan and by the FDA, but is not currently approved in Europe (Cruz, 2018). The exact method of action of edaravone is thought to be via free radical scavenging. However, recently it has been shown to activate NRF2 and produce neuroprotective effects through this pathway (Shou *et al.*, 2019). If the protective effects of edaravone are due to NRF2 activation, this is promising for the effect of M102 in ALS patients. The effects seen with edaravone in the $SOD1^{G93A}$ model in this thesis were mild compared to the effects seen with M102, suggesting that M102 could give greater effects than edaravone in patients. These data are supported by the NRF2 cell reporter assay where edaravone was a much weaker inducer of NRF2 compared to M102.

Other electrophiles that activate NRF2 have been tested for use in ALS and other neurodegenerative diseases. Dimethyl fumarate (DMF) is an electrophilic NRF2 activator that activates NRF2 activity through modification of cysteines on KEAP1 (Brennan *et al.*, 2015), similar to the proposed mechanism of action of M102. DMF has been shown to activate mitochondrial biogenesis in mice and humans (Hayashi *et al.*, 2017) as well activating T cells and promoting anti-inflammatory pathways (Lückel *et al.*, 2019). DMF is currently FDA

approved for the treatment of multiple sclerosis (Gold *et al.*, 2012), and more recently has been studied in ALS patients, however there was no significant improvement in ALS disease progression in a phase 2 clinical trial (Vucic *et al.*, 2021). We have not yet explored if M102 limits the inflammatory response in mice due to issues with abundance in previous studies. However, NanoString analysis suggest that in intermediate stage disease SOD1^{G93A} mice there may be significant effects of M102 upon inflammatory targets. Electrophiles that activate NRF2 also have the potential to activate anti-inflammatory pathways either directly through NRF2 inhibition of inflammatory cytokines (Kobayashi *et al.*, 2016) or through inhibition of the NF-kB pathway (O'Brien and Wendell, 2020). Further research is required to explore if NF-kB is affected with M102 dosing or if there is a significant difference in other anti-inflammatory pathways.

Omaveloxolone is an NRF2 activator that is currently in clinical development for Friedreich's Ataxia, a neurodegenerative disease with no current disease-modifying treatment (Lynch *et al.*, 2021). Gene expression studies were carried out in monkeys and at 24 hours post dose. There was increased expression of GSR and AKR1C1 in the brain with 100mg/kg/day dose, however the gene expression in lung and liver was much higher (Reisman *et al.*, 2019), suggesting lower CNS penetrance of Omaveloxolone compared to M102, as we saw comparable increased gene expression in cortex compared to peripheral tissues at a dose of 5mg/kg subcutaneously.

6.2. Comparisons to other HSF1 activators

Arimoclomol is an activator of HSF1 (Hargitai *et al.*, 2003) that has shown potential in a SOD1^{G93A} mouse model, where mice treated with arimoclomol showed an increase in hindlimb function and had a prolonged survival (Kieran *et al.*, 2004). Recently arimoclomol has been explored in humans with promising effects, although the trial was not powered to explore therapeutic effect (Benatar *et al.*, 2018). In phase 3 trials arimocolomol failed to show any improvement in ALS patients (NCT03491462). However, HSF1 activity combined with NRF2 activity may be able to slow disease progression in ALS. In both the TDP-43^{Q331K} and SOD1^{G93A} studies there was an increase in Hspa1a expression at the end of the experiment in cortex tissue, which looks to be more robust than NRF2 downstream targets, which are sometimes not activated. Although the lack of NRF2 downstream targets may be due to NRF2 pathway dysregulation at later stages of disease, the activation of Hspa1a suggests that the HSF1

pathway is active at this late stage and may be the pathway that is influencing the positive changes seen in the mouse models. Further exploration of HSF1 activation is required with M102 to fully understand the extent of HSF1 involvement in ALS progression.

6.3. M102 in SOD1^{G93A} mice vs TDP-43^{Q331K} mice

Although this SOD1^{G93A} study investigated oral dosing of M102 and the TDP-43^{Q331K} study investigated subcutaneous M102 dosing, some comparisons can be made in terms of M102 activity in ALS models.

Both studies showed a significant improvement in weight for their respective model with the TDP-43^{Q331K} mice having significantly reduced weight when dosed with M102 and the SOD1^{G93A} mice having significantly increased weight with M102 (Table 6.1). Although the mechanisms of this weight gain and loss may be different in the two models, the fact that M102 managed to improve weight in both models suggests it is having a positive impact on disease progression.

Table 6.1: A comparison of effects seen with M102 dosing in the TDP-43^{Q331K} and SOD1^{G93A} mouse models showing the parameters where there were significant differences detected vs SOD1^{G93A} vehicle. *= Not a big enough therapeutic window.

	TDP-43^{Q331K} study		SOD1^{G93A} study		
	2.5mg/kg twice daily	5mg/kg once daily	5mg/kg	12.5mg/kg	25mg/kg
Improvement in weight	✓	✓	✓	×	✓
Improvement in rotarod performance	×	×	×	×	×
Improvement in visible onset of disease	×	×	×	×	×
Improvement in gait paramters	✓	×	×*	×*	×*
Improvement in CMAP amplitude	✓	✓	×	×	✓
Improvement in rep stim	✓	×	×	×	×
Upregulation of NFF2 targets	✓	✓	not complete	not complete	not complete
Upregulation of HSF1 targets	✓	✓	not complete	not complete	not complete
Improvement in glial staining	×	×	N/A	N/A	N/A
Improvement in MN number	×	×	N/A	N/A	N/A

Both studies also showed significant improvement in CMAP amplitude, suggesting that M102 had a positive effect on motor units in the hindlimbs (Harrigan *et al.*, 2019). This positive effect on CMAP amplitude is important, as CMAP amplitude is a translatable marker between animal studies and clinical studies (Arnold *et al.*, 2015). The ability to easily gain measurements of CMAP amplitude in animals or humans in a non-invasive, reproducible way over many time points makes it a powerful tool for tracking disease progression and evaluating potential therapeutic effects of drugs. CMAP amplitude, specifically change in CMAP amplitude over time, in patients correlates well with survival (Yu *et al.*, 2020), which, as well as making it a useful marker of progression, could potentially be a way of finding sub populations of patients with different disease progression rates to stratify patients in future clinical trials.

In the TDP-43^{Q331K} study, there was evidence of a positive impact on gait with M102, which was not seen in the SOD1^{G93A} study possibly due to the shift in the model. Neither study saw an improvement in rotarod performance or visible signs of onset of disease. Overall, the effects of M102 on both models is similar, with the same parameters being significantly improved in both models. This suggests that the changes seen in both models are driven by the same pathways.

One of the main differences between the SOD1^{G93A} and TDP-43^{Q331K} study is the gene expression. In the TDP-43^{Q331K} model there was significant upregulation of a range of NRF2 and HSF1 genes at 3 months of age. However, only Hspa1a was upregulated at 6 months of age, which could be due to dysregulation of the NRF2 pathway at later stages of disease in the models (Mimoto *et al.*, 2012) or repeated dosing with M102. In the SOD1^{G93A} model, gene expression was only analysed at one time point: 90 days. There was no significant upregulation of NRF2 or HSF1 genes. The blood concentration levels are similar between the 5mg/kg subcutaneous dose and the 25mg/kg oral dose. Tissue was collected at 1 hour post dose and previously we have seen upregulation of these targets with M102 doses in the SOD1^{G93A} model at 6- and 24-hours post dose. It could be too soon after dosing to see any gene expression changes, however 1 hour post dose is also 25 hours post dose some gene induction would have been expected. It may be that the upregulation of genes from orally dosed M102 occurs at a different time compared to the subcutaneously dosed M102. Early data from mice dosed orally or subcutaneously with M102 has shown little difference in gene activation. However, this needs to be investigated further.

Although the HSF1 link is not as strong in the SOD1^{G93A} model as in the TDP-43^{Q331K} study, this is an area that needs to be studied further by investigating protein levels of HSF1 and its targets in cortex tissue, or staining for HSP70 in spinal cord tissue in both mouse models (Kieran *et al.*, 2004). In cell models of ALS, M102 has been shown to reduce SOD1 aggregates (in house data), this aligns with the activation of HSF1 downstream markers as chaperones aid with correct protein folding and removal of misfolded proteins, which has been shown in a study by Batulan *et al*, where activation of HSF1 led to reduced accumulation of SOD1 (Batulan *et al.*, 2006).

Having evidence of positive effects of a compound in multiple mouse models is extremely valuable. Different mutations in genes associated with ALS may potentially drive different pathways that cause motor neuron loss in ALS and mouse models for specific mutations may only model certain specific aspects of the pathophysiology of ALS. This is shown in the two mouse models used in this thesis, the $SOD1^{G93A}$ mouse model shows aspects of motor function decline however the $TDP\text{-}43^{Q331K}$ model shows FTD phenotypes alongside the mild motor phenotypes. Notoriously, there has been a lack of translation between SOD1 mouse models and patients in clinical trials, with many drugs showing benefits in the mouse and not showing any benefit in patients (Scott *et al.*, 2008). Although a lot of this lack of translation can be put down to poor study design or underpowered study designs, using multiple mouse models allows more confidence in the action of the therapeutic agent before moving into clinical trials, especially as most clinical trials start with a wide range of ALS patients, not just those with SOD1 mutations.

Overall, the positive effects that are seen in both mouse models indicate that M102 is having a positive impact on disease progression in ALS, suggesting M102 is a promising drug candidate for treating ALS in patients.

6.4. Future work

Throughout the work described in this thesis, there has been analysis of gene expression using RT-qPCR, which has shown increases in NRF2 and HSF1 targets. There are still many different gene targets that could be explored to better understand the function of M102, such as targets from the NF-kB and PPARy pathways, as these have been shown to be activated by other electrophiles that activate NRF2 (Jobbagy *et al.*, 2019).

Analysis of protein levels in tissue would be beneficial to explore to back up the changes seen at mRNA level. This could be carried out via western blot in order to compare protein levels of targets between tissues, or by IHC to determine intensity of staining. Western blot and IHC analysis of HSP70 would be interesting to explore and we are in the process of optimising an antibody to explore this in cortex and spinal cord tissue. Analysis of the protein levels of a few NRF2 targets will also be beneficial, to match with the changes seen at the mRNA level and compare between early stage and intermediate stage of disease in the $SOD1^{G93A}$ animals.

Glutathione levels analysed via HPLC-MS gave an insight into downstream pathways that are activated by NRF2. This analysis would be useful to carry out on cortex tissue from both the long-term dosed mouse studies to compare GSH and GSSG levels. MRI analysis is also being carried out *in vivo* to optimise a protocol for the quantification of glutathione in the brain of living mice. This could be translated into patients and be used to track progression of disease, but also used as a biomarker for M102 activation in clinical trials.

Staining of lumbar spinal cords from the $SOD1^{G93A}$ study for GFAP and Iba1 to explore glial activity is currently being done and will help understand glial activity between the groups dosed. Nissl staining has also been carried out and MN counts are currently underway to explore MN degeneration and the effect of M102, OXA and edaravone on MN number.

6.5. Concluding remarks

Taking the results from the TDP-43^{Q331K} mouse model and $SOD1^{G93A}$ mouse model together shows the potential for M102 to impact on ALS progression, especially in terms of CMAP amplitude and weight, as these were improved in both models. Based on the results of M102 in these mouse models and other *in vitro* data in cell lines, M102 is currently undergoing preclinical safety and toxicology studies to underpin first in man trials. The use of electrophysiology in a clinical trial with M102 would help as a measure of tracking the effects of the treatment on patients over time, as this is where we have seen the most significant changes in the mouse models.

Bibliography

Abe, K., Aoki, M., Tsuji, S., Itoyama, Y., Sobue, G., Togo, M., *et al.*, 2017. Safety and efficacy of edaravone in well defined patients with amyotrophic lateral sclerosis: a randomised, double-blind, placebo-controlled trial. Lancet Neurol. 16, 505–512.

Abe, K., Itoyama, Y., Sobue, G., Tsuji, S., Aoki, M., Doyu, M., *et al.*, 2014. Confirmatory double-blind, parallel-group, placebo-controlled study of efficacy and safety of edaravone (MCI-186) in amyotrophic lateral sclerosis patients. Amyotroph. Lateral Scler. Front. Degener. 15, 610–617.

Abramzon, Y.A., Fratta, P., Traynor, B.J., Chia, R., 2020. The Overlapping Genetics of Amyotrophic Lateral Sclerosis and Frontotemporal Dementia. Front. Neurosci. 14, 42.

Ackerley, S., Grierson, A.J., Brownlees, J., Thornhill, P., Anderton, B.H., Leigh, P.N., *et al.*, 2000. Glutamate Slows Axonal Transport of Neurofilaments in Transfected Neurons. J. Cell Biol. 150, 165–176.

Adam, B., Afzali, B., Dominy, K.M., Chapman, E., Gill, R., Hidalgo, L.G., *et al.*, 2016. Multiplexed color-coded probe-based gene expression assessment for clinical molecular diagnostics in formalin-fixed paraffin-embedded human renal allograft tissue. Clin. Transplant. 30, 295–305.

Ahmad, R., Raina, D., Meyer, C., Kharbanda, S., Kufe, D., 2006. Triterpenoid CDDO-Me blocks the NF-κB pathway by direct inhibition of IKKβ on Cys-179. J. Biol. Chem. 281, 35764–35769.

Ahmed, R.M., Irish, M., Piguet, O., Halliday, G.M., Ittner, L.M., Farooqi, S., *et al.*, 2016. Amyotrophic lateral sclerosis and frontotemporal dementia: distinct and overlapping changes in eating behaviour and metabolism. Lancet Neurol.

Ahuja, M., Ammal Kaidery, N., Attucks, O.C., McDade, E., Hushpulian, D.M., Gaisin, A., *et al.*, 2021. Bach1 derepression is neuroprotective in a mouse model of Parkinson's disease. Proc. Natl. Acad. Sci. U. S. A. 118.

Al-Chalabi, A., Jones, A., Troakes, C., King, A., Al-Sarraj, S., van den Berg, L.H., 2012. The genetics and neuropathology of amyotrophic lateral sclerosis. Acta Neuropathol. 124, 339–352.

Al-Saif, A., Al-Mohanna, F., Bohlega, S., 2011. A mutation in sigma-1 receptor causes juvenile amyotrophic lateral sclerosis. Ann. Neurol. 70, 913–919.

Alanazy, M.H., Hegedus, J., White, C., Korngut, L., 2017. Decremental responses in patients with motor neuron disease. Brain Behav. 7, e00846.

Alexander, G.M., Erwin, K.L., Byers, N., Deitch, J.S., Augelli, B.J., Blankenhorn, E.P., *et al.*, 2004. Effect of transgene copy number on survival in the G93A SOD1 transgenic mouse model of ALS. Mol. Brain Res. 130, 7–15.

Alqahtani, M.S., Kazi, M., Alsenaidy, M.A., Ahmad, M.Z., 2021. Advances in Oral Drug Delivery. Front. Pharmacol. 12, 62.

Ang, Z.Y., Boddy, M., Liu, Y., Sunderland, B., 2016. Stability of apomorphine in solutions containing selected antioxidant agents. Drug Des. Devel. Ther. 10, 3253–3265.

Anraku, M., Iohara, D., Wada, K., Taguchi, K., Maruyama, T., Otagiri, M., *et al.*, 2016. Antioxidant and renoprotective activity of 2-hydroxypropyl-β-cyclodextrin in nephrectomized rats. J. Pharm. Pharmacol. 68, 608–614.

Anton, A., Mead, R.J., Shaw, P.J., Edden, R.A.E., Bigley, J., Jenkins, T.M., *et al.*, 2022. Assessment of the Precision in Measuring Glutathione at 3 T With a MEGA-PRESS Sequence in Primary Motor Cortex and Occipital Cortex. J. Magn. Reson. Imaging 55, 435–442.

Aoki, M., Warita, H., Mizuno, H., Suzuki, N., Yuki, S., Itoyama, Y., 2011. Feasibility study for functional test battery of SOD transgenic rat (H46R) and evaluation of edaravone, a free radical scavenger. Brain Res. 1382, 321–325.

Arai, T., Hasegawa, M., Akiyama, H., Ikeda, K., Nonaka, T., Mori, H., *et al.*, 2006. TDP-43 is a component of ubiquitin-positive tau-negative inclusions in frontotemporal lobar degeneration and amyotrophic lateral sclerosis. Biochem. Biophys. Res. Commun. 351, 602–611.

Armada-Moreira, A., Gomes, J.I., Pina, C.C., Savchak, O.K., Gonçalves-Ribeiro, J., Rei, N., *et al.*, 2020. Going the Extra (Synaptic) Mile: Excitotoxicity as the Road Toward Neurodegenerative Diseases. Front. Cell. Neurosci.

Arnold, E.S., Ling, S.-C., Huelga, S.C., Lagier-Tourenne, C., Polymenidou, M., Ditsworth, D., *et al.*, 2013. ALS-linked TDP-43 mutations produce aberrant RNA splicing and adult-onset motor neuron disease without aggregation or loss of nuclear TDP-43. Proc. Natl. Acad. Sci. 110, E736–E745.

Arnold, W.D., Porensky, P.N., McGovern, V.L., Iyer, C.C., Duque, S., Li, X., *et al.*, 2014. Electrophysiological biomarkers in spinal muscular atrophy: proof of concept. Ann. Clin. Transl. Neurol. 1, 34.

Arnold, W.D., Sheth, K.A., Wier, C.G., Kissel, J.T., Burghes, A.H., Kolb, S.J., 2015. Electrophysiological motor unit number estimation (MUNE) measuring compound muscle action potential (CMAP) in mouse hindlimb muscles. J. Vis. Exp. 2015, 52899.

Arthur, K.C., Calvo, A., Price, T.R., Geiger, J.T., Chiò, A., Traynor, B.J., 2016. Projected increase in amyotrophic lateral sclerosis from 2015 to 2040. Nat. Commun. 7, 12408.

Auffret, M., Drapier, S., Vérin, M., 2018. Pharmacological Insights into the Use of Apomorphine in Parkinson's Disease: Clinical Relevance. Clin. Drug Investig.

Baba, A., Kawakami, Y., Saito, K., Murashima, Y.L., Itoh, Y., 2016. Effects of edaravone on hippocampal antioxidants in EL mice. J. Nippon Med. Sch. 83, 100–106.

Baird, L., Yamamoto, M., 2020. The Molecular Mechanisms Regulating the KEAP1-NRF2 Pathway. Mol. Cell. Biol. 40.

Bakkar, N., Kousari, A., Kovalik, T., Li, Y., Bowser, R., 2015. RBM45 Modulates the Antioxidant Response in Amyotrophic Lateral Sclerosis through Interactions with KEAP1. Mol. Cell.

Biol. 35, 2385–2399.

Balendra, R., Isaacs, A.M., 2018. C9orf72-mediated ALS and FTD: multiple pathways to disease. Nat. Rev. Neurol.

Bannwarth, S., Ait-El-Mkadem, S., Chaussenot, A., Genin, E.C., Lacas-Gervais, S., Fragaki, K., *et al.*, 2014. A mitochondrial origin for frontotemporal dementia and amyotrophic lateral sclerosis through CHCHD10 involvement. Brain 137, 2329–2345.

Barber, S.C., Mead, R.J., Shaw, P.J., 2006. Oxidative stress in ALS: A mechanism of neurodegeneration and a therapeutic target. Biochim. Biophys. Acta - Mol. Basis Dis.

Batulan, Z., Taylor, D.M., Aarons, R.J., Minotti, S., Doroudchi, M.M., Nalbantoglu, J., *et al.*, 2006. Induction of multiple heat shock proteins and neuroprotection in a primary culture model of familial amyotrophic lateral sclerosis.

Benatar, M., 2007. Lost in translation: Treatment trials in the SOD1 mouse and in human ALS. Neurobiol. Dis.

Benatar, M., Wuu, J., Andersen, P.M., Atassi, N., David, W., Cudkowicz, M., *et al.*, 2018. Randomized, double-blind, placebo-controlled trial of arimoclomol in rapidly progressive SOD1 ALS. Neurology 90, 10.1212/WNL.0000000000004960.

Bennett, E.J., Mead, R.J., Azzouz, M., Shaw, P.J., Grierson, A.J., 2014. Early detection of motor dysfunction in the SOD1G93A mouse model of amyotrophic lateral sclerosis (ALS) using home cage running wheels. PLoS One 9, e107918.

Bennion Callister, J., Ryan, S., Sim, J., Rollinson, S., Pickering-Brown, S.M., 2016. Modelling C9orf72 dipeptide repeat proteins of a physiologically relevant size. Hum. Mol. Genet. 25, 5069–5082.

Bergbower, E.A.S., Pierson, R.N., Azimzadeh, A.M., 2020. Multi-gene technical assessment of qPCR and NanoString n-Counter analysis platforms in cynomolgus monkey cardiac allograft recipients. Cell. Immunol. 347, 104019.

Bilbey, D.L.J., Salem, H., Grossman, M.H., 1960. The Anantomical Basis of the Straub Phenomenon. Br. J. Pharmacol. Chemother. 15, 540–543.

Bono, S., Feligioni, M., Corbo, M., 2021. Impaired antioxidant KEAP1-NRF2 system in amyotrophic lateral sclerosis: NRF2 activation as a potential therapeutic strategy. Mol. Neurodegener. 16, 1–26.

Boyle, A., Ondo, W., 2015. Role of apomorphine in the treatment of Parkinson's Disease. CNS Drugs 29, 83–89.

Brennan, M.S., Matos, M.F., Li, B., Hronowski, X., Gao, B., Juhasz, P., *et al.*, 2015. Dimethyl fumarate and monoethyl fumarate exhibit differential effects on KEAP1, NRF2 activation, and glutathione depletion in vitro. PLoS One 10.

Brenner, D., Müller, K., Wieland, T., Weydt, P., Böhm, S., Lule, D., *et al.*, 2016. NEK1 mutations in familial amyotrophic lateral sclerosis. Brain.

Brenner, D., Yilmaz, R., Müller, K., Grehl, T., Petri, S., Meyer, T., *et al.*, 2018. Hot-spot KIF5A mutations cause familial ALS. Brain 141, 688–697.

Brettschneider, J., Toledo, J.B., Van Deerlin, V.M., Elman, L., McCluskey, L., Lee, V.M.-Y., *et al.*, 2012. Microglial Activation Correlates with Disease Progression and Upper Motor Neuron Clinical Symptoms in Amyotrophic Lateral Sclerosis. PLoS One 7, e39216.

Bristol, L.A., Rothstein, J.D., 1996. Glutamate transporter gene expression in amyotrophic lateral sclerosis motor cortex. Ann. Neurol. 39, 676–679.

Broekkamp, C.L., Rijk, H.W., Joly-Gelouin, D., Lloyd, K.L., 1986. Major tranquillizers can be distinguished from minor tranquillizers on the basis of effects on marble burying and swim-induced grooming in mice. Eur. J. Pharmacol. 126, 223–229.

Burberry, A., Wells, M.F., Limone, F., Couto, A., Smith, K.S., Keaney, J., *et al.*, 2020. C9orf72 suppresses systemic and neural inflammation induced by gut bacteria. Nature 582, 89–94.

Burrell, J.R., Halliday, G.M., Kril, J.J., Ittner, L.M., Götz, J., Kiernan, M.C., *et al.*, 2016. The frontotemporal dementia-motor neuron disease continuum. Lancet.

Burrell, J.R., Kiernan, M.C., Vucic, S., Hodges, J.R., 2011. Motor Neuron dysfunction in frontotemporal dementia. Brain 134, 2582–2594.

Canning, P., Sorrell, F.J., Bullock, A.N., 2015. Structural basis of Keap1 interactions with Nrf2. Free Radic. Biol. Med. 88, 101–107.

Chance, P.F., Rabin, B.A., Ryan, S.G., Ding, Y., Scavina, M., Crain, B., *et al.*, 1998. Linkage of the gene for an autosomal dominant form of juvenile amyotrophic lateral sclerosis to chromosome 9q34. Am. J. Hum. Genet. 62, 633–40.

Chang, Y., Kong, Q., Shan, X., Tian, G., Ilieva, H., Cleveland, D.W., *et al.*, 2008. Messenger RNA oxidation occurs early in disease pathogenesis and promotes motor neuron degeneration in ALS. PLoS One 3.

Chen, X., Liu, Y., Zhu, J., Lei, S., Dong, Y., Li, L., *et al.*, 2016. GSK-3β downregulates Nrf2 in cultured cortical neurons and in a rat model of cerebral ischemia-reperfusion. Sci. Rep. 6, 20196.

Chi, L., Ke, Y., Luo, C., Gozal, D., Liu, R., 2007. Depletion of reduced glutathione enhances motor neuron degeneration in vitro and in vivo. Neuroscience 144, 991–1003.

Chia, R., Chiò, A., Traynor, B.J., 2018. Novel genes associated with amyotrophic lateral sclerosis: diagnostic and clinical implications. Lancet Neurol.

Chiu, A.Y., Zhai, P., Dal Canto, M.C., Peters, T.M., Kwon, Y.W., Prattis, S.M., *et al.*, 1995. Age-Dependent Penetrance of Disease in a Transgenic Mouse Model of Familial Amyotrophic Lateral Sclerosis. Mol. Cell. Neurosci. 6, 349–362.

Chow, C.Y., Landers, J.E., Bergren, S.K., Sapp, P.C., Grant, A.E., Jones, J.M., *et al.*, 2009. Deleterious variants of FIG4, a phosphoinositide phosphatase, in patients with ALS. Am. J. Hum. Genet. 84, 85–8.

Ciervo, Y., Gatto, N., Allen, C., Grierson, A., Ferraiuolo, L., Mead, R.J., *et al.*, 2021. Adipose-derived stem cells protect motor neurons and reduce glial activation in both in vitro and in vivo models of ALS. Mol. Ther. - Methods Clin. Dev. 21, 413–433.

Cleasby, A., Yon, J., Day, P.J., Richardson, C., Tickle, I.J., Williams, P.A., *et al.*, 2014. Structure of the BTB domain of Keap1 and its interaction with the triterpenoid antagonist CDDO. PLoS One 9, e98896.

Cohen, T.J., Hwang, A.W., Restrepo, C.R., Yuan, C.-X., Trojanowski, J.Q., Lee, V.M.Y., 2015. An acetylation switch controls TDP-43 function and aggregation propensity. Nat. Commun. 6, 5845.

Cooper-Knock, J., Moll, T., Ramesh, T., Castelli, L., Beer, A., Robins, H., *et al.*, 2019. Mutations in the Glycosyltransferase Domain of GLT8D1 Are Associated with Familial Amyotrophic Lateral Sclerosis. Cell Rep. 26, 2298-2306.e5.

Cooper-Knock, J., Walsh, M.J., Higginbottom, A., Highley, J.R., Dickman, M.J., Edbauer, D., *et al.*, 2014. Sequestration of multiple RNA recognition motif-containing proteins by C9orf72 repeat expansions. Brain 137, 2040–2051.

Cristofani, R., Crippa, V., Rusmini, P., Cicardi, M.E., Meroni, M., Licata, N. V., *et al.*, 2017. Inhibition of retrograde transport modulates misfolded protein accumulation and clearance in motoneuron diseases. Autophagy 13, 1280–1303.

Cruz, M.P., 2018. Edaravone (Radicava): A Novel Neuroprotective Agent for the Treatment of Amyotrophic Lateral Sclerosis. P T 43, 25–28.

Cuadrado, A., 2015. Structural and functional characterization of Nrf2 degradation by glycogen synthase kinase 3/β-TrCP. Free Radic. Biol. Med. 88, 147–157.

Cullinan, S.B., Gordan, J.D., Jin, J., Harper, J.W., Diehl, J.A., 2004. The Keap1-BTB protein is an adaptor that bridges Nrf2 to a Cul3-based E3 ligase: oxidative stress sensing by a Cul3-Keap1 ligase. Mol. Cell. Biol. 24, 8477–86.

Dafinca, R., Barbagallo, P., Talbot, K., 2021. The Role of Mitochondrial Dysfunction and ER Stress in TDP-43 and C9ORF72 ALS. Front. Cell. Neurosci. 15, 653688.

Davies, T.G., Wixted, W.E., Coyle, J.E., Griffiths-Jones, C., Hearn, K., McMenamin, R., *et al.*, 2016. Monoacidic Inhibitors of the Kelch-like ECH-Associated Protein 1: Nuclear Factor Erythroid 2-Related Factor 2 (KEAP1:NRF2) Protein-Protein Interaction with High Cell Potency Identified by Fragment-Based Discovery. J. Med. Chem. 59, 3991–4006.

Dayalan Naidu, S., Kostov, R. V, Dinkova-Kostova, A.T., 2015. Transcription factors Hsf1 and Nrf2 engage in crosstalk for cytoprotection. Trends Pharmacol. Sci.

de Brouwer, G., Fick, A., Harvey, B.H., Wolmarans, D.W., 2019. A critical inquiry into marble-burying as a preclinical screening paradigm of relevance for anxiety and obsessive–compulsive disorder: Mapping the way forward. Cogn. Affect. Behav. Neurosci.

de Carvalho, M., Dengler, R., Eisen, A., England, J.D., Kaji, R., Kimura, J., *et al.*, 2008. Electrodiagnostic criteria for diagnosis of ALS. Clin. Neurophysiol. 119, 497–503.

De Vos, K.J., Chapman, A.L., Tennant, M.E., Manser, C., Tudor, E.L., Lau, K.-F., *et al.*, 2007. Familial amyotrophic lateral sclerosis-linked SOD1 mutants perturb fast axonal transport to reduce axonal mitochondria content. Hum. Mol. Genet. 16, 2720–2728.

De Vos, K.J., Hafezparast, M., 2017. Neurobiology of axonal transport defects in motor neuron diseases: Opportunities for translational research? Neurobiol. Dis.

de Zeeuw, D., Akizawa, T., Audhya, P., Bakris, G.L., Chin, M., Christ-Schmidt, H., *et al.*, 2013. Bardoxolone Methyl in Type 2 Diabetes and Stage 4 Chronic Kidney Disease. N. Engl. J. Med. 369, 2492–2503.

Deacon, R.M.J., 2006. Digging and marble burying in mice: Simple methods for in vivo identification of biological impacts. Nat. Protoc. 1, 122–124.

DeJesus-Hernandez, M., Mackenzie, I.R.R., Boeve, B.F.F., Boxer, A.L.L., Baker, M., Rutherford, N.J.J., *et al.*, 2011. Expanded GGGGCC Hexanucleotide Repeat in Noncoding Region of C9ORF72 Causes Chromosome 9p-Linked FTD and ALS. Neuron 72, 245–256.

Deng, H.-X., Chen, W., Hong, S.-T., Boycott, K.M., Gorrie, G.H., Siddique, N., *et al.*, 2011. Mutations in UBQLN2 cause dominant X-linked juvenile and adult-onset ALS and ALS/dementia. Nature 477, 211–5.

Deng, H., Gao, K., Jankovic, J., 2014. The role of FUS gene variants in neurodegenerative diseases. Nat. Rev. Neurol. 10, 337–348.

Dhakshinamoorthy, S., Jain, A.K., Bloom, D.A., Jaiswal, A.K., 2005. Bach1 Competes with Nrf2 Leading to Negative Regulation of the Antioxidant Response Element (ARE)-mediated NAD(P)H:Quinone Oxidoreductase 1 Gene Expression and Induction in Response to Antioxidants. J. Biol. Chem. 280, 16891–16900.

Dinkova-Kostova, A.T., Kostov, R. V, Canning, P., 2017. Keap1, the cysteine-based mammalian intracellular sensor for electrophiles and oxidants. Arch. Biochem. Biophys. 617, 84–93.

Ederle, H., Dormann, D., 2017. TDP-43 and FUS en route from the nucleus to the cytoplasm. FEBS Lett.

Eisele, Y.S., Monteiro, C., Fearns, C., Encalada, S.E., Wiseman, R.L., Powers, E.T., *et al.*, 2015. Targeting protein aggregation for the treatment of degenerative diseases. Nat. Rev. Drug Discov.

Elden, A.C., Kim, H.-J., Hart, M.P., Chen-Plotkin, A.S., Johnson, B.S., Fang, X., *et al.*, 2010. Ataxin-2 intermediate-length polyglutamine expansions are associated with increased risk for ALS. Nature 466, 1069–1075.

Eleutherio, E.C.A., Silva Magalhães, R.S., de Araújo Brasil, A., Monteiro Neto, J.R., de Holanda Paranhos, L., 2021. SOD1, more than just an antioxidant. Arch. Biochem. Biophys. 697, 108701.

Esmaeili, M.A., Panahi, M., Yadav, S., Hennings, L., Kiaei, M., 2013. Premature death of TDP-43 (A315T) transgenic mice due to gastrointestinal complications prior to development of full neurological symptoms of amyotrophic lateral sclerosis. Int. J. Exp. Pathol. 94, 56–64.

Farhan, S.M.K., Howrigan, D.P., Abbott, L.E., Klim, J.R., Topp, S.D., Byrnes, A.E., *et al.*, 2019. Exome sequencing in amyotrophic lateral sclerosis implicates a novel gene, DNAJC7, encoding a heat-shock protein. Nat. Neurosci.

Fecto, F., Yan, J., Vemula, S.P., Liu, E., Yang, Y., Chen, W., *et al.*, 2011. SQSTM1 mutations in familial and sporadic amyotrophic lateral sclerosis. Arch. Neurol. 68, 1440–1446.

Feeney, S.J., McKelvie, P.A., Austin, L., Jean-Francois, M.J., Kapsa, R., Tombs, S.M., *et al.*, 2001. Presymptomatic motor neuron loss and reactive astrocytosis in the SOD1 mouse model of amyotrophic lateral sclerosis. Muscle Nerve 24, 1510–1519.

Fernadez-checa, J.C., Kaplowitz, N., Garcia-ruiz, C., Colell, A., Mirandam, M., Mari, M., *et al.*, 1997. GSH transport l in mitochondria: defense against TNF-induced oxidative stress and alcohol-induced defect. Am. Physiol. Soc.

Ferraiuolo, L., Kirby, J., Grierson, A.J., Sendtner, M., Shaw, P.J., 2011. Molecular pathways of motor neuron injury in amyotrophic lateral sclerosis. Nat. Rev. Neurol. 7, 616–630.

Festing, M.F.W., 2020. The “completely randomised” and the “randomised block” are the only experimental designs suitable for widespread use in pre-clinical research. Sci. Rep. 10, 17577.

Freischmidt, A., Wieland, T., Richter, B., Ruf, W., Schaeffer, V., Müller, K., *et al.*, 2015. Haploinsufficiency of TBK1 causes familial ALS and fronto-temporal dementia. Nat. Neurosci. 18, 631–636.

Fu, L.L., Yin, H.X., Liu, M.S., Cui, L.Y., 2019. Study on variation trend of repetitive nerve stimulation waveform in amyotrophic lateral sclerosis. Chin. Med. J. (Engl). 132, 542–550.

Fuse, Y., Kobayashi, M., 2017. Conservation of the Keap1-Nrf2 system: An evolutionary journey through stressful space and time. Molecules 22, 1–22.

Geiss, G.K., Bumgarner, R.E., Birditt, B., Dahl, T., Dowidar, N., Dunaway, D.L., *et al.*, 2008. Direct multiplexed measurement of gene expression with color-coded probe pairs. Nat. Biotechnol. 26, 317–325.

Goelz, M.F., Mahler, J., Harry, J., Myers, P., Clark, J., Thigpen, J.E., *et al.*, 1998. Neuropathologic Findings Associated with Seizures in FVB Mice.

Gold, R., Kappos, L., Arnold, D.L., Bar-Or, A., Giovannoni, G., Selmaj, K., *et al.*, 2012. Placebo-Controlled Phase 3 Study of Oral BG-12 for Relapsing Multiple Sclerosis. N. Engl. J. Med. 367, 1098–1107.

Gordon, T., Hegedus, J., Tam, S.L., 2004. Adaptive and maladaptive motor axonal sprouting in aging and motoneuron disease. Neurol. Res.

Gould, S., Scott, R.C., 2005. 2-Hydroxypropyl-β-cyclodextrin (HP-β-CD): A toxicology review. Food Chem. Toxicol.

Greenway, M.J., Andersen, P.M., Russ, C., Ennis, S., Cashman, S., Donaghy, C., *et al.*, 2006. ANG mutations segregate with familial and “sporadic” amyotrophic lateral sclerosis. Nat. Genet. 38, 411–413.

Guo, C., Sun, L., Chen, X., Zhang, D., 2013. Oxidative stress, mitochondrial damage and neurodegenerative diseases. Neural Regen. Res. 8, 2003–14.

Gurney, M.E., 1997. The use of transgenic mouse models of amyotrophic lateral sclerosis in preclinical drug studies, in: Journal of the Neurological Sciences. pp. 67–73.

Gurney, M.E., Pu, H., Chiu, A.Y., Dal Canto, M.C., Polchow, C.Y., Alexander, D.D., *et al.*, 1994. Motor neuron degeneration in mice that express a human Cu,Zn superoxide dismutase mutation. Science (80-.). 264, 1772–1775.

Haeusler, A.R., Donnelly, C.J., Rothstein, J.D., 2016. The expanding biology of the C9orf72 nucleotide repeat expansion in neurodegenerative disease. Nat. Rev. Neurosci. 17, 383.

Haidet-Phillips, A.M., Hester, M.E., Miranda, C.J., Meyer, K., Braun, L., Frakes, A., *et al.*, 2011. Astrocytes from familial and sporadic ALS patients are toxic to motor neurons. Nat. Biotechnol. 29, 824–8.

Hall, E.D., Oostveen, J.A., Gurney, M.E., 1998. Relationship of microglial and astrocytic activation to disease onset and progression in a transgenic model of familial ALS. Glia 23, 249–256.

Hardiman, O., Al-Chalabi, A., Chio, A., Corr, E.M., Logroscino, G., Robberecht, W., *et al.*, 2017. Amyotrophic lateral sclerosis. Nat. Rev. Dis. Prim. 3, 1–18.

Hargitai, J., Lewis, H., Boros, I., Rácz, T., Fiser, A., Kurucz, I., *et al.*, 2003. Bimoclomol, a heat shock protein co-inducer, acts by the prolonged activation of heat shock factor-1. Biochem. Biophys. Res. Commun. 307, 689–695.

Harrigan, M.E., Filous, A.R., Tosolini, A.P., Morris, R., Schwab, J.M., Arnold, W.D., 2019. Assessing Rat Forelimb and Hindlimb Motor Unit Connectivity as Objective and Robust Biomarkers of Spinal Motor Neuron Function. Sci. Rep. 9, 16699.

Hartl, F.U., Bracher, A., Hayer-Hartl, M., 2011. Molecular chaperones in protein folding and proteostasis. Nature.

Harvey, C.J., Thimmulappa, R.K., Singh, A., Blake, D.J., Ling, G., Wakabayashi, N., *et al.*, 2009. Nrf2-regulated glutathione recycling independent of biosynthesis is critical for cell survival during oxidative stress. Free Radic. Biol. Med. 46, 443–53.

Hatzipetros, T., Bogdanik, L.P., Tassinari, V.R., Kidd, J.D., Moreno, A.J., Davis, C., *et al.*, 2014. C57BL/6J congenic Prp-TDP43A315T mice develop progressive neurodegeneration in the myenteric plexus of the colon without exhibiting key features of ALS. Brain Res. 1584, 59–72.

Hayashi, G., Jasoliya, M., Sahdeo, S., Saccà, F., Pane, C., Filla, A., *et al.*, 2017. Dimethyl fumarate mediates Nrf2-dependent mitochondrial biogenesis in mice and humans. Hum. Mol. Genet. 26.

He, X., Ma, Q., 2009. NRF2 cysteine residues are critical for oxidant/electrophile-sensing, Kelch-like ECH-associated protein-1-dependent ubiquitination-proteasomal degradation, and transcription activation. Mol. Pharmacol. 76, 1265–78.

Healy, S., McMahon, J., Owens, P., Dockery, P., FitzGerald, U., 2018. Threshold-based segmentation of fluorescent and chromogenic images of microglia, astrocytes and oligodendrocytes in FIJI. J. Neurosci. Methods 295, 87–103.

Heiman-Patterson, T.D., Sher, R.B., Blankenhorn, E.A., Alexander, G., Deitch, J.S., Kunst, C.B., *et al.*, 2011. Effect of genetic background on phenotype variability in transgenic mouse models of amyotrophic lateral sclerosis: A window of opportunity in the search for genetic modifiers. Amyotroph. Lateral Scler. 12, 79–86.

Herdewyn, S., Cirillo, C., Van Den Bosch, L., Robberecht, W., Vanden Berghe, P., Van Damme, P., 2014. Prevention of intestinal obstruction reveals progressive neurodegeneration in mutant TDP-43 (A315T) mice. Mol. Neurodegener. 9, 24.

Higashi, C., Kawaji, A., Tsuda, N., Hayashi, M., Saito, R., Yagishita, Y., *et al.*, 2017. The novel Nrf2 inducer TFM-735 ameliorates experimental autoimmune encephalomyelitis in mice. Eur. J. Pharmacol. 802, 76–84.

Holland, R., Hawkins, A.E., Eggler, A.L., Mesecar, A.D., Fabris, D., Fishbein, J.C., 2008. Prospective Type 1 and Type 2 Disulfides of Keap1 Protein HHS Public Access. Chem Res Toxicol 21, 2051–2060.

Hroudová, J., Singh, N., Fišar, Z., 2014. Mitochondrial dysfunctions in neurodegenerative diseases: Relevance to alzheimer's disease. Biomed Res. Int.

Hsu, C.-H., Lin, S., Ho, A.-C., Johnson, T.D., Wang, P.C., Scafidi, J., *et al.*, 2021. Comparison of in vivo and in situ detection of hippocampal metabolites in mouse brain using 1 H-MRS. NMR Biomed. 34, e4451.

Hybertson, B.M., Gao, B., Bose, S.K., McCord, J.M., 2011. Oxidative stress in health and disease: The therapeutic potential of Nrf2 activation. Mol. Aspects Med. 32, 234–246.

Hyung, S., Jeong, Y.S., Yeo, J., Song, Y.K., Kim, M.S., Im, Y.J., *et al.*, 2018. Identification of the primary determining factor(s) governing the oral absorption of edaravone in rats. Eur. J. Pharm. Sci. 123, 312–320.

Iguchi, Y., Katsuno, M., Niwa, J., Takagi, S., Ishigaki, S., Ikenaka, K., *et al.*, 2013. Loss of TDP-43 causes age-dependent progressive motor neuron degeneration. Brain 136, 1371–1382.

Ito, Hidefumi, Wate, R., Zhang, J., Ohnishi, S., Kaneko, S., Ito, Hisashi, *et al.*, 2008. Treatment with edaravone, initiated at symptom onset, slows motor decline and decreases SOD1 deposition in ALS mice. Exp. Neurol. 213, 448–455.

Itoh, K., Chiba, T., Takahashi, S., Ishii, T., Igarashi, K., Katoh, Y., *et al.*, 1997. An Nrf2/Small Maf Heterodimer Mediates the Induction of Phase II Detoxifying Enzyme Genes through Antioxidant Response Elements. Biochem. Biophys. Res. Commun. 236, 313–322.

Ittner, L.M., Halliday, G.M., Kril, J.J., Götz, J., Hodges, J.R., Kiernan, M.C., 2015. FTD and ALS-translating mouse studies into clinical trials. Nat. Rev. Neurol. 11, 360–366.

Iwanami, T., Sonoo, M., Hatanaka, Y., Hokkoku, K., Oishi, C., Shimizu, T., 2011. Decremental responses to repetitive nerve stimulation (RNS) in motor neuron disease. Clin. Neurophysiol. 122, 2530–2536.

Jaarsma, D., Haasdijk, E.D., Grashorn, J.A.C., Hawkins, R., Van Duijn, W., Verspaget, H.W., *et al.*, 2000. Human Cu/Zn superoxide dismutase (SOD1) overexpression in mice causes mitochondrial vacuolization, axonal degeneration, and premature motoneuron death and accelerates motoneuron disease in mice expressing a familial amyotrophic lateral sclerosis mutant SO. Neurobiol. Dis. 7, 623–643.

Jacobs, A.T., Marnett, L.J., 2007. Heat Shock Factor 1 Attenuates 4-Hydroxynonenal-mediated Apoptosis: CRITICAL ROLE FOR HEAT SHOCK PROTEIN 70 INDUCTION AND STABILIZATION OF Bcl-XL*. J. Biol. Chem. 282, 33412–33420.

Jiang, T., Harder, B., De La Vega, R., Wong, P.K., Chapman, E., Zhang, D.D., *et al.*, 2015. p62 links autophagy and Nrf2 signaling. Free Radic. Biol. Med. 88, 199–204.

Jiménez-Villegas, J., Ferraiuolo, L., Mead, R.J.J., Shaw, P.J.J., Cuadrado, A., Rojo, A.I.I., 2021. NRF2 as a therapeutic opportunity to impact in the molecular roadmap of ALS. Free Radic. Biol. Med. 173, 125–141.

Jobbagy, S., Vitturi, D.A., Salvatore, S.R., Turell, L., Pires, M.F., Kansanen, E., *et al.*, 2019. Electrophiles modulate glutathione reductase activity via alkylation and upregulation of glutathione biosynthesis. Redox Biol. 21, 101050.

Johnson, J.O., Mandrioli, J., Benatar, M., Abramzon, Y., Van Deerlin, V.M., Trojanowski, J.Q., *et al.*, 2010. Exome sequencing reveals VCP mutations as a cause of familial ALS. Neuron 68, 857–64.

Johnson, J.O., Pioro, E.P., Boehringer, A., Chia, R., Feit, H., Renton, A.E., *et al.*, 2014. Mutations in the Matrin 3 gene cause familial amyotrophic lateral sclerosis. Nat. Neurosci. 17, 664–666.

Jonsson, P.A., Graffmo, K.S., Andersen, P.M., Brännström, T., Lindberg, M., Oliveberg, M., *et al.*, 2006. Disulphide-reduced superoxide dismutase-1 in CNS of transgenic amyotrophic lateral sclerosis models. Brain 129, 451–464.

Joyce, P.I., Mcgoldrick, P., Saccon, R.A., Weber, W., Fratta, P., West, S.J., *et al.*, 2014. A novel SOD1-ALS mutation separates central and peripheral effects of mutant SOD1 toxicity. Hum. Mol. Genet. 24, 1883–1897.

Jung, B.-J., Yoo, H.-S., Shin, S., Park, Y.-J., Jeon, S.-M., 2018. Dysregulation of NRF2 in Cancer: from Molecular Mechanisms to Therapeutic Opportunities. Biomol. Ther. (Seoul). 26, 57–68.

Kabashi, E., Valdmanis, P.N., Dion, P., Rouleau, G.A., 2007. Oxidized/misfolded superoxide dismutase-1: the cause of all amyotrophic lateral sclerosis? Ann. Neurol. 62, 553–559.

Katoh, Y., Itoh, K., Yoshida, E., Miyagishi, M., Fukamizu, A., Yamamoto, M., 2001. Two domains of Nrf2 cooperatively bind CBP, a CREB binding protein, and synergistically activate transcription. Genes to Cells 6, 857–868.

Keerie, A., Brown-Wright, H., Kirkland, I., Grierson, A., Alix, J.J.P., Holscher, C., *et al.*, 2021. The GLP-1 receptor agonist, liraglutide, fails to slow disease progression in SOD1G93A and TDP-43Q331K transgenic mouse models of ALS. Sci. Rep. 11, 17027.

Keum, Y.S., Choi, B.Y., 2014. Molecular and chemical regulation of the keap1-Nrf2 signaling pathway. Molecules.

Kieran, D., Kalmar, B., Dick, J.R.T., Riddoch-Contreras, J., Burnstock, G., Greensmith, L., 2004. Treatment with arimoclomol, a coinducer of heat shock proteins, delays disease progression in ALS mice. Nat. Med. 10, 402–405.

Kim, E., White, M.A., Phillips, B.U., Lopez-Cruz, L., Kim, H., Heath, C.J., *et al.*, 2020. Coexistence of perseveration and apathy in the TDP-43 Q331K knock-in mouse model of ALS-FTD. Transl. Psychiatry 10, 377.

Kim, H.J., Kim, N.C., Wang, Y.-D., Scarborough, E.A., Moore, J., Diaz, Z., *et al.*, 2013. Mutations in prion-like domains in hnRNPA2B1 and hnRNPA1 cause multisystem proteinopathy and ALS. Nature 495, 467–473.

Kim, K., 2021. Glutathione in the Nervous System as a Potential Therapeutic Target to Control the Development and Progression of Amyotrophic Lateral Sclerosis. Antioxidants (Basel, Switzerland) 10.

Kirby, J., Halligan, E., Baptista, M.J., Allen, S., Heath, P.R., Holden, H., *et al.*, 2005. Mutant SOD1 alters the motor neuronal transcriptome: Implications for familial ALS. Brain 128, 1686–1706.

Kobayashi, A., Kang, M.-I., Okawa, H., Ohtsuji, M., Zenke, Y., Chiba, T., *et al.*, 2004. Oxidative stress sensor Keap1 functions as an adaptor for Cul3-based E3 ligase to regulate proteasomal degradation of Nrf2. Mol. Cell. Biol. 24, 7130–9.

Kobayashi, E.H., Suzuki, T., Funayama, R., Nagashima, T., Hayashi, M., Sekine, H., *et al.*, 2016. Nrf2 suppresses macrophage inflammatory response by blocking proinflammatory cytokine transcription. Nat. Commun. 7.

Kobayashi, M., Li, L., Iwamoto, N., Nakajima-Takagi, Y., Kaneko, H., Nakayama, Y., *et al.*, 2009. The Antioxidant Defense System Keap1-Nrf2 Comprises a Multiple Sensing Mechanism for Responding to a Wide Range of Chemical Compounds. Mol. Cell. Biol. 29, 493–502.

Komatsu, M., Kurokawa, H., Waguri, S., Taguchi, K., Kobayashi, A., Ichimura, Y., *et al.*, 2010. The selective autophagy substrate p62 activates the stress responsive transcription factor Nrf2 through inactivation of Keap1. Nat. Cell Biol. 12, 213–223.

Komine, O., Yamanaka, K., 2015. Neuroinflammation in motor neuron disease. Nagoya J. Med. Sci. 77, 537–49.

Kong, Q., Chang, L.-C., Takahashi, K., Liu, Q., Schulte, D.A., Lai, L., *et al.*, 2014. Small-molecule activator of glutamate transporter EAAT2 translation provides neuroprotection. J. Clin. Invest. 124, 1255–67.

Kopacz, A., Kloska, D., Forman, H.J., Jozkowicz, A., Grochot-Przeczek, A., 2020. Beyond repression of Nrf2: An update on Keap1. Free Radic. Biol. Med. 157, 63–74.

Kouadjo, K.E., Nishida, Y., Cadrin-Girard, J.F., Yoshioka, M., St-Amand, J., 2007. Housekeeping and tissue-specific genes in mouse tissues. BMC Genomics 8.

Kovács, D., Sigmond, T., Hotzi, B., Bohár, B., Fazekas, D., Deák, V., *et al.*, 2019. HSF1Base: A Comprehensive Database of HSF1 (Heat Shock Factor 1) Target Genes. Int. J. Mol. Sci. 20.

Kwiatkowski, T.J., Bosco, D.A., Leclerc, A.L., Tamrazian, E., Vanderburg, C.R., Russ, C., *et al.*, 2009. Mutations in the FUS/TLS gene on chromosome 16 cause familial amyotrophic lateral sclerosis. Science 323, 1205–8.

Lastres-Becker, I., García-Yagüe, A.J., Scannevin, R.H., Casarejos, M.J., Kügler, S., Rábano, A., *et al.*, 2016. Repurposing the NRF2 Activator Dimethyl Fumarate as Therapy Against Synucleinopathy in Parkinson's Disease. Antioxid. Redox Signal. 25, 61–77.

Lau, A., Wang, X.-J., Zhao, F., Villeneuve, N.F., Wu, T., Jiang, T., *et al.*, 2010. A noncanonical mechanism of Nrf2 activation by autophagy deficiency: direct interaction between Keap1 and p62. Mol. Cell. Biol. 30, 3275–85.

Le Ber, I., De Septenville, A., Millecamps, S., Camuzat, A., Caroppo, P., Couratier, P., *et al.*, 2015. TBK1 mutation frequencies in French frontotemporal dementia and amyotrophic lateral sclerosis cohorts. Neurobiol. Aging 36, 3116.e5-3116.e8.

Le Gall, L., Anakor, E., Connolly, O., Vijayakumar, U.G., Duddy, W.J., Duguez, S., 2020. Molecular and Cellular Mechanisms Affected in ALS. J. Pers. Med. 10.

Lee, Y.B., Chen, H.J., Peres, J.N., Gomez-Deza, J., Attig, J., Štalekar, M., *et al.*, 2013. Hexanucleotide repeats in ALS/FTD form length-dependent RNA Foci, sequester RNA binding proteins, and are neurotoxic. Cell Rep. 5, 1178–1186.

Leermakers, P.A., Skov, M., Riisager, A., Nielsen, O.B., Pedersen, T.H., 2021. Alterations in fast-twitch muscle membrane conductance regulation do not explain decreased muscle function of SOD1G93A rats. Muscle and Nerve.

Lehmann, J.C.U., Listopad, J.J., Rentzsch, C.U., Igney, F.H., Von Bonin, A., Hennekes, H.H., *et al.*, 2007. Dimethylfumarate induces immunosuppression via glutathione depletion and subsequent induction of heme oxygenase 1. J. Invest. Dermatol. 127, 835–845.

Levonen, A.-L., Hill, B.G., Kansanen, E., Zhang, J., Darley-Usmar, V.M., 2014. Redox regulation of antioxidants, autophagy, and the response to stress: implications for electrophile therapeutics. Free Radic. Biol. Med. 71, 196–207.

Li, X., Zhang, D., Hannink, M., Beamer, L.J., 2004. Crystal Structure of the Kelch Domain of Human Keap1. J. Biol. Chem. 279, 54750–54758.

Liao, B., Zhao, W., Beers, D.R., Henkel, J.S., Appel, S.H., 2012. Transformation from a neuroprotective to a neurotoxic microglial phenotype in a mouse model of ALS. Exp. Neurol. 237, 147–52.

Liby, K., Hock, T., Yore, M.M., Suh, N., Place, A.E., Risingsong, R., *et al.*, 2005. The Synthetic Triterpenoids, CDDO and CDDO-Imidazolide, Are Potent Inducers of Heme Oxygenase-1 and Nrf2/ARE Signaling.

Lin, P.-Y., Simon, S.M., Koh, W.K., Folorunso, O., Umbaugh, C.S., Pierce, A., 2013. Heat shock factor 1 over-expression protects against exposure of hydrophobic residues on mutant SOD1 and early mortality in a mouse model of amyotrophic lateral sclerosis. Mol.

Neurodegener. 8, 43.

Lin, P.-Y.Y., Folorunso, O., Taglialatela, G., Pierce, A., 2016. Overexpression of heat shock factor 1 maintains TAR DNA binding protein 43 solubility via induction of inducible heat shock protein 70 in cultured cells. J. Neurosci. Res. 94, 671–682.

Lin, Z., Kim, E., Ahmed, M., Han, G., Simmons, C., Redhead, Y., *et al.*, 2020. MRI-guided histology of TDP-43 knock-in mice implicates parvalbumin interneuron loss, impaired neurogenesis and aberrant neurodevelopment in ALS-FTD. bioRxiv 2020.05.24.107177.

Liu, Y., Pattamatta, A., Zu, T., Reid, T., Bardhi, O., Borchelt, D.R., *et al.*, 2016. C9orf72 BAC Mouse Model with Motor Deficits and Neurodegenerative Features of ALS/FTD. Neuron 90, 521–534.

Lu, S.C., 2009. Regulation of glutathione synthesis. Mol. Aspects Med. 30, 42–59.

Lückel, C., Picard, F., Raifer, H., Carrascosa, L.C., Guralnik, A., Zhang, Y., *et al.*, 2019. IL-17+ CD8+ T cell suppression by dimethyl fumarate associates with clinical response in multiple sclerosis. Nat. Commun. 10.

Ludolph, A.C., Bendotti, C., Blaugrund, E., Chio, A., Greensmith, L., Loeffler, J.P., *et al.*, 2010. Guidelines for preclinical animal research in ALS/MND: A consensus meeting. Amyotroph. Lateral Scler. 11, 38–45.

Lynch, D.R., Chin, M.P., Delatycki, M.B., Subramony, S.H., Corti, M., Hoyle, J.C., *et al.*, 2021. Safety and Efficacy of Omaveloxolone in Friedreich Ataxia (MOXIe Study). Ann. Neurol. 89, 212.

Ma, Q., 2013. Role of Nrf2 in Oxidative Stress and Toxicity. Annu. Rev. Pharmacol. Toxicol. 53, 401–426.

Mackenzie, I.R., Nicholson, A.M., Sarkar, M., Messing, J., Purice, M.D., Pottier, C., *et al.*, 2017. TIA1 Mutations in Amyotrophic Lateral Sclerosis and Frontotemporal Dementia Promote Phase Separation and Alter Stress Granule Dynamics. Neuron 95, 808-816.e9.

Magrané, J., Cortez, C., Gan, W.-B., Manfredi, G., 2014. Abnormal mitochondrial transport and morphology are common pathological denominators in SOD1 and TDP43 ALS mouse models. Hum. Mol. Genet. 23, 1413–1424.

Majounie, E., Renton, A.E., Mok, K., Dopper, E.G.P., Waite, A., Rollinson, S., *et al.*, 2012. Frequency of the C9orf72 hexanucleotide repeat expansion in patients with amyotrophic lateral sclerosis and frontotemporal dementia: a cross-sectional study. Lancet. Neurol. 11, 323–30.

Malik, R., Wiedau, M., 2020. Therapeutic Approaches Targeting Protein Aggregation in Amyotrophic Lateral Sclerosis. Front. Mol. Neurosci. 13, 98.

Mancuso, R., Oliván, S., Mancera, P., Pastén-Zamorano, A., Manzano, R., Casas, C., *et al.*, 2012. Effect of genetic background on onset and disease progression in the SOD1-G93A model of amyotrophic lateral sclerosis. Amyotroph. Lateral Scler. 13, 302–310.

Mancuso, R., Osta, R., Navarro, X., 2014. Presymptomatic electrophysiological tests predict

clinical onset and survival in SOD1G93A ALS mice. Muscle and Nerve 50, 943–949.

Mancuso, R., Santos-Nogueira, E., Osta, R., Navarro, X., 2011. Electrophysiological analysis of a murine model of motoneuron disease. Clin. Neurophysiol. 122, 1660–1670.

Maruyama, H., Morino, H., Ito, H., Izumi, Y., Kato, H., Watanabe, Y., *et al.*, 2010. Mutations of optineurin in amyotrophic lateral sclerosis. Nature 465, 223–226.

Matus, S., Valenzuela, V., Medinas, D.B., Hetz, C., 2013. ER Dysfunction and Protein Folding Stress in ALS. Int. J. Cell Biol. 2013, 674751.

McBride, H.M., Neuspiel, M., Wasiak, S., 2006. Mitochondria: More Than Just a Powerhouse. Curr. Biol.

McMahon, M., Thomas, N., Itoh, K., Yamamoto, M., Hayes, J.D., 2004. Redox-regulated turnover of Nrf2 is determined by at least two separate protein domains, the redox-sensitive Neh2 degron and the redox-insensitive Neh6 degron. J. Biol. Chem. 279, 31556–31567.

Mead, R.J., Bennett, E.J., Kennerley, A.J., Sharp, P., Sunyach, C., Kasher, P., *et al.*, 2011. Optimised and rapid pre-clinical screening in the SOD1 G93A transgenic mouse model of amyotrophic lateral sclerosis (ALS). PLoS One 6, 1–12.

Mead, R.J., Higginbottom, A., Allen, S.P., Kirby, J., Bennett, E., Barber, S.C., *et al.*, 2013. S[+] Apomorphine is a CNS penetrating activator of the Nrf2-ARE pathway with activity in mouse and patient fibroblast models of amyotrophic lateral sclerosis. Free Radic. Biol. Med. 61, 438–452.

Meng, L., Bian, A., Jordan, S., Wolff, A., Shefner, J.M., Andrews, J., 2018. Profile of medical care costs in patients with amyotrophic lateral sclerosis in the Medicare programme and under commercial insurance. Amyotroph. Lateral Scler. Front. Degener. 19, 134–142.

Millecamps, S., Salachas, F., Cazeneuve, C., Gordon, P., Bricka, B., Camuzat, A., *et al.*, 2010. SOD1, ANG, VAPB, TARDBP, and FUS mutations in familial amyotrophic lateral sclerosis: Genotype-phenotype correlations. J. Med. Genet. 47, 554–560.

Miller, R.G., Mitchell, J.D., Lyon, M., Moore, D.H., 2003. Riluzole for amyotrophic lateral sclerosis (ALS)/motor neuron disease (MND). Amyotroph. Lateral Scler. Other Mot. Neuron Disord. 4, 191–206.

Mimoto, T., Miyazaki, K., Morimoto, N., Kurata, T., Satoh, K., Ikeda, Y., *et al.*, 2012. Impaired antioxydative Keap1/Nrf2 system and the downstream stress protein responses in the motor neuron of ALS model mice. Brain Res. 1446, 109–118.

Mitsumoto, H., Brooks, B.R., Silani, V., 2014. Clinical trials in amyotrophic lateral sclerosis: Why so many negative trials and how can trials be improved? Lancet Neurol. 13, 1127–1138.

Mitsumoto, H., Santella, R.M., Liu, X., Bogdanov, M., Zipprich, J., Wu, H.-C., *et al.*, 2008. Oxidative stress biomarkers in sporadic ALS. Amyotroph. Lateral Scler. 9, 177–83.

Mizunoe, Y., Kobayashi, M., Sudo, Y., Watanabe, S., Yasukawa, H., Natori, D., *et al.*, 2018. Trehalose protects against oxidative stress by regulating the Keap1-Nrf2 and autophagy

pathways. Redox Biol. 15, 115–124.

Mordes, D.A., Morrison, B.M., Ament, X.H., Cantrell, C., Mok, J., Eggan, P., *et al.*, 2020. Absence of Survival and Motor Deficits in 500 Repeat C9ORF72 BAC Mice. Neuron 108, 775-783.e4.

Moujalled, D., Grubman, A., Acevedo, K., Yang, S., Ke, Y.D., Moujalled, D.M., *et al.*, 2017. TDP-43 mutations causing amyotrophic lateral sclerosis are associated with altered expression of RNA-binding protein hnRNP K and affect the Nrf2 antioxidant pathway. Hum. Mol. Genet. 26, 1732–1746.

Münch, C., O'Brien, J., Bertolotti, A., 2011. Prion-like propagation of mutant superoxide dismutase-1 misfolding in neuronal cells. Proc. Natl. Acad. Sci. U. S. A. 108, 3548–3553.

Murphy, J.M., Henry, R.G., Langmore, S., Kramer, J.H., Miller, B.L., Lomen-Hoerth, C., 2007. Continuum of frontal lobe impairment in amyotrophic lateral sclerosis. Arch. Neurol. 64, 530–534.

Namani, A., Li, Y., Wang, X.J., Tang, X., 2014. Modulation of NRF2 signaling pathway by nuclear receptors: Implications for cancer. Biochim. Biophys. Acta - Mol. Cell Res. 1843, 1875–1885.

Neef, D.W., Jaeger, A.M., Thiele, D.J., 2011. Heat shock transcription factor 1 as a therapeutic target in neurodegenerative diseases. Nat. Rev. Drug Discov. 10, 930–44.

Neymotin, A., Calingasan, N.Y., Wille, E., Naseri, N., Petri, S., Damiano, M., *et al.*, 2011. Neuroprotective effect of Nrf2/ARE activators, CDDO ethylamide and CDDO trifluoroethylamide, in a mouse model of amyotrophic lateral sclerosis. Free Radic. Biol. Med. 51, 88–96.

Nguyen, L., Laboissonniere, L.A., Guo, S., Pilotto, F., Scheidegger, O., Oestmann, A., *et al.*, 2020. Survival and Motor Phenotypes in FVB C9-500 ALS/FTD BAC Transgenic Mice Reproduced by Multiple Labs. Neuron 108, 784-796.e3.

Nicolas, A., Kenna, K.P., Renton, A.E., Ticozzi, N., Faghri, F., Chia, R., *et al.*, 2018. Genome-wide Analyses Identify KIF5A as a Novel ALS Gene. Neuron 97, 1268-1283.e6.

Nishimura, A.L., Mitne-Neto, M., Silva, H.C.A., Oliveira, J.R.M., Vainzof, M., Zatz, M., 2004. A novel locus for late onset amyotrophic lateral sclerosis/motor neurone disease variant at 20q13. J. Med. Genet. 41, 315–20.

Nordin, A., Akimoto, C., Wuolikainen, A., Alstermark, H., Jonsson, P., Birve, A., *et al.*, 2015. Extensive size variability of the GGGGCC expansion in C9orf72 in both neuronal and non-neuronal tissues in 18 patients with ALS or FTD.

O'Brien, J., Wendell, S.G., 2020. Electrophile modulation of inflammation: A two-hit approach. Metabolites.

Obrador, E., Salvador, R., López-Blanch, R., Jihad-Jebbar, A., Vallés, S.L., Estrela, J.M., 2020. Oxidative Stress, Neuroinflammation and Mitochondria in the Pathophysiology of Amyotrophic Lateral Sclerosis. Antioxidants (Basel, Switzerland) 9.

Orlacchio, A., Babalini, C., Borreca, A., Patrono, C., Massa, R., Basaran, S., *et al.*, 2010. SPATACSIN mutations cause autosomal recessive juvenile amyotrophic lateral sclerosis. Brain 133, 591–598.

Oyake, T., Itoh, K., Motohashi, H., Hayashi, † Norio, Hoshino, H., Nishizawa, M., *et al.*, 1996. Bach Proteins Belong to a Novel Family of BTB-Basic Leucine Zipper Transcription Factors That Interact with MafK and Regulate Transcription through the NF-E2 Site, MOLECULAR AND CELLULAR BIOLOGY.

Paganoni, S., Karam, C., Joyce, N., Bedlack, R., Carter, G.T., 2015. Comprehensive rehabilitative care across the spectrum of amyotrophic lateral sclerosis. NeuroRehabilitation 37, 53–68.

Pajarillo, E., Rizor, A., Lee, J., Aschner, M., Lee, E., 2019. The role of astrocytic glutamate transporters GLT-1 and GLAST in neurological disorders: Potential targets for neurotherapeutics. Neuropharmacology 161, 107559.

Paré, B., Lehmann, M., Beaudin, M., Nordström, U., Saikali, S., Julien, J.-P., *et al.*, 2018. Misfolded SOD1 pathology in sporadic Amyotrophic Lateral Sclerosis. Sci. Rep. 8, 14223.

Parkinson, N., Ince, P.G., Smith, M.O., Hughley, R., Skibinski, G., Andersen, P.M., *et al.*, 2006. ALS phenotypes with mutations in CHMP2B (charged multivesicular body protein 2B). Neurology 67, 1074–1077.

Petri, S., Körner, S., Kiaei, M., 2012. Nrf2/ARE signaling pathway: Key mediator in oxidative stress and potential therapeutic target in ALS. Neurol. Res. Int. 2012, 1–7.

Poltawski, L., Edwards, H., Todd, A., Watson, T., James, C.-A., Lees, A., 2008. Cutaneous side effects of infused apomorphine: The patient and carer experience. Br. J. Neurosci. Nurs. 4, 576–580.

Polymenidou, M., Lagier-Tourenne, C., Hutt, K.R., Huelga, S.C., Moran, J., Liang, T.Y., *et al.*, 2011. Long pre-mRNA depletion and RNA missplicing contribute to neuronal vulnerability from loss of TDP-43. Nat. Publ. Gr. 14.

Prasad, A., Bharathi, V., Sivalingam, V., Girdhar, A., Patel, B.K., 2019. Molecular Mechanisms of TDP-43 Misfolding and Pathology in Amyotrophic Lateral Sclerosis. Front. Mol. Neurosci. 12, 25.

Proctor, E.A., Fee, L., Tao, Y., Redler, R.L., Fay, J.M., Zhang, Y., *et al.*, 2016. Nonnative SOD1 trimer is toxic to motor neurons in a model of amyotrophic lateral sclerosis. Proc. Natl. Acad. Sci. U. S. A. 113, 614–9.

Prokopec, S.D., Watson, J.D., Waggott, D.M., Smith, A.B., Wu, A.H., Okey, A.B., *et al.*, 2013. Systematic evaluation of medium-throughput mRNA abundance platforms. RNA 19, 51–62.

Rachakonda, G., Xiong, Y., Sekhar, K.R., Stamer, S.L., Liebler, D.C., Freeman, M.L., 2008. Covalent modification at Cys151 dissociates the electrophile sensor Keap1 from the ubiquitin ligase CUL3. Chem. Res. Toxicol. 21, 705–710.

Rada, P., Rojo, A.I., Chowdhry, S., McMahon, M., Hayes, J.D., Cuadrado, A., 2011. SCF/{beta}-

TrCP promotes glycogen synthase kinase 3-dependent degradation of the Nrf2 transcription factor in a Keap1-independent manner. Mol. Cell. Biol. 31, 1121–33.

Radakovic, R., Stephenson, L., Colville, S., Swingler, R., Chandran, S., Abrahams, S., 2016. Multidimensional apathy in ALS: Validation of the Dimensional Apathy Scale. J. Neurol. Neurosurg. Psychiatry 87, 663–669.

Rao, R. V, Ellerby, H.M., Bredesen, D.E., 2004. Coupling endoplasmic reticulum stress to the cell death program. Cell Death Differ. 11, 372–380.

Ratti, A., Buratti, E., 2016. Physiological functions and pathobiology of TDP-43 and FUS/TLS proteins. J. Neurochem. 138, 95–111.

Reisman, S.A., Gahir, S.S., Lee, C.-Y.I., Proksch, J.W., Sakamoto, M., Ward, K.W., 2019. Pharmacokinetics and pharmacodynamics of the novel Nrf2 activator omaveloxolone in primates. Drug Des. Devel. Ther. 13, 1259.

Renton, A.E., Majounie, E., Waite, A., Simón-Sánchez, J., Rollinson, S., Gibbs, J.R., *et al.*, 2011. A hexanucleotide repeat expansion in C9ORF72 is the cause of chromosome 9p21-linked ALS-FTD. Neuron 72, 257–268.

Ringholz, G.M., Appel, S.H., Bradshaw, M., Cooke, N.A., Mosnik, D.M., Schulz, P.E., 2005. Prevalence and patterns of cognitive impairment in sporadic ALS. Neurology 65, 586–590.

Robledinos-Antón, N., Fernández-Ginés, R., Manda, G., Cuadrado, A., 2019. Activators and Inhibitors of NRF2: A Review of Their Potential for Clinical Development. Oxid. Med. Cell. Longev. 2019, 9372182.

Rosen, D.R., Siddique, T., Patterson, D., Figlewicz, D.A., Sapp, P., Hentati, A., *et al.*, 1993. Mutations in Cu/Zn superoxide dismutase gene are associated with familial amyotrophic lateral sclerosis. Nature 362, 59–62.

Ross, C.A., Poirier, M.A., 2004. Protein aggregation and neurodegenerative disease. Nat. Med. 2004 107 10, S10–S17.

Saito, R., Suzuki, T., Hiramoto, K., Asami, S., Naganuma, E., Suda, H., *et al.*, 2015. Characterizations of Three Major Cysteine Sensors of Keap1 in Stress Response. Mol. Cell. Biol. 36, MCB.00868-15.

Salehi, M., Nikkhah, M., Ghasemi, A., Arab, S.S., 2015. Mitochondrial membrane disruption by aggregation products of ALS-causing superoxide dismutase-1 mutants. Int. J. Biol. Macromol. 75, 290–297.

Sam, E.E., Verbeke, N., 1995. Free radical scavenging properties of apomorphine enantiomers and dopamine: Possible implication in their mechanism of action in parkinsonism. J. Neural Transm. - Park. Dis. Dement. Sect. 10, 115–127.

Santamaria, N., Alhothali, M., Alfonso, M.H., Breydo, L., Uversky, V.N., 2017. Intrinsic disorder in proteins involved in amyotrophic lateral sclerosis. Cell. Mol. Life Sci. 74, 1297–1318.

Sarlette, A., Krampfl, K., Grothe, C., Von Neuhoff, N., Dengler, R., Petri, S., 2008. Nuclear Erythroid 2YRelated Factor 2-Antioxidative Response Element Signaling Pathway in

Motor Cortex and Spinal Cord in Amyotrophic Lateral Sclerosis. J Neuropathol Exp Neurol 67, 1055–1062.

Satoh, T., Lipton, S., 2017. Recent advances in understanding NRF2 as a druggable target: development of pro-electrophilic and non-covalent NRF2 activators to overcome systemic side effects of electrophilic drugs like dimethyl fumarate. F1000Research 6, 2138.

Satoh, T., Rezaie, T., Seki, M., Sunico, C.R., Tabuchi, T., Kitagawa, T., *et al.*, 2011. Dual Neuroprotective Pathways of a Pro-Electrophilic Compound via HSF-1-activated Heat Shock Proteins and Nrf2-activated Phase 2 Antioxidant Response Enzymes HHS Public Access. J Neurochem 119, 569–578.

Schönfelder, E., Osmanovic, A., Müschen, L.H., Petri, S., Schreiber-Katz, O., 2020. Costs of illness in amyotrophic lateral sclerosis (ALS): a cross-sectional survey in Germany. Orphanet J. Rare Dis. 15, 149.

Scott, S., Kranz, J.E., Cole, J., Lincecum, J.M., Thompson, K., Kelly, N., *et al.*, 2008. Design, power, and interpretation of studies in the standard murine model of ALS. Amyotroph. Lateral Scler. 9, 4–15.

Seibenhener, M.L., Wooten, M.C., 2015. Use of the open field maze to measure locomotor and anxiety-like behavior in mice. J. Vis. Exp. 52434.

Sekhar, K.R., Rachakonda, G., Freeman, M.L., 2009. Cysteine-based regulation of the CUL3 adaptor protein Keap1. Toxicol. Appl. Pharmacol. 244, 21–26.

Sephton, C.F., Cenik, C., Kucukural, A., Dammer, E.B., Cenik, B., Han, Y., *et al.*, 2011. Identification of neuronal RNA targets of TDP-43-containing ribonucleoprotein complexes. J. Biol. Chem. 286, 1204–15.

Shang, Y., Huang, E.J., 2016. Mechanisms of FUS mutations in familial amyotrophic lateral sclerosis. Brain Res.

Shaw, P.J., Ince, P.G., Falkous, G., Mantle, D., 1995. Oxidative damage to protein in sporadic motor neuron disease spinal cord. Ann. Neurol. 38, 691–695.

Shou, L., Bei, Y., Song, Y., Wang, L., Ai, L., Yan, Q., *et al.*, 2019. Nrf2 mediates the protective effect of edaravone after chlorpyrifos-induced nervous system toxicity. Environ. Toxicol. 34, 626–633.

Simone, M., Trabacca, A., Panzeri, E., Losito, L., Citterio, A., Bassi, M.T., 2018. KIF5A and ALS2 Variants in a Family With Hereditary Spastic Paraplegia and Amyotrophic Lateral Sclerosis. Front. Neurol. 9, 1078.

Simpson, J.T., Workman, R.E., Zuzarte, P.C., David, M., Dursi, L.J., Timp, W., 2017. Detecting DNA cytosine methylation using nanopore sequencing. Nat. Methods 14, 407–410.

Smith, B.N., Ticozzi, N., Fallini, C., Gkazi, A.S., Topp, S., Kenna, K.P., *et al.*, 2014. Exome-wide Rare Variant Analysis Identifies TUBA4A Mutations Associated with Familial ALS. Neuron 84, 324–331.

Smith, B.N., Topp, S.D., Fallini, C., Shibata, H., Chen, H.-J., Troakes, C., *et al.*, 2017. Mutations in the vesicular trafficking protein annexin A11 are associated with amyotrophic lateral sclerosis. Sci. Transl. Med. 9.

Sotelo-Silveira, J.R., Lepanto, P., Elizondo, V., Horjales, S., Palacios, F., Martinez-Palma, L., *et al.*, 2009. Axonal mitochondrial clusters containing mutant SOD1 in transgenic models of ALS. Antioxidants Redox Signal. 11, 1535–1545.

Sreedharan, J., Blair, I.P., Tripathi, V.B., Hu, X., Vance, C., Rogelj, B., *et al.*, 2008. TDP-43 mutations in familial and sporadic amyotrophic lateral sclerosis. Science 319, 1668–72.

Steinmetz, K.L., Spack, E.G., 2009. The basics of preclinical drug development for neurodegenerative disease indications. BMC Neurol. 9, S2.

Stephenson, J., Amor, S., 2017. Modelling amyotrophic lateral sclerosis in mice. Drug Discov. Today Dis. Model. 25–26, 35–44.

Suzuki, T., Yamamoto, M., 2015. Molecular basis of the Keap1-Nrf2 system. Free Radic. Biol. Med.

Taft, R.A., Davisson, M., Wiles, M. V., 2006. Know thy mouse. Trends Genet. 22, 649–653.

Takahashi, Y., Fukuda, Y., Yoshimura, J., Toyoda, A., Kurppa, K., Moritoyo, H., *et al.*, 2013. Erbb4 mutations that disrupt the neuregulin-erbb4 pathway cause amyotrophic lateral sclerosis type 19. Am. J. Hum. Genet. 93, 900–905.

Takei, K., Watanabe, K., Yuki, S., Akimoto, M., Sakata, T., Palumbo, J., 2017. Edaravone and its clinical development for amyotrophic lateral sclerosis. Amyotroph. Lateral Scler. Front. Degener.

Tang, M., Ji, C., Pallo, S., Rahman, I., Johnson, G.V.W., 2018. Nrf2 mediates the expression of BAG3 and autophagy cargo adaptor proteins and tau clearance in an age-dependent manner. Neurobiol. Aging 63, 128–139.

Thomas, A., Burant, A., Bui, N., Graham, D., Yuva-Paylor, L.A., Paylor, R., 2009. Marble burying reflects a repetitive and perseverative behavior more than novelty-induced anxiety. Psychopharmacology (Berl). 204, 361–373.

Tian, X., Cong, F., Guo, H., Fan, J., Chao, G., Song, T., 2019. Downregulation of Bach1 protects osteoblasts against hydrogen peroxide-induced oxidative damage in vitro by enhancing the activation of Nrf2/ARE signaling. Chem. Biol. Interact. 309, 108706.

Tollervey, J.R., Curk, T., Rogelj, B., Briese, M., Cereda, M., Kayikci, M., *et al.*, 2011. Characterizing the RNA targets and position-dependent splicing regulation by TDP-43. Nat. Publ. Gr. 14.

Tong, K.I., Katoh, Y., Kusunoki, H., Itoh, K., Tanaka, T., Yamamoto, M., 2006. Keap1 Recruits Neh2 through Binding to ETGE and DLG Motifs: Characterization of the Two-Site Molecular Recognition Model. Mol. Cell. Biol. 26, 2887–2900.

Tong, K.I., Padmanabhan, B., Kobayashi, A., Shang, C., Hirotsu, Y., Yokoyama, S., *et al.*, 2007. Different Electrostatic Potentials Define ETGE and DLG Motifs as Hinge and Latch in

Oxidative Stress Response. Mol. Cell. Biol. 27, 7511–7521.

Tuntland, T., Ethell, B., Kosaka, T., Blasco, F., Zang, R.X., Jain, M., *et al.*, 2014. Implementation of pharmacokinetic and pharmacodynamic strategies in early research phases of drug discovery and development at Novartis Institute of Biomedical Research. Front. Pharmacol. 0, 174.

van Blitterswijk, M., DeJesus-Hernandez, M., Niemantsverdriet, E., Murray, M.E., Heckman, M.G., Diehl, N.N., *et al.*, 2013. Association between repeat sizes and clinical and pathological characteristics in carriers of C9ORF72 repeat expansions (Xpansize-72): a cross-sectional cohort study. Lancet Neurol. 12, 978–988.

Van Damme, P., Braeken, D., Callewaert, G., Robberecht, W., Van Den Bosch, L., 2005. GluR2 deficiency accelerates motor neuron degeneration in a mouse model of amyotrophic lateral sclerosis. J Neuropathol Exp Neurol 64, 605–612.

van der Ende, E.L., Jackson, J.L., White, A., Seelaar, H., van Blitterswijk, M., Van Swieten, J.C., 2021. Unravelling the clinical spectrum and the role of repeat length in C9ORF72 repeat expansions. J. Neurol. Neurosurg. Psychiatry 92, 502–509.

van Hooft, J.., Vijverberg, H.P.., 1998. Agonist and antagonist effects of apomorphine enantiomers on 5-HT3 receptors. Neuropharmacology 37, 259–264.

Vance, C., Rogelj, B., Hortobágyi, T., De Vos, K.J., Nishimura, A.L., Sreedharan, J., *et al.*, 2009. Mutations in FUS, an RNA processing protein, cause familial amyotrophic lateral sclerosis type 6. Science (80-.). 323, 1208–1211.

Vande Velde, C., Miller, T.M., Cashman, N.R., Cleveland, D.W., 2008. Selective association of misfolded ALS-linked mutant SOD1 with the cytoplasmic face of mitochondria. Proc. Natl. Acad. Sci. U. S. A. 105, 4022–7.

Vargas, M.R., Johnson, D.A., Sirkis, D.W., Messing, A., Johnson, J.A., 2008. Nrf2 activation in astrocytes protects against neurodegeneration in mouse models of familial amyotrophic lateral sclerosis. J. Neurosci. 28, 13574–81.

Vihervaara, A., Sistonen, L., 2014. HSF1 at a glance. J. Cell Sci. 261–266.

Vucic, S., Henderson, R.D., Mathers, S., Needham, M., Schultz, D., Kiernan, M.C., 2021. Safety and efficacy of dimethyl fumarate in ALS: randomised controlled study. Ann. Clin. Transl. Neurol. 8, 1991–1999.

Wakabayashi, N., Itoh, K., Wakabayashi, J., Motohashi, H., Noda, S., Takahashi, S., *et al.*, 2003. Keap1-null mutation leads to postnatal lethality due to constitutive Nrf2 activation. Nat. Genet. 35, 238–245.

Wang, H., Liu, K., Geng, M., Gao, P., Wu, X., Hai, Y., *et al.*, 2013. RXRα inhibits the NRF2-ARE signaling pathway through a direct interaction with the Neh7 domain of NRF2. Cancer Res. 73, 3097–3108.

Wang, S., Tan, Y., Zhang, J.-E., Luo, M., 2013. Pharmacogenetic activation of midbrain dopaminergic neurons induces hyperactivity. Neurosci Bull 29, 517–524.

Wang, Y., Qin, Z., 2010. Molecular and cellular mechanisms of excitotoxic neuronal death. Apoptosis 15, 1382–1402.

Wang, Y., Ye, S., Chen, L., Tang, L., Fan, D., 2021. Loss of appetite in patients with amyotrophic lateral sclerosis is associated with weight loss and anxiety/depression. Sci. Reports 2021 111 11, 1–7.

Watkins, J., Ghosh, A., Keerie, A.F.A., Alix, J.J.P., Mead, R.J., Sreedharan, J., 2020. Female sex mitigates motor and behavioural phenotypes in TDP-43Q331K knock-in mice. Sci. Rep. 10.

Watkins, J.A., Alix, J.J.P., Shaw, P.J., Mead, R.J., 2021. Extensive phenotypic characterisation of a human TDP-43Q331K transgenic mouse model of amyotrophic lateral sclerosis (ALS). Sci. Rep. 11, 16659.

Webster, C.P., Smith, E.F., Bauer, C.S., Moller, A., Hautbergue, G.M., Ferraiuolo, L., *et al.*, 2016. The C9orf72 protein interacts with Rab1a and the ULK 1 complex to regulate initiation of autophagy. EMBO J. 35, 1656–1676.

Werdenberg, D., Joshi, R., Wolffram, S., Merkle, H.P., Langguth, P., 2003. Presystemic metabolism and intestinal absorption of antipsoriatic fumaric acid esters. Biopharm. Drug Dispos. 24, 259–273.

West, R.J.H., Sharpe, J.L., Voelzmann, A., Munro, A.L., Hahn, I., Baines, R.A., *et al.*, 2020. Co-expression of C9orf72 related dipeptide-repeats over 1000 repeat units reveals age-A nd combination-specific phenotypic profiles in Drosophila. Acta Neuropathol. Commun. 8, 158.

Weydt, P., Hong, S.Y., Kliot, M., Möller, T., 2003. Assessing disease onset and progression in the SOD1 mouse model of ALS. Neuroreport 14, 1051–1054.

White, M.A., Kim, E., Duffy, A., Adalbert, R., Phillips, B.U., Peters, O.M., *et al.*, 2018. TDP-43 gains function due to perturbed autoregulation in a Tardbp knock-in mouse model of ALS-FTD. Nat. Neurosci. 21, 1–12.

White, M.A., Lin, Z., Kim, E., Henstridge, C.M., Pena Altamira, E., Hunt, C.K., *et al.*, 2019. Sarm1 deletion suppresses TDP-43-linked motor neuron degeneration and cortical spine loss. Acta Neuropathol. Commun. 7.

Whitelaw, E., Sutherland, H., Kearns, M., Morgan, H., Weaving, L., Garrick, D., 2001. Epigenetic Effects on Transgene Expression, in: Gene Knockout Protocols. Humana Press, New Jersey, pp. 351–368.

Wils, H., Kleinberger, G., Janssens, J., Pereson, S., Joris, G., Cuijt, I., *et al.*, 2010. TDP-43 transgenic mice develop spastic paralysis and neuronal inclusions characteristic of ALS and frontotemporal lobar degeneration. Proc. Natl. Acad. Sci. U. S. A. 107, 3858–3863.

Wu, J., Shen, E., Shi, D., Sun, Z., Cai, T., 2012. Identification of a novel Cys146X mutation of SOD1 in familial amyotrophic lateral sclerosis by whole-exome sequencing. Genet. Med. 14, 823–826.

Xu, Y.-F., Gendron, T.F., Zhang, Y.-J., Lin, W.-L., D'Alton, S., Sheng, H., *et al.*, 2010. Wild-type

human TDP-43 expression causes TDP-43 phosphorylation, mitochondrial aggregation, motor deficits, and early mortality in transgenic mice. J. Neurosci. 30, 10851–9.

Xu, Y.-F., Zhang, Y.-J., Lin, W.-L., Cao, X., Stetler, C., Dickson, D.W., *et al.*, 2011. Expression of mutant TDP-43 induces neuronal dysfunction in transgenic mice. Mol. Neurodegener. 6, 73.

Yang, J., Bridges, K., Chen, K.Y., Liu, A.Y.-C., 2008. Riluzole increases the amount of latent HSF1 for an amplified heat shock response and cytoprotection. PLoS One 3, e2864.

Yang, Y., Hentati, A., Deng, H.-X., Dabbagh, O., Sasaki, T., Hirano, M., *et al.*, 2001. The gene encoding alsin, a protein with three guanine-nucleotide exchange factor domains, is mutated in a form of recessive amyotrophic lateral sclerosis. Nat. Genet. 29, 160–165.

Yore, M.M., Kettenbach, A.N., Sporn, M.B., Gerber, S.A., Liby, K.T., 2011. Proteomic analysis shows synthetic oleanane triterpenoid binds to mTOR. PLoS One 6, 22862.

Yu, F., Wang, Z., Tchantchou, F., Chiu, C.-T., Zhang, Y., Chuang, D.-M., 2012. Lithium ameliorates neurodegeneration, suppresses neuroinflammation, and improves behavioral performance in a mouse model of traumatic brain injury. J. Neurotrauma 29, 362–74.

Yu, H., Chen, L., Zhang, S., He, J., Fan, D., 2020. Early Axonal Dysfunction of the Peripheral Nervous System Influences Disease Progression of ALS: Evidences From Clinical Neuroelectrophysiology.

Zarrindast, M.R., Bayat, A., Shafaghi, B., 1993. Involvement of dopaminergic receptor subtypes in straub tail behaviour in mice. Gen. Pharmacol. Vasc. Syst. 24, 127–130.

Zhou, J., Yi, J., Fu, R., Liu, E., Siddique, T., Ríos, E., *et al.*, 2010. Hyperactive intracellular calcium signaling associated with localized mitochondrial defects in skeletal muscle of an animal model of amyotrophic lateral sclerosis. J. Biol. Chem. 285, 705–12.

Zhou, Y., Zhang, T., Zhang, Q.-K., Jiang, Y., Xu, D.-G., Zhang, M., *et al.*, 2014. Unstable expression of transgene is associated with the methylation of CAG promoter in the offspring from the same litter of homozygous transgenic mice. Mol. Biol. Rep. 41, 5177–5186.

Zhu, C., Beck, M. V, Griffith, J.D., Deshmukh, M., Dokholyan, N. V, 2018. Large SOD1 aggregates, unlike trimeric SOD1, do not impact cell viability in a model of amyotrophic lateral sclerosis. Proc. Natl. Acad. Sci. U. S. A. 115, 4661–4665.

Zhu, M., Fahl, W.E., 2001. Functional Characterization of Transcription Regulators That Interact with the Electrophile Response Element.

Zimmer, S., Grebe, A., Bakke, S.S., Bode, N., Halvorsen, B., Ulas, T., *et al.*, 2016. Cyclodextrin promotes atherosclerosis regression via macrophage reprogramming. Sci. Transl. Med. 8, 333ra50.

Zou, Z.Y., Zhou, Z.R., Che, C.H., Liu, C.Y., He, R.L., Huang, H.P., 2017. Genetic epidemiology of amyotrophic lateral sclerosis: A systematic review and meta-analysis. J. Neurol. Neurosurg. Psychiatry 88, 540–549.

Zu, T., Liu, Y., Banez-Coronel, M., Reid, T., Pletnikova, O., Lewis, J., *et al.*, 2013. RAN proteins and RNA foci from antisense transcripts in C9ORF72 ALS and frontotemporal dementia. Proc. Natl. Acad. Sci. 110, E4968–E4977.

Zuo, X., Zhou, J., Li, Y., Wu, K., Chen, Z., Luo, Z., *et al.*, 2021. TDP-43 aggregation induced by oxidative stress causes global mitochondrial imbalance in ALS. Nat. Struct. Mol. Biol. 28, 132–142.

7. Project outcomes

- Poster presentation at the virtual MNDA 31st international symposium, December 2020.
- Poster presentation at the Medical School Research Day, University of Sheffield, June 2019.
- 3rd place oral presentation at the Medical School Research Day, University of Sheffield, June 2021
- Data used in application for a grant
- Data used in a patent: W02020081973 – treatment of neurological diseases.

8. Appendices

Appendix 1: A complete table of all primer pairs that were optimised including product size and if the primers passed optimisation. The gene name, accession number and primer sequences for all primer pairs analysed in this thesis. Where primers say not completes in ready to use means that they did not make it through the two-stage optimisation protocol, which will either be due to another primer pair working or mediocre data from stage one of optimisation.

Primer pair number	Gene name	Common name	Forward Primer	Reverse primer	Product size (bp)	Gene ID	Accession number	Ready to use
1	Gapdh glyceraldehyde-3-phosphate dehydrogenase	GAPDH	CATCACTGCCACCCAGAAGACTG	ATGCCAGTGAGCTTCCCGTTCAG	153	14433	NM_001289726, NM_008084	yes
2	Actin beta	Actin	CATTGCTGACAGGATGCAGAAGG	TGCTGGAAGGTGGACAGTGAGG	138	11461	NM_007393	yes
3	Glutamate-cycteine ligase, modifier subunit	GCLM	TCCTGCTGTGTGATGCCACCAG	GCTTCCTGGAAACTTGCCTCAG	113	14630	NM_008129	yes
4	Ppargc1a peroxisome proliferative activated receptor gamma coactivator 1 alpha	PGC1a	GAATCAAGCCACTACAGACACCG	CATCCCTCTTGAGCCTTTCGTG	136	19017	NM_008904	yes
5	DnaJ heat shock protein family (HSP40) member B1	Hsp40 member B1	TTCGACCGCTATGGAGAGGAAG	CCGAAGAACTCAGCAAACATGGC	131	81489	NM_001308227, NM_018808	yes
6	heat shock protein 1A	Hsp70 (Hspa1a)	ACAAGTCGGAGAACGTGCAGGA	GTTGTCCGAGTAGGTGGTGAAG	155	193740	NM_010479	yes
7	DnaJ heat shock protein family (Hsp40) member B2	HSP40 member B2	AGCGGGTAGAAGTGGAAGAGGA	GCAACTGAAGGTTGCTGCTCAC	115	56812	NM_001159883, NM_001159884, NM_001159885, NM_020266, NM_178055	not completed
8	Heme oxygenase 1	HMOX1	CACTCTGGAGATGACACCTGAG	GTGTTCCTCTGTCAGCATCACC	115	15368	NM_010442	no
9	NAD(P)H dehydrogenase quinone 1	NQO1	GCCGAACACAAGAAGCTGGAAG	GGCAAATCCTGCTACGAGCACT	120	18104	NM_008706	yes

10	nuclear respiratory factor 1	Nrf1	GGCAACAGTAGCCACATTGGCT	GTCTGGATGGTCATTTCACCGC	141	18181	NM_001164226, NM_001164227, NM_001164228, NM_001164229, NM_001164230, NM_010938	no
11	Nup62, nucleoporin 62	Nup62	ACACCTGCTTCTGGAGGAACAG	TTGGAGGTGCTGCCACTTGAGA	158	18226	NM_053074	yes
12	Ppargc1a peroxisome proliferative activated receptor gamma coactivator 1 beta	PGC1b	CAGCCTCAGTTCCAGAAGTCAG	CACCGAAGTGAGGTGCTTATGC	124	170826	NM_133249	no
13	Oxidative stress induced growth inhibitor 1	Osgin 1	AGACTCTGTGCTCTCCTGGAAG	GCCTTGGCTCAAGGTCACCATG	124	71839	NM_027950	no
14	Heme oxygenase 1	Hmox1	CTAAGACCGCCTTCCTGCTC	CTCTGACGAAGTGACGCCAT	109	15368	NM_010442	no
15	Heme oxygenase 1	Hmox1	CAGAAGAGGCTAAGACCGCC	TAGCAGGCCTCTGACGAAGT	126	15368	NM_010442	not completed
16	NAD(P)H dehydrogenase quinone 1	NQo1	TAGCCTGTAGCCAGCCCTAA	GCCTCCTTCATGGCGTAGTT	187	18104	NM_008706	not completed
17	NAD(P)H dehydrogenase quinone 1	NQo1	AGCTTTAGGGTCGTCTTGGC	ACAATCAGGGCTCTTCTCGC	105	18104	NM_008706	no
18	NAD(P)H dehydrogenase quinone 1	NQo1	AGGATGGGAGGTACTCGAATC	AGGCGTCCTTCCTTATATGCTA	144	18104	NM_008706	not completed
19	nuclear respiratory factor 1	Nrf1	CAGCACCTTTGGAGAATGTG	CCTGGGTCATTTTGTCCACA	162	18181	NM_001164226, NM_001164227, NM_001164228, NM_001164229, NM_001164230, NM_010938	no
20	nuclear respiratory factor 1	Nrf1	AGTGCAGGGTGTGTGTGTGT	GTGAGGCAGTCTCCTCTGCT	177	18181	NM_001164226, NM_001164227, NM_001164228, NM_001164229, NM_001164230, NM_010938	no
21	nuclear respiratory factor 1	Nrf1	CAACAGGGAAGAAACGGAAA	CCACATTCTCCAAAGGTGCT	210	18181	NM_001164226, NM_001164227, NM_001164228,	yes

							NM_001164229, NM_001164230, NM_010938	
22	Nup62, nucleoporin 62	Nup62	GTGTGAGCGGAGAGTGAAGG	GCGGTCCCAAATGTAAAGCC	162	18226	NM_053074	not completed
23	Nup62, nucleoporin 62	Nup62	TCTTCAGTGGGTGGACCAGA	TCAACAACCAACCACGGGAA	187	18226	NM_053074	not completed
24	Oxidative stress induced growth inhibitor 1	Osgin 1	CTCTCTGGACACATCCCCTAC	GAAAGGTACTCTAGGTCCTGGT	119	71839	NM_027950	no
25	Oxidative stress induced growth inhibitor 1	Osgin 1	TGCGGAAGAAATGCAGAGGT	CATGCTCGGACTTAGCCCAC	153	71839	NM_027950	no
26	Glutathione S transferase pi 1	Gstp1	TGGAAGGAGGAGGTGGTTACCA	GGTAAAGGGTGAGGTCTCCATC	109	14870	NM_013541	yes
27	Glutathione S transferase pi 1	Gstp1	TGCTCAAGCCCACTTGTCTG	CACCATATCCATCTGGGCGG	152	14870	NM_013541	no
28	glutamate-cysteine ligase, catalytic subunit	Gclc	ACACCTGGATGATGCCAACGAG	CCTCCATTGGTCGGAACTCTAC	131	14629	NM_010295	yes
29	glutamate-cysteine ligase, catalytic subunit	Gclc	GCACATCTACCACGCAGTCA	GTCTCAAGAACATCGCCTCCA	138	14629	NM_010295	not completed
30	estrogen related receptor, alpha	Esrra	ACTACGGTGTGGCATCCTGTGA	GGTGATCTCACACTCATTGGAGG	104	26379	NM_007953	no
31	estrogen related receptor, alpha	Esrra	CTACGGTGTGGCATCCTGTG	AGACGCACACCCTCCTTGA	183	26379	NM_007953	not completed
32	cytochrome c oxidase assembly protein 11	Cox11	GGAACAAGACGGTGCTCACCTA	CACTGCTGATCCTCCAAGTCCA	122	69802	NM_199008	no
33	cytochrome c oxidase assembly protein 11	Cox11	TGCTGCTATCCTGTGATGGT	AGGCCTATGTGGCAAACACTT	190	69802	NM_199008	yes
34	interleukin 6	Il6	TACCACTTCACAAGTCGGAGGC	CTGCAAGTGCATCATCGTTGTTC	116	16193	NM_001314054, NM_031168	not completed
35	interleukin 6	Il6	CACGGCCTTCCCTACTTCAC	TTTCTGCAAGTGCATCATCGT	191	16193	NM_001314054, NM_031168	not completed
36	interleukin 1 beta	Il1b	TGGACCTTCCAGGATGAGGACA	GTTCATCTCGGAGCCTGTAGTG	148	16176	NM_008361	not completed
37	interleukin 1 beta	Il1b	GTGTCTTTCCCGTGGACCTT	ATGGGAACGTCACACACCAG	128	16176	NM_008361	not completed
38	heat shock protein 8	Hspa8	CCGATGAAGCTGTTGCCTATGG	CCAAGGGAAAGAGGAGTGACATC	112	15481	NM_031165	yes
39	heat shock protein 8	Hspa8	TGGCATTTGTGTGGTCTCGT	TTCCATGCTGGAAGACACCC	126	15481	NM_031165	not completed

40	DnaJ heat shock protein family (Hsp40) member C6	Dnajc6	TGCTAAGCCACCAGGTCAGGAT	CTGGATGTTCACAGCAGGAGTAC	136	72685	NM_198412	yes
41	DnaJ heat shock protein family (Hsp40) member C6	Dnajc6	TGGCCCTGCTGTTCGATTAC	GGCTGACAGTGATTGCCTTG	155	72685	NM_198412	not completed
42	heat shock protein 8	Hspb8	AGCAGGAAGGTGGGATTGTCTC	GGAGCCTCGATGATGAGCAGG	121	80888	NM_030704	no
43	heat shock protein 8	Hspb8	CGTCAGCCTTGGTCCTTCT	GTTCGGTTCTCCCTCCCATC	128	80888	NM_030704	yes
44	BCL2-associated athanogene 3	Bag3	CCAGACAGATAAACAGTGTGGAC	GGAAGAGGATGAGCAGTCAGAG	124	29810	NM_013863	yes
45	BCL2-associated athanogene 3	Bag3	GCCAAGTTCTCTGGATGGGA	CCTCTGTGTAGCCGATGTGT	191	29810	NM_013863	no
46	discs large MAGUK scaffold protein 4	Dlg4	TCAGACGGTCACGATCATCGCT	GTTGCTTCGCAGAGATGCAGTC	130	13385	NM_001109752, NM_007864	no
47	discs large MAGUK scaffold protein 4	Dlg4	TTGACGCCAGCGACGAAG	CCAGTCCTTGGCCTTTAACCT	134	13385	NM_001109752, NM_007864	yes
48	synapsin I	Syn1	TATGCCACTGCTGAGCCCTTCA	ATGGCAATCTGCTCAAGCATAGC	146	20964	NM_001110780, NM_013680	yes
49	synapsin I	Syn1	TCTTTCGCCAGCCTCTTCTC	TAGGACCAGGTTTCTCAAGGG	187	20964	NM_001110780, NM_013680	not completed
50	tumor necrosis factor	Tnf	GGTGCCTATGTCTCAGCCTCTT	GCCATAGAACTGATGAGAGGGAG	139	21926	NM_001278601, NM_013693	no
51	tumor necrosis factor	Tnf	CAGCCGATGGGTTGTACCTT	GATAGCAAATCGGCTGACGG	101	21926	NM_001278601, NM_013693	no
52	nitric oxide synthase 2, inducible	Nos2	GAGACAGGGAAGTCTGAAGCAC	CCAGCAGTAGTTGCTCCTCTTC	127	18126	NM_001313921, NM_001313922, NM_010927	no
53	nitric oxide synthase 2, inducible	Nos2	AGCTACGCCTTCAACACCAA	GCTGGGACAGTCTCCATTCC	117	18126	NM_001313921, NM_001313922, NM_010927	no
54	prostaglandin-endoperoxide synthase 2	Ptgs2	GCGACATACTCAAGCAGGAGCA	AGTGGTAACCGCTCAGGTGTTG	132	19225	NM_011198	yes
55	prostaglandin-endoperoxide synthase 2	Ptgs2	AGTGTGACTGTACCCGGACT	CTCCCTTGAAGTGGGTCAGG	129	19225	NM_011198	not completed
56	Fas ligand (TNF superfamily, member 6)	Fasl	GAAGGAACTGGCAGAACTCCGT	GCCACACTCCTCGGCTCTTTTT	117	14103	NM_001205243, NM_010177	no
57	Fas ligand (TNF superfamily, member 6)	Fasl	TCCGTGAGTTCACCAACCAA	CAGAGATCAGAGCGGTTCCA	177	14103	NM_001205243, NM_010177	no

58	DnaJ heat shock protein family (Hsp40) member C5	Dnajc5	GGACTGGACAAGAATGCAACCTC	CTTTTCGTGGCGTCTGTCAGGA	158	13002	NM_001271584, NM_001271585, NM_016775	yes
59	DnaJ heat shock protein family (Hsp40) member C5	Dnajc5	CCCTGAAGACTTGGAGGCAC	TGAACCCGTCGGTGTGATAG	140	13002	NM_001271584, NM_001271585, NM_016775	not completed
60	Sequestosome 1	Sqstm1	GCTCTTCGGAAGTCAGCAAACC	GCAGTTTCCCGACTCCATCTGT	128	18412	NM_001290769, NM_011018	yes
61	Sequestosome 1	Sqstm1	GATAGCCTTGGAGTCGGTGG	CTAGAGAGCTTGGCCCTTCC	164	18412	NM_001290769, NM_011018	not completed
62	eukaryotic translation elongation factor 2	Eef2	CAGAAGTACCGTTGTGAGCTGC	GTCAGAGGTTGGCACCATCTTG	126	13629	NM_007907	not completed
63	eukaryotic translation elongation factor 2	Eef2	CCCAGTGCGTGTTTGACC	GCAGCATGTGGCAGTATCAG	174	13629	NM_007907	yes
64	Oxidative stress induced growth inhibitor 1	Osgin1	CACCGTGTGACCAAGTTCCT	TGCCGATGATGACTACTGGG	189	71839	NM_027950	no
65	Oxidative stress induced growth inhibitor 1	Osgin1	TCACCGTGTGACCAAGTTCC	AGGAGGTCATAGCTCGGTGG	130	71839	NM_027950	no
66	Heme oxygenase 1	Hmox1	ATGGCGTCACTTCGTCAGAG	GCCAACAGGAAGCTGAGAGT	143	15368	NM_010442	not completed
67	Heme oxygenase 1	Hmox1	AGAACCAGCCTGAACTAGCC	CTGGACACCTGACCCTTCTG	161	15368	NM_010442	yes
68	interleukin 6	Il6	ACAAAGCCAGAGTCCTTCAGAG	TTGGATGGTCTTGGTCCTTAGC	164	16193	NM_001314054, NM_031168	no
69	interleukin 6	Il6	TGTAGCTCATTCTGCTCTGGAG	ACCAGCATCAGTCCCAAGAAG	116	16193	NM_001314054, NM_031168	no
70	interleukin 6	Il6	TCTGCAAGAGACTTCCATCCAG	CCACGATTTCCCAGAGAACATG	178	16193	NM_001314054, NM_031168	no
71	interleukin 1 beta	Il1b	TGTGCAAGTGTCTGAAGCAG	ATGTGCTGCTGCGAGATTTG	189	16176	NM_008361	no
72	interleukin 1 beta	Il1b	AGCTTCCTTGTGCAAGTGTC	TGCTGCGAGATTTGAAGCTG	191	16176	NM_008361	no
73	interleukin 1 beta	Il1b	TGAAGCAGCTATGGCAACTG	TGCTGCTGCGAGATTTGAAG	174	16176	NM_008361	yes
74	tumor necrosis factor	Tnf	AGCACAGAAAGCATGATCCG	GCCATTTGGGAACTTCTCATCC	198	21926	NM_001278601, NM_013693	yes
75	tumor necrosis factor	Tnf	TCGTAGCAAACCACCAAGTG	AGCCTTGTCCCTTGAAGAGAAC	159	21926	NM_001278601, NM_013693	yes

76	tumor necrosis factor	Tnf	TGGGCTTTCCGAATTCACTG	TTGCACCTCAGGGAAGAATCTG	151	21926	NM_001278601, NM_013693	no
77	nitric oxide synthase 2, inducible	Nos2	ACAAGCTGCATGTGACATCG	AAATCCGATGTGGCCTTGTG	106	18126	NM_001313921, NM_001313922, NM_010927	not completed
78	nitric oxide synthase 2, inducible	Nos2	TGCTTTGTGCGAAGTGTCAG	ACCCAAACACCAAGCTCATG	172	18126	NM_001313921, NM_001313922, NM_010927	no
79	nitric oxide synthase 2, inducible	Nos2	ACACCAAGGTTGTCTGCATG	AAGGCCAAACACAGCATACC	182	18126	NM_001313921, NM_001313922, NM_010927	no
80	Fas ligand (TNF superfamily, member 6)	Fasl	TTTCCCTTGACTGCGGAAAC	AATTCATGGGCTGCTGCATG	153	14103	NM_001205243, NM_010177	no
81	Fas ligand (TNF superfamily, member 6)	Fasl	AAAGACCTCATGACCGCAAG	TCTGCATTGTCACACAGCAG	153	14103	NM_001205243, NM_010177	not completed
82	Fas ligand (TNF superfamily, member 6)	Fasl	AGTGTGGCCCATTTAACAGG	TGGTTGTTGCAAGACTGACC	182	14103	NM_001205243, NM_010177	no
83	Oxidative stress induced growth inhibitor 1	Osgin1	CGGTGACATCGCCCACTAC	GCTCGGACTTAGCCCACTC		71839	NM_027950	yes